The Effects of Reduced *Mrpl54* Expression on Mouse Lifespan, Metabolic Health Span, and Skeletal Muscle Aging

Kimberly Reid

Thesis submitted to the University of Ottawa
in partial fulfillment of the requirements for the
Doctorate in Philosophy degree in Biology

Department of Biology
Faculty of Science
University of Ottawa

1. Descriptive Note

INSTITUTION: University of Ottawa

LOCATION: Ottawa, Ontario

DEGREE: Doctor of Philosophy (2024)

PROGRAM: Biology

TITLE: The effects of reduced *Mrpl54* expression on mouse lifespan, metabolic health span, and skeletal muscle aging

AUTHOR: Kimberly J. Reid, B.Sc. (Royal Military College), B.Sc. Honours (University of Victoria), M.Sc. (University of British Columbia)

SUPERVISORS: Professors Emily Standen and Keir Menzies

SUPERVISORY COMMITTEE: Professors Mary-Ellen Harper, Bill Willmore, and Jan Mennigen

NUMBER OF PAGES: 197

2. Lay Abstract

In wealthy populations, the oldest adults have the greatest health issues due to aging and age-related disease. We need interventions to maintain and improve health and functionality as we age – in other words, we need to increase human health span. Mitochondria are cell organelles responsible for adenosine triphosphate (ATP) production and for signaling the health of a cell. They have machinery called mitochondrial ribosomes (mitoribosomes) that generate functional proteins important to ATP generation. With age, mitochondria become less efficient and dysfunctional, and coordination breaks down between the cell and the mitochondria. The result is an increase in stress signaling via the mitochondrial unfolded protein response (UPR^{mt}). The goal of the UPR^{mt} is to attempt to repair dysfunctional mitochondria. One type of intervention to insulate mitochondria and cells from age-related decline is mitohormesis, where a mild mitochondrial stressor is introduced to generate a beneficial health effect. The cell responds by adapting to the stressor and increasing resilience so that the organism becomes resistant to future stressors. A well-known mitohormetic is regular physical exercise, during which mitochondria send stress signals to the nucleus, invoking the UPR^{mt}, and ultimately improving health span. In the roundworm *Caenorhabditis elegans*, reducing the amount of mitoribosome protein subunits (MRPs) results in a mild reduction in mitoribosome function, which invokes the UPR^{mt} and extends worm lifespan and health span. In this study, we mutated the gene of a critical MRP (*Mrpl54*$^{+/-}$) to introduce mild mitochondrial stress in a mouse model. Like the roundworm *Mrp* longevity model, we predicted the mouse would have an increased life span and/or health span due to a mitohormetic response to mild mitochondrial stress. However, our mouse model showed no difference in metabolic health with age or lifespan when compared to control mice. We noticed that myoblasts (a type of cell that can turn into mature muscle cells during development or in response to stress or injury) have

reduced amounts of mitochondrial proteins that are critical to ATP production. Since we know that MRP levels reduce with age and that *Mrpl54*$^{+/-}$ myoblast mitochondria start with lower levels of proteins, we predicted that the *Mrpl54*$^{+/-}$ mouse model will show premature muscle aging, despite not showing major whole-body metabolic deficits. This is because myoblasts start with less proteins that are necessary to ATP production. By the age of 12-months (i.e., middle age), male *Mrpl54*$^{+/-}$ mice had reduced grip strength, decreased muscle force, and disrupted muscle fibers, which suggested compensatory changes in muscle that recapitulated aging. Unexpectedly, 12-month male *Mrpl54*$^{+/-}$ mice also showed better running endurance and better recovery from fatigue that may be the result of changes in muscle fiber characteristics during aging in these mice. However, by age 18-months, male *Mrpl54*$^{+/-}$ mice had lost their running endurance advantage. Altogether, the results from the *Mrpl54*$^{+/-}$ mouse model failed to show an effect on lifespan or health span. On the contrary, male *Mrpl54*$^{+/-}$ mice appeared to display altered muscle characteristics during aging.

3. Résumé

Dans les populations riches, ce sont les adultes les plus âgés qui connaissent les plus grands problèmes de santé dus au vieillissement et aux maladies liées à l'âge. Nous avons besoin d'interventions pour maintenir et améliorer la santé et la fonctionnalité à mesure que nous vieillissons – en d'autres termes, nous devons augmenter la durée de vie de l'humanité. Les mitochondries sont des organites cellulaires responsables de la production d'ATP et de signaler la santé d'une cellule. Ils possèdent des machineries appelées ribosomes mitochondriaux (mitoribosomes) qui génère des protéines fonctionnelles essentielles à la production d'ATP. Avec l'âge, les mitochondries deviennent moins efficaces et dysfonctionnelles, et la communication entre la cellule et les mitochondries se dégrade. Le résultat est une augmentation de la signalisation du stress via la réponse protéine dépliée mitochondriale (UPR^{mt}). L'objectif de l'UPR^{mt} est de tenter de réparer les mitochondries dysfonctionnelles. Un type d'intervention visant à protéger les mitochondries et les cellules du déclin lié à l'âge est la mitohormèse, dans laquelle un faible stress mitochondrial est introduit pour générer un effet bénéfique sur la santé. La cellule réagit en s'adaptant au facteur de stress et en augmentant sa résilience afin que l'organisme devienne résistant aux futurs facteurs de stress. Un mitohormétique bien connu est l'exercice physique régulier, au cours duquel les mitochondries envoient des signaux de stress au noyau, invoquant l'UPR^{mt} et améliorant finalement la santé. Chez le ver rond *Caenorhabditis elegans*, la réduction de la quantité de sous-unités protéines des mitoribosomes (MRP) entraîne une petite réduction de la fonction des mitoribosomes, ce qui invoque l'UPR^{mt} et prolonge la durée de vie et la santé du ver. Dans cette étude, nous avons muté le gène d'un MRP critique ($Mrpl54^{+/-}$) pour introduire un faible stress mitochondrial dans un modèle de souris. Comme le modèle de longévité *Mrp* de vers rond, nous avons prédit que la souris aurait une durée de vie et/ou une durée de santé améliorée en

raison d'une réponse mitohormétique à un faible stress mitochondrial. Cependant, notre modèle de souris n'a montré aucune différence en termes de santé métabolique en fonction de l'âge ou de la durée de vie par rapport aux souris de contrôle. Nous avons remarqué que les myoblastes (un type de cellule qui peut se transformer en cellules musculaires matures au cours du développement ou en réponse à un stress ou à une blessure) contiennent des quantités réduites de protéines mitochondriales essentielles à la production d'énergie. Nous savons que les niveaux de MRP diminuent avec l'âge et que les mitochondries des myoblastes *Mrpl54*$^{+/-}$ démarrent avec des niveaux de protéines plus faibles. Nous avons prédit que le modèle souris *Mrpl54*$^{+/-}$ montrerait un vieillissement musculaire prématuré, même s'il ne présentait pas de déficits métaboliques majeurs dans l'ensemble du corps. En effet, les myoblastes commencent avec moins de protéines essentielles à la production d'ATP. À l'âge de 12 mois (c'est-à-dire d'âge moyen), les souris mâles *Mrpl54* $^{+/-}$ présentaient une force de préhension réduite, une diminution de la force musculaire et des fibres musculaires perturbées, ce qui suggérait des changements compensatoires dans les muscles qui récapitulaient le vieillissement. De manière inattendue, les souris mâles *Mrpl54*$^{+/-}$ de 12 mois ont également montré une meilleure endurance à la course et une meilleure récupération de la fatigue, ce qui pourrait être le résultat de changements dans les caractéristiques des fibres musculaires au cours du vieillissement chez ces souris. Dans l'ensemble, les résultats du modèle de souris *Mrpl54*$^{+/-}$ n'ont pas réussi à montrer d'effet sur la durée de vie ou sur la santé. Au contraire, les souris mâles *Mrpl54*$^{+/-}$ semblaient présenter des caractéristiques musculaires altérées au cours du vieillissement.

4. Abstract

With age comes a decline in the dynamic regulation of a balanced and functional mitochondrial proteome (proteostasis) that leads to an increase in oxidative stress and macromolecule damage, with a decline in ATP production. Compromised protein networks and reduced available energy leaves an organism susceptible to accelerated aging and the onset of age-related disease. Since mitochondrial respiratory complexes are composed of protein subunits from both mitochondria and nuclear genomes, their assembly relies on the coordination of mitochondrial and cytoplasmic translation machinery. Disruption of mitochondrial translation generates an imbalance in the ratio of mitochondrial (mtDNA) to nuclear DNA (nDNA) encoded proteins, which is called a mitonuclear protein imbalance. In response to the protein imbalance, a retrograde stress signal is sent from the mitochondria to the nucleus, invoking the mitochondrial unfolded protein response (UPR^{mt}) to resolve the mitoproteostatic stress. In a young healthy cell, the UPR^{mt} upregulates protein folding chaperones and proteases to resolve the consequences of a mitonuclear protein imbalance. In the early stages of aging, the UPR^{mt} appears to be upregulated in response to age-related mitochondrial proteostatic stress. In aged senescent cells however, the UPR^{mt} response is blunted. There is cross-species evidence that induction of the UPR^{mt} through moderate-intensity exercise or through genetic disruption of the mitochondrial translation machinery will act as a hormetic – resulting in health benefits in the long term. *Caenorhabditis elegans* longevity models demonstrate that a reduction in mitochondrial ribosomal protein (*Mrp*) gene expression or disturbed mitochondrial translation will function as a hormetic. The disruption of the mitochondrial ribosome leads to a mitonuclear protein imbalance, invokes the nematode UPR^{mt}, which then robustly extends *C. elegans* lifespan and health span. To determine whether the hormetic effects of mild mitochondrial ribosome disruption can be recapitulated in a mammalian

model, this thesis tests a C57/BL6/NTaconic mouse model altered in the germline to have reduced *Mrpl54* expression through heterozygous mutation. Mice were metabolically tested at ages 6-, 18-, and 24-months and followed through their natural lifespan to determine whether reduction in the expression of a critical *Mrp* (*Mrpl54*) impacts lifespan or metabolic health span. While *Mrpl54* mRNA expression was ~50% of wildtype in all *Mrpl54*$^{+/-}$ tissues tested, there were no differences observed in metabolic health with age or lifespan in either male or female mice. Cultured *Mrpl54*$^{+/-}$ primary myoblasts had lower absolute levels of nDNA- and mtDNA-encoded respiratory complex subunits relative to wildtype; however, the ratio between nDNA- and mtDNA-encoded protein subunits remained like wildtype. Further testing of the model revealed that *Mrpl54*$^{+/-}$ males had weaker grip strength by age 12-months, which was also found in the data from multiple heterozygous *Mrp* (*Mrp*$^{+/-}$) mouse models available at the International Mouse Phenotyping Consortium. 12-month-old *Mrpl54*$^{+/-}$ males displayed reduced tetanic force and better fatigue recovery in *ex vivo* skeletal muscles, and the transmission electron micrographs of skeletal muscle sarcomeres revealed an early aging phenotype. Unlike the *C. elegans* reduced *Mrp* longevity model, reduced expression of a critical *Mrp* did not result in lifespan or metabolic health span benefits in a mouse model. In contrast, the *Mrpl54*$^{+/-}$ male model showed evidence of premature skeletal muscle aging. While the results of this research do not support the role of *Mrpl54* reduced expression in mammalian lifespan or health span extension, they do point to a premature aging phenotype for certain muscle parameters that may be relevant to people living with heterozygous mitochondrial protein mutations. Typically, these individuals are regarded as carriers and free of phenotype associated with their mitochondrial protein mutation. The results in this thesis suggest that those with a heterozygous mitochondrial protein gene mutation may manifest a phenotype as they grow older and are less resilient to external or internal challenges.

5. Acknowledgement

I dedicate this thesis to my partner, Phillip Rennison, and my daughters, Paige and Isla Rennison, for their unwavering support and encouragement. And I acknowledge the following people for their mentorship, support, and friendship:

Adriana Gambarotta – Adriana taught me all she knows about mouse breeding, colony maintenance, IVF and she became my dear friend in the process. Adriana, thank you for answering my many questions, your valuable time and continuous support, and your excellent sense of humour.

Danielle Dewar-Darch – like Adriana, Danielle was instrumental in my training in mouse handling and colony maintenance, and she taught me how to do a detailed and efficient necropsy. And she became my dear friend in the process. Danielle, thank you for always being there for me when I needed a shoulder to lean on.

Christine Kitchen – Christine was my go-to person in the management of my mouse longevity colony, particularly in resolving male aggression issues and, as the mice aged, she helped me with identifying difficult humane endpoints. She was always present and available to advise and resolve problems. Most importantly, she took over my mouse colony for me for three months in 2019, so that I could pursue *C. elegans* research in Amsterdam. Christine, I could not have finished my mouse studies without your help.

Courtney Reeks – Courtney was my trainer for all things mouse related (including but not limited to weaning and breeding mice, tissue sampling, performing the OGTT and ipITT, saphenous vein blood sampling, and cardiac puncture). She is a natural and excellent teacher and was able to put me, her student, at ease. Courtney, I appreciate your patience as I slowly became proficient.

Alex Green – when Alex joined the Menzies lab as a post-doctorate, my PhD trajectory changed for the better. As someone who is highly knowledgeable in his field, he is an excellent mentor, advisor, and trainer. Alex, thank you for always being willing to listen and to give productive and critical feedback when I most needed it.

Keegan Lutek and Trina Du – in the Standen Lab, Keegan was my fellow PhD student and Trina was a post-doctorate. Both Keegan and Trina became my rock-solid friends and mentors, especially in all things statistics. Keegan and Trina, I learned a great deal from you, both in how to do science properly and how to lead. I will miss our Friday afternoon stats and evolution discussions at the Noz.

Keir Menzies – as my co-supervisor, Professor Menzies was always supportive, kind, and his office door always open for discussions. His lab is a gentle place where mistakes are learning opportunities. Professor Menzies, thank you for providing this opportunity for me.

Emily Standen – as my co-supervisor, Professor Standen always had my back and was my staunch supporter and defender. I admire her leadership and her advocacy for students at the University of Ottawa. Professor Standen, thank you for providing this opportunity and for supporting me in every single step of my journey.

Martin René Alexander Leduc – thank you for reading my lay abstract, asking excellent clarifying questions, and then translating it into French for me.

6. Indigenous Affirmation

We pay respect to the Algonquin People, who are the traditional guardians of this land. We acknowledge their longstanding relationship with this territory, which remains unceded. We pay respect to all Indigenous People in this region, from all nations across Canada, who call Ottawa home. We acknowledge the traditional knowledge keepers, both young and old. And we honour their courageous leaders: past, present, and future.

7. Preface

This thesis consists of two data chapters (Sections 15 and 16), which are prepared in manuscript style. This thesis was supported by the Canadian Institutes of Health Research (CIHR MOP 159455 Grant to Keir J. Menzies), Natural Sciences and Engineering Research Council (NSERC Collaborative Research and Training Experience program grant RGPIN 2018-06838 and NSERC Discovery Grant DGECR 2018-00012 to Keir J. Menzies), and the Netherlands Organisation for Scientific Research (NWO VIDI grant 917.15.305 to Riekelt H. Houtkooper). I was a holder of the NSERC Alexander Graham Bell Canada Graduate Scholarship-Doctoral Program (CGS-D) for three years during this thesis and I was awarded a Michael Smith Foreign Study Supplement, which allowed me to conduct *C. elegans* work at the Amsterdam University Medical Centre in Professor Riekelt Houtkooper's laboratory.

8. Table of Contents

9. List of Figures

10. List of Abbreviations

8W	8 weeks
6M	6 months
12M	12 months
18M	18 months
24M	24 months
AA	Antimycin A
Aβ	Amyloid beta peptide
AD	Alzheimer's Disease
ADP	Adenosine diphosphate
AF	Assembly factor
ANCOVA	Analysis of covariance
ANOVA	Analysis of variance
APP	Amyloid precursor protein
Asc	Ascorbate
ATF4	Activating transcription factor-4 (mammalian ISR master regulator)
ATF5	Activating transcription factor-5 (mammalian UPR^{mt} master regulator)
Atf-5	*C. elegans* activating transcription factor-5 (orthologue of ATF4)
Atfs-1	Activating transcription factor-1 stress-associated (*C. elegans* UPR^{mt} master regulator)
ATP	Adenosine triphosphate
ATP5A	ATP-5A protein subunit
AUC	Area under curve
B2m	Beta-r-microglobulin
BAT	Brown adipose tissue
BP	Blood pressure
BRASTO	Brain-specific overexpression of Sirt1

BXD	Multigenerational C57BL/6J intercrosses with DBA/2J mouse strains
CCCP	Carbonyl cyanide m-chlorophenylhydrazone
CHOP	CAAT/enhancer binding homology protein
CI	Complex I (NADH-dehydrogenase) or confidence interval
CII	Complex II (succinate dehydrogenase)
CIII	Complex III (cytochrome *c* oxidoreductase)
CIV	Complex IV (cytochrome *c* oxidase)
CIV	Complex V (ATP-synthase)
CLAMS	Comprehensive Lab Animal Monitoring System (Columbus Instruments)
CoQ/CoQH$_2$	Ubiquinol/ubiquinone
COX	Cytochrome *c* oxidase subunit
CRU	Ca^{2+}-release units
Cyt *c*	Cytochrome *c*
DELE1	DAP3-binding cell death enhancer-1
DNA	Deoxyribonucleic acid
EchoMRI	Magnetic resonance imager
EDL	Extensor digitorum longus
eIF2α	Eukaryotic translation initiation factor-2 alpha subunit
ETC	Electron transport chain
FADH	Oxidized form of flavin adenine dinucleotide
FADH$_2$	Reduced form of flavin adenine dinucleotide
FCCP	Carbonyl cyanide-p-trifluoromethoxyphenylhydrazine
FGF21	Fibroblast growth factor-21
GCN2	General control non-depressible protein-2
GDP	Guanosine diphosphate
G/M or GM	Glutamate and malate
HDAC	Histone deacetylase

HeLa	Henrietta Lacks immortalized cell line
HEP	Humane endpoint
H_2O_2	Hydrogen peroxide
Hom	Muscle tissue homogenate
HR	Heart rate or hazard ratio
HRI	Heme-regulated inhibitor
HSP10	Heat shock protein-10
HSP60	Heat shock protein-60
Hz	Hertz
ipITT	Intraperitoneal insulin tolerance test
IMF	Intermyofibrillar
IMM	Inner mitochondrial membrane
IMPC	International Mouse Phenotype Consortium
IMS	Intermembrane space
ISR	Integrated stress response
IVF	*in vitro* fertilization
LC-MS/MS	Liquid chromatography with tandem mass spectrometry
LFQ	Label-free quantification
LiCl	Lithium chloride
LONP1	LON protease-1
m-AAA	Matrix ATPases associated with diverse activities
MITRAC	Mitochondrial translation regulation assembly intermediate of CIV
mPTP	Mitochondrial permeability transition pore
mRNA	Messenger RNA
MRP	Mitochondrial ribosomal protein
MRPL	Mitochondrial ribosomal protein of the large subunit
MRPS	Mitochondrial ribosomal protein of the small subunit

MTCO1	Mitochondria cytochrome *c* oxidase subunit-1
mtHSP70	Mitochondrial heat shock protein-70
mtLSU	Large subunit of the mitochondrial ribosome
mtSSU	Small subunit of the mitochondrial ribosome
mTOR	Mammalian target of rapamycin
NAD^+	Oxidized form of nicotinamide adenine dinucleotide
NADH	Reduced form of nicotinamide adenine dinucleotide
nDNA	Nuclear DNA
OGTT	Oral glucose tolerance test
OMA1	Overlapping proteolytic activity with m-AAA protease-1
OMM	Outer mitochondrial membrane
ORF	Open reading frame
OXA1L	Oxidase assembly-3-like insertase
OXPHOS	Oxidative phosphorylation
PGC-1α	Peroxisome proliferator-activated receptor *γ*-assisted activating factor 1-alpha
Pi	Inorganic phosphate
PIT1	Pituitary-specific positive transcription factor-1
RER	Respiratory exchange ratio
RM-ANOVA	Repeated measures ANOVA
RNA	Ribonucleic acid
RNAi	RNA interference
ROS	Reactive oxygen species
Rot	Rotenone
RPLP0	Ribosomal protein P0
rRNA	Ribosomal RNA
RT-qPCR	Quantitative reverse transcription polymerase chain reaction
S-DELE1	Short form of DELE1

SDHB	Succinate dehydrogenase complex iron sulphur subunit-B
SEM	Standard error of the mean
SIRT1	Silent information regulator-1
SSBP	Single-stranded binding protein
Succ	Succinate
SURF1-KO	Surfeit locus protein-1 knock out
TCA	Tricarboxylic acid cycle
TEM	Transmission electron microscopy
TFAM	Mitochondrial transcription factor A
TMPD	Tetramethyl-p-phenylenediamine dihydrochloride
TNFα	Tumor necrosis factor-alpha
TOM	Translocase of the outer membrane
tRNA	Transfer RNA
UQCRC2	Ubiquinol-cytochrome *c* reductase core protein-2
UPR^{mt}	Mitochondrial unfolded protein response
VCO_2	CO_2 volume
VO_2	O_2 volume
WHO	World Health Organization
WT	Wildtype

11. Declaration of Academic Achievement

Contributions:

- Kimberly J. Reid, MSc – Study design, method development, mouse breeding, mouse colony monitoring and maintenance, monthly/weekly/daily body weighing, necropsy, tissue harvesting, cardiac puncture, genotyping, *in vivo* metabolic tests at ages 6-, 18-, and 24-months (EchoMRI, CLAMS, ipITT, OGTT, cold tolerance, treadmill endurance, HR & BP monitoring), mitochondrial respiration polarography, sample preparation for TEM, TEM, myocyte primary culture, western blotting, sample preparation for LC-MS/MS, data management, data analysis (except for LC-MS/MS), and manuscript writing and submission.
- Keir J. Menzies, PhD – Study design, method development, financial support, tissue harvesting, manuscript writing and review
- Riekelt H. Houtkooper, PhD – Study conception, study design, method development, financial support, and manuscript review
- Emily Standen, PhD – Financial support and manuscript review
- Eileen G. Daniels, MSc – Study design, method development, *in vivo* metabolic tests at ages 6-and 24-months, and manuscript review
- Goutham Vasam, PhD – LC-MS/MS data analysis and tissue harvesting
- Alexander E. Green, PhD – Tissue harvesting and manuscript review
- Fahmida Jahan, MSc – Tissue harvesting
- Rashmi Kamble, MSc – RT-qPCR
- Tarek Ammar, PhD – *Ex vivo* muscle contraction
- Abolfazl Nik-Akhtar, BSc – RT-qPCR
- Adriana Gambarotta, MSc – IVF
- Sara Kealey, BSc – Grip strength
- Harry Coenraad (CHEO Electron Microscopy) – Staining and Ultra Microtome preparation of TEM tissue section grids
- NorthOmics, Ottawa – Mass spectrophotometry proteomics (LC-MS/MS)
- Institute Clinique de la Souris, France – Establishment of *Mrpl54* mouse mutant line

12. Academic Contributions

12.1 Published/Submitted Manuscripts

1. **Reid, K.**, Daniels, E. G., Vasam, G., Kamble, R., Janssens, G. E., Hu, I. M., Green, A. E., Houtkooper, R. H., & Menzies, K. J. (2023). Reducing mitochondrial ribosomal gene expression does not alter metabolic health or lifespan in mice. *Scientific reports*, *13*(1), 8391. https://doi.org/10.1038/s41598-023-35196-3
2. Zeidler, J. D., Chini, C. C. S., Kanamori, K. S., Kashyap, S., Espindola-Netto, J. M., Thompson, K., Warner, G., Cabral, F. S., Peclat, T. R., Gomez, L. S., Lopez, S. A., Wandersee, M. K., Schoon, R. A., **Reid, K.**, Menzies, K., Beckedorff, F., Reid, J. M., Brachs, S., Meyer, R. G., Meyer-Ficca, M. L., … Chini, E. N. (2022). Endogenous metabolism in endothelial and immune cells generates most of the tissue vitamin B3 (nicotinamide). *iScience*, *25*(11), 105431. https://doi.org/10.1016/j.isci.2022.105431
3. Vasam, G., **Reid, K.**, Burelle, Y., & Menzies, K. J. (2019). Nutritional Regulation of Mitochondrial Function. *Mitochondria in Obesity and Type 2 Diabetes: Comprehensive Review on Mitochondrial Functioning and Involvement in Metabolic Diseases*, 93–126. https://doi.org/10.1016/B978-0-12-811752-1.00004-3
4. Tammaro, A., Daniels, E. G., Hu, I. M., 't Hart, K. C., **Reid, K.**, Juni, R. P., Butter, L. M., Vasam, G., Kamble, R., Jongejan, A., Aviv, R. I., Roelofs, J. J. T. H., Aronica, E., Boon, R. A., Menzies, K. J., Houtkooper, R. H., & Janssens, G. E. (2023). HDAC1/2 inhibitor therapy improves multiple organ systems in aged mice. *iScience*, *27*(1), 108681. https://doi.org/10.1016/j.isci.2023.108681

13. Introduction

13.1 Literature Review

13.1.1 Countering Aging by Mitigating the Loss of Intrinsic Capacity

A child born before 1840 had an average life expectancy of less than 40 years (Human Mortality Database, 2023; Vachon & Sestier, 2013). Since then, life expectancy has increased by ~2.5 years per decade in wealthy countries (Vaupel et al., 2021). In Canada, an individual born in 2020 is expected to live 81.72 years (Statistics Canada, 2022). This increase in life expectancy is attributed to extrinsic factors – reduced impact of infectious diseases with immunization, antibiotics, and improved medical care, as well as improved nutrition and living conditions with access to clean water, hygiene, and sanitation (Mathers et al., 2015). Today, the oldest humans have the highest proportion of ill health primarily due to chronic age-related diseases and conditions such as type 2 diabetes, heart disease, dementia, and osteoarthritis (Beard et al., 2016) with all the concomitant economic and social burdens that accompany this trend (World Health Organization, 2022). As declared by the *World Health Organisation (WHO) 2016 Policy Framework Report on Aging and Health*, there is a pressing need to keep people healthy for longer and reverse the expanding period of morbidity that accompanies an increasing life span – in other words, to compress morbidity to the very end of life (Beard et al., 2016).

The WHO intrinsic capacity paradigm of aging includes the physiological capacity of an individual to resist health deterioration (Beard et al., 2019; Kemoun et al., 2022). The ability to adapt to stressors is termed resilience and age-related susceptibility to chronic disease and conditions is thought to result from the loss of resilience (Kirkland et al., 2016). Provided an individual has the functional reserves to adapt to or overcome a stressor, they are considered robust

and can maintain proper function (Kemoun et al., 2022). Homeostasis is associated with robustness (i.e., biological function is actively maintained despite perturbations), where energy balance and critical life-maintaining structural and functional relationships and networks at the subcellular level are optimized for survival (Kitano et al., 2004; Ramsay & Woods, 2014). In contrast, allostasis (achieving stability through change) refers to a sub-optimal response, where the optimal balance-point is altered in response to chronic challenges and comes at a cost to the organism (i.e., allostatic load) (Ramsay & Woods, 2014).

Model eukaryotic organisms like *Caenorhabditis elegans* (roundworm), *Drosophila melanogaster* (fruit fly), and *Mus musculus* (house mouse) have shown that lifespans can be modulated by extrinsic and intrinsic factors. For example, dietary restriction and reduced insulin signaling will extend lifespan in all three model organisms (Holzenberger et al., 2002; Mair et al., 2003; Murphy et al., 2003). These lifespan modulating factors appear to converge on shared molecular mechanisms that mitigate the accumulation of damaged organelles or macromolecules within the cell, helping to maintain cellular homeostasis in the face of chronic challenges (Tomtheelnganbee et al., 2022). The age-associated decline of these molecular mechanisms (and thereby the decline in cellular homeostasis) leads to aging phenotypes including chronic disease (e.g., type 2 diabetes), cognitive decline (e.g., Alzheimer's Disease), and physical decline (e.g., sarcopenia, also known as age-related loss of muscle mass) (Campbell & Drucker, 2015; Cruz-Jentoft et al., 2019; Tan et al., 2020; Tiernan et al., 2016) .

A critical element underlying cellular homeostasis is energy redox balance, where an organism obtains energy through the process of oxidizing electron donors (i.e., stripping electrons from metabolized dietary sugars and fats) via net energy-releasing reactions. The released energy is stored in a chemical form (e.g., adenosine triphosphate or ATP) (Martin et al., 2020). Energy

management is critical to survival, even at a cost to the organism (Kemoun et al., 2022). This is illustrated with prolonged starvation where energy levels are maintained at the cost of stored protein (Kerndt et al., 1982). In the same context, sarcopenia can be viewed as the body's attempt to maintain energy allostasis (a new balance point) with age, but at a cost to muscle strength and function (Kemoun et al., 2022).

A cellular homeostasis mechanism that is prone to age-related decline is mitochondrial proteostasis (mitoproteostasis). Mitoproteostasis is the maintenance of protein levels and protein function within mitochondria, an organelle that produces ATP, the energy currency of the cell, and is responsible for cellular energy transduction (López-Otín et al., 2023). Mitoproteostasis is a dynamic and complex network of nuclear, cytosolic, and mitochondrial processes that control protein production. Production of mitochondrial proteins (i.e., the mitoproteome) includes protein translation (i.e., protein generation from mRNA), maturation, trafficking, targeting, and degradation. Mitochondrial protein quality control involves chaperones that properly fold proteins, re-fold misfolded proteins, or shuttle dysfunctional proteins to proteasomes and lysosomes for targeted degradation. A properly functioning mitoproteostasis network buffers protein levels and protein function against perturbations and external assaults. A healthy (young) mitochondrion maintains its function because it has a mitoproteostasis network that successfully responds to external stressors and maintains the mitoproteome.

A pool of healthy mitochondria is essential for cellular, tissue, and organismal health since the mitochondrion is central to energy metabolism. With age, mitochondrial proteins are damaged through dysregulation of redox homeostasis (i.e., imbalance between oxidation and reduction reactions) leading to an increase in reactive oxygen species (ROS), which directly damage macromolecules in the mitochondria such as lipids, proteins, and mitochondrial DNA (mtDNA).

The results are misfolded proteins, a perturbed mitoproteome, decreased ATP production, and a further increase in ROS production (Moehle et al., 2019). Since mitochondria rely on proteins translated from both the nuclear and mitochondrial genomes, intracellular retrograde communication (i.e., mitochondria to nucleus communication) of stress signals is integral to mitochondrial functioning and, with age, retrograde communication is altered (Fang et al., 2016).

Counterintuitively, mitochondria health can be maintained with age in several animal models with the early introduction of mild stress. This stress evokes retrograde signalling from the mitochondria to the nucleus and cytosol and results in system-wide positive effects (Cox et al., 2018; Houtkooper et al., 2013; Kang et al., 2021; Owusu-Ansah et al., 2013; A. Tapia et al., 2021). The process leading to beneficial health effects is called mitochondrial hormesis (mitohormesis) where a mild stressor within the mitochondria results in a beneficial long term systemic response, such as increased lifespan or health span (the period of an organism's lifespan that is free of age-related disorders) (P. C. Tapia, 2006; Yun & Finkel, 2014). An example of mitohormesis at the organismal level are regular bouts of exercise, which will transiently increase ROS production in skeletal muscle mitochondria (Webb et al., 2017). Exercise-induced ROS from the mitochondria signals the muscle cell to undergo mitochondrial biogenesis (mitobiogenesis – involving new protein synthesis and increasing the number of mitochondria) and to increase fusion to form mitochondria networks, all of which increase cellular ATP-generating efficiency and capacity (Kasai et al., 2020). While the initial exercise-induced ROS signal originates in skeletal muscle, the beneficial effects are transmitted throughout the body and, in the long term, will increase human health span (Musci et al., 2019). For example, exercise stimulates the production and release of myokines (peptides produced by muscle fibers that have autocrine, paracrine and/or

endocrine effects (L. Zhang et al., 2022)), such as fibroblast growth factor-21 (FGF21) and musclin with potentially cardioprotective effects (Harris et al., 2023; Jin et al., 2022).

An example of mitohormesis at the subcellular level, is the early introduction of mild mitochondrial translation stress. This is accomplished by mildly challenging the mitochondrial ribosome (mitoribosome), which is responsible for translating mtDNA-encoded mRNA transcripts into proteins essential to ATP production. In *C. elegans,* successful examples of mitohormesis through mitoribosomal challenge include treatment with doxycycline and reduction in the expression levels of mitochondrial ribosomal proteins (MRPs) (Houtkooper et al., 2013; Perry et al., 2021). A third mitohormetic that challenges the mitoribosome is the genetic knock-down of *tars-1* (gene encoding mitochondrial tRNA synthetase for threonine) (M. Guo et al., 2023). Doxycycline is an antibiotic that will knock out bacterial ribosome function. It will also reduce the efficiency of the eukaryotic mitoribosome because it shares a common ancestor with the prokaryotic bacterial ribosome (Perry et al., 2021; Seely & Gagnon, 2022). In *C. elegans*, doxycycline treatment, MRP reduction, and *tars-1* knock-down result in an imbalance in the ratio of mtDNA-encoded versus nuclear (nDNA)-encoded proteins (mitonuclear protein imbalance), followed by a reduction in ATP production (M. Guo et al., 2023; Houtkooper et al., 2013; Tsang et al., 2001). Subsequent invocation of the mitochondrial unfolded protein response (UPR^{mt} - a stress response to resolve the mitonuclear protein imbalance) leads to an increase in *C. elegans* health span and lifespan (M. Guo et al., 2023; Houtkooper et al., 2013).

Ultimately, aging biological processes and an age-related shift toward allostasis (new set-points with costs to the organism) are thought to be main drivers of the susceptibility to chronic disease. Mitochondrial degradation is implicated in the aging process; therefore, targeting age-related degradation of mitoproteostasis and mitochondrial function through mitohormesis is

proposed to slow the onset and progression of aging and age-related diseases (Kennedy et al., 2014; López-Otín et al., 2013, 2023; Zimmermann et al., 2021). In the next sections, maintaining mitoproteostasis with age will be explored through the following topics:

- Origin and structure of mitochondria, and signalling the energy status of the cell,
- Mitoribosome assembly, mtDNA-encoded protein translation, and the disruption of translation leading to mitohormesis,
- Coordination of mitochondrial and cytosolic translation and the generation of a mitonuclear protein imbalance,
- Stress responses to mitonuclear protein imbalance,
- Role of UPR^{mt} in aging and age-related diseases, and
- Mitohormesis as a mitigating strategy to maintain mitoproteostasis with age.

13.1.2 About the Mitochondria

Mitochondria are cellular organelles with a unique origin. Approximately 2.1 to 1.2 billion years ago, a prokaryotic archaeon cell engulfed an alpha-proteobacterium (Betts et al., 2018), likely through microbial metabolic symbiosis (i.e., physiological interactions) (Bremer et al., 2022). The bacterium stayed on to become present day mitochondria, or the derivative mitosomes and hydrogenosomes (Roger et al., 2017). A symbiotic relationship arose where the archaeon host provided resources to its tenant bacteria, which then shared the ATP they produced with its host. For the first time in evolutionary history, an organism generated and transduced its own energy from dedicated internal organelles, rather than relying on external sources (Lane & Martin, 2010). Critically, this singular symbiotic event gave rise to all eukaryotic organisms and the increased availability of energy likely drove this advancement (Lane & Martin, 2010; Tria et al., 2021). Over time, most of the genes from the bacterium tenant were transferred to the nuclear genome, leaving

an organelle (now called the mitochondrion) wholly dependent on its host and vice versa (Janouškovec et al., 2017; Sloan et al., 2018).

A few critical genes remain within the mitochondrial genome, all necessary to produce ATP via oxidative phosphorylation – where oxygen is reduced to water, generating high energy ATP in the process (Daley & Whelan, 2005; Sloan et al., 2018). Today, the mitochondrion is a double-membrane organelle with the following structures (Fig. 13.1) (Sherratt, 1991):

- An inner alkaline matrix that houses the processes that breakdown dietary-sourced fuels and release electrons (i.e., tricarboxylic acid (TCA) cycle and β-oxidation),
- A highly selectively permeable inner mitochondrial membrane (IMM) with convoluted invaginations (cristae). The IMM maintains an electrochemical potential and houses ATP synthase and the electron transport chain complexes essential for oxidative phosphorylation,
- A relatively permeable outer mitochondrial membrane (OMM), and
- An acidic intermembrane space (IMS) between the outer and inner membranes.

To generate energy, the cell breaks down mainly dietary sources of protein, glucose, and fat into amino acids, pyruvate, and fatty acids and delivers them to the mitochondria. Inside the matrix, pyruvate and fatty acids are broken down by the TCA cycle and β-oxidation, respectively, to provide electrons and protons via the redox couple proteins NAD^+/NADH (nicotinamide adenine dinucleotide) and FADH/$FADH_2$ (flavin adenine dinucleotide). NAD^+ is reduced to NADH, which then carries its electrons and proton to the IMM-spanning Complex I (CI), aptly known as NADH-dehydrogenase. After NADH gives up its pair of electrons and proton, CI pumps four protons from the matrix into the IMS and transfers its electrons via the IMM-bound mobile electron carrier

ubiquinone/ubiquinol ($CoQ/CoQH_2$) to Complex III (CIII – cytochrome *c* oxidoreductase), regenerating/oxidizing NAD^+ in the process. After FADH is reduced to $FADH_2$, Complex II (succinate dehydrogenase) receives one pair of electrons from $FADH_2$ and transfers them to CIII via $CoQ/CoQH_2$, regenerating/oxidizing FADH in the process. Unlike CI, CII does not span the inner membrane and does not contribute protons to the IMS. Once CIII receives electrons from CI and CII, it pumps four protons into the IMS and transfers its electrons to Complex IV (CIV – cytochrome *c* oxidase) via the mobile electron carrier cytochrome *c* (Cyt *c*). Subsequently, CIV pumps two protons into the IMS. The electrons that arrive at CIV are destined for their final acceptor, which is oxygen (O_2) in mammals and, after accepting the electrons from CIV, will form water.

All together, the complexes CI, CII, $CoQ/CoQH_2$, CIII, Cyt *c* and CIV are called the electron transport chain (ETC). According to the Chemiosmotic Theory, the main purpose of the ETC is to generate a high concentration (i.e., pressure) of protons within the IMS relative to the matrix, creating an electrochemical gradient (aka electrochemical proton potential) (Mitchell, 1961, 1970). The pressure of protons within the IMS is analogous to a dam that uses water pressure to drive an electricity-generating mechanical turbine. In mitochondria, the turbine is IMM-spanning ATP-synthase (aka Complex V or CV), which allows protons to flow back into the matrix from the IMS, creating the membrane electrochemical potential. With every four protons that return to the matrix, ATP-synthase turns and generates ATP from adenosine diphosphate (ADP) and inorganic phosphate (Pi). The combined ETC and ATP-synthase process is called oxidative phosphorylation (OXPHOS) – oxidative because the ETC complexes strip electrons from NADH and $FADH_2$, ultimately transferring them to an acceptor (like O_2); phosphorylation because ADP

is phosphorylated to produce ATP, which is then used to transport and generate energy throughout the cell (Sherratt, 1991).

It is important to note here that the OXPHOS process constitutively leads to the generation of reactive oxygen species (ROS), particularly from CI and CIII (Brand, 2016; Kudin et al., 2004). Specifically, electrons escape the ETC at CI and CIII and react with O_2 to form superoxide ion ($O_2^{\cdot-}$), which is converted to hydrogen peroxide (H_2O_2) by superoxide dismutases (SODs) in the matrix and IMS (Okado-Matsumoto & Fridovich, 2001). H_2O_2 is an important mitochondrial ROS second messenger signal that readily diffuses through the IMM and OMM into the cytosol. Low levels (~1-10 nM) of cytosolic H_2O_2 affect cellular metabolism and physiology (Sies, 2017). Disruption of OXPHOS (e.g., through the disruption of the membrane electric potential), will increase ROS production at CI and CIII and signal a stress response to either recover mitochondrial function (an adaptive response) or induce mitophagy (where dysfunctional mitochondria are targeted for degradation and removal) (Sies, 2017). ROS is an important signal from the mitochondria to the nucleus and cytosol, signalling the functional status of both ETC components and the membrane potential. And so, the structures that contribute to ATP generation within the mitochondria are also involved in signaling the energy transduction status and health of the mitochondria.

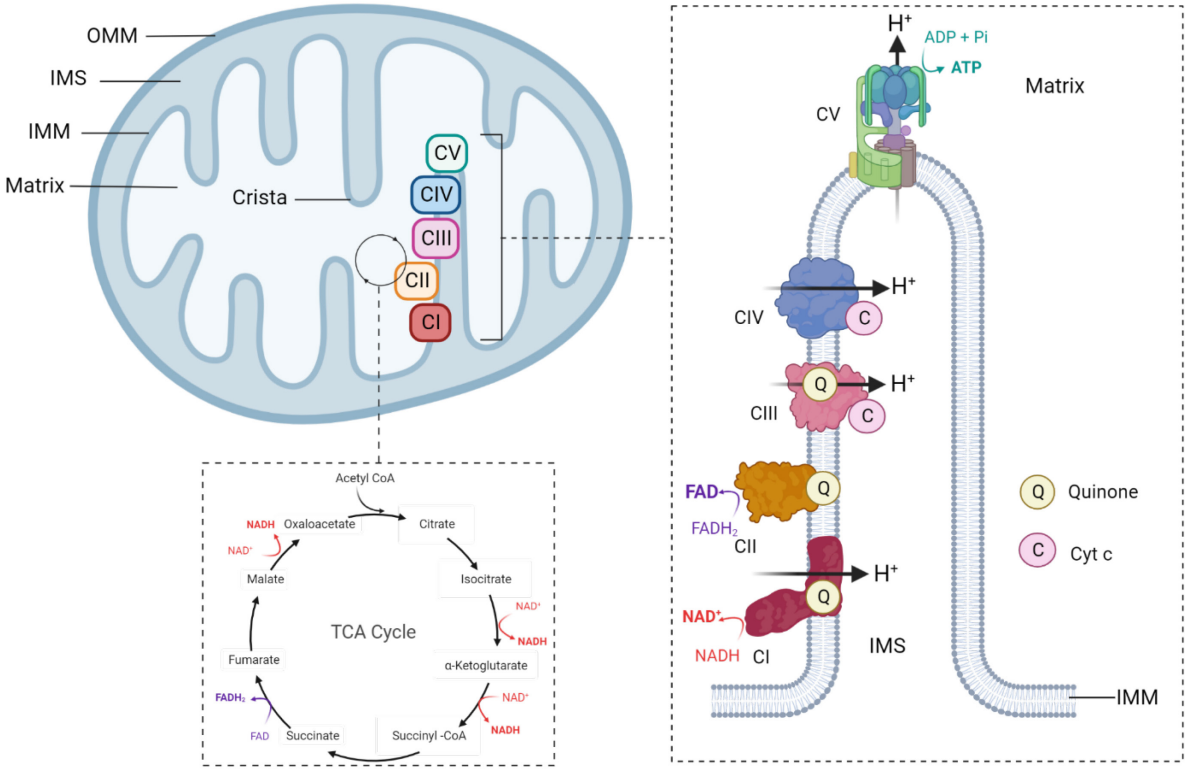

Figure 13.1 Structures of the mitochondrion.

ADP/ATP – adenosine diphosphate/triphosphate; CI – Complex I (NADH-dehydrogenase); CII – Complex II (succinate dehydrogenase); CIII – Complex III (cytochrome c oxidoreductase); CIV – Complex CIV (cytochrome c oxidase); CV – Complex V (ATP synthase); FADH/FADH2 – oxidized and reduced forms of flavin adenine dinucleotide); H+ – protons ; IMS – intermembrane space; IMM – inner mitochondrial membrane; NAD+/NADH – oxidized and reduced forms of nicotinamide adenine dinucleotide; OMM – outer mitochondrial membrane; Pi – inorganic phosphate; TCA – tricarboxylic acid cycle. Created with BioRender.com.

13.1.3 Health Benefits from the Disruption of Mitochondrial Translation

The mammalian mitochondrial ribosome (mitoribosome) has the essential function of translating 11 mtDNA-encoded mRNA transcripts into 13 hydrophobic OXPHOS proteins. These mtDNA-encoded OXPHOS proteins are critical to mitochondrial ATP production. To introduce mild mitochondrial translation stress and induce mitohormesis (i.e., lifespan and health span extension) within *C. elegans*, Houtkooper et al. (2013) used RNA-interference (RNAi) methodology to reduce the expression of mitochondrial ribosomal proteins (MRPs) (Conte et al., 2015; Houtkooper et al., 2013). This section explores the structure, assembly process, and function of the mammalian mitoribosome to better understand how mild disruption of individual MRPs could lead to mitohormesis in mammals.

The mitoribosome consists of a large and small subunit, both made of nDNA-encoded MRPs and mtDNA-encoded mitoribosomal RNAs (mito-rRNAs). Mitoribosomes are relatively low in abundance (~34,000 mitoribosomes vs. 6,000,000 cytoplasmic ribosomes in a HeLa cell (Bogenhagen et al., 2014)) and reside in the matrix tethered to the IMM such that the polypeptide exit tunnel is aligned with oxidase assembly-1-like insertase (OXA1L) (Fig. 13.2). With cardiolipin (a negatively charged lipid abundant in the IMM), OXA1L aids the insertion of newly translated OXPHOS proteins into the IMM (Greber et al., 2014; Itoh et al., 2021; R. G. Lee et al., 2020; Liu & Spremulli, 2000).

In mammals, mitoribosome assembly begins within nucleoids, which are nucleus-like regions in the matrix that contain one or more copies of circular mtDNA folded with mitochondrial transcription factor-A (TFAM) and single-stranded binding protein (SSBP) (Bogenhagen et al., 2014) (Box 13.1; Fig. 13.3). Mitoribosome assembly moves to RNA granules, which are processing bodies peripheral to the nucleoids where mito-rRNAs are matured (Antonicka &

Shoubridge, 2015). Since mitoribosome assembly begins in nucleoids and RNA granules, mtDNA replication and transcription are linked with mRNA processing and protein translation (Bogenhagen et al., 2014; De Silva et al., 2015) (Fig. 13.2). Furthermore, nucleoids in the matrix are found indirectly connected to the cytoskeleton via the IMM and OMM, and RNA granules co-localize with protein import machinery (like the translocase in the outer membrane [TOM] complex) (Iborra et al., 2004). The physical connections between nucleoids and the cytoskeleton and between RNA granules and TOM suggest that mitochondrial and cytoplasmic translation complexes are efficiently coordinated (De Silva et al., 2015). Since OXPHOS complexes require both nDNA- and mtDNA-encoded proteins, efficient coordination between cytoplasmic and mitochondrial translation machinery is essential to maintain a mitonuclear protein balance.

The 82 nDNA-encoded MRPs (30 small subunit and 52 large subunit MRPs) that make up the mammalian mitoribosome are imported into the matrix in considerable excess (Bogenhagen et al., 2018; Bogenhagen & Haley, 2020). Mitoribosome assembly takes 2-3 hours after which excess MRPs are degraded to avoid accumulation (Bogenhagen et al., 2018). Over synthesis of MRPs is possibly to ensure an adequate supply for mitoribosome assembly, especially during sustained growth and high turnover rates. Near the mtDNA-containing nucleoids where mitoribosome biogenesis begins, there appears to be a larger steady-state pool of small subunit MRPs (MRPSs) compared to large subunit MRPs (MRPLs). This relative MRPL excess may reflect a higher MRPL turnover rate (i.e., MRPL proteins spend less time assembling) (Bogenhagen et al., 2014). Excess MRPs in general may be required for slow or sterically restricted assembly stages. For example, early-stage processing of mito-rRNAs in RNA granules is a time-consuming process and possibly rate-limiting for mitoribosome assembly (Bogenhagen et al., 2014).

As mentioned, early introduction of mild stress through the disruption of mitoribosomal function has the mitohormetic effect of increasing health span and lifespan in *C. elegans* (M. Guo et al., 2023; Houtkooper et al., 2013). Houtkooper *et al.* (2013) introduced RNAi to the roundworm prior to the onset of adulthood (i.e., before larval 4 [L4] stage) to reduce *Mrp* expression. In brief, *C. elegans* were fed RNAi-expressing *Escherichia coli*, which specifically reduced the expression of individual MRPSs (MRPS5, MRPS27, or MRPS30) or MRPLs (MRPL1, MRPL2, MRPL15, MRPL23, MRPL37, MRPL47, or MRPL54) in worm tissues by ~50% (Fig. 13.3). All MRP reduction experiments demonstrated a mitonuclear protein imbalance where the disruption of mitochondrial translation resulted in fewer mtDNA-encoded relative to nDNA-encode proteins. The mitonuclear protein imbalance activated the nematode mitochondrial unfolded protein response (UPR^{mt}) and increased lifespan compared to empty vector controls (lifespan extension ranged from +37.2% for *Mrpl54* RNAi to +124% for *Mrpl15* RNAi) (Houtkooper et al., 2013).

The authors propose that a mitonuclear protein imbalance is a conserved longevity mechanism because it is a common feature linking other *C. elegans* longevity pathways. These other pathways include treatment with antibiotics like doxycycline or chloramphenicol (i.e., inhibition of mitochondrial translation), as well as treatment with rapamycin or resveratrol. Both rapamycin and resveratrol treatment extend lifespan in multiple animal models (Hector et al., 2012; Weichhart, 2018) and result in a mitonuclear protein imbalance in *C. elegans* through the reduction in nDNA-encoded relative to mtDNA-encoded proteins (Houtkooper et al., 2013). The reduction of nDNA-encoded proteins by rapamycin may be due to the activation of general control non-depressible-2 (GCN2) kinase (Kubota et al., 2003). Activated GCN2 phosphorylates eIF2α (cytosolic eukaryotic translation initiation factor-2 alpha subunit) and inhibits global cytosolic translation, reducing the number of nDNA-encoded proteins relative to mtDNA-encoded proteins.

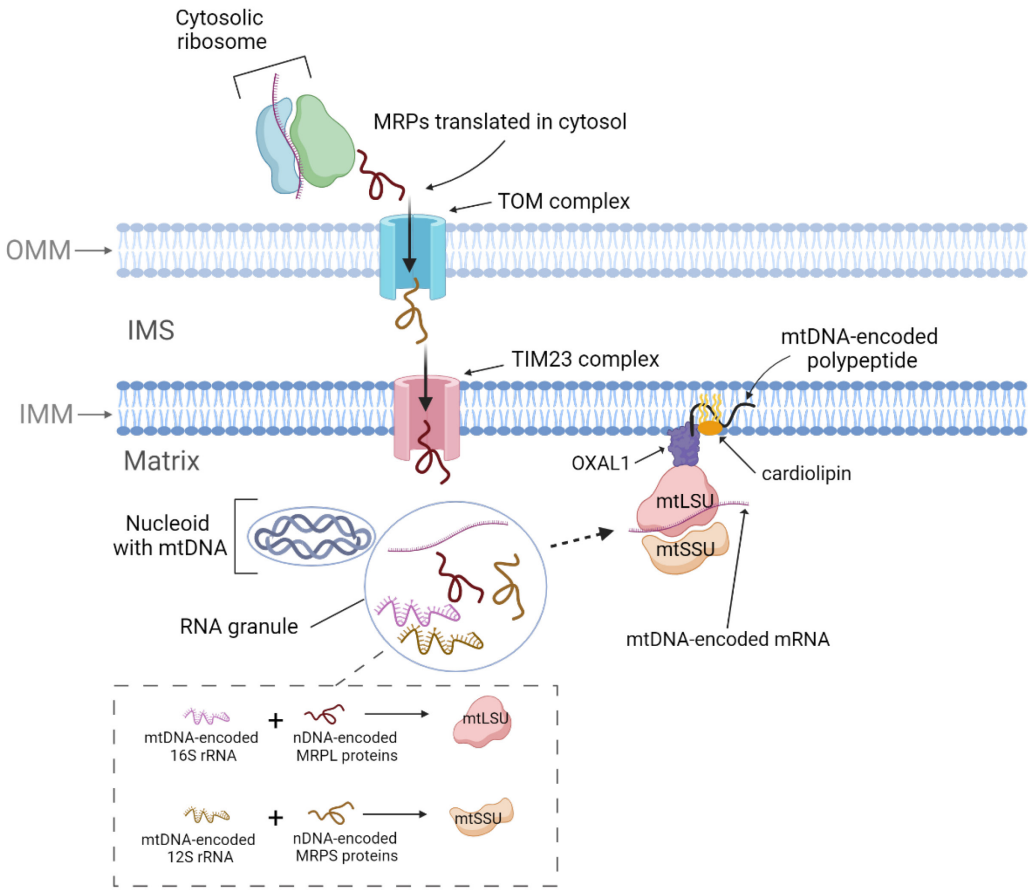

Figure 13.2 Overview of the mitoribosome.

IMM – inner mitochondrial membrane; IMS – intermembrane space; MRP – mitochondrial ribosomal protein; MRPL – large subunit mitochondrial ribosomal protein; MRPS – small subunit mitochondrial ribosomal protein; mtDNA – mitochondrial DNA; mtLSU – large subunit of the mitochondrial ribosome; mtSSU – small subunit of the mitochondrial ribosome; nDNA – nuclear DNA; OMM – outer mitochondrial membrane; OXA1L – oxidase assembly-1-like insertase; TOM – translocase of the outer membrane; TIM23 – translocase of the inner membrane-23. Created with BioRender.com

BOX 13.1 Mitoribosome assembly

The mammalian mitoribosome sediments as a 55S particle consisting of a 39S large subunit (mtLSU) and 28S small subunit (mtSSU). The mtLSU consists of 16S rRNA, $tRNA^{Val}$, and 52 mtLSU mitochondrial ribosomal proteins (MRPLs). The mtSSU consists of 12S rRNA and 30 mtSSU MRPs (MRPSs). All 82 MRPs and their assembly factors (AF) are encoded by the nuclear genome and translated in the cytosol, close to import machinery that transport them to the matrix (Fig. 13.2). Both the mtLSU and mtSSU are assembled in stages (Amunts et al., 2015; Bogenhagen et al., 2014), where the latter stages are dependent on prior assembly intermediates; however, mtLSU and mtSSU complexes can arise from parallel assembly pathways (Bogenhagen et al., 2018; Khawaja et al., 2023). The mtSSU has two main assembly stages – early and late (Fig. 13.3). Early mtSSU assembly begins with 12S rRNA and the binding of 18 MRPSs, including MRPS5, which bridges 12S rRNA to early-stage MRPs, and was reduced to induce mitohormesis in Houtkooper et al. (2013) (Amunts et al., 2015; Houtkooper et al., 2013; Lopez Sanchez et al., 2021). Recruitment of the remaining 12 late-stage MRPSs enable the interface between the mtLSU and mtSSU.

Assembly of the mtLSU has three stages: early, intermediate, and late (Fig. 13.3). The mtLSU early stage begins with 16S rRNA and 23 MRPLs, including MRPL45, which tethers the mtLSU to the IMM. The polypeptide exit tunnel is formed during the intermediate stage with the addition of 12 MRPLs (Brown et al., 2014; Lopez Sanchez et al., 2021). Late-stage mtLSU assembly involves the remaining 17 MRPLs to complete the interface with the mtSSU, including MRPL54, which interacts with intermediate-stage MRPL11 and is critical to stabilizing the L7/L12 stalk, which functions to promote recruitment of AFs (Aibara et al., 2020; Diaconu et al., 2005; Tobiasson et al., 2021).

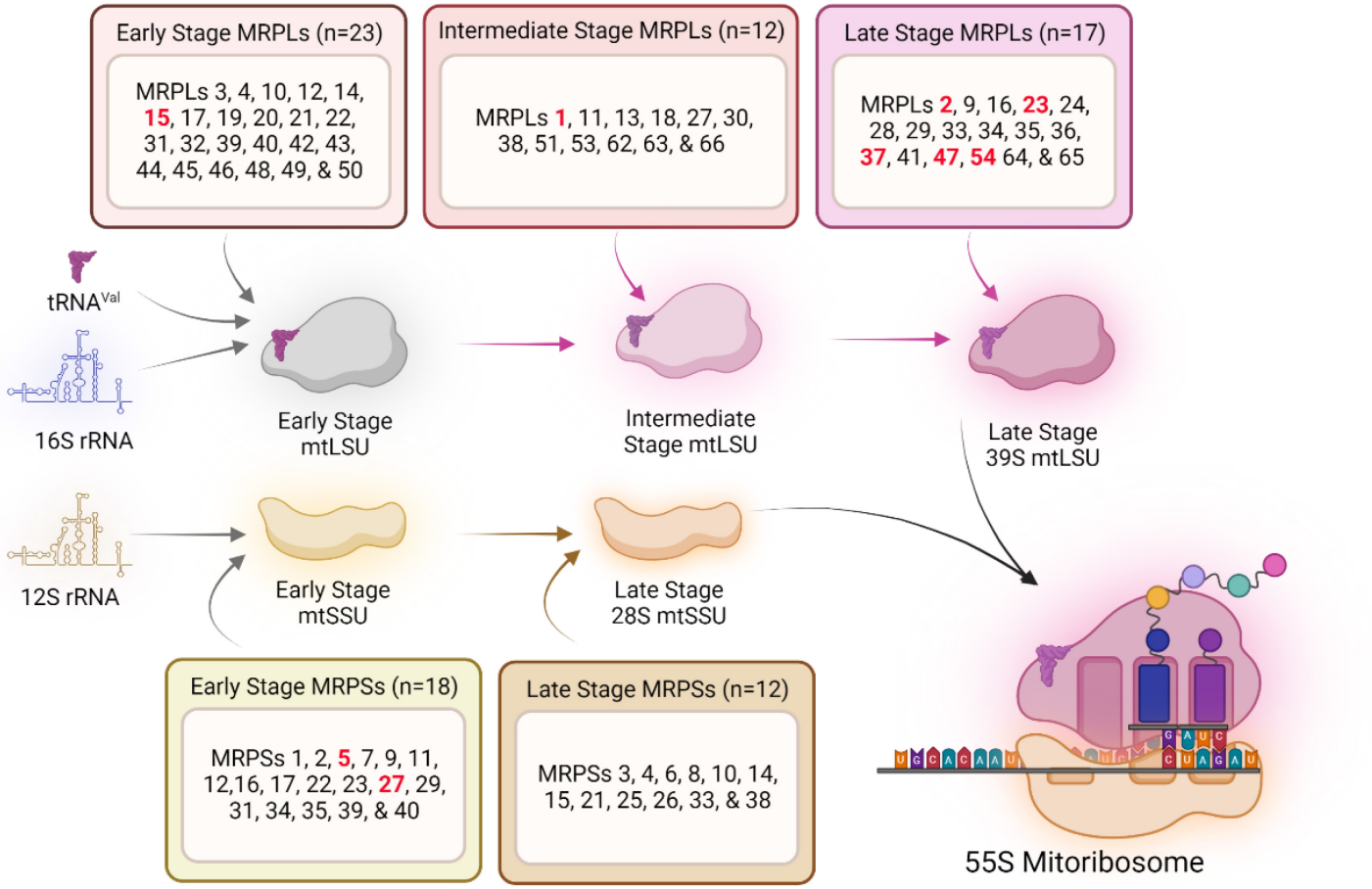

Figure 13.3 55S mitoribosome assembly.

Bold MRPs in red are the proteins that were reduced by ~50% in a *C. elegans* longevity model to generate a mitonuclear protein imbalance, UPR^{mt} response, and lifespan extension (Houtkooper et al., 2013). MRP – mitochondrial ribosomal protein; MRPL – large subunit mitochondrial ribosomal protein; MRPS – small subunit mitochondrial ribosomal protein; mtLSU – large subunit of the mitochondrial ribosome; mtSSU – small subunit of the mitochondrial ribosome; rRNA – ribosomal RNA; $tRNA^{Val}$ – transfer RNA for valine; UPR^{mt} – mitochondrial unfolded protein response. Created with BioRender.com

13.1.4 Generation of a Mitonuclear Protein Imbalance

Except for CII, which is entirely nDNA-encoded, the multimeric OXPHOS complexes (CI, CIII, CIV, and CV) require both nDNA- and mtDNA-encoded protein subunits. For example, mammalian CI has 45 structural protein subunits of which 38 are nDNA-encoded (Hirst et al., 2003) and 7 are mtDNA-encoded (Mercer et al., 2011). That subunit proteins are dual sourced indicates the construction of OXPHOS complexes requires responsive and synchronous coordination between cytosolic and mitochondrial translation machinery, to prevent the accumulation of unassembled subunits.

From yeast to mammals, nDNA-encoded OXPHOS assembly factors (AFs) regulate mitochondrial translation in response to the status of cytosolic translation, which is a form of unidirectional cytosol to mitochondria communication (Couvillion et al., 2016; Richter-Dennerlein et al., 2016). Specifically, OXPHOS AFs adjust mitochondrial translation in response to the availability of nDNA-encoded OXPHOS subunits. For example, when the cytosolic translation of human nDNA-encoded cytochrome *c* oxidase subunit-4 (COX4, or yeast nDNA-encoded COX14) is repressed, the mitoribosome pauses the translation of mtDNA-encoded COX1 (Richter-Dennerlein et al., 2016). Pausing the mitoribosome delays the assembly of CIV. In humans, this response is regulated by the AF called MITRAC (mitochondrial translation regulation assembly intermediate of cytochrome *c* oxidase complex), which maintains a partially-translated COX1 in an arrested primed state with the mitoribosome until COX4 is recruited from the cytosol. Therefore, cytosolic translation status is communicated through AF-mediated pausing of the mitoribosome. In this way, the rate of mitochondrial protein production and respiratory complex biogenesis can be directly adapted to meet cellular metabolic demand.

The opposite direction, where the status of mitochondrial translation directly regulates cytosolic translation (i.e., mitochondrial to cytosol communication), has yet to be demonstrated in mammals or yeast (Couvillion et al., 2016; Soto et al., 2022). Current evidence does not support direct communication from the mitoribosome to cytosolic ribosome in response to stalled production of mitochondrial protein subunits. The mammalian and yeast cytosolic translation maintains its pace regardless of the repression of mtDNA-encoded protein synthesis (Couvillion et al., 2016; Soto et al., 2022). However, there is evidence of indirect communication from mitochondria to cytosol translation machinery, where RNAi-mediated reduction of MRPS5 (small mitochondrial ribosomal subunit-5) in *C. elegans* and *in vivo* doxycycline treatment in mice impairs mitochondrial translation and subsequently decreases cytosolic translation (Molenaars et al., 2020). Specifically, mitoribosome disruption results in a cellular stress response (i.e., retrograde mitochondria to nuclear communication) that leads to a reduction in cytosolic translation. A mechanism underlying the reduction in cytosolic translation may involve a shift from polysomes (mRNA with ≥2 cytosolic ribosomes) to monosomes (mRNA associated with a single cytosolic ribosome) (for an example see integrated stress response in Fig. 13.4 (Molenaars et al., 2020)).

There is clear cross-species evidence of direct unidirectional communication between cytosolic and mitochondrial translation machinery, where the mitoribosome will pause and wait for incoming nDNA-encoded proteins to arrive before proceeding. The evidence is less clear for the opposite pathway (i.e., direct mitochondrial to cytosolic translational machinery communication). Importantly (and regardless of whether a compromised mitoribosome directly impacts cytosolic translation), a dysfunctional mitoribosome leads to cellular stress responses that

will attempt to resolve the mitonuclear protein imbalance (Houtkooper et al., 2013; Soto et al., 2022), and reduction of cytosolic translation is part of the stress response (Molenaars et al., 2020).

13.1.5 Mammalian Stress Responses to Mitochondrial Translation Dysfunction

In mammals, there are two known cellular stress responses to mitochondrial translation dysfunction (such as a stalled mitoribosome) - the integrated stress response (ISR) (Quirós et al., 2017) and the mitochondrial unfolded protein response (UPR^{mt}) (Zhao et al., 2002). The ISR is considered the primary response to mitochondrial stressors in mammals and hinges on the phosphorylation status of the cytosolic eukaryotic translation initiation factor-2 alpha subunit (eIF2α). Phosphorylation of eIF2α inhibits the initiation of cytosolic translation, reducing the general global production rate of protein. The ISR and the UPR^{mt} in mammals are strongly coupled in that they both respond to mitoproteostasis stress and the UPR^{mt} appears to be preceded and activated by the ISR (Forsström et al., 2019).

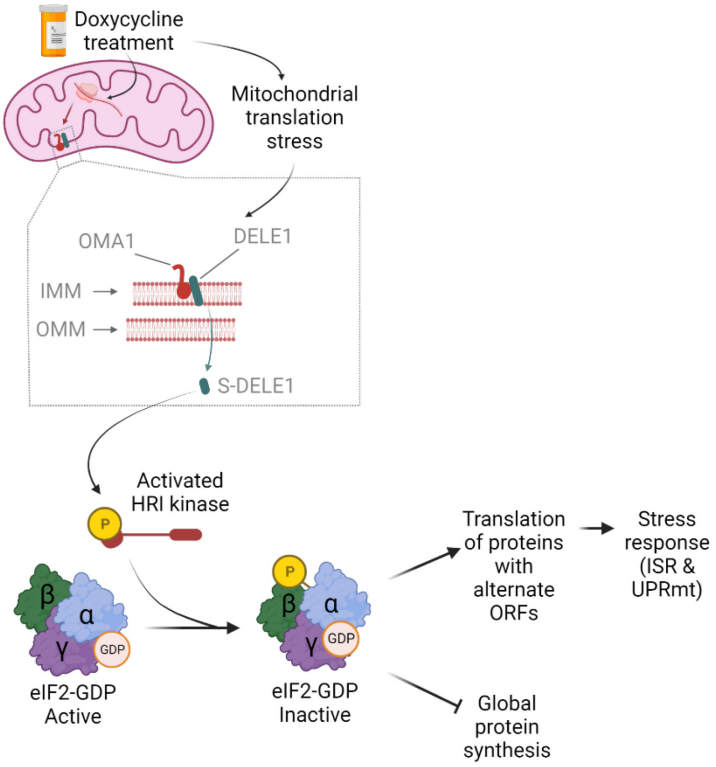

Figure 13.4 HRI-mediated activation of the ISR in response to mito-translation stress.

Doxycycline treatment induces mitoribosomal stress, which causes OMA1 to cleave DELE1, releasing its short form (S-DELE1) into the cytoplasm (X. Guo et al., 2020). S-DELE1 activates HRI, which then phosphorylates eIF2α. Phosphorylated eIF2α reduces global protein synthesis but allows the synthesis of proteins involved in the stress response pathways. DELE1 – DAP3-binding cell death enhancer-1; eIF2α – eukaryotic translation initiation factor-2 alpha subunit; GDP – guanosine diphosphate; HRI – heme-regulated inhibitor; IMM – inner mitochondrial membrane; ISR – integrated stress response; OMA1 – overlapping proteolytic activity with m-AAA protease-1; OMM – outer mitochondrial membrane; ORF – open reading frame; S-DELE1 – short form of DELE1; UPR^{mt} – mitochondrial unfolded protein response. Created with BioRender.com

In mammals, mitochondrial translation stress is known to invoke the ISR through the heme-regulated inhibitor (HRI – which is also canonically activated through cytosolic proteotoxicity) (Girardin et al., 2021; X. Guo et al., 2020; Mick et al., 2020) (Fig. 13.4). For example, in response to mitoribosome dysfunction through doxycycline treatment, the IMM-bound stress-activated metalloendopeptidase OMA1 (overlapping proteolytic activity with m-AAA protease-1) cleaves DELE1 (DAP3-binding cell death enhancer-1) into its short-form (S-DELE1). S-DELE1 is released from the IMM, moves to the cytosol, and then activates HRI kinase and the ISR (X. Guo et al., 2020) (Fig.13.4). Activated HRI kinase will phosphorylate eIF2α, which prevents the initiation of general global cytosolic translation, thereby reducing the load on protein chaperones (Chaveroux et al., 2011; Falcón et al., 2019). To propagate the ISR and subsequently the UPR^{mt}, the proteins involved in these two stress response pathways escape HRI-mediated translation inhibition. Specifically, stress response mRNAs have alternate open reading frames (ORFs) that allow translation to continue (i.e., aka privileged translation) even though global cytosolic translation is inhibited (Anderson & Haynes, 2020; Forsström et al., 2019; X. Guo et al., 2020)

Mitochondrial translation stress activation of the ISR (e.g., through HRI-mediated phosphorylation of eIF2α) upregulates activating transcription factor-4 (ATF4), which is the ISR master regulator in mammals. ATF4 upregulation results in the activation of multiple stress response genes and their protein products. These stress response proteins include ATF5 (the master regulator for the UPR^{mt}), CHOP (CCAAT/enhancer binding protein homology protein, which is thought to fine-tune the ISR and activate ATF5), and FGF21 (a myokine that may transmit the mammalian stress response to other tissues) (Forsström et al., 2019; Kaspar et al., 2021; Teske et al., 2013). Likewise in *C. elegans*, a disrupted mitoribosome (e.g., through decreased MRP production or doxycycline treatment) will result in a decrease in general cytosolic translation with

specific upregulation of Atf-5 (the *C. elegans* orthologue of mammalian ATF4) and Atfs-1 (the *C. elegans* orthologue of mammalian ATF5 and the master regulator of the nematode UPR^{mt}) (Molenaars et al., 2020).

The mammalian UPR^{mt} is a mitochondrial stress response axis that is downstream from the ISR (Zhao et al., 2002). It shares many of the features of the nematode UPR^{mt} (Al-Furoukh et al., 2015; Haynes et al., 2007) where both are critical mechanisms by which mitochondrial protein homeostasis (mitoproteostasis) is regained in response to mitochondrial stressors. The UPR^{mt} helps maintain stable protein levels by refolding misfolded proteins and resolving oxidative stress. Inducers of the mammalian UPR^{mt} include the following:

1) Compromised processes that are required to maintain mitonuclear protein balance (e.g., disrupted mitochondrial translation, mitochondrial protein importation, or respiratory complex assembly) (Melber & Haynes, 2018; Rolland et al., 2019),
2) Compromised processes or drugs that affect mitochondrial membrane potential but do not necessarily affect mitonuclear protein balance (e.g., knockdown of respiratory CII genes, compromised TCA cycle or lipid metabolism proteins, CI inhibitors like rotenone, or CIII inhibitors like antimycin) (Rolland et al., 2019), and
3) Oxidative stress (e.g., tumour necrosis factor alpha [TNFα]-induced ROS production, which transiently opens the mitochondrial permeability transition pore [mPTP] and reduces membrane potential) (Dasgupta et al., 2020).

Stress signals from within the mitochondrion signal a cascade of nuclear gene expression to mitigate or resolve the stressor (Fig. 13.5). In the absence of mitochondrial stress in mammals, ATF5 (the UPR^{mt} master regulator) moves from the cytosol into the mitochondria via the TOM complex using its relatively weak amphipathic amino-terminus sequence signal (Fig. 13.5A). Once

inside the mitochondrial matrix, ATF5 is degraded (Fiorese et al., 2016). However, when a mitochondrial stress signal is detected, (e.g., a reduced membrane potential that prevents the importation of mitochondrial proteins with a low net charge) (Nargund et al., 2012; Rolland et al., 2019), ATF5 accumulates in the cytosol and then moves to the nucleus where it induces the expression of proteins involved in the remodeling of chromatin (Merkwirth et al., 2016; Tian et al., 2016) and the refolding and degradation of misfolded protein. UPR^{mt} upregulated refolding proteins include the mitochondrial chaperones HSP60 (heat shock protein 60) and HSP10. Together, HSP60 and HSP10 form the HSP60/10 chaperonin complex - a football-shaped tetradecamer nanocage that functions to unfold then refold a misfolded protein (Gomez-Llorente et al., 2020; Sadat et al., 2022; Wälti et al., 2021) (Fig. 13.5B). In addition, mtHSP70 and the protein-degradation enzyme LON peptidase-1 (LONP1) are upregulated in response to ATF5 translocation to the nucleus (Fiorese et al., 2016). Under unstressed conditions, LONP1 is proposed to synergistically cooperate with mtHSP70 and works primarily as a housekeeping chaperone by helping to assemble OXPHOS complexes (Shin et al., 2021). However, in the presence of mitochondrial stress, LONP1 is phosphorylated, which increases its protease activity (Ghosh et al., 2019).

In summary, mammalian cells first respond to mitochondrial proteostasis stress through activation of the ISR, which functions to both reduce general cytosolic translation as well as activate the UPR^{mt}. The UPR^{mt} is initiated through the translocation of ATF5 into the nucleus, after which stress response genes are upregulated. The UPR^{mt} stress upregulated HSP60/10 chaperonin complex then attempts to rectify protein misfolding in the mitochondrial matrix. mtHSP70 and LONP1 are also upregulated upon UPR^{mt} activation, and they function to refold or degrade misfolded proteins, respectively.

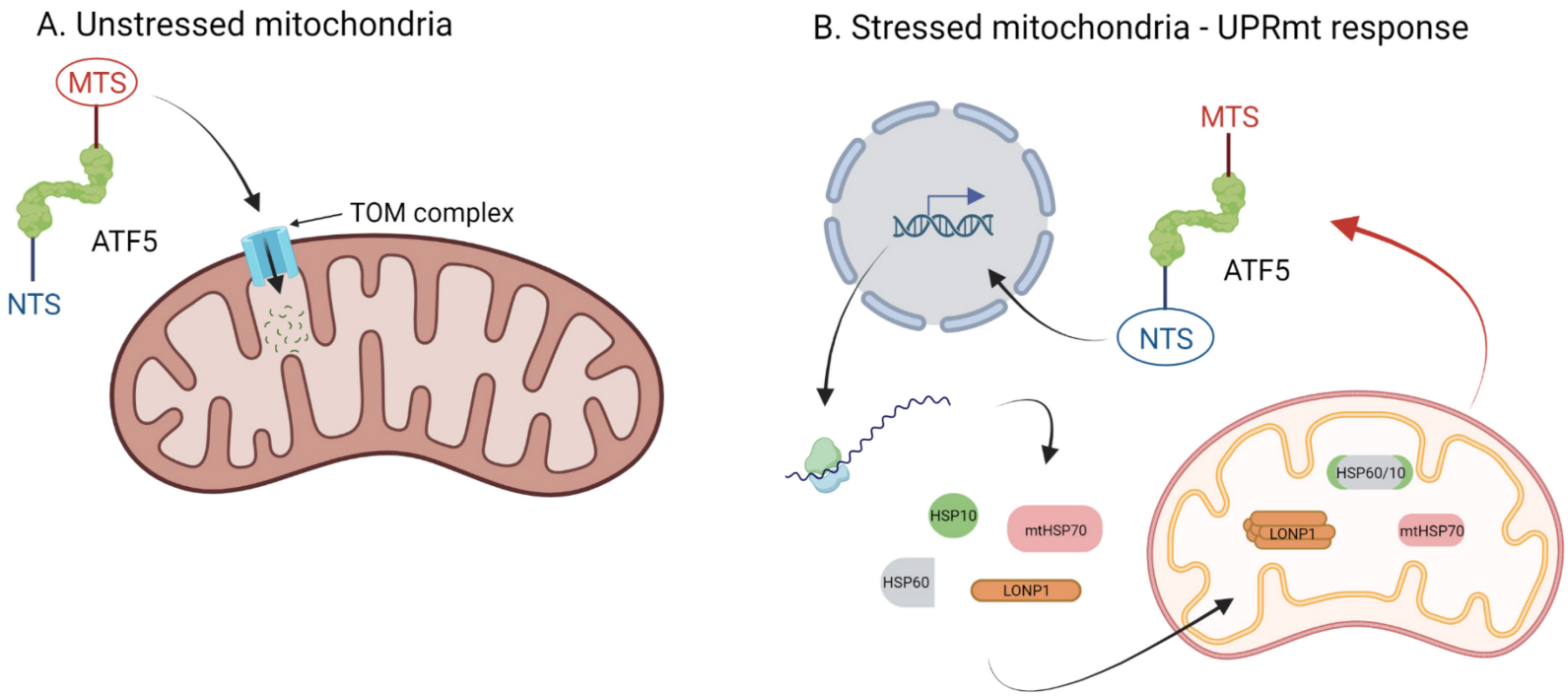

Figure 13.5 UPR^{mt} in the mammalian mitochondrion.

A) In the absence of stress, ATF5 moves to the mitochondrial matrix where it is degraded. B) Mitochondria stress (red arrow) signals ATF5 to move to the nucleus, where UPR^{mt} stress response genes are upregulated. ATF5 – activating transcription factor-5; HSP10 – heat shock protein-10; HSP60 – heat shock protein-60; LONP1 – LON peptidase-1; mtHSP70 – mitochondrial heat shock protein-70; MTS – mitochondrial targeting signal; NTS – nuclear targeting signal; TOM – outer membrane translocase; UPR^{mt} – mitochondrial unfolded protein response. Created with BioRender.com

13.1.6 UPR^{mt} in Aging and Age-related Disease

Initially identified for its role in restoring mitoproteostasis, the UPR^{mt} has since been implicated in aging and in the pathogenesis of age-related conditions. These conditions include Alzheimer's Disease, Parkinson's Disease, cancer, and sarcopenia, among others (Beck et al., 2016; Hu et al., 2019; Urbina-Varela et al., 2020). Mitoproteostasis stress and the UPR^{mt} response both increase with age in certain cell types such as in activated hippocampal neural stem cells (implicated in age-related cognitive decline) (C. L. Wang et al., 2023) and mitochondria-rich (i.e., aerobic) skeletal muscles such as the soleus (implicated in sarcopenia) (Tamura et al., 2017). In contrast, the UPR^{mt} response is blunted in age-related progressive cell senescence (i.e., aged cells that exhibit mitochondrial dysfunction and irreversible growth arrest, secrete components that promote chronic inflammation, and where their accumulation accelerates aging) (Chapman et al., 2019; T. Y. Lee et al., 2020; Regulski, 2017). In senescent cells, a reduced UPR^{mt} response may be due to age-related hypermethylation of histone-3, which would effectively hinder ATF5's access to DNA in response to mitochondrial stress (Y. Guo et al., 2023; Snigdha et al., 2016). In many cancers (e.g., cancers of the prostate, large bowel, and liver), upregulation of the UPR^{mt} contributes to tumour survival (Inigo & Chandra, 2022; S. F. Wang et al., 2020), suggesting that shutting down the UPR^{mt} in senescent cells may in fact provide protection through tumor suppression (Q. Chen et al., 2023).

Intriguingly, inducing the UPR^{mt} through extrinsic or intrinsic methods appears to mitigate mitoproteostatic stress in age-related disease models. In a *C. elegans* Alzheimer's Disease (AD) model, inducing UPR^{mt} through treatment with doxycycline or a reduction in small mitoribosomal subunit-5 (*Mrps5*) expression results in reduced amyloid-β proteotoxicity and increased worm fitness and lifespan (Sorrentino et al., 2017). In both AD neuroblastoma cell and AD mouse

models, an activated UPR^{mt} has a cytoprotective effect (Shen et al., 2020). Likewise, in a Parkinson's Disease neuroblastoma cell model and sarcopenia mouse models, activation of the UPR^{mt} reduces mitoproteostatic stress and has cytoprotective effects (Cordeiro et al., 2020; Hu et al., 2021; Kayani et al., 2010).

Overall, mitochondrial dysfunction is recognized as a hallmark of aging (López-Otín et al., 2013, 2023), with age-related increased ROS production and oxidative stress (i.e., persistent imbalance between ROS/free radical generation and the inability of a cell to deactivate them) along with the accumulation of misfolded proteins, all shown to contribute to age-related diseases (Y. Guo et al., 2023). The induction of the UPR^{mt} in response to mitoproteostatic stress appears to be protective at least in the early stages of aging. However, the dampening of the UPR^{mt} in senescent cells may be in response to overactivation of the UPR^{mt}, as observed in tumour cells.

13.1.7 UPR^{mt} as a Mitohormetic Leading to Beneficial Health Effects

Mitohormesis describes a situation where a small level of mitochondrial stress elicits a beneficial adaptive response that primes the cell, tissue, and/or organism to be resistant to future stressors. A well-studied mitohormetic is moderate-intensity exercise. Regular exercise is a stressor that causes skeletal muscle mitochondria to release retrograde signals to the nucleus in the form of ROS and the UPR^{mt} (Cordeiro et al., 2020; Goh et al., 2023; Memme et al., 2016; Qiu et al., 2023; Slavin et al., 2022; Z. Wang et al., 2022), with positive health effects transmitted throughout the organism. The beneficial effects of a hormetic are generally depicted as a biphasic dose-response relationship in the form of a J-curve or U-curve. There typically is a low-dose beneficial stimulation threshold (below which there is either no effect or a negative effect) and a high-dose limit (above which there is inhibition or a negative effect) (Calabrese et al., 2012). The mitohormetic adaptive response to regular moderate-intensity exercise results in the following: 1)

maintenance of mitochondrial function and protein homeostasis through stimulated mitobiogenesis and mitochondrial network formation (Musci et al., 2018), 2) increased health span and life span (Arem et al., 2015; Chakravarty et al., 2008), and 3) reduced DNA damage (Schmidt et al., 2016). However, excess or over-strenuous exercise induces an overabundance of ROS and oxidative stress that can lead to DNA damage (Wagner et al., 2011).

Genetic mutation or RNAi-induced mild mitoproteostatic stress has been implicated as a mitohormetic in several animal models from *C. elegans* to mammals (Dell'Agnello et al., 2007; M. Guo et al., 2023; Houtkooper et al., 2013; Ozkurede & Miller, 2019). There are at least two long-lived mouse models where an genetic mutation-induced UPR^{mt} response is associated with an increased lifespan – 1) Snell dwarf mice with homozygous mutations on pituitary-specific positive transcription factor-1 gene (*Pit1*) that downregulates growth hormone signalling and leads to ~40% lifespan extension (Ozkurede & Miller, 2019), and 2) surfeit locus protein-1 (*Surf1*) KO mice, where SURF1 is an IMM-embedded accessory factor that assists in the assembly of mtDNA-encoded subunits of respiratory complex CIV (Dell'Agnello et al., 2007). In *C. elegans* models, both lifespan and health span are extended after mitochondrial protein translation is disrupted, which generates a mitonuclear protein imbalance and invokes the UPR^{mt} (M. Guo et al., 2023; Houtkooper et al., 2013).

Compared to wildtype mice, both long-lived Snell dwarf mice and SURF1-KO mice show stronger UPR^{mt} basal activity in cultured fibroblasts (i.e., higher HSP60 and LONP1 levels) (Flurkey et al., 2002; Ozkurede & Miller, 2019; Pharaoh et al., 2016). Snell dwarf mice treated with doxycycline show a stronger UPR^{mt} in response to mitoproteotoxic stress in both cultured fibroblasts and liver samples of treated mice, which results in an improved ability to maintain mitoproteostasis (e.g., mitoribosomal production of mtDNA-encoded COX1 protein quickly

recovers after doxycycline treatment in Snell mice) (Ozkurede & Miller, 2019). Likewise, cultured fibroblasts from SURF1-KO mice challenged with oxidative stressors (paraquat or tert-Butyl H_2O_2) show a strong UPR^{mt} response and enhanced cell survival (Pharaoh et al., 2016). SURF1-KO mouse skeletal muscle and heart tissue show both an upregulated UPR^{mt} and antioxidant response (Pulliam et al., 2014). Importantly from a mitohormesis standpoint, SURF1 deficiency in humans is the leading cause of Leigh Syndrome (a neurometabolic disorder leading to early death). However, the same *Surf1* mutation in mice leads to a milder response (~50% decline in mouse CIV activity vs. >90% CIV decline in humans) and an extended mouse lifespan (Dell'Agnello et al., 2007; Wedatilake et al., 2013). Dell'Agnello et al. (2007) suggest the milder response to SURF1 deficiency in mice may be due to genetic compensation (i.e., `COX assembly function was partly taken over by other factors).

A reduction in *Mrp* expression was initially found to correlate with lifespan extension through quantitative trait locus mapping in BXD mice (multigenerational intercrosses between C57BL/6J and DBA/2J mouse strains generating recombinant inbred mice with a genetic complexity that matches many human populations) (Houtkooper et al., 2013; Peirce et al., 2004). Lifespan extension also correlated with *Mrp* reduction in skeletal muscle microarray analyses of aged and calorie restricted C57BL/6J mice (Edwards et al., 2007). To test the hypothesis that *Mrp* reduction will lead to a lifespan extension, Houtkooper *et al.* (2013) reduced *Mrp* expression in a *C. elegans* model using RNAi. The results were robustly increased lifespan and health span (i.e., induced delay in the expected age-related decline of both pharyngeal pumping and muscle fibre organization). A mitonuclear protein imbalance and subsequent activation of the UPR^{mt} were identified as the underlying mechanisms for lifespan extension in *C. elegans*. This was considered a conserved response since a mitonuclear protein imbalance and UPR^{mt} induction are shared with

other mitoproteostasis-implicated longevity pathways including ETC component knockdown and doxycycline treatment (M. Guo et al., 2023; Houtkooper et al., 2013).

A reduction in *Mrp* expression and the mitonuclear protein imbalance that follows generates a mild mitoproteostatic stress retrograde signal that invokes the UPR^{mt} and leads to an improved health span and life span in *C. elegans* models. In mammals, the SURF1-KO mouse and Snell dwarf mouse models suggest that mild mitoproteostatic stress and subsequent induction of the UPR^{mt} from an early age plays a role in the lifespan extension observed in these two longevity models. This thesis investigates whether a germline reduction in the expression of a critical *Mrp* gene (*Mrpl54*) in a mouse model likewise generates a UPR^{mt} mitohormetic response and examines the effects of *Mrpl54* reduction on mouse lifespan, metabolic health span, and skeletal muscle aging.

14. Aims and Objectives

Based on the *C. elegans* reduced *Mrp* longevity model (Houtkooper et al., 2013), we hypothesized that germline reduction of *Mrpl54* expression (*Mrpl54*$^{+/-}$) in a mouse model will: 1) improve mouse metabolic health span, and 2) increase mouse lifespan. The specific aims of this thesis were as follows:

1) To characterize the *Mrpl54*$^{+/-}$ mouse model (quantitative analysis of tissue *Mrpl54* expression using reverse transcriptase quantitative polymerase chain reaction [RT-qPCR], semi-quantitative analysis of levels of proteins involved in UPR^{mt} upregulation using western blot, and detection of mitonuclear imbalance using western blot and protein mass spectrometry)

2) To assess *Mrpl54*$^{+/-}$ metabolic health with age through the assessment of body composition, indirect calorimetry, glucose and insulin challenge, endurance treadmill, cold challenge, and heart rate and blood pressure monitoring, and

3) To assess *Mrpl54*$^{+/-}$ median lifespan, maximum life expectancy, and 24-month life expectancy.

During the characterization of the *Mrpl54*$^{+/-}$ mouse model, we observed reductions in ETC complex subunit proteins in cultured primary myoblasts. These observations led us to a second hypothesis that an aging *Mrpl54*$^{+/-}$ mouse model will have premature reduction in 1) grip strength, 2) treadmill endurance, and 3) *ex vivo* skeletal muscle tetanic force, fatigue resistance, and fatigue recovery, as well as 4) premature disruption of skeletal muscle sarcomeres and/or Ca^{2+}-release units (CRUs).

15. Reducing mitochondrial ribosomal gene expression does not alter metabolic health or lifespan in mice

Kim Reid* [1]

Eileen G. Daniels* [2,3]

Goutham Vasam[4]

Rashmi Kamble[2]

Georges E. Janssens[2,3]

Iman M. Hu[2,3]

Alexander E. Green[4,5]

Riekelt H. Houtkooper** [2,3,6]

Keir J. Menzies** [4,5]

1. Department of Biology & Ottawa Institute of Systems Biology, University of Ottawa, 30 Marie Curie Private, Ottawa, Ontario, Canada
2. Laboratory Genetic Metabolic Diseases, Amsterdam UMC location University of Amsterdam, Meibergdreef 9, 1105 AZ Amsterdam, The Netherlands
3. Amsterdam Gastroenterology Endocrinology and Metabolism institute, Amsterdam, The Netherlands
4. Interdisciplinary School of Health Sciences, University of Ottawa, 451 Smyth Road, K1H 8M5 Ottawa, Ontario, Canada
5. Ottawa Institute of Systems Biology and the Éric Poulin Centre for Neuromuscular Disease, Department of Biochemistry, Microbiology and Immunology, Faculty of Medicine, University of Ottawa, Ottawa, Ontario, Canada
6. Amsterdam Cardiovascular Sciences institute, Amsterdam, The Netherlands

*co-first authors

**co-last authors

Correspondence – r.h.houtkooper@amsterdamumc.nl (R.H.H.) and kmenzies@uottawa.ca (K.J.M.)

Note: This study was published in Scientific Reports 2023 13:1 doi: 10.1038/s41598-023-35196-3 (Reid et al., 2023).

15.1 Abstract

Maintaining mitochondrial function is critical to an improved health span and lifespan. Introducing mild stress by inhibiting mitochondrial translation invokes the mitochondrial unfolded protein response (UPR^{mt}) and increases lifespan in several animal models. Notably, lower mitochondrial ribosomal protein (MRP) expression also correlates with increased lifespan in a reference population of mice. In this study, we tested whether partially reducing the expression of a critical MRP, *Mrpl54*, reduced mitochondrial DNA-encoded protein content, induced the UPR^{mt}, and affected lifespan or metabolic health using germline heterozygous *Mrpl54* mice. Despite reduced *Mrpl54* expression in multiple organs and a reduction in mitochondrial-encoded protein expression in myoblasts, we identified few significant differences between male or female $Mrpl54^{+/-}$ and wild type mice in initial body composition, respiratory parameters, energy intake and expenditure, or ambulatory motion. We also observed no differences in glucose or insulin tolerance, treadmill endurance, cold tolerance, heart rate, or blood pressure. There were no differences in median life expectancy or maximum lifespan. Overall, we demonstrate that genetic manipulation of *Mrpl54* expression reduces mitochondrial-encoded protein content but is not sufficient to improve health span in otherwise healthy and unstressed mice.

Key words: mitochondrial translation, mitochondrial ribosomal proteins, MRPL54, nDNA, mtDNA, mitonuclear protein imbalance, UPR^{mt}, stress response, longevity, metabolic health, aging, metabolism

15.2 Introduction

Since 1972, mitochondria have been implicated in the aging process[1-4], initially as a source of free radicals in the mitochondrial theory of aging, and more recently as an indicator where reduced mitochondrial respiratory chain efficiency is considered a cellular hallmark of aging[5,6]. This is because mitochondrial dysfunction: (1) occurs during normal aging[7-9]; (2) is implicated in age-related pathologies such as type 2 diabetes, cardiovascular disease, and cancer[10-12]; and (3) aggravation of mitochondrial dysfunction accelerates aging[13]. If mitochondrial dysfunction contributes to aging, then improving mitochondrial function should slow normal aging[14]. Although seemingly contradictory, mitochondrial stress early in development maintains mitochondrial function with age in several animal models[15-19]. This stress triggers a compensatory beneficial response – i.e., a mitochondrial hormetic (mitohormetic) response, which is suggested to improve health span and/or lifespan[6,20]. If mild mitochondrial stress improves health span or extends lifespan in mammals, then this opens new possibilities in human health span and longevity research.

Specifically, mitochondrial translation stress is emerging as a promising mitohormetic strategy[15,21,22]. The mitochondrial ribosome (mitoribosome), which consists of ~80 mitoribosomal proteins (MRPs)[23], conducts mitochondrial translation to produce essential electron transport chain (ETC) complex protein subunits encoded by mitochondrial DNA. Previously, we showed that partial knockdown of any individual *Mrp*, and the subsequent disruption of mitochondrial translation, improved metabolic health and extended the lifespan of *Caenorhabditis elegans*[15]. Reducing the expression of a single *Mrp* induced a mitonuclear protein imbalance, a stoichiometric imbalance between nuclear- (nDNA) and mitochondrial-DNA (mtDNA) encoded ETC subunits. This imbalance subsequently activated the mitochondrial unfolded protein response (UPR^{mt}) – a

nuclear transcriptional response that maintains or restores mitochondrial proteostasis[24-26]. Strikingly, the variation in expression of MRP genes amongst recombinant-inbred BXD mouse strains[27,28], e.g., *Mrps5* expression, inversely correlated with a ~250-day increase in lifespan[15]. Further, fibroblast cell cultures from long-lived Snell dwarf mice had greater expression of UPR^{mt} markers, including elevated 60kDa mitochondrial heat shock protein (HSP60 or HSPD1)[29]. Therefore, chronic disruption of mitochondrial translation and induction of the UPR^{mt} may promote both longevity and an improved health span via mitohormesis[15,30-35].

The observation that the reduction of *Mrp* expression and consequent induction of mitonuclear imbalance induced the UPR^{mt} and promoted longevity across species led us to a general hypothesis: partial disruption of a critical *Mrp* gene in a mouse model would result in improved metabolic health with age and/or an increased lifespan. To test this hypothesis, we engineered a whole-body mouse model heterozygous for the *Mrpl54* gene (*Mrpl54*$^{+/-}$). The MRPL54 protein was selected because: (1) reduced expression of *Mrpl54* invokes the UPR^{mt} and extends *C. elegans* lifespan[15]; (2) MRPL54 is evolutionarily conserved between species[36]; and (3) MRPL54 is essential to both recruitment of essential factors for mitochondrial translation[37,38] and ETC function[39]. To assess metabolic health with age, we subjected both male and female *Mrpl54*$^{+/-}$ and *Mrpl54*$^{+/+}$ (wildtype, WT) littermate mice to *in vivo* metabolic phenotyping at 6-, 18-, and 24-months of age. In parallel, we conducted a longevity study to assess the effect of mitochondrial stress on life expectancy and lifespan.

15.3 Results

15.3.1 Generation of Mrpl54$^{+/-}$ mice

To investigate the effect of reduced *Mrpl54* expression on whole body metabolism and longevity, we generated mice heterozygous for *Mrpl54* (Fig. 15.1a) by deleting exon 2 in the *Mrpl54* gene. Homozygous *Mrpl54* exon 2 deletion proved lethal, as no *Mrpl54*$^{-/-}$ mice were observed at weaning, yet WT and *Mrpl54*$^{+/-}$ were born at the expected Mendelian ratio (Fig. 15.1b). This agrees with current understanding that there is little functional redundancy in *Mrp* genes[40]. Next, to assess if *Mrpl54*$^{+/-}$ led to reduced expression of the targeted gene, we performed qPCR analysis in gastrocnemius, heart, liver, interscapular brown adipose tissue (BAT), and proximal colon tissues from 7-week-old male and female mice. We found that the relative expression of *Mrpl54* was highest in gastrocnemius and lowest in the liver (Fig. 15.1c). Additionally, in all tissues tested, *Mrpl54* expression was reduced by ~50% in *Mrpl54*$^{+/-}$ mice compared to WT (Fig. 15.1d).

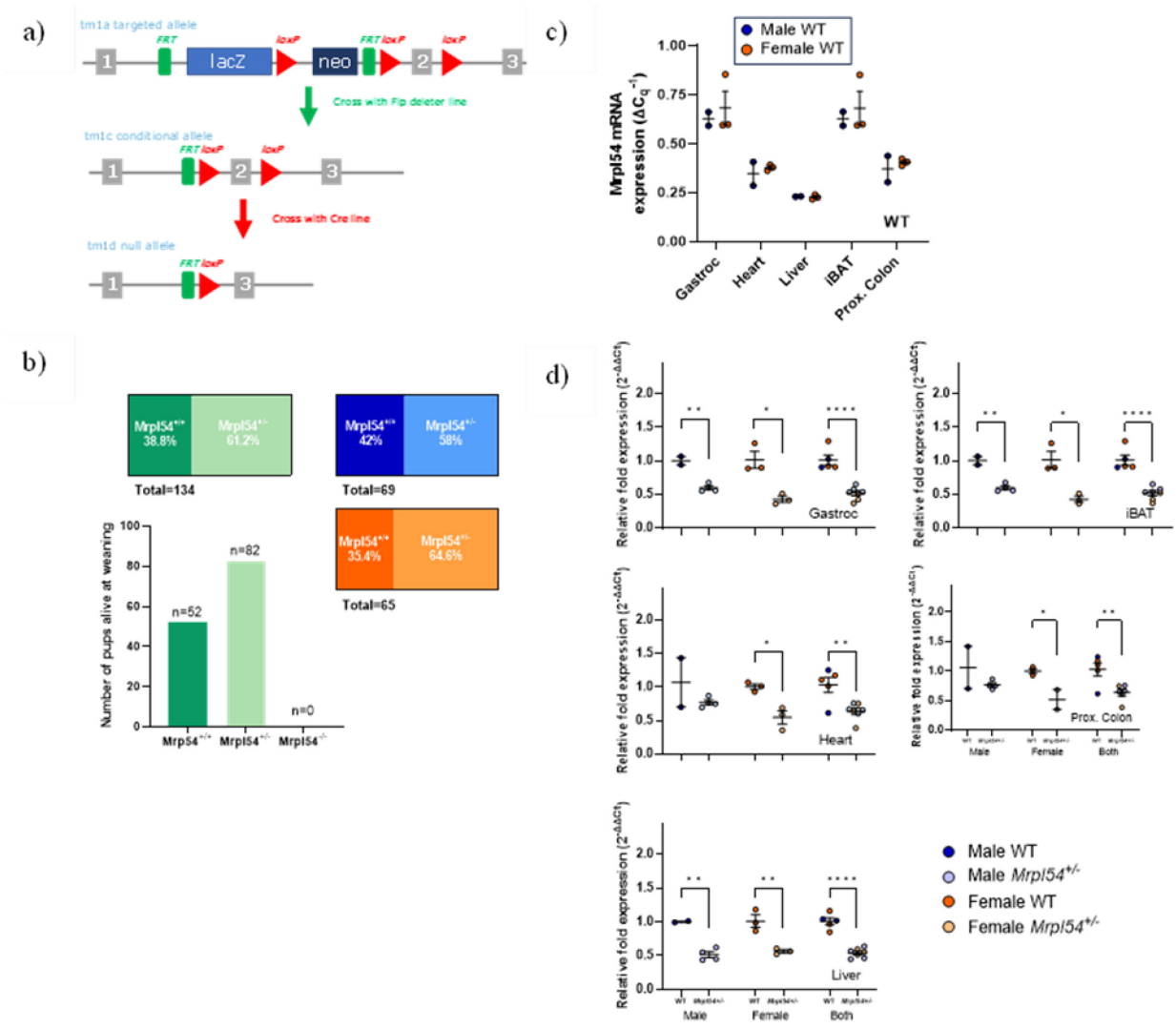

Figure 15.1 Generation and basic characterization of the Mrpl54+/- model

a) Generation of the *Mrpl54*$^{+/-}$ mouse model through the deletion of exon 2 at the *Mrpl54* allele. Adapted from the Mouse Genome Database[61].

b) The number of WT and *Mrpl54*$^{+/-}$ pups born to 28 *Mrpl54*$^{+/-}$ breeding pairs followed a Mendelian ratio for homozygous lethality.

c) Relative *Mrpl54* gene expression in tissues from 7-week-old WT males (blue, n=2) and females (orange, n=3) as determined by RT-qPCR. Values were normalized to 60S acidic ribosomal protein P0 (*36b4* or *RPLP0*) and beta-2-microglobulin (*B2m*) expression.

d) Reduced *Mrpl54* gene expression (~50%) in tissues derived from 7-week-old *Mrpl54*$^{+/-}$ males (light blue, n=2) and females (light orange, n=3) compared to WT male (blue, n=4) and female (orange, n=3). Values were normalized to *36b4* and *B2m* expression. Graphs show mean ± SEM, *P ≤ 0.05, **P ≤ 0.01, and ****P ≤ 0.0001

15.3.2 No major metabolic phenotype in adult Mrpl54$^{+/-}$ mice

To examine the effect of reduced *Mrpl54* expression on metabolic health in adult mice, we subjected male and female *Mrpl54*$^{+/-}$ and WT mice to a comprehensive metabolic phenotyping protocol (Supplemental Fig. 15.7). In both males and females in the combined longevity and metabolic study cohorts (the latter study animals included up until entering metabolic phenotyping, as described in methods), there were no differences in body mass between *Mrpl54*$^{+/-}$ and WT mice (Fig. 15.2a). Both genotypes had similar lean- or fat-mass body composition across genotypes in males; although, females in the metabolic health study at 6 months (6M) had slightly lower lean and fat mass (Fig. 15.2b). Body composition as a percentage of body mass, however, remained the same between 6M female *Mrpl54*$^{+/-}$ and WT (Supplemental Fig. 15.8). Metabolic indices, examined via indirect calorimetry, exhibited no differences in mean O_2 volume (VO_2) (Fig. 15.2c) or mean respiratory exchange ratio (RER) (Fig. 15.2d). Mean VO_2 was lower in 6M female *Mrpl54*$^{+/-}$ animals during the less active light phase; however, an ANCOVA analysis[41] attributed this difference to their reduced body mass (Fig 15.2c inset). Male spontaneous ambulatory activity in testing cages was not different, yet there was an increase in activity in 6M *Mrpl54*$^{+/-}$ females when compared to WT (Fig. 15.2e), possibly in line again with the effect of reduced body weight and VO_2. Like the increase in ambulatory activity of female *Mrpl54*$^{+/-}$ mice, 6M females exhibited improved running capacity in a forced exercise treadmill test (Fig. 15.2f). Whole body glucose handling was not different between genotypes during an oral glucose tolerance test (OGTT; Fig. 15.2g) or an intraperitoneal insulin tolerance test (ipITT; Fig. 15.2h) in 6M male and female mice. Since skeletal muscle exhibited the highest relative levels of *Mrpl54* gene expression and BAT tissue the second highest (Fig. 15.1c), and because of their importance for non-shivering and shivering thermogenesis, we evaluated potential differences in metabolic heat production by

exposing mice to an acute cold challenge (4°C). Mice from both genotypes maintained their core body temperature similarly for four hours for 6M males and females (Fig. 15.2i). At sacrifice, the masses of the heart, spleen and kidney were reduced as a percentage of body mass in *Mrpl54*$^{+/-}$ males with no changes in skeletal muscle, brain, or liver (Fig. 15.2j). In females, there were no changes in organ masses expressed as a percentage of body mass. Overall, there were no robust morphological or metabolic changes in adult *Mrpl54*$^{+/-}$ mice apart from the increased physical activity in female *Mrpl54*$^{+/-}$ mice.

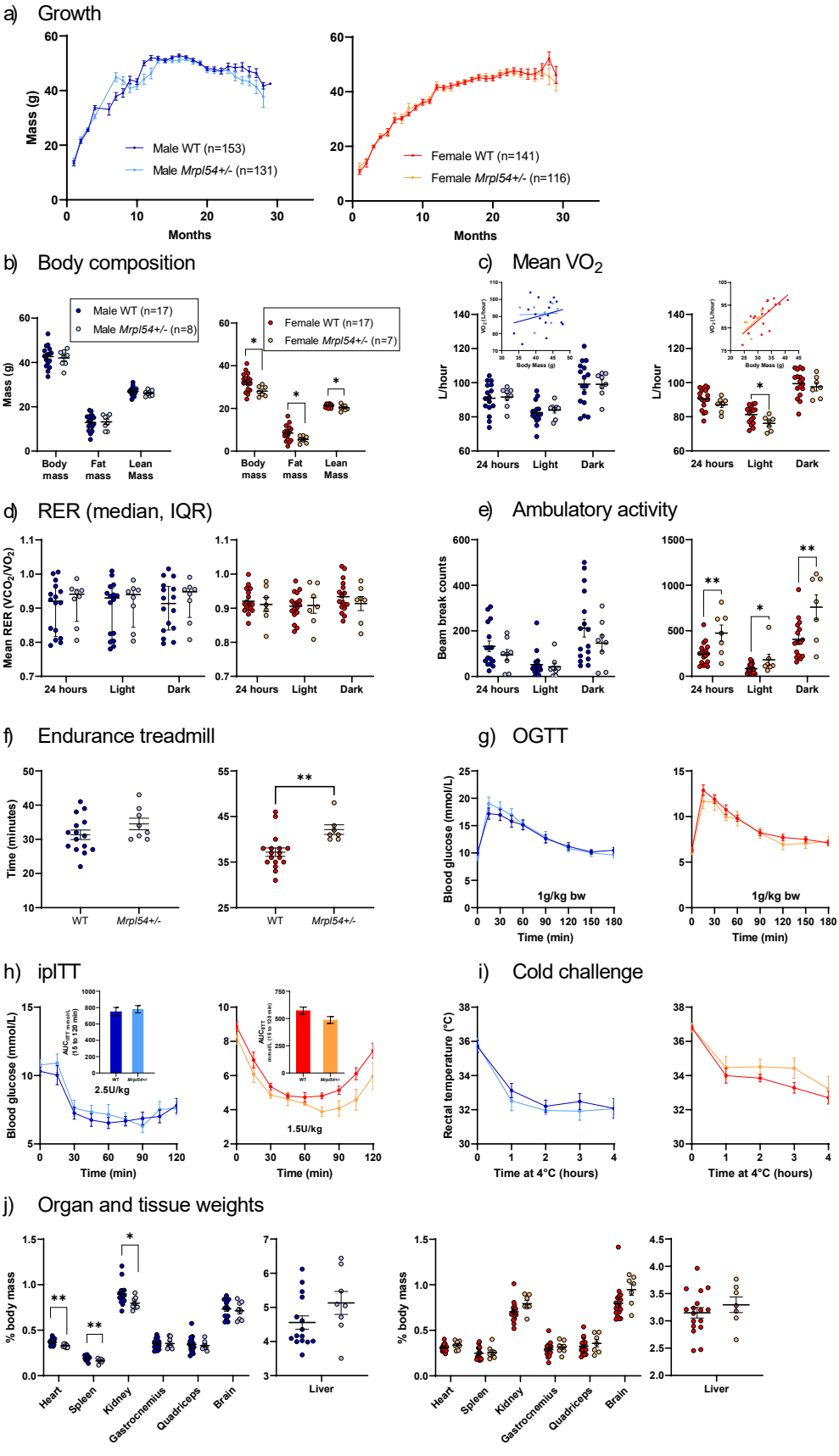
a) Growth
Mass (g)
Months
Male WT (n=153)
Male Mrpl54+/- (n=131)
Female WT (n=141)
Female Mrpl54+/- (n=116)
b) Body composition
Male WT (n=17)
Male Mrpl54+/- (n=8)
Female WT (n=17)
Female Mrpl54+/- (n=7)
Body mass
Fat mass
Lean Mass
c) Mean VO2
L/hour
24 hours
Light
Dark
d) RER (median, IQR)
Mean RER (VCO2/VO2)
e) Ambulatory activity
Beam break counts
f) Endurance treadmill
Time (minutes)
WT
Mrpl54+/-
g) OGTT
Blood glucose (mmol/L)
1g/kg bw
Time (min)
h) ipITT
2.5U/kg
1.5U/kg
i) Cold challenge
Rectal temperature (°C)
Time at 4°C (hours)
j) Organ and tissue weights
% body mass
Heart
Spleen
Kidney
Gastrocnemius
Quadriceps
Brain
Liver

Figure 15.2 Metabolic phenotyping in 6M-old male and female *Mrpl54*$^{+/-}$ and wild type mice

a) Body mass (g) comparison between male *Mrpl54*$^{+/-}$ (n=131) and WT (n=153) and female *Mrpl54*$^{+/-}$ (n=116) and WT (n=141) over lifespan.

b) Body composition (g) by EchoMRI in 6M adult *Mrpl54*$^{+/-}$ and WT male and female mice.

c) Mean VO_2 (L/hour) by CLAMS in 6M adult mice. ANCOVA results (insets) indicate the difference in mean female VO_2 are explained by the difference in female body mass.

d) Mean RER by CLAMS in 6M adult *Mrpl54*$^{+/-}$ and WT male and female mice.

e) Mean ambulatory motion (beam break counts) in 6M adult *Mrpl54*$^{+/-}$ and WT male and female mice.

f) Mean duration (minutes) on an endurance treadmill for 6M adult male *Mrpl54*$^{+/-}$ (n=8) and WT (n=15) male and *Mrpl54*$^{+/-}$ and WT female mice.

g) Mean blood glucose levels (mmol/L) over time in response to an oral glucose challenge (OGTT) in 6M *Mrpl54*$^{+/-}$ and WT male and female mice.

h) Mean blood glucose levels (mmol/L) over time in response to intraperitoneal insulin challenge (ipITT) in 6M adult *Mrpl54*$^{+/-}$ and WT male and female mice with area under the curve (AUC) (insets).

i) Mean rectal temperature (°C) in response to a 4-hour 4°C cold challenge in 6M male *Mrpl54*$^{+/-}$ (n=7) and WT (n=16) mice and female *Mrpl54*$^{+/-}$ and WT mice.

j) Relative organ weights (% body mass) in 6M adult necropsied male *Mrpl54*$^{+/-}$ (n=7-8) vs. WT (n=14-15) and female *Mrpl54*$^{+/-}$ vs. WT mice.

Graphs show mean ± SEM, *P ≤ 0.05, **P ≤ 0.01, and ****P ≤ 0.0001. Unless otherwise indicated, the number analysed are as follows: male WT (blue, n=16); male *Mrpl54*$^{+/-}$ (light blue, n=8); female WT (orange, n=17); and female *Mrpl54*$^{+/-}$ (light orange, n=7).

15.3.3 Aged Mrpl54$^{+/-}$ mice did not show an improved metabolic phenotype

Given that disruption of mitochondrial translation and/or UPR^{mt} induction has been linked to improved health span in several animal models[15,30-35], we examined whether reduced *Mrpl54* expression altered whole body metabolism during the aging trajectory. Female and male *Mrpl54*$^{+/-}$ and WT mice were aged 24 months (24M) before performing the same metabolic phenotyping tests used for adult 6M mice. While there were no differences in body composition between *Mrpl54*$^{+/-}$ and WT, female mice had increased fat mass and decreased lean mass with age, as a proportion of body mass, while the opposite was observed in males – fat mass decreased and lean mass increased with age, as a proportion of body mass (Supplemental Fig. 15.9, Fig. 15.3a). Like 6M animals, we did not observe any differences in indirect calorimetry measurements between *Mrpl54*$^{+/-}$ and WT at 24M (Fig. 15.3b, 15.3c, & 15.3d). At 24M, there were no differences in running capacity (Fig. 15.3e), which contrasts our observations in 6M *Mrpl54*$^{+/-}$ female mice where running capacity was higher (Fig. 15.2f) but can be attributed to the difference in body weight at 6M. In the 24M mice, the response to OGTT was similar between *Mrpl54*$^{+/-}$ and WT (Fig. 15.3f), as was the response to the ipITT (Fig. 15.3g). There were no differences between genotypes when exposed to a cold challenge at 24M (Fig. 15.3h). There were no differences in heart rate, diastolic blood pressure, or systolic blood pressure between genotypes for either males or females at 24M (Fig. 15.3i). Finally, at 24M there were no differences in organ mass as a percentage of body mass (Fig. 15.3j). The 18M cohort displayed the same results as the 24M cohort for both males and females (Supplemental Fig. 15.10a-h, 15.10j); except 18M male *Mrpl54*$^{+/-}$ mice demonstrated a mean diastolic blood pressure that was higher than WT (Supplemental Fig. 15.10i). Altogether, aging *Mrpl54*$^{+/-}$ mice did not reveal robust differences from WT in metabolic parameters.

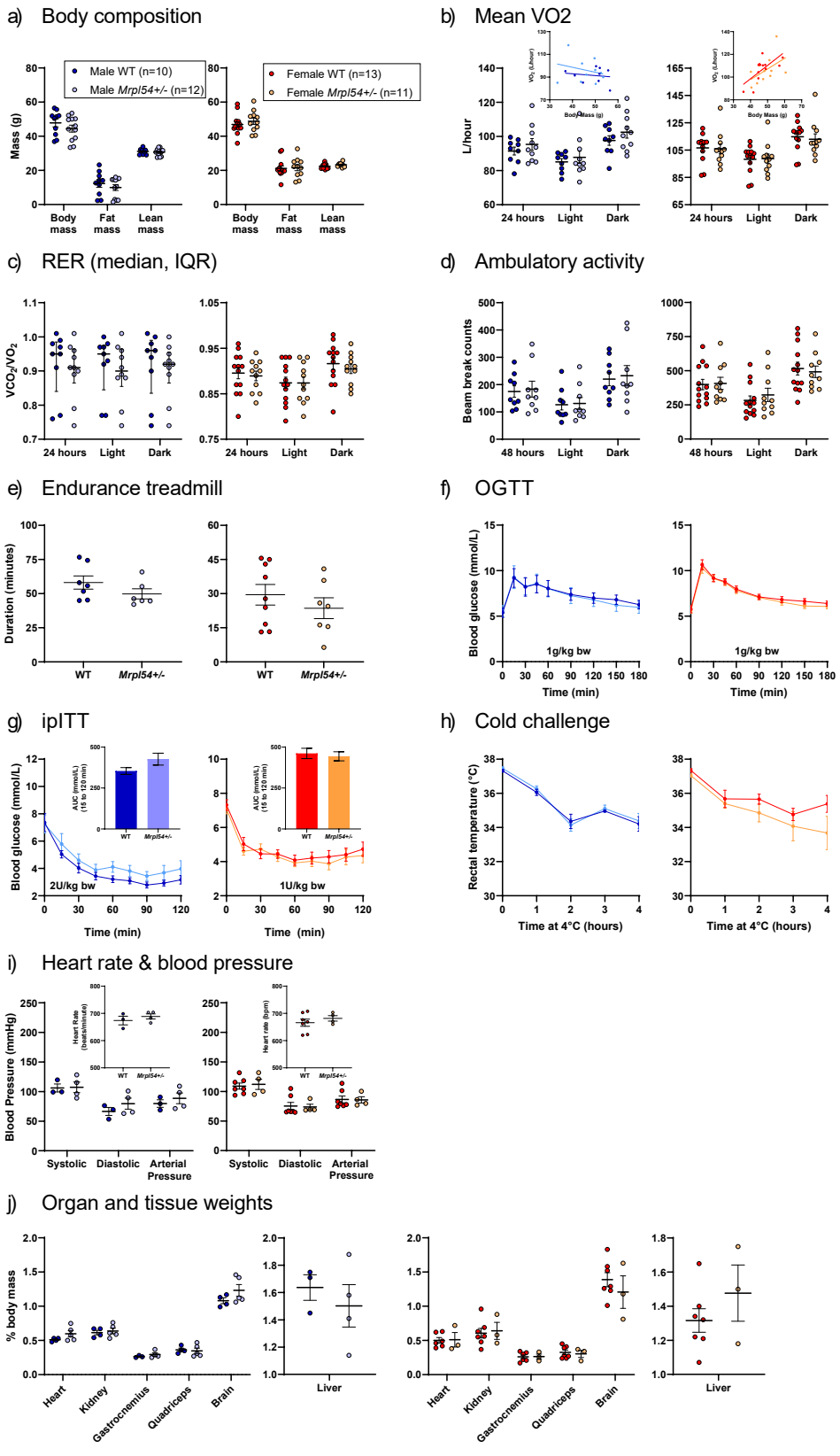
a) Body composition
Male WT (n=10)
Male Mrpl54+/- (n=12)
Female WT (n=13)
Female Mrpl54+/- (n=11)
Mass (g)
Body mass
Fat mass
Lean mass
b) Mean VO2
L/hour
24 hours
Light
Dark
c) RER (median, IQR)
VCO2/VO2
d) Ambulatory activity
Beam break counts
48 hours
e) Endurance treadmill
Duration (minutes)
WT
Mrpl54+/-
f) OGTT
Blood glucose (mmol/L)
1g/kg bw
Time (min)
g) ipITT
AUC (mmol/L) (15 to 120 min)
2U/kg bw
1U/kg bw
h) Cold challenge
Rectal temperature (°C)
Time at 4°C (hours)
i) Heart rate & blood pressure
Blood Pressure (mmHg)
Heart Rate (beats/minute)
Heart rate (bpm)
Systolic
Diastolic
Arterial Pressure
j) Organ and tissue weights
% body mass
Heart
Kidney
Gastrocnemius
Quadriceps
Brain
Liver

Figure 15.3 Metabolic phenotyping in 24M *Mrpl54*$^{+/-}$ and wild type mice

a) Body composition (g) by EchoMRI in 24M male *Mrpl54*$^{+/-}$ (n=12) and WT (n=10) and female *Mrpl54*$^{+/-}$ (n=11) and WT (n=13).

b) Mean VO_2 (L/hour) by CLAMS and body mass ANCOVA analysis (insets) in 24M old male *Mrpl54*$^{+/-}$ (n=10) and WT (n=9) and female *Mrpl54*$^{+/-}$ and WT.

c) Mean RER by CLAMS in 24M old male *Mrpl54*$^{+/-}$ (n=10) and WT (n=9) and female *Mrpl54*$^{+/-}$ and WT.

d) Mean ambulatory motion (beam break counts) in 24M old male *Mrpl54*$^{+/-}$ (n=9) and WT (n=9) and female *Mrpl54*$^{+/-}$ (n=10) and WT (n=13).

e) Mean duration (minutes) on an endurance treadmill for 24M old mice male *Mrpl54*$^{+/-}$ (n=6) and WT (n=7) and female *Mrpl54*$^{+/-}$ (n=7) and WT (n=9).

f) Mean blood glucose level (mmol/L) over time in response to an oral glucose challenge (OGTT) in 24M old male *Mrpl54*$^{+/-}$ (n=10) and WT (n=8) and female *Mrpl54*$^{+/-}$ (n=10) and WT (n=12).

g) Mean blood glucose level (mmol/L) and AUC (insets) over time in response to intraperitoneal insulin challenge (ipITT) in 24M old male *Mrpl54*$^{+/-}$ (n=8) and WT (n=8) and female *Mrpl54*$^{+/-}$ (n=10) and WT (n=11).

h) Mean rectal temperature (°C) in response to a 4-hour 4°C cold challenge in 24M old male *Mrpl54*$^{+/-}$ (n=4) and WT (n=3) and female *Mrpl54*$^{+/-}$ (n=4) and WT (n=7).

i) Mean heart rate (beats/min) and blood pressure (mmHg) in 24M old male *Mrpl54*$^{+/-}$ (n=6) and WT (n=5) and female *Mrpl54*$^{+/-}$ (n=5) and WT (n=8).

j) Relative organ weights (% body mass) in 24M necropsied male *Mrpl54*$^{+/-}$ (n=4-5) and WT (n=3-4) and female *Mrpl54*$^{+/-}$ (n=3) and WT (n=6-7).

Graphs show mean ± SEM; male WT (blue); male *Mrpl54*$^{+/-}$ (light blue); female WT (orange); and female *Mrpl54*$^{+/-}$ (light orange).

15.3.4 Lifespan and life expectancies were not altered in Mrpl54$^{+/-}$ mice

Since reduced *Mrp* gene expression extended lifespan in *C. elegans* and correlated with long lifespan in BXD mouse strains, we tested whether reducing *Mrpl54* expression affected lifespan or life expectancy in mice. We followed *Mrpl54*$^{+/-}$ male and female mice until they reached a humane endpoint or a natural death and assessed mean and 24-month life expectancy and maximum lifespan. We included 24-month life expectancy because strain-specific conditions and diseases affect C57BL/6 mice after the age of 24-months, which can confound results of aging studies[42]. We observed no significant differences in median life expectancy, 24-month life expectancy, or maximum lifespan between *Mrpl54*$^{+/-}$ and WT, for either males or females (Fig. 15.4a).

During the lifespan study, some males were separated due to injuries or deaths from aggression and fighting, which resulted in a population of male mice that were housed individually (i.e., a single animal per cage from age 3-4 months onward). When individually and group-housed animals were analysed separately, it was evident that individually housed males had better median life expectancy than grouped-housed males for both genotypes (777 days vs. 714 days; Fig. 15.4b), which may be due to conspecific aggression increasing stress levels and shortening lifespan in group-housed males[43]. While not statistically significant, survival data for individually housed *Mrpl54*$^{+/-}$ males suggested a better 24-month life expectancy compared to WT (24-month HR 1.85, 95% CI 0.86, 4.01, p = 0.12) (Supplemental Fig. 15.11a). Group-housed males (n=2-9 males per cage) showed no differences in median or 24-month life expectancy between genotypes (Supplemental Fig. 15.11b).

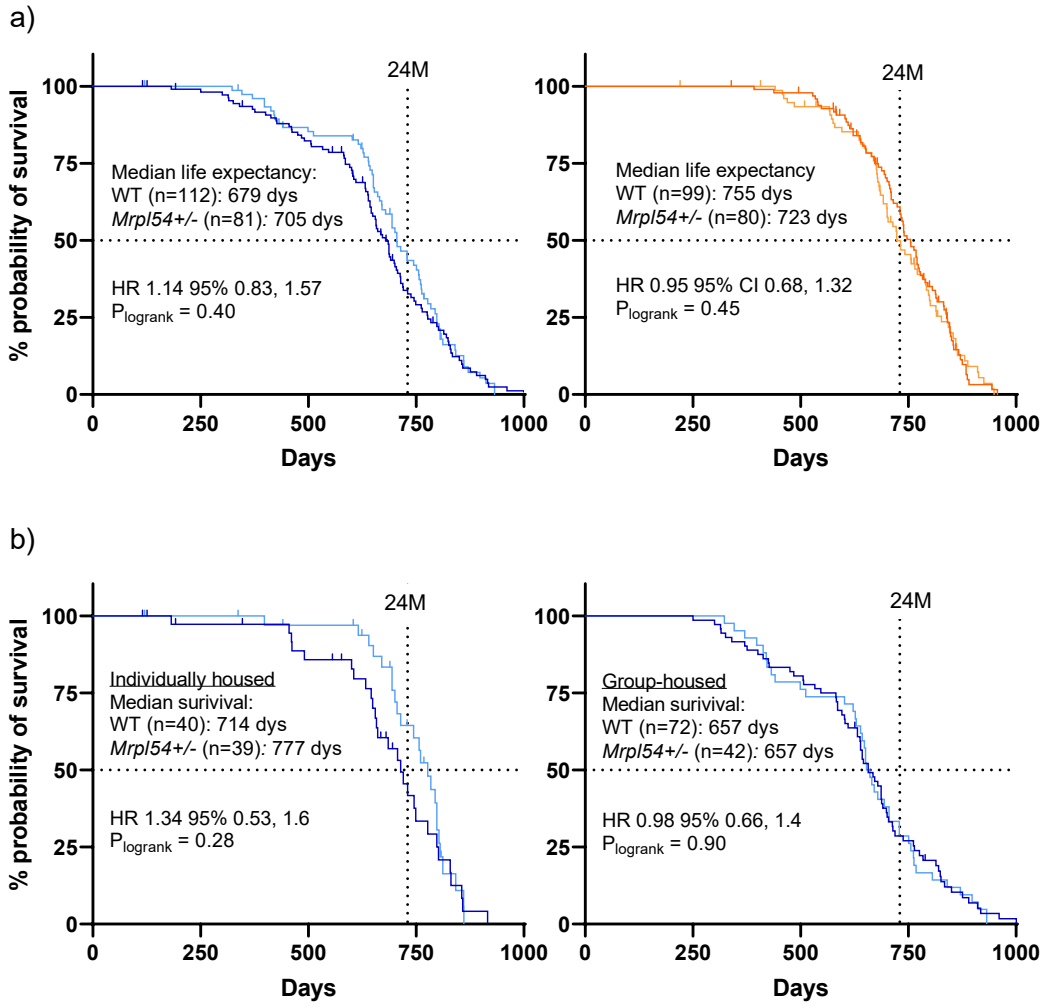

Figure 15.4 Life expectancy and lifespan in male and female Mrpl54+/- mice

a) Kaplan Meier survival curves showed no difference in overall lifespan (top 10% of surviving animals) between either male *Mrpl54*$^{+/-}$ (n=81) and WT (n=112) or female *Mrpl54*$^{+/-}$ (n=80) and WT (n=99) mice. No differences were observed in median life expectancy between *Mrpl54*$^{+/-}$and WT for either males or females.

b) Kaplan Meier survival curves showed no difference in overall lifespan between either individual-housed male *Mrpl54*$^{+/-}$ (n=39) and WT (n=40) or group-housed male *Mrpl54*$^{+/-}$ (n=42) and WT (n=72). Individual-housed *Mrpl54*$^{+/-}$ male mice had better median life expectancy compared to individual-housed WT, with no difference in median life expectancy between group-housed male *Mrpl54*$^{+/-}$ and WT.

15.3.5 Mrpl54$^{+/-}$ did not activate the UPR^{mt} in liver mitochondria or primary myoblasts

Since MRP proteins play a crucial role in the translation of mtDNA-encoded mRNAs into protein subunits for oxidative phosphorylation (OXPHOS), we determined whether mitochondrial oxygen consumption was affected in the liver, a major metabolic organ. Using a Clark-type oxygen electrode, purified mitochondria from the liver of 7-week-old WT and *Mrpl54*$^{+/-}$ males demonstrated similar rates of oxygen consumption (Fig. 15.5a). We then examined if reductions in *Mrpl54* induced a mitonuclear protein imbalance and induced the UPR^{mt}. Using purified mitochondria from the liver of 7-week-old WT and *Mrpl54*$^{+/-}$ males, we found no significant difference in HSP60 (HSPD1) protein levels, a classical marker for UPR^{mt} activation[44,45] (Fig. 15.5b, uncropped gel images in Supplemental Fig. 15.12a). This result was confirmed by mass spectrometry-based proteomics on purified liver mitochondria from 7-week-old males showing no differences in the levels of nDNA- or mtDNA-encoded proteins between WT and *Mrpl54*$^{+/-}$ animals (Fig. 15.5c). Combined, these results suggest that the mitochondrial translational capacity was not affected in the liver tissue of *Mrpl54*$^{+/-}$ animals.

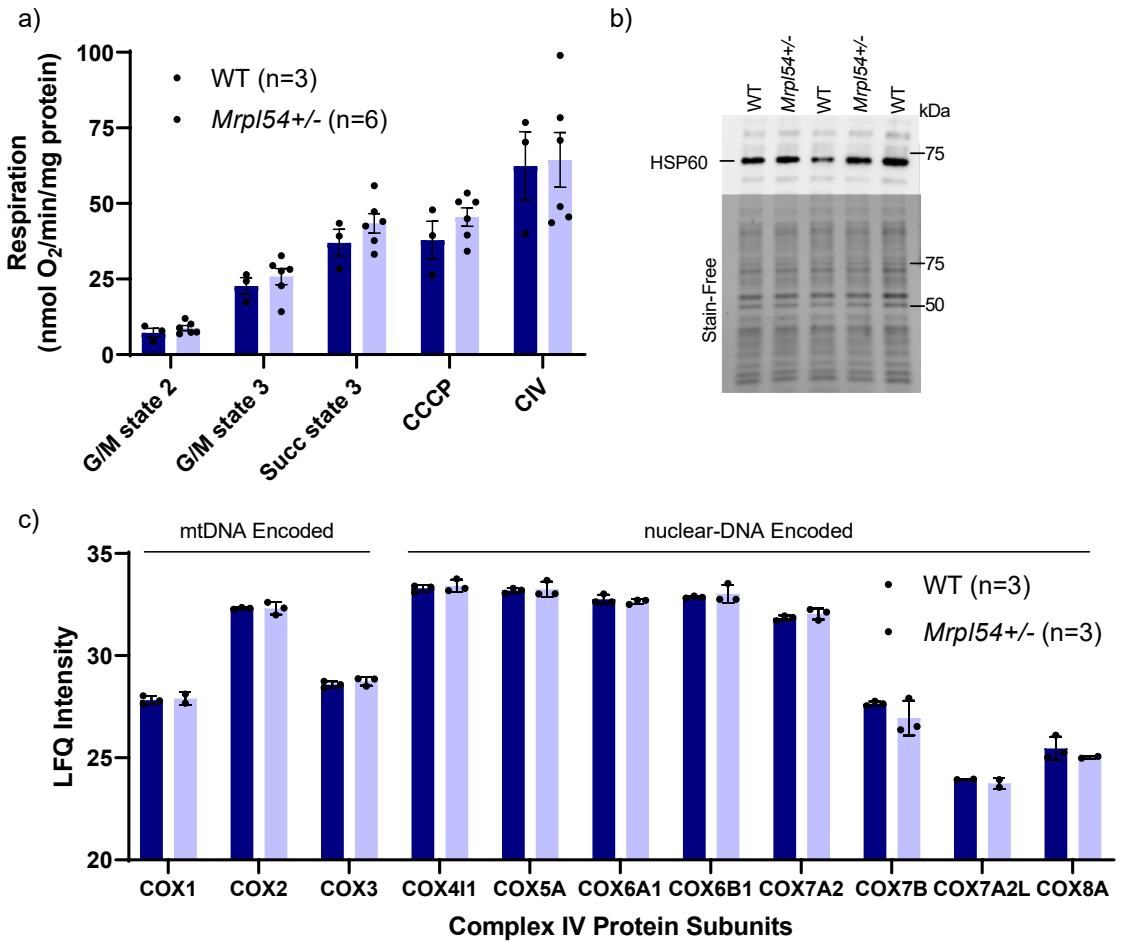

Figure 15.5 Biochemical profiling of Mrpl54+/- and wild type mouse liver.

a) Oxygraph respiration analysis of isolated liver mitochondria showed no difference in state 2, state 3, or maximal respiration between *Mrpl54*$^{+/-}$ (n=6) and WT (n=3).

b) Semiquantitative western blot analysis of HSP60 expression in isolated liver mitochondria showed no difference between *Mrpl54*$^{+/-}$ (n=2) and WT (n=3).

c) Mass spectrometry analysis of protein from isolated liver mitochondria showed no difference between levels (label-free quantification, LFQ) of nDNA- and mtDNA-encoded protein subunits of ETC complex IV between *Mrpl54*$^{+/-}$ (n=3) and WT (n=3).

Graphs show mean ± SEM; male WT (blue); male *Mrpl54*$^{+/-}$ (light blue).

Since the relative *Mrpl54* expression is highest in skeletal muscle tissue (Fig. 15.1c), we examined the effect of reduced *Mrpl54* expression on the levels of OXPHOS protein subunits and the UPR^{mt} marker HSP60 in primary myoblasts. Primary myoblast cultures were established from 7-week-old male *Mrpl54*$^{+/-}$ and WT hindlimb skeletal muscle. In cell lysates from these myoblasts, levels of mitochondrial OXPHOS subunits (including both nDNA- and mtDNA-encoded proteins) were lower in *Mrpl54*$^{+/-}$ mice compared to WT (Fig 15.6a, uncropped gel images in Supplemental Fig. 15.12b-c). The level of succinate dehydrogenase complex iron sulphur subunit B (SDHB), a nDNA-encoded protein subunit of Complex II of the ETC, and the level of MTCO1, a mtDNA-encoded protein subunit of Complex IV of the ETC, were both lower in *Mrpl54*$^{+/-}$ primary myoblasts (Fig 15.6a, uncropped gel images in Supplemental Fig 15.12b-c). Notably, considering that both MTCO1 and SDHB were similarly decreased, the ratio of mtDNA- to nDNA-encoded proteins was not different in *Mrpl54*$^{+/-}$ myoblasts. In line with this, HSP60 levels in *Mrpl54*$^{+/-}$ myoblasts were not increased, suggesting that UPR^{mt} was not invoked in *Mrpl54*$^{+/-}$ myoblasts (Fig 15.6b, uncropped gel images in Supplemental Fig. 15.12b). These results suggest that reduced *Mrpl54*$^{+/-}$ expression in primary myoblasts lowered levels of various ETC complexes but this reduction was insufficient to activate the UPR^{mt}.

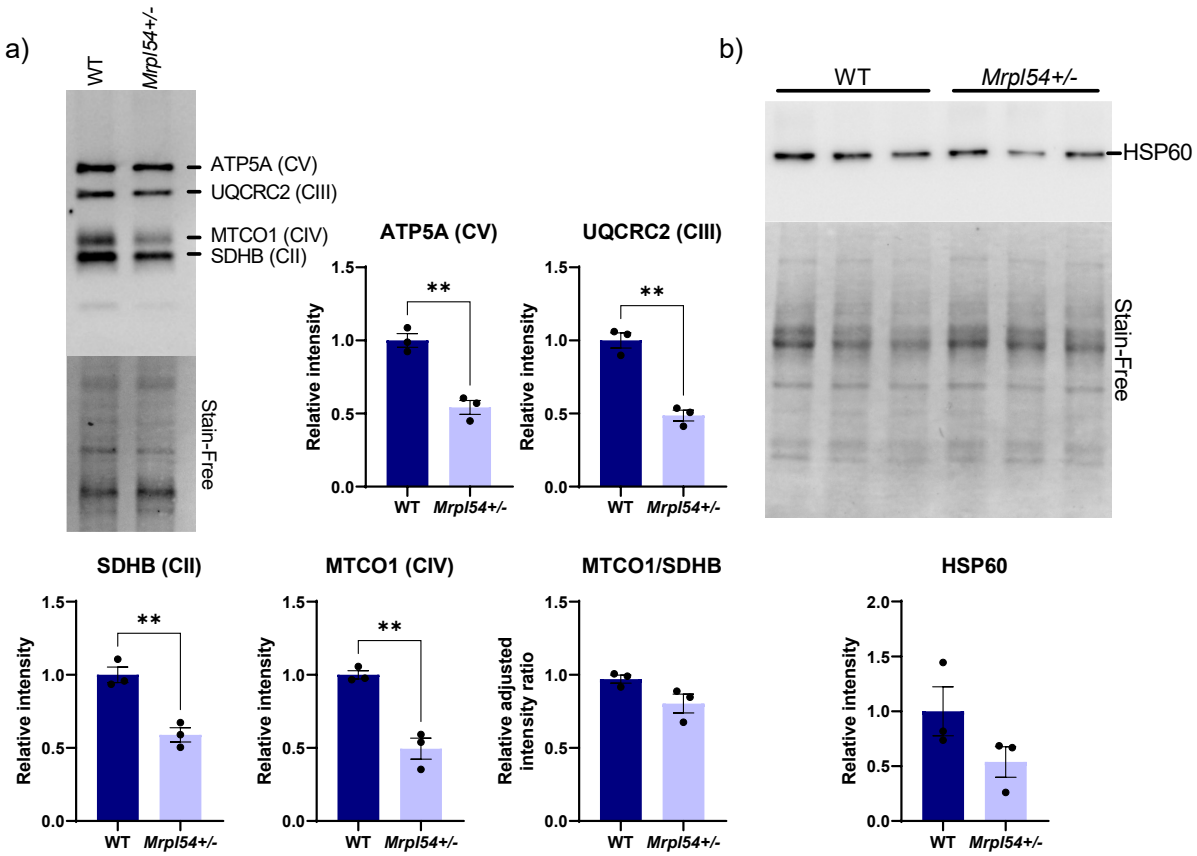

Figure 15.6 Biochemical profiling of *Mrpl54*$^{+/-}$ and wild type mouse muscle.

a) Semiquantitative representative western blot of ETC nDNA-encoded subunits (ATP5A, QCRC2, and SDHB) and mtDNA-encoded MTCO1 subunit in cell lysate from primary myoblasts showed a decrease in ETC subunit expression in *Mrpl54*$^{+/-}$ (n=3) compared to WT (n=3).

b) Semiquantitative western blot analysis of HSP60 expression in cell lysate from primary myoblasts showed no difference in HSP60 levels in *Mrpl54*$^{+/-}$ (n=3) compared to WT (n=3).

Graphs show mean ± SEM; male WT (blue); male *Mrpl54*$^{+/-}$ (light blue); *P ≤ 0.05, **P ≤ 0.01, and ***P ≤ 0.001.

15.4 Discussion

Reduced expression of MRP proteins in *C. elegans* results in an increase in both health span and lifespan through the induction of the UPR^{mt} that results from a mitonuclear protein imbalance[15]. Similarly, long lifespan is correlated with low expression of *Mrps5* and other MRP genes in a genetic reference population of mice and elevated UPR^{mt} markers are observed in cell cultures of the long-lived Snell dwarf mouse strain[15,29]. The UPR^{mt} is also induced in mice treated with doxycycline[46], an antibiotic that inhibits mitochondrial translation[47], which potentially reduces energy expenditure[46]. To determine whether reduced expression of *Mrpl54* in heterozygote mice alters metabolism or lifespan, we compared metabolic health at 6-, 18-, and 24-months as well as assessed lifespan and life expectancy in $Mrpl54^{+/-}$ and WT animals.

While *Mrpl54* mRNA expression was reduced in multiple metabolic organs from $Mrpl54^{+/-}$ animals, we found no compelling metabolic changes in 6-month-old adult mice. However, in line with previous reports showing an increase in rearing activity during test cage monitoring in mice treated with doxycycline[46], female $Mrpl54^{+/-}$ mice exhibited an increase in ambulatory activity along with elevated treadmill endurance when compared to WT. Like doxycycline-treated mice[15,46], we observed a lower VO_2 in adult female $Mrpl54^{+/-}$ mice, but this is likely explained by their reduced body weight[41], and not consistent with observations in male mice, or female mice at later time points.

We compared the life expectancy and lifespan in large cohorts of $Mrpl54^{+/-}$ and WT male and female mice. As a result of injury or death associated with male aggression, the male cohort was divided into individual-housed and group-housed cages. Male mice tended to experience stress associated with conspecific aggression under group housing conditions. Individually housed male $Mrpl54^{+/-}$ mice had better median life expectancy than male WT mice, while group-housed males

had no difference in median life expectancy between *Mrpl54*$^{+/-}$ and WT. Male C57BL/6 mice can be successfully housed together in low numbers[43]; however, it may be that the high level of conspecific aggression experienced in male group housing overcame any survival advantage afforded by the *Mrpl54*$^{+/-}$ genotype.

Finally, we observed neither a mitonuclear imbalance nor an induction of the UPR^{mt} in *Mrpl54*$^{+/-}$ mouse liver, a major metabolic organ. Within primary myoblasts, however, there was evidence of decreased OXPHOS protein expression, but no evidence of UPR^{mt} induction. It remains to be seen whether there is an induction of the UPR^{mt} in other *Mrpl54*$^{+/-}$ mouse tissues and organs, or in a temporal fashion – neither of which was captured in this study. Previous work demonstrated that reductions in MRP expression (through RNAi of *Mrp* genes, or inhibition of mitochondrial translation through doxycycline treatment) can increase health span and lifespan in *C. elegans* through a mitohormetic response[15]. Our work demonstrates that a reduction in *Mrpl54* expression in the germline may have implications in energy expenditure and activity levels in adult female mice, along with a potential increase in median and 24-month life expectancy of individual-housed male mice that are removed from the conspecific stress associated with group housing conditions. However, our findings also demonstrate that a reduction of *Mrpl54* is not sufficient to drive the induction of UPR^{mt} in mouse liver tissue or primary myoblasts, nor is it able to alter metabolism of older mice or affect lifespan.

It may be that reducing *Mrpl54* expression through the mammalian germline allows the mouse to adjust to lower MRPL54 protein levels through adaptations during developmental processes from embryogenesis onward – for example, genetic compensation where mutant mRNA degradation leads to transcriptional adaptation[48]. In other words, the levels of MRP expression are adjusted early in development to optimize mitochondrial output and maintain mitochondrial

protein homeostasis. Alternatively, our results may indicate that the level of mitochondrial translation stress instigated by the *Mrpl54*$^{+/-}$ genotype is not high enough to generate a mitonuclear imbalance, mito-cytosolic translational imbalance, or induce mitochondrial stress responses like the UPR^{mt} or ATF4-dependent signalling[15,21,22]. This explanation implies that any mitohormetic effect that affects metabolic health or lifespan requires a mitochondrial translational stress level above a specific threshold, and that this threshold was not met by the *Mrpl54*$^{+/-}$ model.

In conclusion, our results demonstrate that the reduction of *Mrpl54* expression through the mouse germline does not induce a mitonuclear protein imbalance or a subsequent UPR^{mt} response. Furthermore, reduction in *Mrpl54* expression does not result in an improved life expectancy or overall lifespan. We recommend that future work pursue the hypothesis of a minimum threshold of mitochondrial translational stress necessary to invoke a mitohormetic impact on metabolic health with age or lifespan. As well, since reduced *Mrpl54* expression in male mice may mitigate the lifespan effects of stressful housing conditions, we recommend that the *Mrpl54*$^{+/-}$ model be tested under various stress conditions, such as genotoxic or metabolic stress through a high fat diet.

15.5 Methods

15.5.1 Approval for animal experiments

All procedures for animal care and experimentation were performed according to protocol HS-2847, which was approved by the University of Ottawa Animal Care Committee, and following guidelines provided by the Canadian Council on Animal Care (CCAC). In addition, these procedures followed the guidelines provided by ARRIVE (Animals in Research: Reporting In Vivo Experiments).

15.5.2 Animal breeding

The Institute Clinique de la Souris (ICS) generated a *Mrpl54* constitutive knock-down mouse model on a C57BL/6N(Taconic) background (C57BL/6NTac-Mrpl54$^{tm1b(EUCOMM)Wtsi/IcsOrl}$; colony name ICS-EPD1076_5_A09)[49,50]. *Mrpl54*$^{+/-}$ breeding pairs were kept in ventilated racks and their progeny were housed in groups of 2-5 mice until their transfer to the metabolic health and longevity studies. Litter sizes were small (mean 4-5 pups) and production dropped off after the fourth litter. To generate the cohorts needed, CD1 host mothers were used for three rounds of *in vitro* fertilization, in addition to traditional breeding. At age 21-days, animals were weaned, ear-tagged, and tissue sampled from the ear for genotyping.

15.5.3 Genotyping

DNA for genotyping was extracted from the ear tissue sample according to the Phire Animal Direct PCR protocol (F-170, Thermo Scientific). Genotyping proceeded according to the ICS protocol (Forward primer Ef 4877 5'-GACCCACATAAGCAGGGAAGGAGATG-3', reverse primer L3r 4879 5'-CAATCTCCTGAGAATGTAGCCCACCAT-3', Invitrogen). The *Mrpl54* knock-out allele generated a 402 base-pair (bp) fragment, and the WT allele generated a 1095 bp fragment.

15.5.4 Animal husbandry

WT and *Mrpl54*$^{+/-}$ animals, separated by sex, were housed under a 12:12-hour light-dark cycle in a dedicated room set to 23°C (temperature and humidity were checked every 5 minutes using an automatic delta system; verified daily by staff). All mice were fed a standard chow diet (Envigo; Teklad Global 2018; 18.6% crude protein, 6.2% fat, 44.2% available carbohydrates). Female and male mice were initially housed 5-10 per cage in a ventilated rat cage (at least 90.4cm^2 per mouse) to reduce stress[51]. Male cages experienced aggression and fighting and the male mice

in cages that experienced injuries or deaths due to male-on-male aggression were reassigned to individual-housing. Animals in the metabolic health study were handled or weighed at least once per week. Animals in the longevity study were weighed once per month until age-related weight loss was observed, after which mice were weighed weekly or daily as needed.

15.5.5 RNA isolation and Real-time qPCR

For total RNA isolation, a small piece of snap frozen mouse tissue was placed in 1ml TRIzol (Sigma-Aldrich or Invitrogen). Samples were homogenized with a 5 mm steel bead using a TissueLyser II (Qiagen) for 3 min at a frequency of 30 Hz. RNA was isolated according to manufacturer's protocol. From 1 μg of extracted RNA, genomic DNA was eliminated with a gDNA Wipeout Buffer and subsequently reverse transcribed into cDNA using the QuantiTect Reverse Transcription Kit (Qiagen). The diluted cDNA was prepared with SYBR Green (Roche), and the quantitative gene expression was measured using the LightCycler 480 Instrument (Roche). The primer pairs used were as follows: *Mrpl54* forward 5'-AAAAAGCCAGTTGGCAAGGG-3', reverse 5'-ATGTGTGGTGAGCTGAGTGG-3'; *36B4* (acidic ribosomal phosphoprotein gene) forward 5′-ACGGGTACAAACGAGTCCTG-3′, reverse 5′-GCCTTGACCTTTTCAGCAAG-3′; and *B2m* (beta2 microglobulin) forward 5′-GGCTCACACTGAATTCACCC-3, 5′-GTCTCGATCCCAGTAGACGG-3′. To normalize tissue sample expression (threshold cycle [Ct] values) to the expression of housekeeping genes, the delta-delta Ct method was used. The geometric means of *36B4* and *B2m* genes were used to normalize *Mrpl54* tissue sample expression (delta Ct values) to the WT samples.

15.5.6 Metabolic Health Analyses

The metabolic health of male and female WT and *Mrpl54*$^{+/-}$ mice (n=7-17 in each group) were tested in three separate cohorts at 6-, 18-, and 24-months of age. The battery of tests started

with EchoMRI body composition (EchoMRI-700 Analyzer), followed by indirect calorimetry using the comprehensive laboratory animal monitoring system (CLAMS, Columbus Instruments), oral glucose tolerance, intraperitoneal insulin tolerance, endurance treadmill, cold tolerance, heart rate and blood pressure measurement (at 18- and 24-months), and then necropsy (Supplemental Fig. S1). Mice were allowed to recover 1-2 weeks between tests.

15.5.7 EchoMRI and Indirect Calorimetry

Each mouse was loaded into an A100 antenna insert and placed into the EchoMRI (EchoMRI-700 Analyzer) to determine body composition (whole-body, lean, and fat mass). Immediately afterward, mice were placed in individual CLAMS (Columbus Instruments Oxymax System) plexiglass cages for 48-72 hours (24-hours acclimation, followed by 24-48 hours of data collection). The ambient temperature was set to thermoneutrality (28°C) to gain an understanding of basal metabolism that mimicked human energy expenditure and to reduce thermogenic stress on mice housed individually without bedding or enrichment[52]. The light-dark cycle was 12:12. Mice had *ad libitum* access to water and powdered chow (Teklad 2018 Diet). At regular intervals (every 18-26 min), the following measurements were recorded: O_2 volume (VO_2), CO_2 volume (VCO_2), respiratory exchange ratio (RER), ambulatory and rearing motion, and the amount of food consumed in grams.

15.5.8 Oral Glucose Tolerance Test (OGTT)

Mice were fasted overnight for 16-hours prior to the OGTT. Whole-blood glucose levels were measured using the Accu-check Performa glucometer and accompanying strips (Roche Diagnostics, Canada). For the 6M cohort, mice were placed in a restraint tube during the blood sampling from the left lateral tail vein. For the 18M and 24M cohorts, mice remained unrestrained on the home-cage hopper during blood sampling. At time zero, freshly made 20% α-D-glucose

(Sigma-Aldrich PN158968) was orally administered using a flexible straight metal gavage at a dose of 1.0g per kg of body mass. Blood glucose was measured at baseline (prior to oral glucose dose), and at 15-, 30-, 45-, 60-, 90-, 120-, 150-, and 180-min post-gavage.

15.5.9 Intraperitoneal Insulin Tolerance Test (ipITT)

Two weeks prior to the ipITT, intraperitoneal insulin titrations were conducted on a subset of mice to determine the correct dose to elicit an insulin response. Mice were fasted in the morning for 5-6 hours prior to the ipITT. Whole-blood glucose levels were measured using the Accu-check Performa glucometer and accompanying strips (Roche Diagnostics, Canada). During blood sampling from the right lateral tail vein, mice remained unrestrained on their home-cage hopper. At time zero, mice received an intraperitoneal injection of insulin (NovoRapid Insulin aspart, 100U/mL, DIN 02245397). For the 6M cohort, females received an insulin dose of 1.5 U/kg body mass and males received 2.5 U/kg. For the 18M cohort, females received an insulin dose of 2 U/kg and males received 4.5 U/kg. For the 24M cohort, females received an insulin dose of 1 U/kg and males received 2 U/kg. Blood glucose was measured at baseline (prior to insulin injection), and at 15-, 30-, 45-, 60-, 75-, 90-, 105-, and 120-min post-injection. In the event the blood glucose level dropped below 2.0 mmol/L, emergency α-D-glucose (Sigma-Aldrich PN 158968) was orally administered at a dose of 1 g per kg of body mass.

15.5.10 Endurance Treadmill

Mice were acclimated to the treadmill (Exer-3/6, Columbus Instruments) over three consecutive days where they were placed on an unmoving belt for 5 min, then ran at a constant speed of 15 cm/s at an elevation of +5° with an electro-stimulus (0.1 mA, 1 Hz) applied to the resting grid. Those mice that achieved fewer than five electro-stimulations over 5 min by the third acclimation day were permitted to continue with the endurance test. The endurance test was

conducted the day following the last day of acclimation using the following profile – accelerate to 15 cm/s in 30 sec and then run at 15 cm/s for 12 min, accelerating +3.0 cm/s over 30 sec every 12 min[53]. Mice ran until the exhaustion criterion was met (5 electro-stimulus contacts [0.1 mA, 1 Hz] within 5 sec) at which point the electro-stimulus was stopped, and the running time and maximum speed attained were recorded.

15.5.11 Cold Tolerance

The baseline rectal temperature of each mouse was measured using a lubricated rectal thermometer at an insertion depth ~2 cm. Mice were placed in individual cages with access to fresh water and a plastic house, but without access to bedding or food, and then placed in a +4° C refrigerated room with all cages at the same height. Rectal temperature was measured every hour for up to 4-6 hours. If rectal temperature reached 25° C or below[54], the mouse was removed from the cold room and placed in a 37° C incubator with access to food and water.

15.5.12 Heart Rate & Blood Pressure

Mice in the 18M and 24M cohorts were acclimated to the blood pressure and heart rate monitoring equipment (BP-2000-M-6 Series II Blood Pressure Analysis System, Visitech Systems) over a period of 3-5 days[55]. The procedure for acclimation and testing was the same – mice were individually placed in an opaque mouse holder on a warmed 36° C plate with the tail pulled through an inflatable tail cuff. Mice rested in position for 5 min, followed by five preliminary readings and then 10 actual readings. The program parameters were as follows: 2.5-sec pause between readings, 10-sec analysis pulse, system maximum set to 170 mmHg. Test day immediately followed the last day of successful acclimation, where blood pressure was recorded for at least 6 out of 10 readings. The outcomes recorded were diastolic blood pressure, systolic blood pressure, and heart rate.

15.5.13 EchoMRI & Necropsy

The day before the necropsy, body composition was determined using the EchoMRI-700 as described above. The mice were fasted overnight for 10-12 hours and then refed 1-2 hours before the necropsy. Mice were euthanized through injection with ketamine/xylazine cocktail (0.1 mg/kg body weight) followed by exsanguination through cardiac puncture. The following tissues and organs were collected, weighed, fast-frozen in liquid N_2 and then stored at -80° C for further analysis: pancreas, spleen, diaphragm, heart, liver, kidneys, quadriceps, gastrocnemius, soleus, tibialis anterior, and brain[56]. For the 24-month cohort necropsy, the right kidney, quadriceps, and gastrocnemius/soleus were suspended in Optimal Cutting Temperature fixative (Fisher Health Care, Cat# 4585) and placed on dry ice (kidney) or in isopentane (Sigma, CAT# 1003301470) supercooled in liquid N_2 (muscles), then stored at -80°C for further analysis.

15.5.14 Longevity Study and Growth

Male and female WT and *Mrpl54*$^{+/-}$ mice (n=80-112 per group) were initially group-housed 5-10 per cage (at least 100 cm^2 per mouse). Male cages experienced aggression and fighting from age 3-months onward. In case of a fight-related injury or death, the males were reassigned to individual cages to improve animal welfare. Mice were weighed monthly, and median life expectancy (50% survival time point), 24-month life expectancy (all mice alive at 24 months were censored), and maximum lifespan (lifespan of top 10% of surviving animals) were calculated. Where a human-endpoint (HEP) was identified and time-permitting, mice were necropsied to identify tumour burden and to collect tissue and plasma for future analysis. HEPs included (a) >15% weight loss over 2 weeks, (b) skin lesions not responding to treatment, (c) head tilt/rolling or loss of balance, (d) ulcerated or bulging eye, (e) ulcerated mass, (f) respiratory distress, (g) inability to express bladder, or (h) a distended abdomen or growing internal mass[51]. Mice that were

euthanized because of ulcerative dermatitis that did not respond to treatment (a C57BL/6 strain-specific condition[57]), or because of an unacceptable pain level from an ulcerated or bulging eye, were censored from the longevity analysis.

To assess growth over time, the body mass of WT and *Mrpl54*$^{+/-}$ male and female animals were weighed monthly. Animals destined for the 6-, 18-, and 24-month metabolic health analyses were included in the growth analysis, up until the month they entered the metabolic health study.

15.5.15 Respiration of Isolated Liver Mitochondria

7-week-old male WT and *Mrpl54*$^{+/-}$ mice were fasted overnight for 12 hours, killed by cervical dislocation, and their livers weighed then rapidly dissected directly into ice-cold isolation buffer (300 mM D-sucrose, 10 mM Tris-HCl, 1 mM EGTA-Tris Base; pH 7.2)[58]. The suspension was homogenized in a 15 mL Potter-Elvehjem homogenizer, and the supernatant centrifuged twice at 1000*g* for 10 min at 4° C (Sorvall RC-6 Plus Centrifuge, Thermo Scientific). The supernatant was centrifuged 8000*g* for 10 min at 4° C and then aspirated without disturbing the pellet. The pellet was gently resuspended in ice-cold suspension buffer (300 mM D-sucrose, 10 mM Tris-HCl, 0.05 mM EGTA-Tris Base; pH 7.2) and centrifuged at 8000*g* for 10 min at 4° C. The final pellet was gently re-suspended in 300 µL suspension buffer and kept on ice.

The respiratory function of isolated liver mitochondria was measured using a Clark-type electrode (Oxygraph System, Hansatech Instruments Ltd.). The chambers were calibrated at 23° C with continuous stirring with a PTFE-coated magnetic follower bar. The mitochondrial suspension was quantified (Bio-Rad DC Protein Assay, BMG Labtech POLARstar Omega plate reader) and then suspended in miR05 respiration buffer (110 mM D-sucrose, 60 mM lactobionic acid, 20 mM taurine, 20 mM HEPES, 10 mM KH2PO4, 3 mM MgCl2, 0.5 mM EGTA, 1 g/L fatty-acid free BSA; pH 7.1 at 23° C)[59] at 0.5 mg protein/mL. The function of isolated liver

mitochondria was examined at less than 37°C to prolong mitochondrial activity and maximize the duration of the experiment, such that O_2 did not become rate-limiting[60]. Following a baseline recording, O_2 consumption rate was measured following sequential additions of: 1) glutamate + malate (G/M, 5:2.5 mM) to give Complex I (CI)-driven State 2 respiration, 2) ADP (2 mM) to give CI-driven State 3 respiration, 3) Amytal (2 mM) to inhibit CI, 4) succinate (10 mM) to give Complex II (CII)-driven State 3 respiration, 5) carbonyl cyanide m-chlorophenylhydrazone (CCCP) titrations to decouple OXPHOS until maximum respiration was reached (0.01-0.05 µM); 6) antimycin-A (8 µM) to inhibit Complex III (CIII); 7) N,N,N',N'-Tetramethyl-p-phenylenediamine dihydrochloride (TMPD) + ascorbate (5:0.3 mM) to test Complex IV (CIV) respiration; and finally 8) KCN (0.6 mM) to inhibit CIV.

15.5.16 Mass Spectrometry (MS)-based Proteomics

Crude mitochondria were isolated from the livers of WT (n=3) and *Mrpl54*$^{+/-}$ (n=3) male mice, as described above, and then purified using 30% Percoll gradient ultracentrifugation at 95,000*g* for 30 min at +4° C (Beckman sv41 rotor). Purified mitochondria were treated 1:200 with a protease inhibitor cocktail (Thermo Fisher Scientific HALT PI) then the mitochondrial proteins were left to precipitate overnight in precipitation buffer (50% acetone, 49.9% ethanol, 0.1% acetic acid). Proteins were suspended in 50 mM ammonium bicarbonate in 8 M urea and then quantified (Bio-Rad DC Protein Assay, BMG Labtech POLARstar Omega plate reader). To reduce disulphide bonds, 140 µg of mitochondrial protein was incubated with 1:100 of 1 M dithiothreitol (Sigma-Aldrich, SKU 43815), followed by 1:50 dark incubation in 1 M iodoacetamide (Sigma-Aldrich, SKU I1149). The urea concentration was reduced to <2 M and the protein sample was digested overnight at 37° C with 1:100 Trypsin Gold (Promega V5280). The following day, the digested proteins were passed through a Sep-Pak Vac 1 cc tC18 cartridge (Waters, WAT054960)

to rid the sample of salts and contaminants. The sample was dried in a Savant DNA120 SpeedVac Concentrator (Thermo Electron Corporation) at room temperature and analysed using a nano-LC-MS/MS with an Orbitrap Elite mass spectrometer (Thermo Fisher Scientific) coupled to an ultraperformance LC system (Ultimate 3000 RSLC; Thermo Fisher Scientific). Data analysis was performed with Proteome Discoverer (version 1.3), and searches were performed with Mascot and Sequest against a mouse database (UniProt). Data were further processed, inspected, and visualized with Scaffold 4 (Proteome Software).

15.5.17 Generation of Primary Myoblasts

Hind limb skeletal muscles were excised from euthanized 7-week-old male WT (n=3) and *Mrpl54*$^{+/-}$ (n=3) mice. Under aseptic conditions, the muscles were rinsed in phosphate buffered solution (PBS, Wisent Inc., Cat# 311-010-CL), the fat excised, and the remaining muscle tissue placed in collagenase B-dispase solution, 1.5 mL per 0.5 g tissue (4 mg/mL dispase II [Sigma D4693], 10 mg/mL collagenase B [Roche 11088831001] in Hams-F10 [Multicell, Wisent Inc. Cat# 318 050-CL]). The tissue was mulched with a razor blade, incubated at 37° C for 30 min, and then homogenized through trituration until smooth. The homogenate was passed through a 100-micron cell strainer with PBS washes. The muscle cells were centrifuged at 300*g* for 5 min and the cell pellet resuspended in Ham's Complete growth medium (4% bovine calf serum [cytiva, Cat# SH30077.03], 1% penicillin and streptomycin [gibco by Life Technologies, Cat# 15140122], 2.5 ng/µL human basic fibroblast growth factor [bFGF, Stemcell, Cat# 78003]). To rid the culture of fibroblasts, the cells were allowed to rest on a non-collagen-coated plate for two hours at 37° C before plating onto a 10 cm collagen-coated plate. To enrich myoblasts, 80% confluent plates were pre-plated on non-collagen-coated plates for one hour before plating on a collagen-coated plate.

15.5.18 Western Blotting

Protein was extracted by suspending isolated WT and *Mrpl54*$^{+/-}$ liver mitochondria or primary myoblast cells (10 cm plates at 80% confluence) in radioimmunoprecipitation (RIPA) lysis buffer (50 mM Tris HCl, 150 mM NaCl, 1% v/v Triton X-100, 0.5% w/v sodium deoxycholate, 0.1% w/v SDS; pH 8.0) augmented with protease and phosphatase inhibitors (1:100 HALT PI cocktail, Thermofisher Sci Cat# 78440; or Roche cOmplete ULTRA [Cat# 05892970001] plus phosStop [Cat# 4906845001] tablets), then flash frozen in liquid N_2. The solution was centrifuged 16,000*g* for 10 min at 4°C and the supernatant containing the mitochondrial or cell lysate proteins quantified (Bio-Rad DC Protein Assay, BMG Labtech POLARstar Omega plate reader).

Protein samples were diluted to 1 µg/µL in Laemmli Buffer (Bio-Rad Cat# 1610737) augmented with 10% β-mercaptoethanol (Fisher Bioreagents, BP176-100) and run on a 10% SDS-PAGE using the TGX Stain-free FastCast Acrylamide Kit (Bio-Rad Cat# 1610183) and the Mini-PROTEAN system (Bio-Rad Cat# 1658006). SDS-PAGE was run at a constant 90 volts across the gel for 30 min and then 120 volts for 50-60 min in a 4° C cold room. The StainFree gels were activated once for 45 sec using a ChemiDoc Touch Imaging System (Bio-Rad) and then the proteins transferred to TransBlot Turbo Mini size 0.2 µm nitrocellulose membrane (Bio-Rad) using the Trans-Blot TurboTransfer System (Bio-Rad Cat# 1704150EDU).

The nitrocellulose membrane was imaged for total protein and then blocked for one hour in blocking buffer (5% w/v bovine serum albumin [Sigma, SKU A7906] in TBS-T buffer [50 mM Tris-HCl, pH 7.6; 150 mM NaCl; 0.1% Tween]), rocking gently at room temperature. Membranes were then incubated with primary antibody diluted in TBS-T buffer (1:1000 Total OXPHOS Rodent WB Antibody Cocktail [abcam Cat# ab110413] or 1:1000 HSP60 XP Rabbit mAB [Cell

Signaling Technology CAT#12165]) overnight at 4°C with gentle rocking. After three washes with TBS-T, the membrane was incubated for one hour with the matching IgG, horseradish peroxidase (HRP)-conjugated secondary antibody (1:10,000 Cell Signaling Technology Anti-rodent Cat# 7076, or Anti-rabbit Cat# 7074P2), rocking at room temperature. After three washes in TBS-T, the membrane was visualized using enhanced chemiluminescent detection (BioRad Clarity Cat# 1705061) on the ChemiDoc Touch Imaging System (Bio-Rad).

To semi-quantify the protein levels in the western blot analyses, dilutions of protein were first loaded onto an SDS-PAGE to determine the linear range of protein concentrations. Protein concentrations within the linear range were chosen for subsequent semi-quantitative SDS-PAGE, where the selected protein band was normalized to total loaded protein and analysed using Image Lab Software (Bio-Rad).

15.5.19 Statistical Analysis

All data are presented as mean ± SEM, unless otherwise stated. Differences between two groups were assessed using two-tailed t-tests. Analysis of covariance (ANCOVA) was used to eliminate unwanted variance on the dependent variable. To compare the interaction between time and treatment, a two-way analysis of variance (ANOVA) tests was performed. Survival curves were analysed using the Kaplan-Meier method. Hazard ratios were calculated using the Log rank test. GraphPad Prism 9.4.1 (GraphPad Software, Inc.) was used for all statistical analyses, and $p<0.05$ was considered significant.

15.6 References

1 Harman, D. Aging: A Theory Based on Free Radical and Radiation Chemistry. *Journal of Gerontology* **11**, 298-300 (1956). https://doi.org:10.1093/geronj/11.3.298

2 Harman, D. The Biologic Clock: The Mitochondria? *Journal of the American Geriatrics Society* **20**, 145-147 (1972). https://doi.org:10.1111/j.1532-5415.1972.tb00787.x

3 Gruber, J., Schaffer, S. & Halliwell, B. The mitochondrial free radical theory of ageing-where do we stand? *Frontiers in Bioscience-Landmark* **13**, 6554-6579 (2008). https://doi.org:10.2741/3174

4 Balaban, R. S., Nemoto, S. & Finkel, T. Mitochondria, Oxidants, and Aging. *Cell* **120**, 483-495 (2005). https://doi.org:10.1016/j.cell.2005.02.001

5 López-Otín, C., Blasco, M. A., Partridge, L., Serrano, M. & Kroemer, G. The Hallmarks of Aging. *Cell* **153**, 1194-1217 (2013). https://doi.org:10.1016/j.cell.2013.05.039

6 López-Otín, C. & Kroemer, G. Hallmarks of Health. *Cell* **184**, 33-63 (2021). https://doi.org:10.1016/j.cell.2020.11.034

7 Joseph, A.-M. *et al.* The impact of aging on mitochondrial function and biogenesis pathways in skeletal muscle of sedentary high- and low-functioning elderly individuals. *Aging Cell* **11**, 801-809 (2012). https://doi.org:10.1111/j.1474-9726.2012.00844.x

8 Andreux, P. A. *et al.* Mitochondrial function is impaired in the skeletal muscle of pre-frail elderly. *Sci. Rep.* **8** (2018). https://doi.org:10.1038/s41598-018-26944-x

9 Sonjak, V. *et al.* Reduced Mitochondrial Content, Elevated Reactive Oxygen Species, and Modulation by Denervation in Skeletal Muscle of Prefrail or Frail Elderly Women. *The Journals of Gerontology: Series A* **74**, 1887-1895 (2019). https://doi.org:10.1093/gerona/glz066

10 Kelley, D. E., He, J., Menshikova, E. V. & Ritov, V. B. Dysfunction of mitochondria in human skeletal muscle in type 2 diabetes. *Diabetes* **51**, 2944-2950 (2002).

11 Boudina, S. *et al.* Mitochondrial Energetics in the Heart in Obesity-Related Diabetes. *Diabetes* **56**, 2457-2466 (2007). https://doi.org:10.2337/db07-0481

12 Wallace, D. C. Mitochondria and cancer. *Nature Reviews Cancer* **12**, 685-698 (2012). https://doi.org:10.1038/nrc3365

13 Ferrucci, L. & Zampino, M. A mitochondrial root to accelerated ageing and frailty. *Nature Reviews Endocrinology* **16**, 133-134 (2020). https://doi.org:10.1038/s41574-020-0319-y

14 Zimmermann, A., Madreiter-Sokolowski, C., Stryeck, S. & Abdellatif, M. Targeting the Mitochondria-Proteostasis Axis to Delay Aging. *Frontiers in Cell and Developmental Biology* **9** (2021). https://doi.org:10.3389/fcell.2021.656201

15 Houtkooper, R. H. *et al.* Mitonuclear protein imbalance as a conserved longevity mechanism. *Nature* **497**, 451-457 (2013). https://doi.org:10.1038/nature12188

16 Owusu-Ansah, E., Song, W. & Perrimon, N. Muscle Mitohormesis Promotes Longevity via Systemic Repression of Insulin Signaling. *Cell* **155**, 699-712 (2013). https://doi.org:10.1016/j.cell.2013.09.021

17 Cox, C. S. *et al.* Mitohormesis in Mice via Sustained Basal Activation of Mitochondrial and Antioxidant Signaling. *Cell Metab.* **28**, 776-786.e775 (2018). https://doi.org:10.1016/j.cmet.2018.07.011

18 Kang, G. M. *et al.* Mitohormesis in Hypothalamic POMC Neurons Mediates Regular Exercise-Induced High-Turnover Metabolism. *Cell Metab.* **33**, 334-349.e336 (2021). https://doi.org:10.1016/j.cmet.2021.01.003

19 Tapia, A. *et al.* Mild Muscle Mitochondrial Fusion Distress Extends Drosophila Lifespan through an Early and Systemic Metabolome Reorganization. *Int. J. Mol. Sci.* **22** (2021). https://doi.org:10.3390/ijms222212133

20 Tapia, P. C. Sublethal mitochondrial stress with an attendant stoichiometric augmentation of reactive oxygen species may precipitate many of the beneficial alterations in cellular physiology produced by caloric restriction, intermittent fasting, exercise and dietary phytonutrients: "Mitohormesis" for health and vitality. *Med. Hypotheses* **66**, 832-843 (2006). https://doi.org:10.1016/j.mehy.2005.09.009

21 Molenaars, M. *et al.* A Conserved Mito-Cytosolic Translational Balance Links Two Longevity Pathways. *Cell Metab.* **31**, 549-563.e547 (2020). https://doi.org:10.1016/j.cmet.2020.01.011

22 Liu, Y. J. *et al.* Mitochondrial translation and dynamics synergistically extend lifespan in C. elegans through HLH-30. *J. Cell Biol.* **219** (2020). https://doi.org:10.1083/jcb.201907067

23 Amunts, A., Brown, A., Toots, J., Scheres, S. H. W. & Ramakrishnan, V. The structure of the human mitochondrial ribosome. *Science* **348**, 95-98 (2015).

24 Yoneda, T. *et al.* Compartment-specific perturbation of protein handling activates genes encoding mitochondrial chaperones. *Journal of Cell Science* **117**, 4055-4066 (2004). https://doi.org:10.1242/jcs.01275

25 Durieux, J., Wolff, S. & Dillin, A. The Cell-Non-Autonomous Nature of Electron Transport Chain-Mediated Longevity. *Cell* **144**, 79-91 (2011). https://doi.org:10.1016/j.cell.2010.12.016

26 Shpilka, T. *et al.* UPRmt scales mitochondrial network expansion with protein synthesis via mitochondrial import in Caenorhabditis elegans. *Nature Communications* **12** (2021). https://doi.org:10.1038/s41467-020-20784-y

27 Taylor, B. A., Heiniger, H. J. & Meier, H. Genetic analysis of resistance to cadmium-induced testicular damage in mice. *Proc Soc Exp Biol Med* **143**, 629-633 (1973). https://doi.org:10.3181/00379727-143-37380

28 Ashbrook, D. G. *et al.* A platform for experimental precision medicine: The extended BXD mouse family. *Cell Syst.* **12**, 235-247.e239 (2021). https://doi.org:10.1016/j.cels.2020.12.002

29 Ozkurede, U. & Miller, R. A. Improved mitochondrial stress response in long-lived Snell dwarf mice. *Aging Cell* **18** (2019). https://doi.org:10.1111/acel.13030

30 Braga, R. R. *et al.* Exercise alters the mitochondrial proteostasis and induces the mitonuclear imbalance and UPRmt in the hypothalamus of mice. *Sci. Rep.* **11** (2021). https://doi.org:10.1038/s41598-021-82352-8

31 Holbrook, M. A. & Menninger, J. R. Erythromycin Slows Aging of *Saccharomyces cerevisiae*. *Journal of Gerontology: Biological Sciences* **57A**, B29-B36 (2002).

32 Caballero, A. *et al.* Absence of Mitochondrial Translation Control Proteins Extends Life Span by Activating Sirtuin-Dependent Silencing. *Molecular Cell* **42**, 390-400 (2011). https://doi.org:10.1016/j.molcel.2011.03.021

33 Jeong, D. E. *et al.* Mitochondrial chaperone HSP-60 regulates anti-bacterial immunity via p38 MAP kinase signaling. *The EMBO Journal* **36**, 1046-1065 (2017). https://doi.org:10.15252/embj.201694781

34 Silva, J. *et al.* EXD2 governs germ stem cell homeostasis and lifespan by promoting mitoribosome integrity and translation. *Nature Cell Biology* **20**, 162-174 (2018). https://doi.org:10.1038/s41556-017-0016-9

35 Snell, T. W. *et al.* Repurposed FDA-approved drugs targeting genes influencing aging can extend lifespan and healthspan in rotifers. *Biogerontology* **19**, 145-157 (2018). https://doi.org:10.1007/s10522-018-9745-9

36 Koc, E. C. *et al.* The Large Subunit of the Mammalian Mitochondrial Ribosome. *Journal of Biological Chemistry* **276**, 43958-43969 (2001). https://doi.org:10.1074/jbc.m106510200

37 Diaconu, M. *et al.* Structural Basis for the Function of the Ribosomal L7/12 Stalk in Factor Binding and GTPase Activation. *Cell* **121**, 991-1004 (2005). https://doi.org:10.1016/j.cell.2005.04.015

38 Aibara, S., Singh, V., Modelska, A. & Amunts, A. Structural basis of mitochondrial translation. *eLife* **9** (2020). https://doi.org:10.7554/elife.58362

39 Arroyo, J. D. *et al.* A Genome-wide CRISPR Death Screen Identifies Genes Essential for Oxidative Phosphorylation. *Cell Metab.* **24**, 875-885 (2016). https://doi.org:10.1016/j.cmet.2016.08.017

40 Cheong, A., Lingutla, R. & Mager, J. Expression analysis of mammalian mitochondrial ribosomal protein genes. *Gene Expression Patterns* **38** (2020). https://doi.org:10.1016/j.gep.2020.119147

41 Müller, T. D., Klingenspor, M. & Tschöp, M. H. Revisiting energy expenditure: how to correct mouse metabolic rate for body mass. *Nature Meta.* **3**, 1134-1136 (2021). https://doi.org:10.1038/s42255-021-00451-2

42 Hagan, C. *When Are Mice Considered Old?*, <https://www.jax.org/news-and-insights/jax-blog/2017/november/when-are-mice-considered-old> (2017).

43 Melotti, L. *et al.* Can live with 'em, can live without 'em: Pair housed male C57BL/6J mice show low aggression and increasing sociopositive interactions with age, but can adapt to single housing if separated. *Applied Animal Behaviour Science* **214**, 79-88 (2019). https://doi.org:https://doi.org/10.1016/j.applanim.2019.03.010

44 Aldridge, J. E., Horibe, T. & Hoogenraad, N. J. Discovery of Genes Activated by the Mitochondrial Unfolded Protein Response (mtUPR) and Cognate Promoter Elements. *PLoS ONE* **2**, e874 (2007). https://doi.org:10.1371/journal.pone.0000874

45 Wodrich, A. P. K., Scott, A. W., Shukla, A. K., Harris, B. T. & Giniger, E. The Unfolded Protein Responses in Health, Aging, and Neurodegeneration: Recent Advances and Future Considerations. *Front Mol Neurosci* **15**, 831116 (2022). https://doi.org:10.3389/fnmol.2022.831116

46 Moullan, N. *et al.* Tetracyclines Disturb Mitochondrial Function across Eukaryotic Models: A Call for Caution in Biomedical Research. *Cell Rep.* **10**, 1681-1691 (2015). https://doi.org:https://doi.org/10.1016/j.celrep.2015.02.034

47 Dijk, S. N., Protasoni, M., Elpidorou, M., Kroon, A. M. & Taanman, J.-W. Mitochondria as target to inhibit proliferation and induce apoptosis of cancer cells: the effects of doxycycline and gemcitabine. *Sci. Rep.* **10** (2020). https://doi.org:10.1038/s41598-020-61381-9

48 El-Brolosy, M. A. *et al.* Genetic compensation triggered by mutant mRNA degradation. *Nature* **568**, 193-197 (2019). https://doi.org:10.1038/s41586-019-1064-z

49 Codner, G. F. *et al.* Universal Southern blot protocol with cold or radioactive probes for the validation of alleles obtained by homologous recombination. *Methods* **191**, 59-67 (2021). https://doi.org:https://doi.org/10.1016/j.ymeth.2020.06.011

50 Birling, M.-C., Dierich, A., Jacquot, S., Hérault, Y. & Pavlovic, G. Highly-efficient, fluorescent, locus directed cre and FlpO deleter mice on a pure C57BL/6N genetic background. *genesis* **50**, 482-489 (2012). https://doi.org:10.1002/dvg.20826

51 Godbey, T. G., R.; Heon, H.; Turner, P.; St-Arnaud, R.; Smith, E. Canadian Council on Animal Care Guidelines: MIce. (Ottawa, Ontario, 2019).

52 Keijer, J., Li, M. & Speakman, J. R. What is the best housing temperature to translate mouse experiments to humans? *Mol. Metab.* **25**, 168-176 (2019). https://doi.org:https://doi.org/10.1016/j.molmet.2019.04.001

53 Marcaletti, S., Thomas, C. & Feige, J. N. Exercise Performance Tests in Mice. *Current protocols in mouse biology* **1** (2011). https://doi.org:10.1002/9780470942390.MO100160

54 Argmann, C. A., Champy, M. F. & Auwerx, J. Evaluation of Energy Homeostasis. *Current Protocols in Molecular Biology* **73**, 29B.21.21-29B.21.21 (2006). https://doi.org:10.1002/0471142727.mb29b01s73

55 Krege, J. H., Hodgin, J. B., Hagaman, J. R. & Smithies, O. A noninvasive computerized tail-cuff system for measuring blood pressure in mice. *Hypertension* **25**, 1111-1115 (1995). https://doi.org:10.1161/01.HYP.25.5.1111

56 Parkinson, C. M. *et al.* Diagnostic Necropsy and Selected Tissue and Sample Collection in Rats and Mice. *Journal of Visualized Experiments : JoVE*, 2966-2966 (2011). https://doi.org:10.3791/2966

57 Hampton, A. L. *et al.* Progression of ulcerative dermatitis lesions in C57BL/6Crl mice and the development of a scoring system for dermatitis lesions. *J Am Assoc Lab Anim Sci* **51**, 586-593 (2012).

58 Cuillerier, A. *et al.* Loss of hepatic LRPPRC alters mitochondrial bioenergetics, regulation of permeability transition and trans-membrane ROS diffusion. *Human Molecular Genetics* **26**, 3186-3201 (2017). https://doi.org:10.1093/hmg/ddx202

59 Gnaiger, E. C., C.; Cardoso, L.H.D. Mitochondrial respiration medium: MiR05-Kit. *Mitochondrial Physiology Network* **22.10**, 1-3 (2022).

60 Long, Q., Huang, L., Huang, K. & Yang, Q. in *Methods in Molecular Biology* 237-246 (Springer New York, 2019).

61 *Mouse Genome Database (MGD) at the Mouse Genome Informatics website*, <http://www.informatics.jax.org/mgihome/nomen/IKMC_schematics.shtml> (2022).

15.7 Acknowledgements

We thank the Institut Clinique de la Souris – PHENOMIN for the establishment of the *Mrpl54* mouse mutant line. From the University of Ottawa, we thank the following people: Adriana Gambarotta for her IVF expertise; Dr. Kerstin Ure, Mirela Barclay, and Sarah Kealey from the Behavioural Core Unit for help with CLAMS; the staff at the Animal Care and Veterinary Services Unit, in particular Courtney Reeks and Christine Kitchen, for help in mouse-handling training and colony maintenance assistance; and Prof. Daniel Figeys for mass spectrophotometry proteomics collaboration (NorthOmics).

This project was financially supported by the following: CIHR grant (MOP 159455), NSERC Collaborative Research and Training Experience program grant (RGPIN 2018-06838), and NSERC Discovery grant (DGECR 2018-00012) to K.J.M.; VIDI grant (917.15.305) to R.H.H., NSERC CGS-D scholarship awarded to K.R., UvA Lustrum 385 grant to E.G.D., and uOttawa Brain and Mind Research Institute Eric Poulain Centre for Neuromuscular Disease Scholarship in Translational Research awarded to A.E.G.

15.8 Data Availability

The datasets generated during and/or analysed during the current study are available from the corresponding author on reasonable request.

15.9 Author Contributions

Conception of hypotheses: R.H.H. Design of the work: R.H.H., K.J.M., K.R., and E.G.D. Acquisition of the data: K.R., E.G.D., R.K., G.E.J., M.H., and G.V. Analysis and interpretation of the data: K.R., E.G.D., G.V., R.K., G.E.J., M.H., A.E.G., K.J.M. and R.H.H. Drafting of the manuscript and figures: K.R. and K.J.M. All authors approved the final version of the manuscript.

15.10 Declaration of Competing Interests

The author(s) declare no competing interests.

15.11 Supplemental Figures

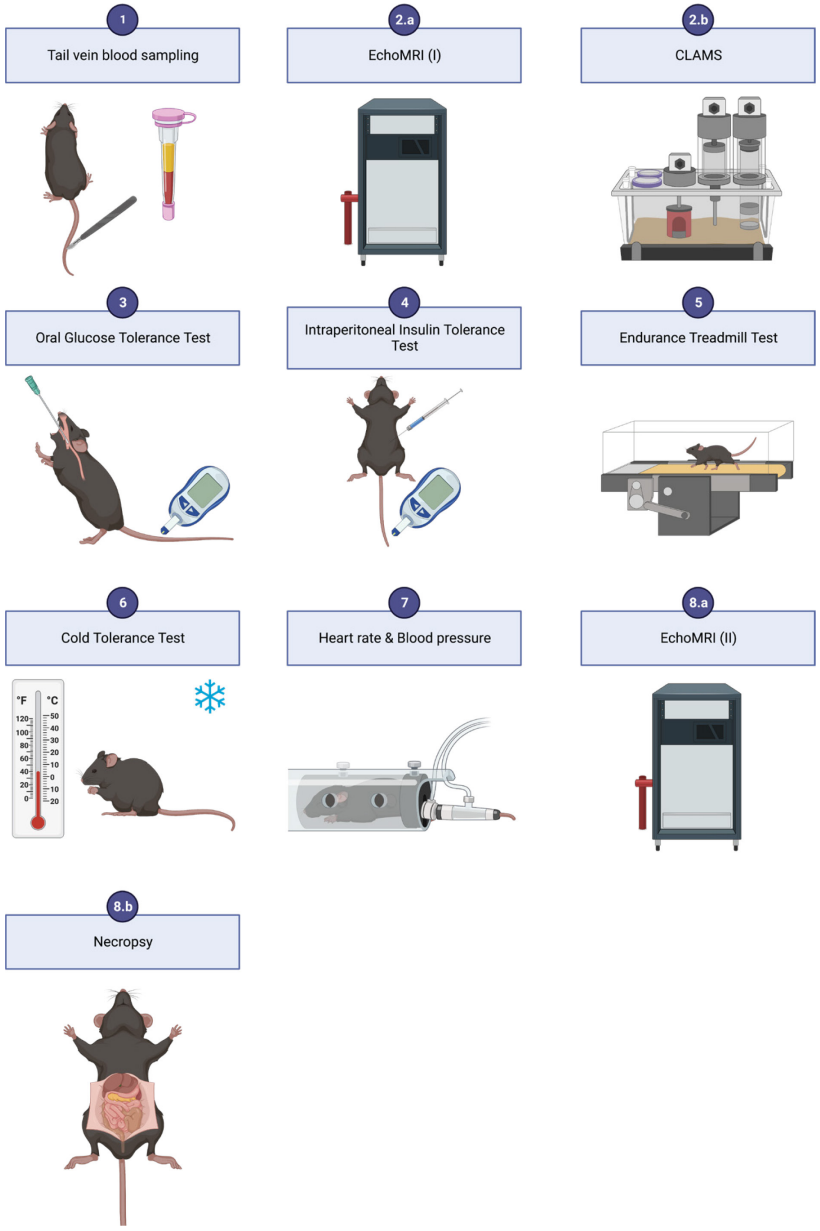

Figure 15.7 Supplemental: Protocol and timeline for metabolic phenotyping of *Mrpl54*$^{+/-}$ and WT mouse cohorts

Metabolic phenotyping in 6-, 18-, and 24-month male and female cohorts began with an assessment of body composition (EchoMRI) followed by 24-48-hour measurement of VO_2, RER, and ambulatory motion (CLAMS). Each cohort was then assessed using the following tests with 1-2 weeks between each test, in order: blood glucose tolerance (OGTT), intraperitoneal insulin tolerance (ipITT), cold challenge (4°C), heart rate and blood pressure monitoring (18M and 24M only), and endurance treadmill, ending with a necropsy and tissue, organ, and plasma collection. Images were created with BioRender.com.

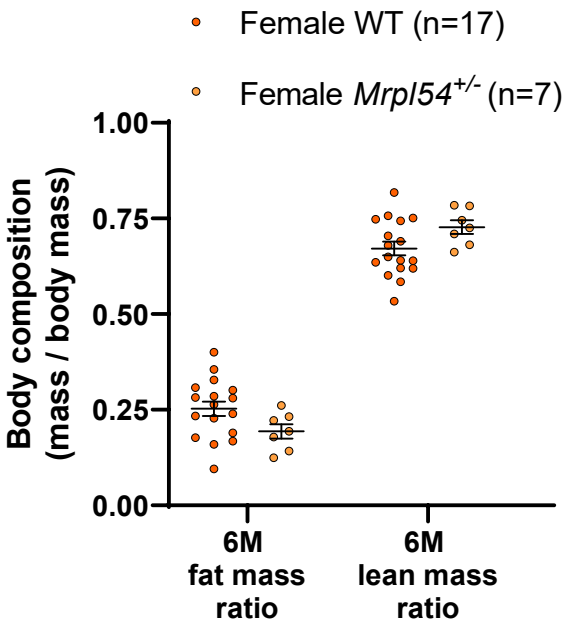

Figure 15.8 Supplemental: 6M *Mrpl54*$^{+/-}$ and WT female body composition as a function of body mass

No difference in body composition as function of body mass between 6M female *Mrpl54*$^{+/-}$ and WT mice. Graphs show mean ± SEM; female WT (orange); and female *Mrpl54*$^{+/-}$ (light orange).

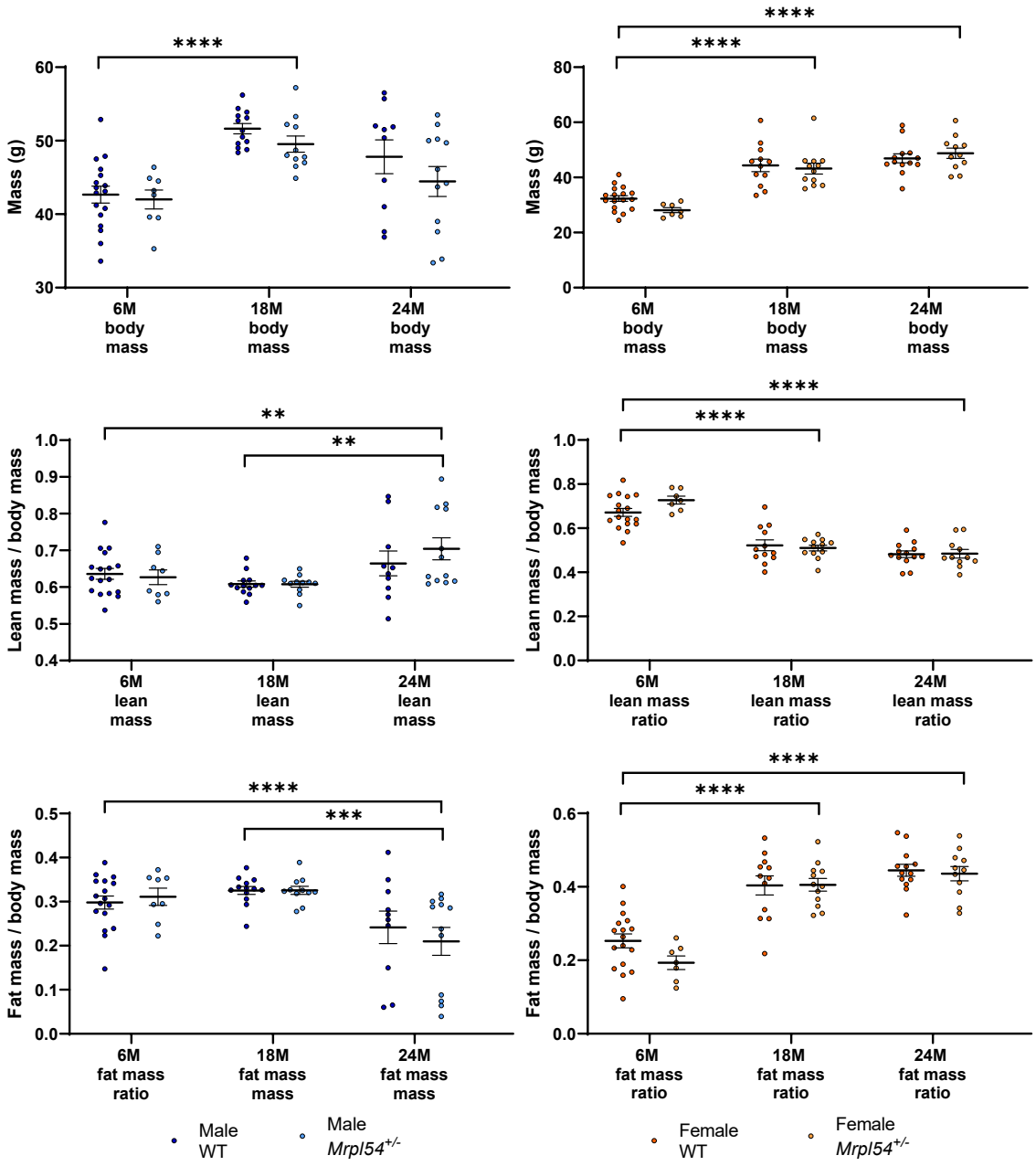

Figure 15.9 Supplemental: *Mrpl54*$^{+/-}$ and WT body composition at age 6M, 18M, & 24M

Body composition (g) by EchoMRI with increasing age for both male and female *Mrpl54*$^{+/-}$ and WT mice. Graphs show mean ± SEM; male WT (blue); male *Mrpl54*$^{+/-}$ (light blue); female WT (orange); and female *Mrpl54*$^{+/-}$ (light orange). **P ≤ 0.01, ***P ≤ 0.001, and ****P ≤ 0.0001

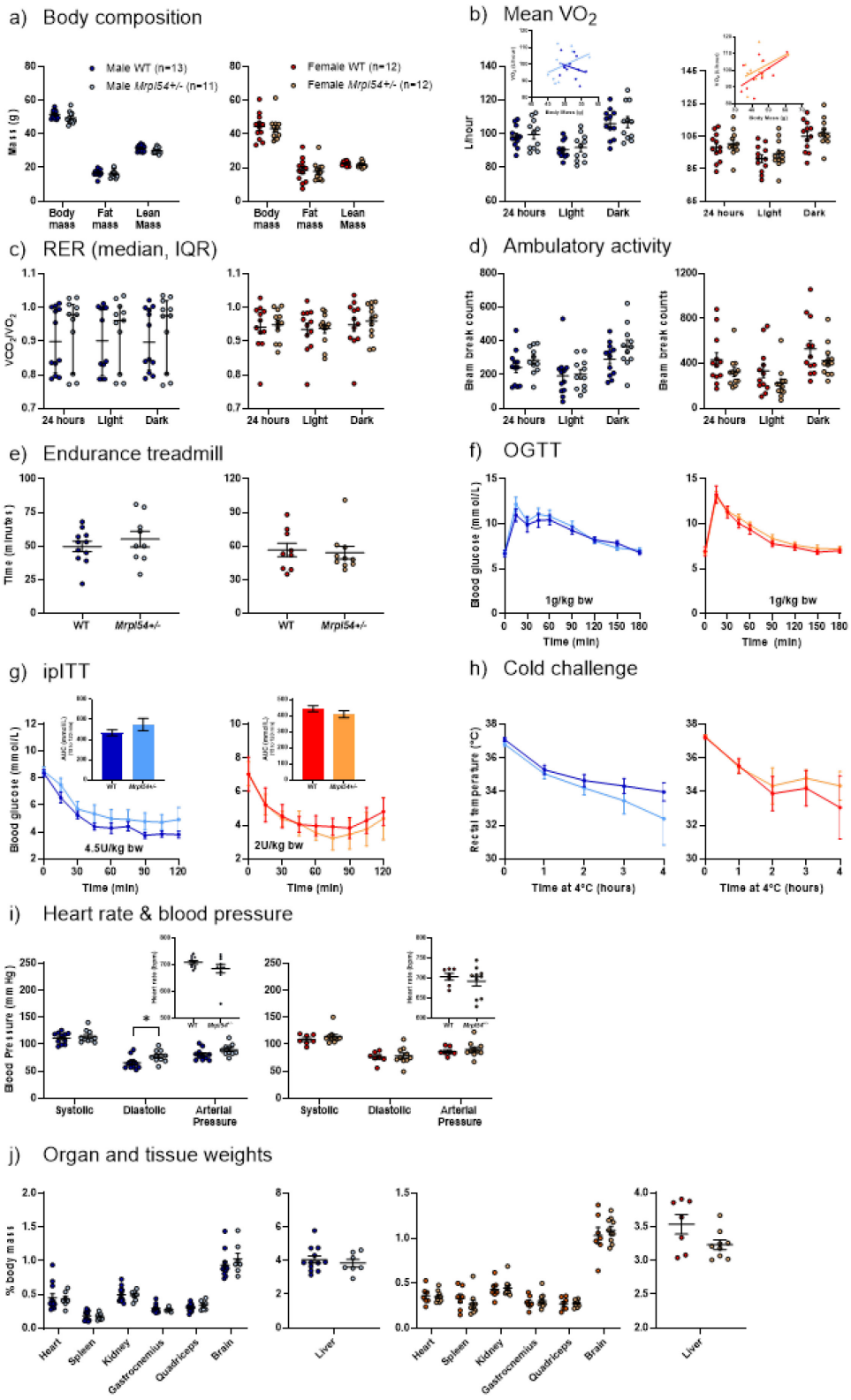
a) Body composition
Male WT (n=13)
Male Mrpl54+/- (n=11)
Female WT (n=12)
Female Mrpl54+/- (n=12)
Mass (g)
Body mass
Fat mass
Lean Mass
b) Mean VO2
L/hour
24 hours
Light
Dark
c) RER (median, IQR)
VCO2/VO2
d) Ambulatory activity
Beam break counts
e) Endurance treadmill
Time (minutes)
WT
Mrpl54+/-
f) OGTT
Blood glucose (mmol/L)
1g/kg bw
Time (min)
g) ipITT
4.5U/kg bw
2U/kg bw
h) Cold challenge
Rectal temperature (°C)
Time at 4°C (hours)
i) Heart rate & blood pressure
Blood Pressure (mm Hg)
Systolic
Diastolic
Arterial Pressure
j) Organ and tissue weights
% body mass
Heart
Spleen
Kidney
Gastrocnemius
Quadriceps
Brain
Liver

Figure 15.10 Supplemental: Body composition and metabolic testing results in 18M aged male and female mice: *Mrpl54*$^{+/-}$ versus WT

a) Body composition (g) by EchoMRI in 18M aged mice showed no difference in total body, fat, or lean mass between either male *Mrpl54*$^{+/-}$ (n=11) and WT (n=13) or female *Mrpl54*$^{+/-}$ (n=12) and WT (n=12).

b) Mean VO_2 (L/hour) by CLAMS and body mass ANCOVA analysis (insets) in 18M aged mice showed no differences for 24-hour, light, or dark periods between either male *Mrpl54*$^{+/-}$ (n=11) and WT (n=12) or female *Mrpl54*$^{+/-}$ (n=12) and WT (n=12).

c) Mean RER by CLAMS in 18M aged mice showed no difference between either male *Mrpl54*$^{+/-}$

(n=11) and WT (n=12) or female *Mrpl54*$^{+/-}$ (n=12) and WT (n=12).

d) Mean ambulatory motion (beam break counts) in 18M aged mice showed no difference between either male *Mrpl54*$^{+/-}$ (n=11) and WT (n=12) or female *Mrpl54*$^{+/-}$ (n=12) and WT (n=12).

e) Mean duration (minutes) on an endurance treadmill for 18M aged mice showed no difference in endurance time between either male *Mrpl54*$^{+/-}$ (n=9) and WT (n=11) or female *Mrpl54*$^{+/-}$ (n=10) and WT (n=9).

f) Mean blood glucose level (mmol/L) over time in response to an oral glucose challenge (OGTT) in 18M aged mice showed no difference between either male *Mrpl54*$^{+/-}$ (n=11) and WT (n=12) or female *Mrpl54*$^{+/-}$ (n=11) and WT (n=12).

g) Mean blood glucose level (mmol/L) and AUC (insets) over time in response to intraperitoneal insulin challenge (ipITT) in 18M aged mice showed no differences between either male *Mrpl54*$^{+/-}$ (n=12) and WT (n=13) or female *Mrpl54*$^{+/-}$ (n=10) and WT (n=11).

h) Mean rectal temperature (°C) in response to a 4-hour 4°C cold challenge in 18M aged mice showed no difference between either male *Mrpl54*$^{+/-}$ (n=10) and WT (n=9) or female *Mrpl54*$^{+/-}$ (n=10) and WT (n=9).

i) Mean heart rate (beats/min) and systolic blood pressure (mmHg) in 18M aged mice showed no differences between either male *Mrpl54*$^{+/-}$ (n=10) and WT (n=11) or female *Mrpl54*$^{+/-}$ (n=10) and WT (n=7). Diastolic blood pressure (mmHg) at 18M was higher in male *Mrpl54*$^{+/-}$ compared to WT, with no differences between female *Mrpl54*$^{+/-}$ and WT.

j) Relative organ weights (% body mass) in 18M aged necropsied mice showed no differences between either male *Mrpl54*$^{+/-}$ (n=7) and WT (n=12) or female *Mrpl54*$^{+/-}$ (n=10) and WT (n=7). Graphs show mean ± SEM; *P ≤ 0.05, male WT (blue); male *Mrpl54*$^{+/-}$ (light blue); female WT (orange); and female *Mrpl54*$^{+/-}$ (light orange).

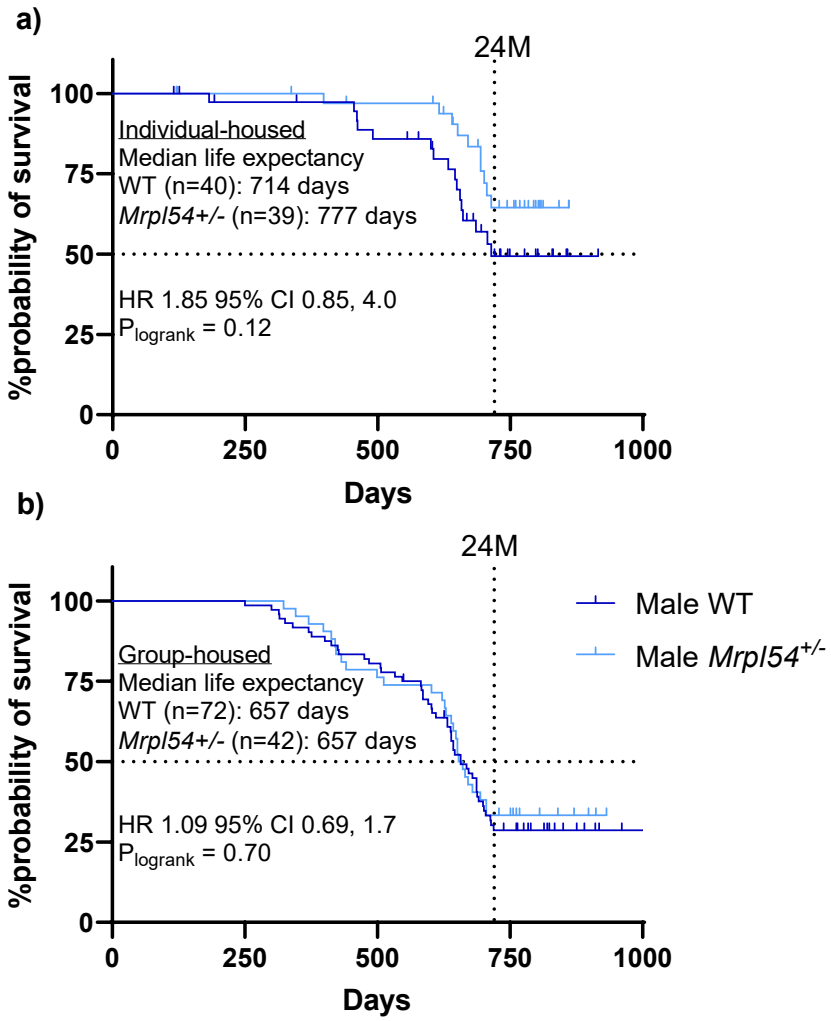

Figure 15.11 Supplemental: 24-month life expectancy in *Mrpl54*$^{+/-}$ versus WT males by housing conditions

a) Kaplan Meier survival curves show a suggested increase in 24-month life expectancy in individual-housed *Mrpl54*$^{+/-}$ (n=39) males compared to WT (n=40).

b) Kaplan Meier survival curves show no difference in 24-month life expectancy (where all mice alive after 24-month are censored) in group-housed males between *Mrpl54*$^{+/-}$ (n=42) and WT (n=72).

a)

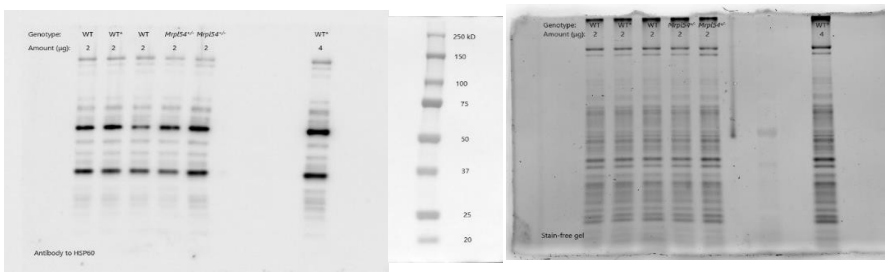
Genotype:
Amount (µg):
Antibody to HSP60
250 kD
150
100
75
50
37
25
20
Stain-free gel

b)

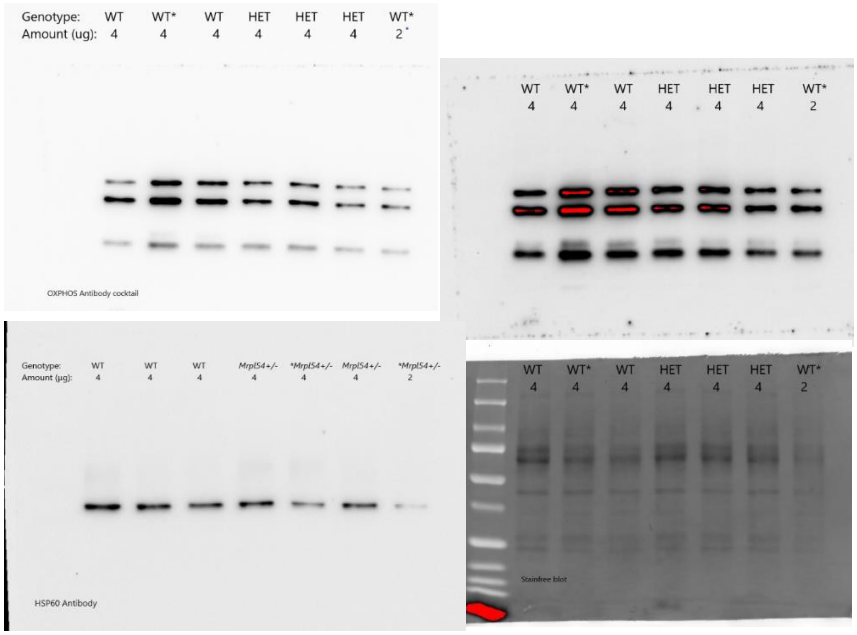
Genotype: WT WT* WT HET HET HET WT*
Amount (ug): 4 4 4 4 4 4 2
OXPHOS Antibody cocktail
WT WT* WT HET HET HET WT*
4 4 4 4 4 4 2
Genotype: WT WT WT Mrpl54+/- *Mrpl54+/- Mrpl54+/- *Mrpl54+/-
Amount (µg): 4 4 4 4 4 4 2
HSP60 Antibody
WT WT* WT HET HET HET WT*
4 4 4 4 4 4 2
Stainfree blot

c)

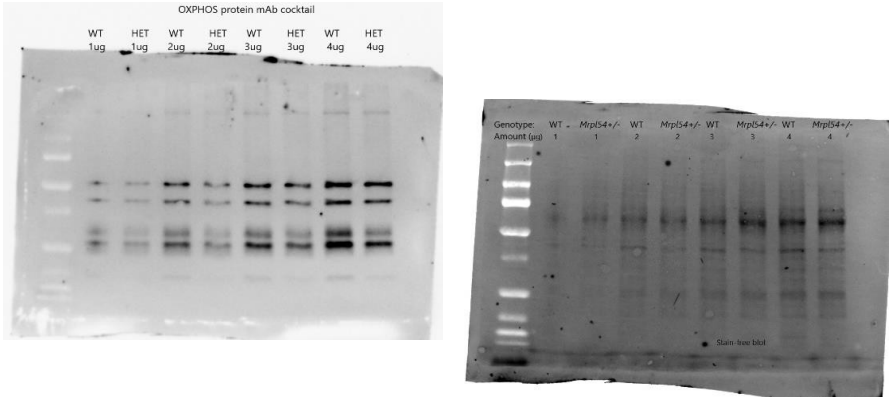
OXPHOS protein mAb cocktail
WT HET WT HET WT HET WT HET
1ug 1ug 2ug 2ug 3ug 3ug 4ug 4ug
Genotype: WT Mrpl54+/- WT Mrpl54+/- WT Mrpl54+/- WT Mrpl54+/-
Amount (µg) 1 1 2 2 3 3 4 4
Stain-free blot

Figure 15.12 Supplemental: Original uncropped western blot images

a) Original uncropped images of western blot (Fig. 5b) of isolated liver mitochondria immunofluorescence with HSP60 antibody (left), protein standard ladder (centre), and stain free gel (right).

b) Original uncropped images of western blot (Fig. 6a and 6b) of myoblast protein lysate immunofluorescence with OXPHOS antibody cocktail (top left and right), HSP60 antibody (bottom left), and stain free blot (bottom right).

c) Original uncropped images of western blot (Fig. 6a- taken from the 4µg loading lanes) of increasing concentration of myoblast protein lysate immunofluorescence with OXPHOS antibody cocktail (left) and stain-free gel (right).

16. A single dysfunctional copy of mitochondrial ribosomal protein L54 gene leads to early skeletal muscle aging in male C57BL/6N mice

Kim Reid[1]

Tarek Ammar[2]

Alexander E. Green[3,4]

Abolfazl Nik-Akhtar[3]

Goutham Vasam[3]

Baptiste Lacoste[5]

Jean-Marc Renaud[2]

Emily Standen[1]

Keir J. Menzies[3,4]

Affiliations:

1. Department of Biology, Faculty of Science, University of Ottawa, Ottawa, Ontario, Canada
2. Department of Cellular and Molecular Medicine, Faculty of Medicine, University of Ottawa, Ottawa, Ontario, Canada.
3. Interdisciplinary School of Health Sciences, Faculty of Health Sciences, University of Ottawa, Ottawa, Ontario, Canada.
4. Ottawa Institute of Systems Biology and the Éric Poulin Centre for Neuromuscular Disease, Department of Biochemistry, Microbiology and Immunology, Faculty of Medicine, University of Ottawa, Ottawa, Ontario, Canada.
5. Ottawa Hospital Research Institute, Neuroscience Program, Department of Cellular and Molecular Medicine, University of Ottawa Brain and Mind Research Institute, Faculty of Medicine, Ottawa, Ontario, Canada

Correspondence:

Correspondence to Keir J. Menzies: kmenzies@uottawa.ca

Keywords: mitochondrial ribosomal proteins, MRPL54, aging, skeletal muscle

Note: This study is awaiting results for skeletal muscle fibre typing before submission for publication.

16.1 Abstract

With age, mice lose skeletal muscle mass and show a decline in the number of intermyofibrillar mitochondria, which become hypertrophic and misaligned within irregular shaped sarcomeres. Age-related reduction in the levels of mitochondrial ribosomal proteins (MRPs) is also observed in skeletal muscle mitochondria. In this study, we analyzed grip strength data from publicly available heterozygous *Mrp* (*Mrp*$^{+/-}$) mouse models, and we examined the effects of a germline heterozygous *Mrpl54* mutation on aging mouse muscle, which previously showed reduced levels of respiratory complex protein subunits in cultured primary myoblasts. Grip strength, treadmill endurance, *ex vivo* maximum generated tetanic muscle force, muscle fatigue resistance, muscle force recovery, and the level of sarcomere disruption were examined. Using the International Mouse Phenotyping Consortium database, we identified multiple *Mrp*–mutation (*Mrp*$^{+/-}$) mouse models with a reduced grip strength phenotype. Male *Mrp54*$^{+/-}$ mice had reduced grip strength by age 12-months and *ex vivo* extensor digitorum longus (EDL) and soleus muscles tended towards a lower maximum tetanic force when compared to wildtype (WT). Both *Mrp54*$^{+/-}$ EDL and soleus muscles had a rightward shift in the force-frequency curve, suggesting a shift towards a slower twitch fiber type when compared to WT. A fiber-type switch would be consistent with an increased treadmill endurance and *ex vivo* EDL muscles exhibiting better recovery compared to WT. Transmission electron micrographs of 15-month-old *Mrp54*$^{+/-}$ EDL tissue show irregular shaped sarcomeres, along with misaligned and hypertrophic intermyofibrillar mitochondria compared to WT. In conclusion, we observed evidence of early skeletal muscle aging characterized by lower tetanic force generation, irregular sarcomere phenotype, and a shift in force frequency curves associated with a fast to slow muscle fiber type switch among male *Mrp54*$^{+/-}$ mice from age 12-months onward.

16.2 Introduction

The function of the mitochondrial ribosome (mitoribosome) is to synthesize proteins encoded by mitochondrial DNA. In humans, the mitoribosome encodes 13 vital protein subunits of electron transport chain (ETC) respiratory complexes I, III, IV, and V[1,2] and consists of 82 nuclear-DNA-encoded mitochondrial ribosomal proteins (MRPs)[3]. Mutations in *Mrp* genes manifest as rare early-onset or severe autosomal recessive diseases[4-7], where both alleles are disrupted for small ribosomal subunit proteins (MRPSs)[8-18] or large subunit proteins (MRPLs)[6,19-24]. Homozygous, compound heterozygous, or uniparental disomy *Mrp* mutations affect mitochondrial protein translation and reduce oxidative phosphorylation[4,6]. These mutations result in abnormal growth as well as neurological and cardiac phenotypes[4,6].

The effects of heterozygous *Mrp* mutations, where the protein product from one allele is functional and the other dysfunctional, are largely unreported. Those who carry disrupting mutations on a single *Mrp* allele are generally considered unaffected carriers[21], where the carrier is apparently free from disease and has no acute or early onset phenotype. While the protein level produced from a single *Mrp* allele may be sufficient in a young animal, this may not hold true with age. Downregulation of MRPs in skeletal muscle tissue is associated with normal aging in humans[27] and impaired synthesis of respiratory chain protein subunits is implicated in age-related chronic diseases[28-30]. In humans, aging results in the loss of muscle mass and strength[31] and defective mitochondrial function and protein quality control are considered aging mechanisms[32,33] and contribute to sarcopenia[34]. With an age-related decline in MRPs, the partially restricted MRP pool in heterozygous *Mrp* carriers may be insufficient to build or maintain functional mitoribosomes. This defect could potentially accelerate age-induced loss of protein quality control[25], leading to sarcopenia[26] and other aging phenotypes.

With aging, skeletal muscles experience numerous changes. In humans, there is an age-related shift in fiber type from fast twitch (i.e., glycolytic, anaerobic) to slow twitch (i.e., oxidative, aerobic)[38]. This age-related fiber type switch has yet to be confirmed in mice[36,39]. Mouse skeletal muscle shows age at around 24-months with a decline in muscle mass and fiber number[35], but without changes in cross-sectional area of individual muscle fibers[36,37]. At the cellular level, aged mice experience a reduction in skeletal muscle sarcoplasmic reticulum Ca^{2+}-pumping capacity, which likely contributes to a reduction in peak force[40]. Within mouse muscle fibers, there is an age-related decrease in the number of intermyofibrillar (IMF) mitochondria as well as onset of mitochondrial hypertrophy, possibly to compensate for the decrease in mitochondrial number or function (i.e., functional mitochondria fuse with dysfunctional organelles to maintain cellular function)[41,42]. Starting at age 24-months, sarcomeres become misaligned with a disruption in Ca^{2+}-release-units (CRUs), where the triads (i.e., two terminal sarcoplasmic reticulum cisternae flanking a central transverse tubule) on either side of the IMF mitochondria are no longer oriented transversally to the main axis of the myofibril[40]. CRU disruption and misalignment with age may interfere with IMF mitochondria communication (CRU-mitochondria uncoupling), which impacts skeletal muscle ATP production, where mitochondrial Ca^{2+} uptake is required to keep up with ATP demand[40,43].

We have previously shown that reducing *Mrpl54* expression through the knockout of one allele in a C57BL/6NTac mouse model ($Mrpl54^{+/-}$) reduces the expression of ETC protein complex subunits in primary myoblasts[44]. Given that downregulation of MRPs is associated with skeletal muscle aging[27], we have examined the effect of a single dysfunctional *Mrpl54* allele on skeletal muscle function with age. When compared to $Mrpl54^{+/+}$ (WT), we found that $Mrpl54^{+/-}$ male mice experienced a premature reduction in grip strength and *ex vivo* maximum generated tetanic muscle

force, as well as earlier age-related evidence of disrupted sarcomeres and CRUs. Unexpectedly, we found that *Mrpl54*$^{+/-}$ male mice experienced better treadmill endurance at age 12-months and improved *ex vivo* muscle fatigue resistance and muscle force recovery.

16.3 Results

16.3.1 Mrp$^{+/-}$ *models show decreased grip strength compared to controls*

To see if differences in muscle strength is associated with a heterozygous *Mrp* genotype (*Mrp*$^{+/-}$), we accessed grip strength data from the International Mouse Phenotype Consortium (IMPC)[45] for all available (*Mrp*$^{+/-}$) mouse models and compared them to their appropriate genetic background control population. Both females and males for several *Mrp*$^{+/-}$ models experienced reduced grip strength with *Mrpl54*$^{+/-}$ having one of the largest and robust effects (Fig. 16.1).

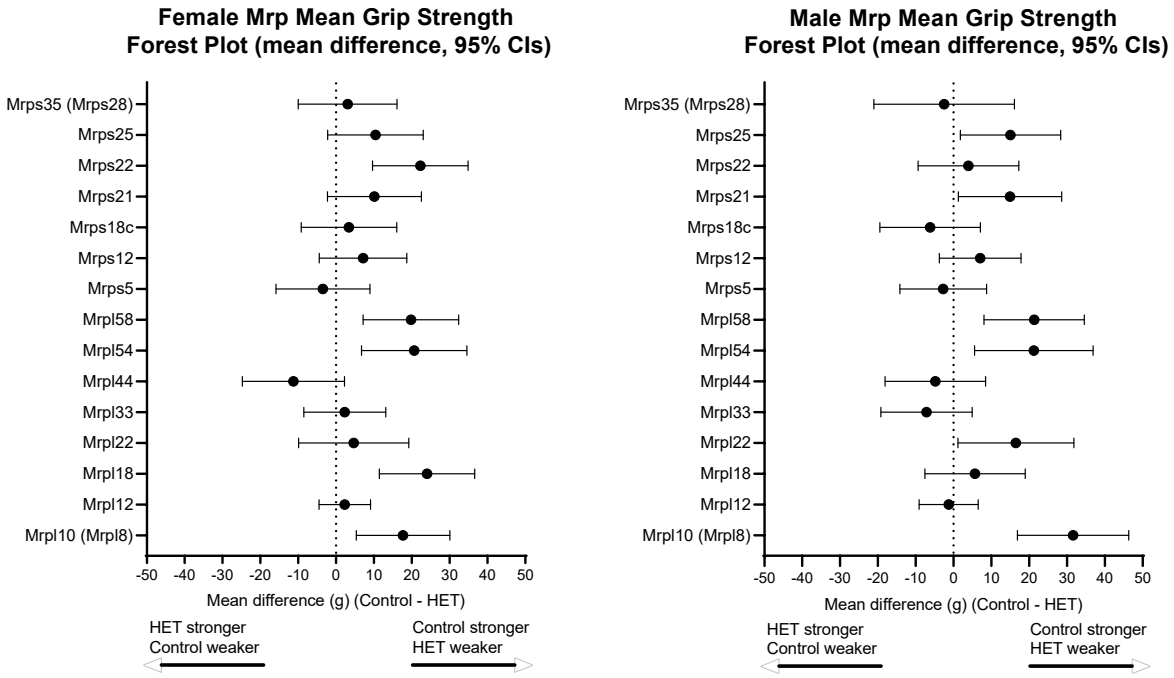

Figure 16.1 Forest plots depicting the mean difference in grip strength comparing control versus heterozygous *Mrp* mouse models (age 7-8 weeks).

Data extracted from the IMPC[45].

CI – confidence interval; HET – heterozygous for *Mrp* (*Mrp*$^{+/-}$); IMPC – International Mouse Phenotype Consortium; Mrps – small subunit of the mitochondrial ribosome protein; Mrpl – large subunit of the mitochondrial ribosome protein.

16.3.2 Aged Mrpl54$^{+/-}$ males have decreased grip strength and increased treadmill endurance compared to WT males

Given the IMPC data demonstrated that many *Mrp*$^{+/-}$ models have reduced grip strength compared to controls and our previous observation that *Mrpl54*$^{+/-}$ male primary myoblasts had lower ETC protein levels compared to WT[44], we monitored *Mrpl54*$^{+/-}$ and WT male and female mice from age 8-weeks until 15-months. Consistent with our previous study[44], 8-week-old *Mrpl54*$^{+/-}$ males had ~50% decrease in *Mrpl54* expression in gastrocnemius muscle compared to WT (Fig. 16.2a). There were no differences between *Mrpl54*$^{+/-}$ and WT in body mass from ages 8-weeks to 15-months nor was there a difference in body composition for males at age 12-months (Fig. 16.2b). Finally, in support of our previous work [44], there were no differences in ETC protein subunit levels in aged skeletal muscle (Fig. 16.2c-d).

To test the association between muscle strength and *Mrpl54* heterozygosity observed with IMPC data, we evaluated muscular strength using the forelimb grip strength assay in *Mrpl54*$^{+/-}$ and WT male and female mice at ages 8-weeks, 6-months, and 12-months. Mean grip strength did not differ between *Mrpl54*$^{+/-}$ and WT for either males or females at age 8-weeks or 6-months, with or without accounting for body mass (Fig. 16.3a-b, Supplemental Fig. 16.6a-d). At 12-months of age, mean grip strength continued to be the same between *Mrpl54*$^{+/-}$ and WT females (Fig. 16.3b, Supplemental Fig. 16.6e); however, male *Mrpl54*$^{+/-}$ mice had reduced grip strength compared to WT (Fig. 16.3a), with or without adjustment for body mass (Fig. 16.3c). Peak grip strength and the mean of the top-3 grip strength trial measurements revealed comparable results (Supplemental Fig. 16.7a-d).

Since 12-month-old male *Mrpl54*$^{+/-}$ mice demonstrated a reduction in grip strength compared to WT, we tested their exercise capacity and endurance using a treadmill exhaustion

test. While grip strength is dependent on muscle size, motor output and maximal force production, endurance tests the ability to resist muscular fatigue. At age 12-months, male *Mrpl54*$^{+/-}$ mice displayed improved running endurance compared to WT males (Fig. 16.3d).

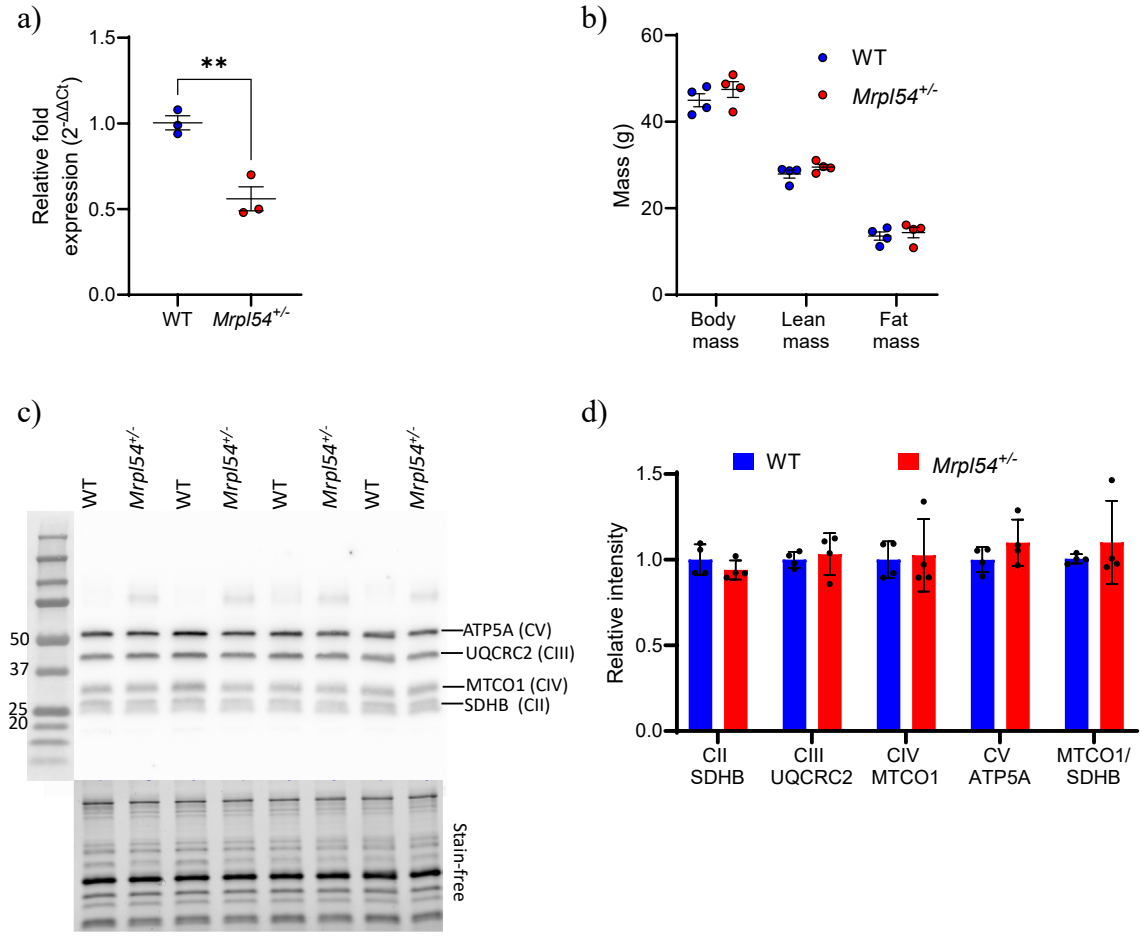

Figure 16.2 Reduced *Mrpl54* expression does not impact body composition or gastrocnemius ETC protein expression.

a) Relative *Mrpl54* expression in 8-week-old male *Mrpl54*+/- and WT mice.

b) Body composition of 12-month-old male *Mrpl54*+/- and WT mice.

c-d) Western blot and quantification of ETC protein subunits in 16-month-old male gastrocnemius whole protein lysate. Values are means ± SE; ** $p<0.01$.

ATP5A – ATPase subunit-5A; ETC – electron transport chain; MTCO1 – mitochondria cytochrome c oxidase subunit-1; SDHB – succinate dehydrogenase complex iron sulfur subunit-B; UQCRC2 – ubiquinol-cytochrome c reductase core protein-2; WT – wildtype.

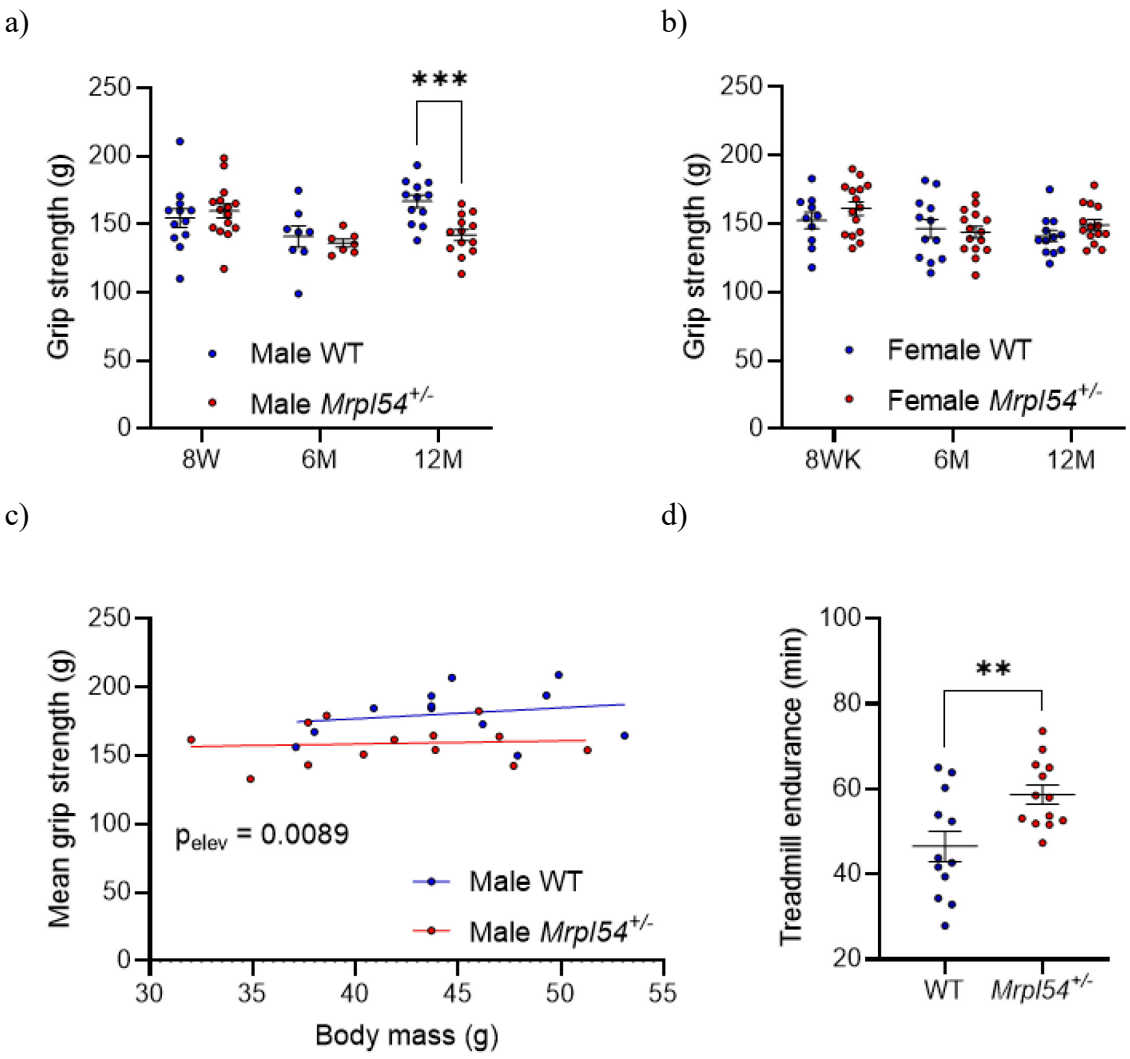

Figure 16.3 Grip strength and treadmill endurance in aging WT vs. *Mrpl54*$^{+/-}$ mice.

a) Grip strength in males aged 8W (n=12 WT; n=15 *Mrpl54*$^{+/-}$), 6M (n=8 WT; n=7 *Mrpl54*$^{+/-}$), and 12M (n=12 WT; n=13 *Mrpl54*$^{+/-}$) (Time x genotype, p=0.028).

b) Grip strength in females aged 8W (n=10 WT; n=15 *Mrpl54*$^{+/-}$), 6M (n=12 WT; n= 15 *Mrpl54*$^{+/-}$), and 12M (n=12 WT; n=14 *Mrpl54*$^{+/-}$).

c) 12M male mean grip strength adjusted for body mass using ANCOVA (n=12 WT; n=13 *Mrpl54*$^{+/-}$).

d) Treadmill endurance of 12M male mice (n=12 WT; n=13 *Mrpl54*$^{+/-}$).

Values are means ± SE; ** p<0.01; *** p<0.001.

6M – 6-months; 8W – 8-weeks; 12M – 12-months; ANCOVA – analysis of covariance; WT - wildtype

16.3.3 Ex vivo muscle contraction experiments demonstrate reduced force generation

Given the reduced grip strength and improved endurance treadmill results in 12-month *Mrpl54*$^{+/-}$ males, we carried out *ex vivo* functional testing of the EDL and soleus muscles from 15-month-old males to determine the force generation and fatigue profiles of specific muscles (Fig. 16.4). The EDL and soleus muscles were chosen because they have accessible tendons for securing the muscles, are small enough to be supported in a superfusion bath with sufficient oxygenation and are representative of fast twitch and slow twitch muscles, respectively[51]. Compared to WT, *Mrpl54*$^{+/-}$ EDL and soleus muscles trended towards a lower maximum tetanic force (Fig. 16.4a). Both *Mrpl54*$^{+/-}$ EDL and soleus had higher Frequency 50 values (the stimulation frequency at which muscles generate 50% of maximum tetanic force) compared to WT (Fig. 16.4b). Repeated measured two-way ANOVA analysis further supported a shift of the absolute force-frequency curve toward higher frequencies indicating that, at similar submaximal stimulation frequencies, *Mrpl54*$^{+/-}$ EDL and soleus muscles generated less force (Fig. 16.4c-d). No significant differences in fatigue or recovery were observed in soleus muscles between *Mrpl54*$^{+/-}$ and WT male mice (Fig. 16.4e-f); however, *Mrpl54*$^{+/-}$ EDL muscles showed better recovery when compared to WT (Fig. 16.4f). Together, the *ex vivo* muscle contraction data support a reduction of force generation and improved force recovery which may suggest impaired sarcomere function and/or a muscle fiber type shift toward slower twitch fibers.

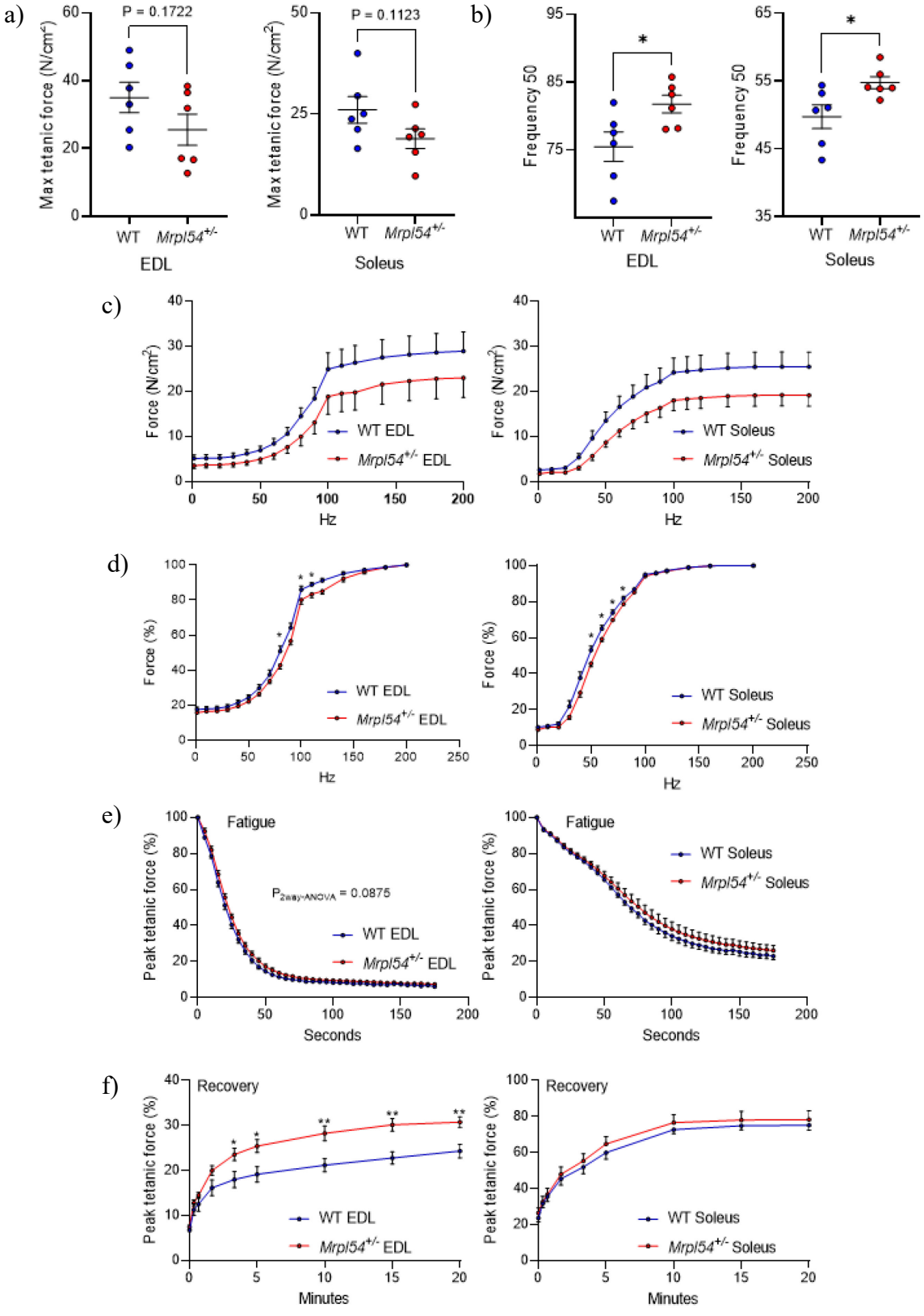
a)
P = 0.1722
Max tetanic force (N/cm²)
WT
Mrpl54+/-
EDL
P = 0.1123
Soleus
b)
Frequency 50
*
c)
Force (N/cm²)
WT EDL
Mrpl54+/- EDL
WT Soleus
Mrpl54+/- Soleus
Hz
d)
Force (%)
e)
Fatigue
P2way-ANOVA = 0.0875
Peak tetanic force (%)
Seconds
f)
Recovery
Minutes

Figure 16.4 Maximum tetanic force, Frequency 50, force-frequency, fatigue, and recovery of *ex vivo* 15-month-old WT (n=6) and *Mrpl54*$^{+/-}$ (n=6) EDL and soleus muscles.

a) Mean normalized tetanic forces (N/cm^2), representing the maximum force generated for EDL and soleus muscles during a 400 ms train of pulses at 200 Hz.

b) Frequency 50 is the stimulation frequency at which muscles generate 50% of maximum tetanic force.

c) Absolute force-frequency relationships for EDL and soleus muscles; RM-ANOVA for soleus (Hz x genotype: F(16, 160)=2.03, p=0.014) and split plot ANOVA (Hz x genotype p=0.049).

d) Force-frequency relationships of EDL and soleus muscles as a percentage of force measured at 200Hz; RM-ANOVA for EDL and soleus (Hz x genotype: F(16, 160)=2.32, p=0.004 and F(16, 160)=3.94, p<0.0001, respectively).

e) Fatigue curves for EDL and soleus muscles as a percentage of peak tetanic force.

f) Recovery curves for EDL and soleus muscles as a percentage of peak tetanic force; RM-ANOVA for EDL (genotype F(1,10)=4.63, p=0.014; Hz x genotype F(8,80)=4.63, p=0.0001). Values are mean ± SEM; *p<0.05; **p<0.01.

ANOVA – analysis of variance analysis; EDL – extensor digitorum longus muscle; F – F distribution test; Hz – Hertz (frequency in cycles per second); RM-ANOVA – repeated measures 2-way analysis of variance analysis; SEM – standard error of the mean.

16.3.4 Transmission electron micrographs

The reduction in grip strength in 12-month-old *Mrpl54*$^{+/-}$ males, combined with a trend toward a reduction in *ex vivo* mean tetanic force for aged *Mrpl54*$^{+/-}$ EDL and soleus muscles may point to sarcomere disruption. To visualize the sarcomeres, we used transmission electron microscopy (TEM) (Fig. 16.5). As expected, 15-month-old WT EDL muscle displayed regularly shaped sarcomeres, aligned Z-lines, and IMF mitochondria with aligned CRUs that lie within the I-band and are perpendicular to the Z-line (Fig. 16.5a). Compared to WT, we identified a series of structural abnormalities in 15-month-old *Mrpl54*$^{+/-}$ male EDL muscle, which displayed sarcomeres with heterogeneous sizes and shapes and with misaligned and disrupted Z-lines (Fig. 16.5b). Both morphology and orientation of the CRUs in *Mrpl54*$^{+/-}$ male EDL muscle were compromised in that the triads were not aligned transversally with the myofibrils, and the IMF mitochondria displayed evidence of hypertrophy comparted to WT (Fig. 16.5c-d).

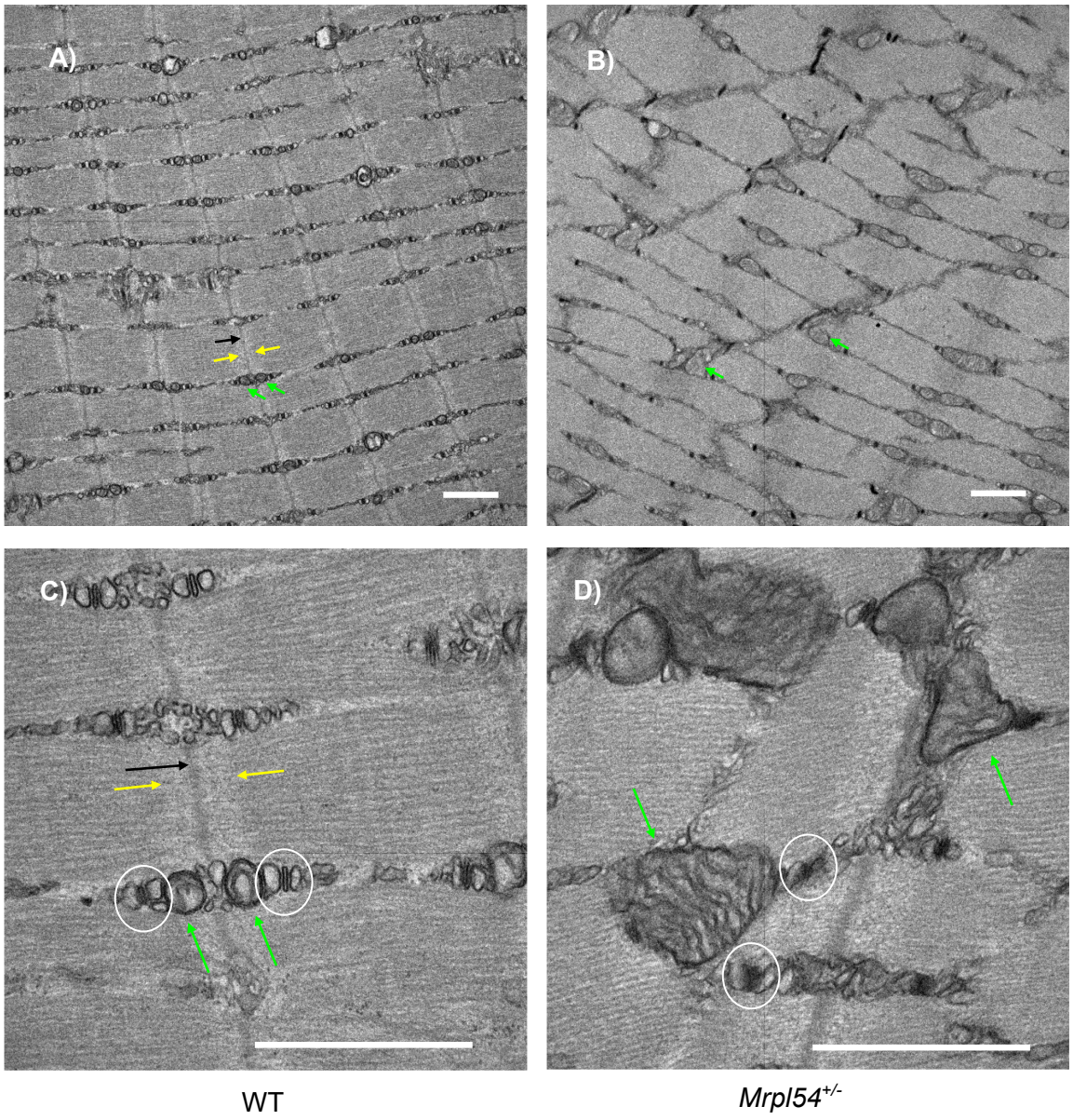

Figure 16.5 Representative transmission electron micrographs of 15M-old male EDL muscle.

a) WT sarcomeres are regular and ordered with IMF mitochondria (green arrows) oriented within the I-band (yellow arrows) of the sarcomere and transverse to the Z-line (black arrow).

b) *Mrpl54*$^{+/-}$ sarcomeres display heterogeneous shapes without alignment and with many IMF mitochondria (green arrows) misaligned.

c) WT CRUs (white circles) are symmetrical, located on either side of the Z-line (black arrow), and contain a transverse tubule element flanked by two terminal cisternae (triad) close to IMF mitochondria (green arrows) lying within the I-band (yellow arrows).

d) *Mrpl54*$^{+/-}$ IMF mitochondria (green arrows) display hypertrophy and are misaligned with the CRU triads (white circles). Scale bar is 1µm.

16.4 Discussion

We had previously identified reduced levels of ETC complex protein subunits in *Mrpl54*$^{+/-}$ primary myoblasts; although, the ratio of mitochondrial-DNA-encoded to nuclear-DNA-encoded ETC complex proteins remained like WT[44]. In the current study, we likewise did not identify a physical or metabolic phenotype in young male or female *Mrpl54*$^{+/-}$ mice, which indicates that the reduced expression of a critical mitochondrial large subunit ribosomal protein had limited effect on mitochondrial ribosomal function in young animals. These results match what is generally observed in human heterozygous carriers of *Mrp* mutations – a damaging phenotype does not manifest in the young unless both mutated alleles are inherited[21]. One exception to the observed human data was observed in the *Mrpl40*$^{+/-}$ mouse model, where the knock down of a single *Mrpl40* allele resulted in a short-term memory deficit (via Serca2-independent deregulation of presynaptic Ca^{2+}) in 16-20-week-old *Mrpl40*$^{+/-}$ mice, which is thought to contribute to 22q11.2-microdeletion-related schizophrenia[46].

Given that mitochondrial dysfunction is a hallmark of aging[33], MRPs are downregulated with age in skeletal muscle[27], and we observed low ETC protein levels in *Mrpl54*$^{+/-}$ primary myoblasts, we hypothesized that a skeletal muscle phenotype will manifest with age in the *Mrpl54*$^{+/-}$ mouse model. We searched the IMPC mouse database for *Mrp*$^{+/-}$ skeletal muscle outcomes and found that, across several *Mrp*$^{+/-}$ models including *Mrp54*$^{+/-}$, grip strength was lower when compared to WT. After following male and female *Mrpl54*$^{+/-}$ and WT mice for 12-months, we confirmed that male *Mrpl54*$^{+/-}$ grip strength declined compared to WT and that this decline was detectable by age 12-months. Searching the literature for aging skeletal muscle phenotypes related to MRPs, we identified one study of a homozygous *Mrps5* mouse model (*Mrps5*$^{V338Y/V338Y}$) that introduced an increased mitochondrial translational error rate resulting in an age-related

skeletal muscle phenotype – while no differences were detected between young 9-month *Mrps5*$^{V338Y/V338Y}$ and WT mice, 19-month-old *Mrps5*$^{V338Y/V338Y}$ showed accelerated aging metabolomic and transcriptomic profiles[47].

Unexpectedly, 12-month-old *Mrpl54*$^{+/-}$ males had better treadmill endurance than WT. This result compliments the rightward shift observed in the force frequency curves in *Mrpl54*$^{+/-}$ male mice, which may have been associated with a switch in muscle fiber type. The *ex vivo* soleus and EDL contraction and fatigue experiments supported both the decreased grip strength results (decreased *ex vivo* tetanic force) as well as the increased treadmill endurance (increased *ex vivo* fatigue recovery). We had previously tested 18-month and 24-month male *Mrpl54*$^{+/-}$ versus WT on the treadmill and found no difference in endurance (Reid et al., 2023). Collectively, these results suggest the *Mrpl54*$^{+/-}$ males show an early aging muscle phenotype with respect to grip strength but there may be a compensatory mechanism in play that strives to maintain overall muscle function, which is lost as the male *Mrpl54*$^{+/-}$ ages past 12-months.

16.5 Methods

16.5.1 International Mouse Phenotype Consortium (IMPC) grip strength data retrieval

On 28 April 2022, raw grip strength data was downloaded from the IMPC website for fifteen *Mrp*$^{+/-}$ mouse models (*Mrps5, Mrps12, Mrps18c, Mrps21, Mrps22, Mrps25, Mrps35, Mrpl10, Mrpl12, Mrpl18, Mrpl22, Mrpl33, Mrpl54, and Mrpl58*). At the time of the grip strength tests, male and female mice were early adults for both *Mrp*$^{+/-}$ (n=7-9) and control animals (n=387-1901). The grip strength test involved three trials and followed the standardized International or European Mouse Phenotyping Resource of Standardised Screens (IMPReSS or EMPReSS) protocols published at the IMPC website[48].

16.5.2 Animal husbandry and genotyping

Institute Clinic de la Souris (ICS, France) generated a *Mrpl54* constitutive knock-down mouse on a C57BL/6N(Taconic) background (C57BL/6NTac-Mrpl54$^{tm1b(EUCOMM)Wtsi/IcsOrl}$). *Mrpl54*$^{+/-}$ breeding pairs were kept in ventilated racks and their progeny weaned, ear-tagged, and tissue sampled for genotyping at age 21 days. DNA for genotyping was extracted from an ear sample according to the Phire Animal Direct PCR protocol (F-170, Thermo Scientific). Genotyping proceeded according to the ICS protocol (Forward primer Ef 4877 5'-GACCCACATAAGCAGGGAAGGAGATG-3', reverse primer L3r 4879 5'-CAATCTCCTGAGAATGTAGCCCACCAT-3', Invitrogen). The *Mrpl54* knock-out allele generated a 402 bp fragment, and the wildtype (WT) allele generated a 1095 bp fragment.

Male *Mrpl54*$^{+/-}$ and WT mice, separated by sex (n=15 mice per group, total 30 mice), were housed 1-5 per cage under a 12:12-hour light-dark cycle at a room temperature of 23°C until age 15 months. All mice were fed a standard chow diet (Envigo; Teklad Global 2018). Humane endpoint criteria included >15% weight loss over 2 weeks, skin lesions not responding to treatment, head tilt/rolling or loss of balance, ulcerated/bulging eye, ulcerated mass, respiratory distress, inability to express bladder, distended abdomen, or growing internal mass. The Animal Care Committee of the University of Ottawa approved all experimental procedures in this study.

16.5.3 RNA isolation and real-time qPCR

For total RNA isolation, a small piece of snap frozen mouse tissue was placed in 1 ml TRIzol (Sigma-Aldrich or Invitrogen). Samples were homogenized with a 2.8 mm ceramic bead using a homogenized in a Bead Mill 24 Homogenizer (Fisherbrand 15340163) with three 40 second cycles at a speed of 2.09 m/s, and a rest time of 22 seconds between cycles. RNA was isolated according to manufacturer's protocol. From 1 μg of extracted RNA, genomic DNA was eliminated with a

gDNA Wipeout Buffer and subsequently reverse transcribed into cDNA using the QuantiTect Reverse Transcription Kit (QIAGEN). The diluted cDNA was prepared with SYBR Green (Roche), and the quantitative gene expression was measured using the LightCycler 480 Instrument (Roche). The primer pairs used were as follows: *Mrpl54* forward 5'-AAAAAGCCAGTTGGCAAGGG-3', reverse 5'-ATGTGTGGTGAGCTGAGTGG-3'; *36B4* forward 5′-ACGGGTACAAACGAGTCCTG-3′, reverse 5′-GCCTTGACCTTTTCAGCAAG-3′; and *B2M* forward 5′-GGCTCACACTGAATTCACCC-3, 5′-GTCTCGATCCCAGTAGACGG-3′. To normalize tissue sample expression (threshold cycle [Ct] values) to the expression of housekeeping genes, the ΔΔCt method was used. The geometric means of *36B4* (acidic ribosomal phosphoprotein gene) and *B2m* (beta2 microglobulin) genes were used to normalize *Mrpl54* tissue sample expression (ΔCt values) to the WT samples.

16.5.4 Western blotting

A single gastrocnemius muscle was dissected from 15-month-old male mice (n=4 WT; n=4 *Mrp54*$^{+/-}$), flash frozen in liquid nitrogen, and powdered. ~50 mg of tissue was transferred to a reinforced homogenization tube containing three 2.8 mm ceramic beads (Fisher Scientific 19-340-162) and 10 mL/mg lysis buffer (20 mM Tris-Buffer [pH 7.8], 100mM KCl, 1mM dithiothreitol, 1mm MgCl2, 1 mM EDTA, 20% w/v glycerol, 1% v/v Triton-X-100) augmented with protease and phosphatase inhibitors (Roche cOmplete ULTRA [Cat# 05892970001] plus phosStop [Cat# 4906845001] tablets). Samples were homogenized in a Bead Mill 24 Homogenizer (Fisherbrand 15340163) with three 40 second cycles at a speed of 2.09 m/s, and a rest time of 22 seconds between cycles. The samples were centrifuged twice at 16,000*g* for 10 minutes at 4°C and the supernatant containing the protein lysate stored at -80°C. Protein levels were quantified using the DC Protein Assay, (Bio-Rad) and POLARstar Omega plate reader (BMG Labtech).

Protein samples were diluted to 1 µg/µL in Laemmli Buffer (Bio-Rad Cat# 1610737) augmented with 10% β-mercaptoethanol (Fisher Bioreagents, BP176-100). Six µg of each sample were run on a 10% SDS-PAGE using the TGX Stain-free FastCast Acrylamide Kit (Bio-Rad Cat# 1610183) and the Mini-PROTEAN system (Bio-Rad Cat# 1658006). SDS-PAGE was run at 4°C at a constant 90 volts across the gel for 30 minutes and then 120 volts for 50-60 minutes. The Stain-Free gels were activated once for 45 seconds using a ChemiDoc Touch Imaging System (Bio-Rad) and then the proteins transferred to TransBlot Turbo Mini size 0.2 µm nitrocellulose membrane (Bio-Rad) using the Trans-Blot TurboTransfer System (Bio-Rad Cat# 1704150EDU).

The nitrocellulose membrane was imaged for total protein and then blocked for one hour in blocking buffer (5% w/v bovine serum albumin [Sigma, SKU A7906] in TBS-T buffer [50mM Tris-HCl, pH 7.6; 150mM NaCl; 0.1% Tween]), rocking gently at room temperature. Membranes were then incubated with primary antibody diluted in TBS-T buffer (1:1000 Total OXPHOS Rodent WB Antibody Cocktail [abcam Cat# ab110413] overnight at 4°C with gentle rocking. After three washes with TBS-T, the membrane was incubated for one hour with the matching IgG, horseradish peroxidase (HRP)-conjugated secondary antibody (1:10,000 Cell Signaling Technology Anti-rodent Cat# 7076, or Anti-rabbit Cat# 7074P2), rocking at room temperature. After three washes in TBS-T, the membrane was visualized using enhanced chemiluminescent detection (BioRad Clarity Cat# 1705061) on the ChemiDoc Touch Imaging System (Bio-Rad).

To semi-quantify the protein levels in the western blot analyses, dilutions of protein were first loaded onto an SDS-PAGE to determine the linear range of protein concentrations. Protein concentrations within the linear range were chosen for subsequent semi-quantitative SDS-PAGE, where the selected protein band was normalized to total loaded protein and analysed using Image Lab Software (Bio-Rad).

16.5.5 Body composition using EchoMRI

Each mouse was loaded into an A100 antenna insert and placed into the EchoMRI (EchoMRI-700 Analyzer) to determine body composition (whole-body, lean, and fat mass).

16.5.6 Grip strength

Forelimb grip strength was measured using a standard grip strength meter (Chantillion DFE, Columbus Instruments) at ages 8-weeks, 6-months, and 12-months. The mouse was allowed to grasp a bar mounted on the meter and, after stabilization, the force transducer meter was set to zero and the mouse tail gently pulled horizontally until the grasp was broken. The moment the mouse released its forepaws from the bar, the tension in grams was recorded. The test was conducted five times consecutively, with a 60-second interval between trials. The same operator conducting all grip strength experiments and was blinded to genotype. Grip strength was evaluated in three ways: the peak measurement, the average of all five measurements, and the top three measurements[49].

16.5.7 Endurance treadmill

At age 12 months, male mice in the grip strength study were tested for endurance[50] on a treadmill (Exer-3/6, Columbus Instruments). Mice were acclimated to the treadmill over three consecutive days where they were placed on an unmoving belt for 5 minutes, then running at a constant speed of 15 cm/s at an elevation of +5° with an electro-stimulus (0.1 mA, 1 Hz) applied to the resting grid. Those mice that achieved fewer than 5 stimulations over 5 minutes by the third acclimation day were permitted to continue with the endurance test. The endurance test was conducted the day following the last day of acclimation using the following profile – accelerate to 15 cm/s in 30 seconds and then run at 15 cm/s for 12 minutes, accelerating +3.0 cm/s over 30 seconds every 12 minutes[7]. Mice ran until the exhaustion criterion was met (3 electro-stimulus contacts [0.1 mA, 1.0 Hz] within 10 seconds) at which point the electro-stimulus was stopped, and

the running time, distance, and maximum speed attained were recorded. The same operator conducted all treadmill experiments and was blinded to genotype.

16.5.8 Ex vivo extensor digitorum longus (EDL) and soleus muscle contraction

Male *Mrpl54*$^{+/-}$ and WT mice aged 15-months (n=6 per group, total 12 mice) were sacrificed by cervical dislocation and the EDL and soleus dissected from one hindlimb. Each muscle was superfused in a physiological saline solution containing (in mM) 118.5 NaCl, 4.7 KCl, 2.4 CaCl2, 3.1 $MgCl_2$, 25 $NaHCO_3$, 2 NaH_2PO_4, and 5.5 D-glucose[51]. The solution was continuously bubbled with 95% O_2 and 5% CO_2 to maintain a pH of 7.4. Experimental temperature was 37°C. Total flow of solution in the muscle chamber was 15 mL/min split just above and below the muscle to prevent buildup of reactive oxygen species[52]. Each muscle was stimulated by passing a current between two parallel platinum wires located 4 mm apart on opposite sides in the middle of the muscle. Stimuli was provided by a Grass S88X stimulator and a Grass stimulation isolation unit (Grass Technologies/Astro-Med).

Muscles were positioned horizontally in a Plexiglas chamber with one end of the muscle fixed to a stationary hook using silk suture, while the other end was attached to a force transducer (model 400A; Aurora Scientific Canada). The transducer was connected to a KCP13104 data acquisition system (Keithley), and data were recorded at 5 kHz. EDL and soleus muscles were allowed to equilibrate for 30 min after the muscle length was adjusted to give maximal tetanic force (200 ms trains of 0.3 ms and 10-V [supramaximal voltage] pulses at 140 Hz and 200 Hz for soleus and EDL, respectively). Maximum tetanic force, defined as the force developed during a tetanic contraction, was calculated as the difference between the maximum force during a contraction and the force measured 5 ms before the contraction was elicited. Tetanic force was normalized as follows[53]:

$F_{normalized} = F_{measured}/CSA*CF$

$CSA = L_e/(W_e*M_{density})$

Where $F_{normalized}$ is the normalized force in N/cm^2; $F_{measured}$ is the measured force in g; CF is the conversion factor of 0.00980665 N/g; CSA is the cross-sectional area in cm^2; L_e is the muscle length in cm; W_e is the muscle mass in g; and $M_{density}$ is the muscle density of 1.06 g/cm^3.

During the 30 min equilibration, tetanic contractions were elicited every 100 s. After the 30 min equilibrium period, a force-frequency curve was generated starting at 1 Hz and increasing by 10-20 Hz every 5 min until 200 Hz. Frequency 50 was calculated from the sigmoidal curve (the stimulation frequency at which muscles generate 50% of maximum tetanic force). A fatigue bout was elicited for each muscle by delivering a tetanic force every second over a 3 min period. Muscles were allowed to recover by eliciting tetanic contractions every 5 min over a 20 min period.

16.5.9 Fiber typing and cross-sectional area

EDL and soleus muscles were embedded in Tissue-Plus medium (Fisher HealthCare Cat. 23-730-571), frozen in isopentane precooled in liquid nitrogen, and stored at −80°C. Ten-micrometer sections were cut at -20°C using a cryostat (Leica CM 1850), placed on positively charged glass slides, and stored at -80°C. Sections were stained using a Mouse-on-Mouse (M.O.M) fluorescein kit (Cat. No. FMK-2201, MJS Biolynx, Canada) for type I, IIA, and IIB fibers. Briefly, a section was incubated 1 hour in 10% M.O.M. Mouse IgG Blocking Reagent and washed with phosphate buffer saline (PBS) and then washed twice in phosphate buffered saline (PBS) for two minutes. Cross sections were incubated 5 min in 10% M.O.M. Protein Diluent in PBS solution before being exposed 1 hour to either mouse monoclonal anti-myosin type I (A4.840), anti-myosin IIA (SC-71), or anti-myosin heavy chain type IIB (BF-F3; Developmental Studies Hybridoma Bank); different cross sections were used to identify fiber types. After three washes with PBS,

cross sections were exposed 10 min to biotinylated anti-mouse IgG reagent solution. Finally, cross sections were incubated 15 min in a fluorescein avidin (1:500) followed by three washes in PBS. Slides were mounted on slide with mounting media and cover it with coverslip. Images were captured on a Zeiss Axio Imager.M2 microscope (Canada) using a digital camera (AxioCam mRm CCD). Pictures were taken from overlapping regions of each muscle and then collaged together to allow fiber typing measurements from all fibers of each muscle using Imaris software (Bitplane an Oxford Instruments company).

16.5.10 Transmission electron microscopy

EDL muscles were dissected from 15-month-old WT and *Mrpl54*$^{+/-}$ males and fixed in glass vials containing 2.5% glutaraldehyde in 0.1 M NaCaCO buffer (pH 7.4) (Cedarlane 16537-15). The vials were gently rocked at room temperature for 30 min, then incubated overnight at 4°C. The muscles were placed in 1% osmium tetroxide for 60 min, rinsed with 0.2 M NaCaCO, dehydrated in a series of ethanol solutions, followed by propylene oxide, and then finally embedded in epoxy resin. An ultramicrotome was used to generate 500 nm sections, which were stained with toluidine blue and viewed using light microscopy. Once the correct orientation was confirmed, the resin block was trimmed to a 1 mm hexagon and thin 60-90 nm sections were sliced using a diamond cutter. The sections were then stained onto mesh grids using uranyl nitrate and lead citrate. Images of sarcomeres for each sample were captured on a JEOL JEM-1400Plus 60-kV transmission electron microscope with magnification set to 6500X or 25,600X.

16.5.11 Statistics

Descriptive statistics were employed to examine the IMPC grip strength data generating Forest plots depicting mean difference in grip strength (average of three trials) with 95% confidence intervals (CIs). *Mrpl54* expression, western blot results, body composition, 12-month

treadmill endurance, maximum tetanic force, and Frequency 50 results were compared using two-tailed unpaired Student's *t*-tests. Mean grip strength over time was analysed using mixed effects analysis corrected for multiple measurements using Šídák's multiple comparisons test and analysis of covariance (ANCOVA) to eliminate the effect of body mass-related variance[54]. Force-frequency, fatigue, and recovery curves were analysed using repeated measures two-way ANOVA using the Geisser-Greenhouse correction for unequal variability of differences[55]. Absolute force-frequency curves were also analysed using split-plot ANOVA analysis. When a main effect or interaction was significant, then Fisher's least significance difference test was employed without adjustments for multiple comparisons. GraphPad Prism 9.4.1 (GraphPad Software, Inc.) was used for statistical analyses except for split-plot ANOVA, which was completed using the general linear model procedures of the Statistical Analysis Software (SAS Institute Inc., Cary, NC). Statistical significance was set at $p<0.05$.

16.6 References

1 Ott, M. & Herrmann, J. M. Co-translational membrane insertion of mitochondrially encoded proteins. *Biochimica et Biophysica Acta (BBA) - Molecular Cell Research* **1803**, 767-775 (2010). https://doi.org:10.1016/j.bbamcr.2009.11.010

2 Englmeier, R., Pfeffer, S. & Förster, F. Structure of the Human Mitochondrial Ribosome Studied In Situ by Cryoelectron Tomography. *Structure* **25**, 1574-1581.e1572 (2017). https://doi.org:10.1016/j.str.2017.07.011

3 Brown, A. *et al.* Structures of the human mitochondrial ribosome in native states of assembly. *Nature Structural & Molecular Biology* **24**, 866-869 (2017). https://doi.org:10.1038/nsmb.3464

4 Boczonadi, V., Ricci, G. & Horvath, R. Mitochondrial DNA transcription and translation: clinical syndromes. *Essays in Biochemistry* **62**, 321-340 (2018). https://doi.org:10.1042/ebc20170103

5 Ferrari, A., Del'Olio, S. & Barrientos, A. The Diseased Mitoribosome. *FEBS Letters* **595**, 1025-1061 (2021). https://doi.org:10.1002/1873-3468.14024

6 Horga, A. *et al.* Uniparental isodisomy of chromosome 2 causing MRPL44-related multisystem mitochondrial disease. *Molecular Biology Reports* **48**, 2093-2104 (2021). https://doi.org:10.1007/s11033-021-06188-1

7 Webb, B. D., Diaz, G. A. & Prasun, P. Mitochondrial translation defects and human disease. *Journal of Translational Genetics and Genomics* (2020). https://doi.org:10.20517/jtgg.2020.11

8 Saada, A. *et al.* Antenatal mitochondrial disease caused by mitochondrial ribosomal protein (MRPS22) mutation. *Journal of Medical Genetics* **44**, 784-786 (2007). https://doi.org:10.1136/jmg.2007.053116

9 Miller, C. *et al.* Defective mitochondrial translation caused by a ribosomal protein (MRPS16) mutation. *Annals of Neurology* **56**, 734-738 (2004). https://doi.org:10.1002/ana.20282

10 Smits, P. *et al.* Mutation in mitochondrial ribosomal protein MRPS22 leads to Cornelia de Lange-like phenotype, brain abnormalities and hypertrophic cardiomyopathy. *European Journal of Human Genetics* **19**, 394-399 (2011). https://doi.org:10.1038/ejhg.2010.214

11 Baertling, F. *et al.* MRPS22 mutation causes fatal neonatal lactic acidosis with brain and heart abnormalities. *neurogenetics* **16**, 237-240 (2015). https://doi.org:10.1007/s10048-015-0440-6

12 Kılıç, M. *et al.* A patient with mitochondrial disorder due to a novel mutation in MRPS22. *Metabolic Brain Disease* **32**, 1389-1393 (2017). https://doi.org:10.1007/s11011-017-0074-5

13 Chen, A. *et al.* Mutations in the mitochondrial ribosomal protein MRPS22 lead to primary ovarian insufficiency. *Human Molecular Genetics* **27**, 1913-1926 (2018). https://doi.org:10.1093/hmg/ddy098

14 Lake, N. J. *et al.* Biallelic Mutations in MRPS34 Lead to Instability of the Small Mitoribosomal Subunit and Leigh Syndrome. *The American Journal of Human Genetics* **101**, 239-254 (2017). https://doi.org:10.1016/j.ajhg.2017.07.005

15 Richman, T. R. *et al.* Mutation in MRPS34 Compromises Protein Synthesis and Causes Mitochondrial Dysfunction. *PLoS Genet.* **11**, e1005089 (2015). https://doi.org:10.1371/journal.pgen.1005089

16 Borna, N. N. *et al.* Mitochondrial ribosomal protein PTCD3 mutations cause oxidative phosphorylation defects with Leigh syndrome. *neurogenetics* **20**, 9-25 (2019). https://doi.org:10.1007/s10048-018-0561-9

17 Liu, C., Zhou, W., Liu, Q. & Peng, Z. Hypoglycemia with lactic acidosis caused by a new MRPS2 gene mutation in a Chinese girl: a case report. *BMC Endocrine Disorders* **22** (2022). https://doi.org:10.1186/s12902-021-00924-1

18 Kline, B. L. *et al.* Integral Role of the Mitochondrial Ribosome in Supporting Ovarian Function: MRPS7 Variants in Syndromic Premature Ovarian Insufficiency. *Genes* **13**, 2113 (2022). https://doi.org:10.3390/genes13112113

19 Serre, V. *et al.* Mutations in mitochondrial ribosomal protein MRPL12 leads to growth retardation, neurological deterioration and mitochondrial translation deficiency. *Biochimica et Biophysica Acta (BBA) - Molecular Basis of Disease* **1832**, 1304-1312 (2013). https://doi.org:10.1016/j.bbadis.2013.04.014

20 Di Nottia, M. *et al.* A homozygous MRPL24 mutation causes a complex movement disorder and affects the mitoribosome assembly. *Neurobiol. Dis.* **141**, 104880 (2020). https://doi.org:10.1016/j.nbd.2020.104880

21 Carroll, C. J. *et al.* Whole-exome sequencing identifies a mutation in the mitochondrial ribosome protein MRPL44 to underlie mitochondrial infantile cardiomyopathy. *Journal of Medical Genetics* **50**, 151 (2013). https://doi.org:10.1136/jmedgenet-2012-101375

22 Distelmaier, F. *et al.* MRPL44 mutations cause a slowly progressive multisystem disease with childhood-onset hypertrophic cardiomyopathy. *neurogenetics* **16**, 319-323 (2015). https://doi.org:10.1007/s10048-015-0444-2

23 Galmiche, L. *et al.* Exome sequencing identifies MRPL3 mutation in mitochondrial cardiomyopathy. *Human Mutation* **32**, 1225-1231 (2011). https://doi.org:10.1002/humu.21562

24 Friederich, M. W. *et al.* Pathogenic variants in MRPL44 cause infantile cardiomyopathy due to a mitochondrial translation defect. *Molecular Genetics and Metabolism* **133**, 362-371 (2021). https://doi.org:10.1016/j.ymgme.2021.06.001

25 Rugarli, E. I. & Langer, T. Mitochondrial quality control: A matter of life and death for neurons. *EMBO J.* **31**, 1336-1349 (2012). https://doi.org:10.1038/emboj.2012.38

26 Fu, W., Kadeer, G., He, Y. & Feng, Y. The regulatory network of potential transcription factors and MiRNAs of mitochondria-related genes for sarcopenia. *Front Genet* **13**, 975886 (2022). https://doi.org:10.3389/fgene.2022.975886

27 Prokopidis, K., Giannos, P., Witard, O. C., Peckham, D. & Ispoglou, T. Aberrant mitochondrial homeostasis at the crossroad of musculoskeletal ageing and non-small cell lung cancer. *PLoS ONE* **17**, e0273766 (2022). https://doi.org:10.1371/journal.pone.0273766

28 Lopez Sanchez, M. I. G., Krüger, A., Shiriaev, D. I., Liu, Y. & Rorbach, J. Human Mitoribosome Biogenesis and Its Emerging Links to Disease. *Int. J. Mol. Sci.* **22**, 3827 (2021). https://doi.org:10.3390/ijms22083827

29 Gonçalves, A. M., Pereira-Santos, A. R., Esteves, A. R., Cardoso, S. M. & Empadinhas, N. The Mitochondrial Ribosome: A World of Opportunities for Mitochondrial Dysfunction Toward Parkinson's Disease. *Antioxidants & Redox Signaling* **34**, 694-711 (2020). https://doi.org:10.1089/ars.2019.7997

30 Scheibye-Knudsen, M., Scheibye-Alsing, K., Canugovi, C., Croteau, D. L. & Bohr, V. A. A novel diagnostic tool reveals mitochondrial pathology in human diseases and aging. *Aging* **5**, 192-208 (2013). https://doi.org:10.18632/aging.100546

31 Robinson, S., Denison, H., Cooper, C. & Aihie Sayer, A. Prevention and optimal management of sarcopenia: a review of combined exercise and nutrition interventions to improve muscle outcomes in older people. *Clinical Interventions in Aging*, 859 (2015). https://doi.org:10.2147/cia.s55842

32 Francisco, S., Ferreira, M., Moura, G., Soares, A. R. & Santos, M. A. S. Does proteostasis get lost in translation? Implications for protein aggregation across the lifespan. *Ageing Res. Rev.* **62**, 101119 (2020). https://doi.org:https://doi.org/10.1016/j.arr.2020.101119

33 Schmauck-Medina, T. *et al.* New hallmarks of ageing: a 2022 Copenhagen ageing meeting summary. *Aging* **14**, 6829-6839 (2022). https://doi.org:10.18632/aging.204248

34 Yang, Y.-F. *et al.* MICU3 regulates mitochondrial Ca2+-dependent antioxidant response in skeletal muscle aging. *Cell Death & Disease* **12** (2021). https://doi.org:10.1038/s41419-021-04400-5

35 Ballak, S. B., Degens, H., De Haan, A. & Jaspers, R. T. Aging related changes in determinants of muscle force generating capacity: A comparison of muscle aging in men and male rodents. *Ageing Res. Rev.* **14**, 43-55 (2014). https://doi.org:10.1016/j.arr.2014.01.005

36 Messa, G. A. M. *et al.* Morphological alterations of mouse skeletal muscles during early ageing are muscle specific. *Exp. Gerontol.* **125**, 110684 (2019). https://doi.org:10.1016/j.exger.2019.110684

37 Sheard, P. W. & Anderson, R. D. Age-related loss of muscle fibres is highly variable amongst mouse skeletal muscles. *Biogerontology* **13**, 157-167 (2012). https://doi.org:10.1007/s10522-011-9365-0

38 Pani, S. & Bal, N. C. in *Models, Molecules and Mechanisms in Biogerontology* 319-345 (Springer Singapore, 2020).

39 Hill, C., James, R. S., Cox, V. M., Seebacher, F. & Tallis, J. Age-related changes in isolated mouse skeletal muscle function are dependent on sex, muscle, and contractility mode. *American Journal of Physiology-Regulatory, Integrative and Comparative Physiology* **319**, R296-R314 (2020). https://doi.org:10.1152/ajpregu.00073.2020

40 Pietrangelo, L. *et al.* Age-dependent uncoupling of mitochondria from Ca2+ release units in skeletal muscle. *Oncotarget* **6**, 35358-35371 (2015). https://doi.org:10.18632/oncotarget.6139

41 Ono, T., Isobe, K., Nakada, K. & Hayashi, J.-I. Human cells are protected from mitochondrial dysfunction by complementation of DNA products in fused mitochondria. *Nature Genetics* **28**, 272-275 (2001). https://doi.org:10.1038/90116

42 Romanello, V. & Sandri, M. Implications of mitochondrial fusion and fission in skeletal muscle mass and health. *Seminars in Cell & Developmental Biology* (2022). https://doi.org:https://doi.org/10.1016/j.semcdb.2022.02.011

43 Protasi, F., Pietrangelo, L. & Boncompagni, S. Improper Remodeling of Organelles Deputed to Ca2+ Handling and Aerobic ATP Production Underlies Muscle Dysfunction in Ageing. *Int. J. Mol. Sci.* **22**, 6195 (2021). https://doi.org:10.3390/ijms22126195

44 Reid, K., Daniels, E. G., Vasam, G., Kamble, R., Janssens, G. E., Hu, I. M., Green, A. E., Houtkooper, R. H., & Menzies, K. J. (2023). Reducing mitochondrial ribosomal gene expression does not alter metabolic health or lifespan in mice. *Scientific Reports 2023 13:1*, *13*(1), 1–15. https://doi.org/10.1038/s41598-023-35196-3

45 Dickinson, M. E. *et al.* High-throughput discovery of novel developmental phenotypes: https://www.mousephenotype.org/. *Nature* **537**, 508-514 (2016). https://doi.org:10.1038/nature19356

46 Devaraju, P. *et al.* Haploinsufficiency of the 22q11.2 microdeletion gene Mrpl40 disrupts short-term synaptic plasticity and working memory through dysregulation of mitochondrial calcium. *Molecular Psychiatry* **22**, 1313-1326 (2017). https://doi.org:10.1038/mp.2016.75

47 Shcherbakov, D. *et al.* Mitochondrial misreading in skeletal muscle accelerates metabolic aging and confers lipid accumulation and increased inflammation. *RNA* **27**, 265-272 (2021). https://doi.org:10.1261/rna.077347.120

48 IMPC. *Defining Protocols - IMPReSS*, <https://www.mousephenotype.org/help/standardized-mouse-phenotyping/defining-protocols-impress/> (2019).

49 Bellantuono, I. *et al.* A toolbox for the longitudinal assessment of healthspan in aging mice. *Nature Protocols* **15**, 540-574 (2020). https://doi.org:10.1038/s41596-019-0256-1

50 Marcaletti, S., Thomas, C. & Feige, J. N. Exercise Performance Tests in Mice. *Current protocols in mouse biology* **1** (2011). https://doi.org:10.1002/9780470942390.MO100160

51 Uwera, F., Ammar, T., Mcrae, C., Hayward, L. J. & Renaud, J.-M. Lower Ca2+ enhances the K+-induced force depression in normal and HyperKPP mouse muscles. *Journal of General Physiology* **152** (2020). https://doi.org:10.1085/jgp.201912511

52 Edwards, J. N., Macdonald, W. A., van der Poel, C. & Stephenson, D. G. O2•− production at 37°C plays a critical role in depressing tetanic force of isolated rat and mouse skeletal muscle. *American Journal of Physiology-Cell Physiology* **293**, C650-C660 (2007). https://doi.org:10.1152/ajpcell.00037.2007

53 Scott, K. *et al.* KATP channel deficiency in mouse FDB causes an impairment of energy metabolism during fatigue. *Am. J. Physiol. Cell Physiol.* **311**, C559-C571 (2016). https://doi.org:10.1152/ajpcell.00137.2015

54 Plichta, S. B. in *Munro's Statistical Methods for Health Care Research: Sixth Edition* 247–262 (2011).

55 Watanabe, D. & Wada, M. Predominant cause of prolonged low-frequency force depression changes during recovery after in situ fatiguing stimulation of rat fast-twitch muscle. *American Journal of Physiology-Regulatory, Integrative and Comparative Physiology* **311**, R919-R929 (2016). https://doi.org:10.1152/ajpregu.00046.2016

16.7 Supplemental Figures

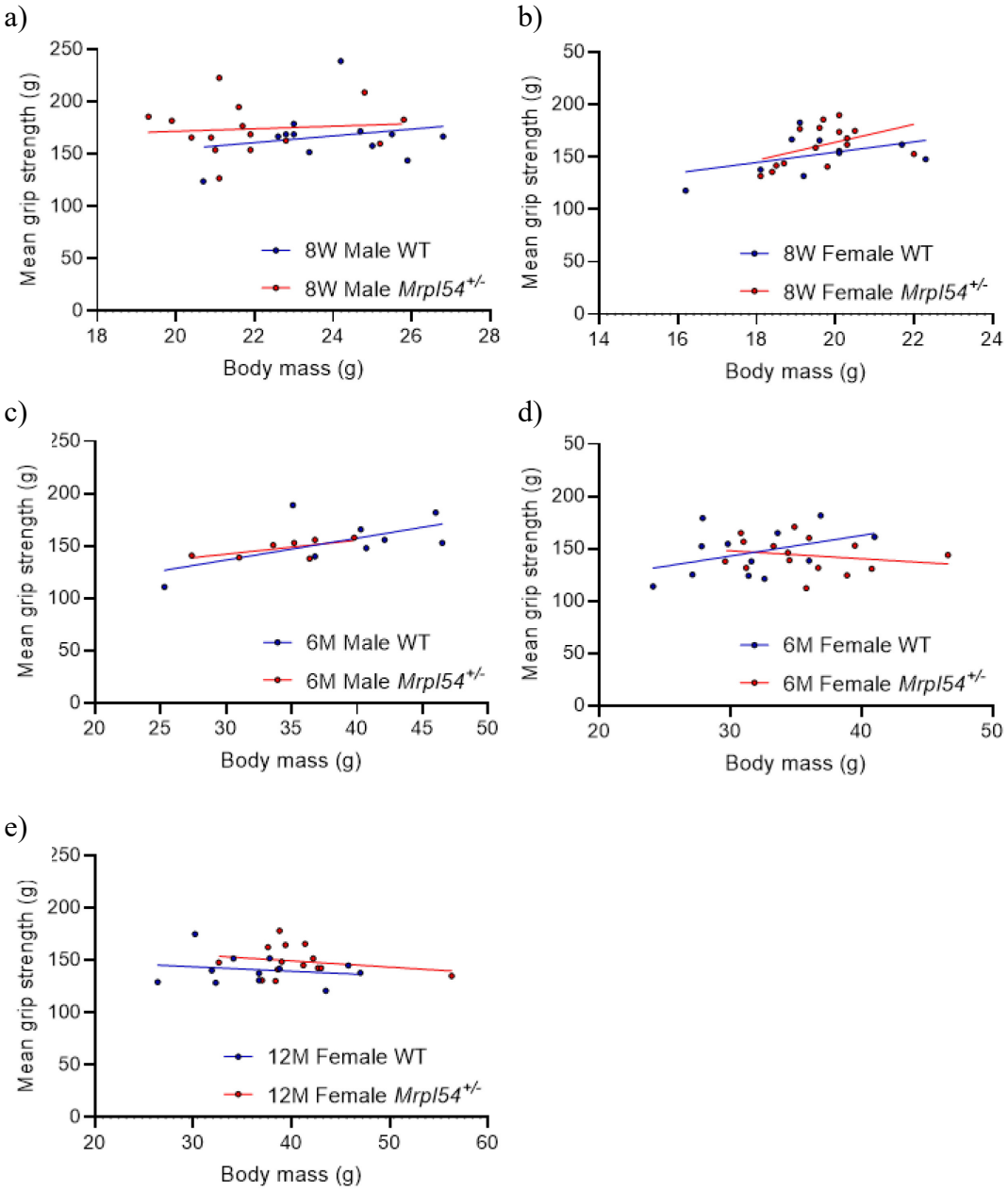

Figure 16.6 Supplemental: Mean grip strength adjusted for body mass using ANCOVA.

a) 8W male mean grip strength adjusted for body mass (n=12 WT; n=15 *Mrpl54*$^{+/-}$).

b) 8W female mean grip strength adjusted for body mass (n=10 WT; n=15 *Mrpl54*$^{+/-}$).

c) 6M male mean grip strength adjusted for body mass (n=8 WT; n=7 *Mrpl54*$^{+/-}$).

d) 6M female mean grip strength adjusted for body mass (n=12 WT; n= 15 *Mrpl54*$^{+/-}$).

e) 12M female mean grip strength adjusted for body mass (n=12 WT; n= 14 *Mrpl54*$^{+/-}$).

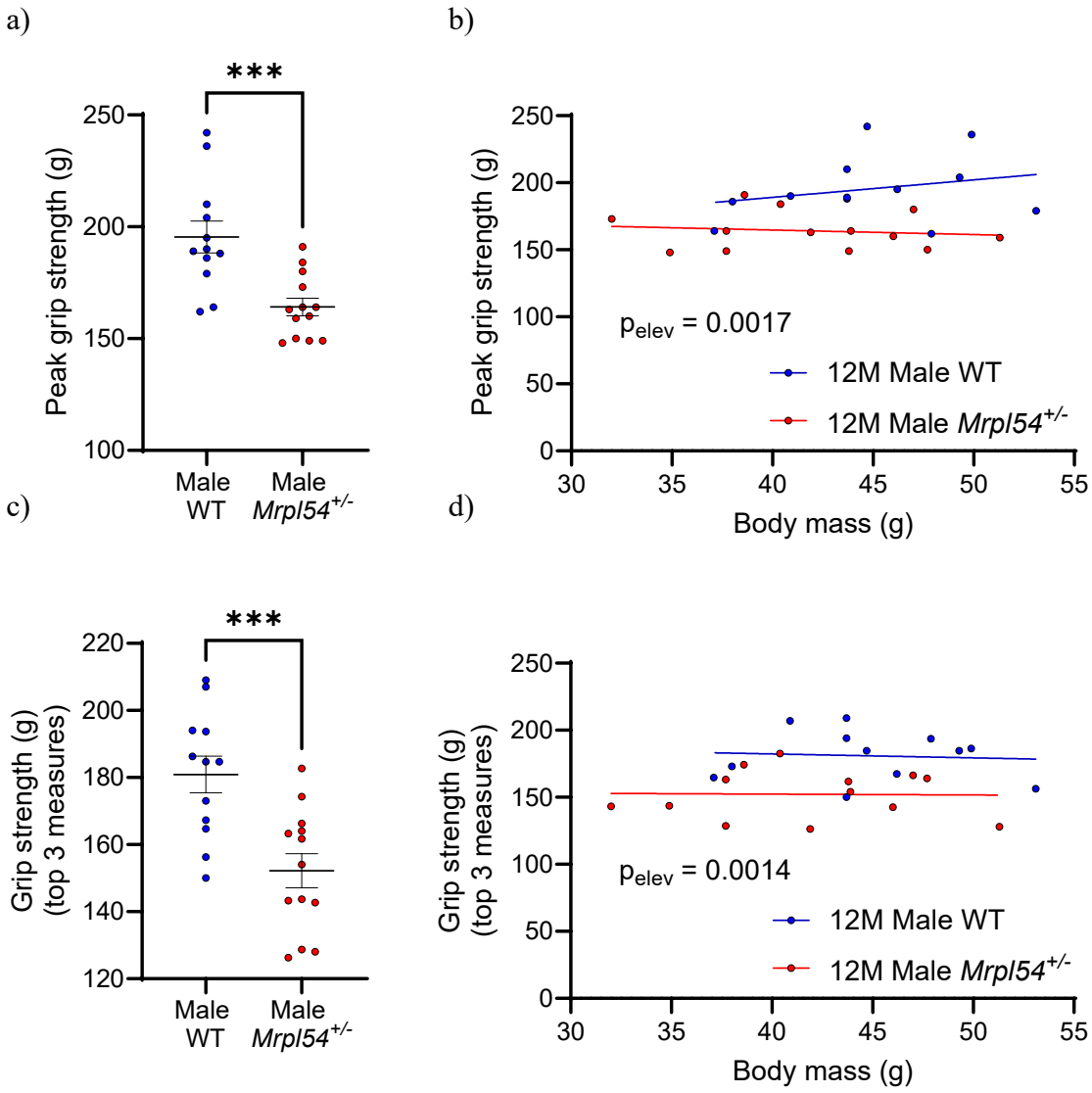

Figure 16.7 Supplemental: Peak grip strength and mean grip strength for top three measurements.

a) 12-month (12M) male peak grip strength (n=12 WT; n=13 *Mrpl54*$^{+/-}$).

b) 12M male peak grip strength adjusted for body mass using ANCOVA.

c) 12M male top three grip strength measurements (n=12 WT; n=13 *Mrpl54*$^{+/-}$).

d) 12M male top three grip strength measurements adjusted for body mass using ANCOVA. Values are means ± SE; **** p<0.0001.

17. Future Direction/Other Work In-Progress

17.1 Future direction – stress testing the *Mrpl54*$^{+/-}$ mouse model

In Sections 12 and 13, data and results were presented characterizing the *Mrpl54*$^{+/-}$ mouse model under low stress conditions. The predictions were that reducing *Mrpl54* gene expression in the mouse would result in mitohormetic effects, such as an increased health span or lifespan, as observed in the *C. elegans* reduced *Mrp* longevity model (Houtkooper et al., 2013). WT and *Mrpl54*$^{+/-}$ mice separated by sex were housed under low stress conditions with 5 to 10 animals in a large cage (at least 90 cm^2 per mouse), *ad libitum* access to food and water, and enrichment in the form of bedding, house domes, and cotton pads that could be shredded for nesting (André et al., 2018). Under these conditions, ~50% reduction in *Mrpl54* expression had no discernible effect on metabolic health with age or lifespan in either male or female mice (Reid et al., 2023).

Housing male C57BL/6NTac mice at greater than 3-5 mice per cage introduced unplanned conspecific aggression, which is known to reduce lifespan through subordination stress (Razzoli et al., 2018). In the *Mrpl54*$^{+/-}$ lifespan study, a male mouse exposed to severe conspecific aggression (i.e., aggression that resulted in either injury or the death of a mouse) was separated from his cage mates and moved to individual housing. If male separation was required, it happened between 3-6-months of age, leaving the male in individual housing for most of his lifespan. A male *Mrpl54*$^{+/-}$ mouse exposed to severe conspecific aggression and then subsequently individually housed may have a better life expectancy than WT (Fig. 17.1). Compared to individually housed WT males, the overall life expectancy hazard ratio (HR) leaned in the direction of favouring individually housed *Mrpl54*$^{+/-}$ males (HR 1.34, 95% CI 0.53, 1.6, p=0.28) (Fig. 17.1a). Compared to group-housed WT males, individually housed *Mrpl54*$^{+/-}$ males had an extended overall life expectancy (HR 1.56, 95% CI 1.02, 2.39, p=0.005) (Fig. 17.1b). 24-month life expectancy results

(the upper limit used for C57/BL6 because of strain-specific age effects (Hagan, 2017)) were even more pronounced (Fig. 17.1c-d). These lifespan results favoring individually housed *Mrpl54*$^{+/-}$ males arose after unplanned aggression and separation of males and so are hypothesis generating only.

By definition, a mitohormetic is the introduction of a mild mitochondrial stressor that then primes an organism to resist future stressors (Yun & Finkel, 2014). Reducing the expression of *Mrpl54* in the mouse failed to affect lifespan or metabolic health span under low stress conditions. However, the seemingly positive lifespan results for *Mrpl54*$^{+/-}$ males individually caged after exposure to conspecific aggression suggest that reduced *Mrpl54* expression may have positive health benefits under high stress conditions. Amongst individually housed male mice that experienced conspecific aggression in the *Mrpl54*$^{+/-}$ longevity study, the high stress likely came from subordination, lack of social housing, or both (Razzoli et al., 2018; Võikar et al., 2005). To test this hypothesis, future lifespan studies could test the *Mrpl54*$^{+/-}$ mouse model using stress conditions that are known to impact lifespan, such as the lifelong chronic psychosocial stress model (Razzoli et al., 2018).

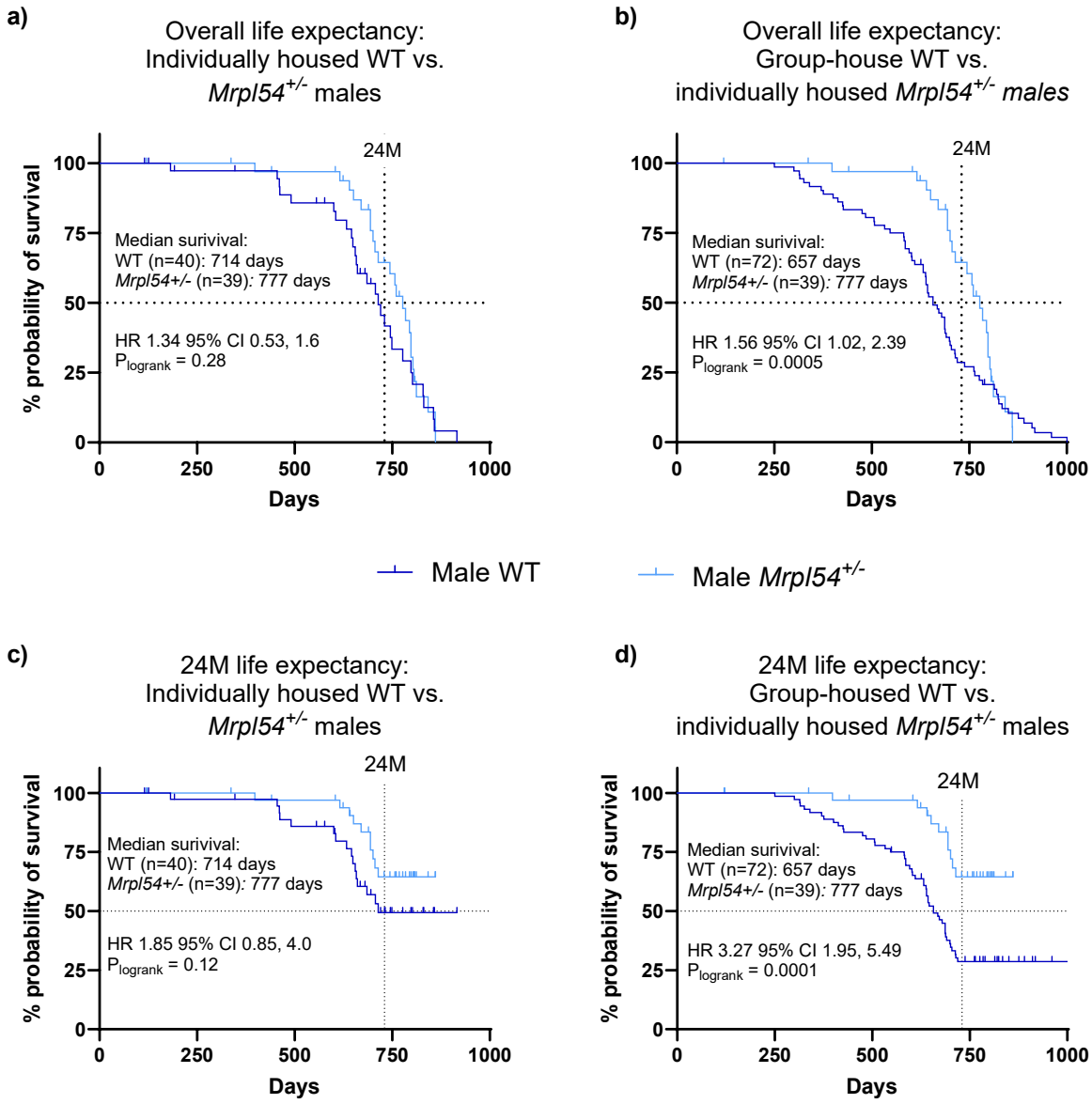

Figure 17.1 Life expectancy comparison between WT and Mrpl54$^{+/-}$ male mice.

Male mice exposed to severe conspecific aggression were individually housed versus group-housed males (Reid et al., 2023).

a) Overall life expectancy of male individually housed WT vs. individually housed Mrpl54+/-.

b) Overall life expectancy of male group-housed WT vs. individually housed Mrpl54+/-.

c) 24M life expectancy of male individually housed WT vs. individually housed Mrpl54+/-.

d) 24M life expectancy of male group-housed WT vs. individually housed Mrpl54+/-.

24M – 24-month, CI – confidence interval, HR – hazard ratio, WT – wildtype

17.2 Work in-progress – *Sirt1*$^{-/-}$ mouse model

Improving or maintaining the function of mitochondria with age (e.g., maintaining mitoproteostasis and reducing excess ROS production) is recognized as an upstream health target to maintain health span and to prevent (or reduce the effects of) neurodegenerative diseases (e.g., Alzheimer's and Parkinson's Disease) (Olagunju et al., 2023). A key player in maintaining mitochondrial function with age is the silent information regulator-1 (SIRT1), which is a NAD^+-dependent lysine deacetylase found in both the nucleus and the cytoplasm. SIRT1 signalling is considered a longevity pathway because it is a hub of intracellular communication that affects multiple cellular processes including cell survival and apoptosis, inflammation, stress adaptation, metabolism, and cellular senescence (C. Chen et al., 2020). With age, SIRT1 levels decrease (along with NAD^+ levels) and this decrease is exacerbated in aged patients with neurodegenerative diseases (Xu et al., 2023).

In the roundworm, overexpression of *Sir-2.1* (the orthologue of mammalian *Sirt1*) will increase lifespan by 10-25% (Mouchiroud et al., 2013; Viswanathan & Guarente, 2011). The increase in lifespan is dependent on the induction of the UPR^{mt} and a mitonuclear protein imbalance (Mouchiroud et al., 2013). Likewise, blocking *Sir-2.1* expression in the roundworm blocks the induction of the UPR^{mt} and abrogates lifespan extension. In primary mouse hepatocytes, increasing SIRT1 signalling will induce a mitonuclear protein imbalance and the UPR^{mt}. Abrogating *Sirt1* expression (via adenovirus-controlled *Cre* recombinase infected *Sirt1* floxed mouse primary hepatocytes) blocks induction of both the mitonuclear imbalance and the UPR^{mt} (Mouchiroud et al., 2013)

While whole-body overexpression of *Sirt1* does not extend mouse lifespan, it does promote healthy aging (e.g., improved glucose tolerance and reduced spontaneous tumour generation)

(Herranz et al., 2010). Brain-specific overexpression of *Sirt1* in transgenic mice (BRASTO mice) shows enhanced neural activity with age, a delayed aging phenotype, as well as an increased lifespan (extension of ~11% for median lifespan and ~10% for maximal lifespan) (Satoh et al., 2013). Delayed aging characteristics in BRASTO mice includes increased skeletal muscle mitochondrial function, dark time physical activity, and sleep quality at age 20 months.

To test whether the absence of SIRT1 will accelerate the decline of metabolic health with age and whether abrogation of the UPR^{mt} and a mitonuclear protein imbalance is involved in a SIRT1-mediated decline, we generated outbred whole-body male *Sirt1* knock out mice (*Sirt1*$^{-/-}$) (McBurney et al., 2003). To examine metabolic health with age, we subjected *Sirt1*$^{-/-}$ mice to EchoMRI and indirect calorimetry at age 7-10 months and again at 13-15 months and compared them to WT. *Sirt1*$^{-/-}$ mice do not synthesize the SIRT1 protein (McBurney et al., 2003) and are ~40% smaller than control mice (Fig. 17.2.1a), although there is no difference in fat or lean mass composition relative to body mass (Fig 17.2.1b). Indirect calorimetry using the Comprehensive Lab Animal Monitoring System (CLAMS, Columbus Instruments Inc.) at 7-10 months and again at 13-15 months revealed that the smaller *Sirt1*$^{-/-}$ male mice inhaled a lower volume of O_2 (VO_2) than WT, particularly during the active dark cycle (Fig. 17.2.2a-b). However, the differences can be explained by a smaller body mass (Fig. 17.2.2c). The respiratory exchange ratio (RER, VCO_2/VO_2) was no different between WT and *Sirt1*$^{-/-}$ mice at 7-10 months or 13-15 months (Fig. 17.2.3a). Ambulatory motion (total beam break counts) for both WT and *Sirt1*$^{-/-}$ mice at both time points was unusually high, which suggests the mice were in a stressed state; however, both the active dark phase and the less active light phase were discernible (Fig. 17.2.3b). No difference in ambulatory motion was noted between WT and *Sirt1*$^{-/-}$ mice at 7-10 months or 13-15 months.

Energy intake (kCal/hour) was lower in *Sirt1*$^{-/-}$ males (Fig. 17.2.3c); however, like VO_2, the difference can be explained by the lower *Sirt1*$^{-/-}$ body mass (Fig. 17.2.3c inset).

These results contradict a previously published study examining the same *Sirt1*$^{-/-}$ mouse model, which reported *Sirt1*$^{-/-}$ mice as hyperphagic (increased food consumption), less active during the dark phase, higher VO_2, and a RER close to 0.7, indicating a reliance on lipid substrates for fuel (Boily et al., 2008). The difference in results can be attributed to dividing parameters by body mass instead of regression through an ANCOVA analysis (Macena & Bueno, 2023; Tschöp et al., 2012). As well, the mice in the present study had unusually high ambulatory motion (total number of beam breaks) in the CLAMS, which is in an indicator of high stress and may have impacted the results.

Like the ambiguous results from whole-body overexpression of *Sirt1* (Herranz et al., 2010), a whole-body knock (*Sirt1*$^{-/-}$) demonstrates ambiguous results with respect to an aging phenotype. *Sirt1*$^{-/-}$ mice are undoubtedly smaller, have a disabling eye phenotype, and do not survive long into adulthood but these affects appear to be developmental rather than related to aging. Since the BRASTO mouse (brain-specific overexpression of SIRT1) showed extended lifespan and healthy aging effects (Satoh et al., 2013), future directions using the *Sirt1*$^{-/-}$ mouse model could investigate the brain-specific knock-out of *Sirt1* through metabolic testing as well as testing for the induction of a mitonuclear imbalance and the UPR^{mt} within brain tissue.

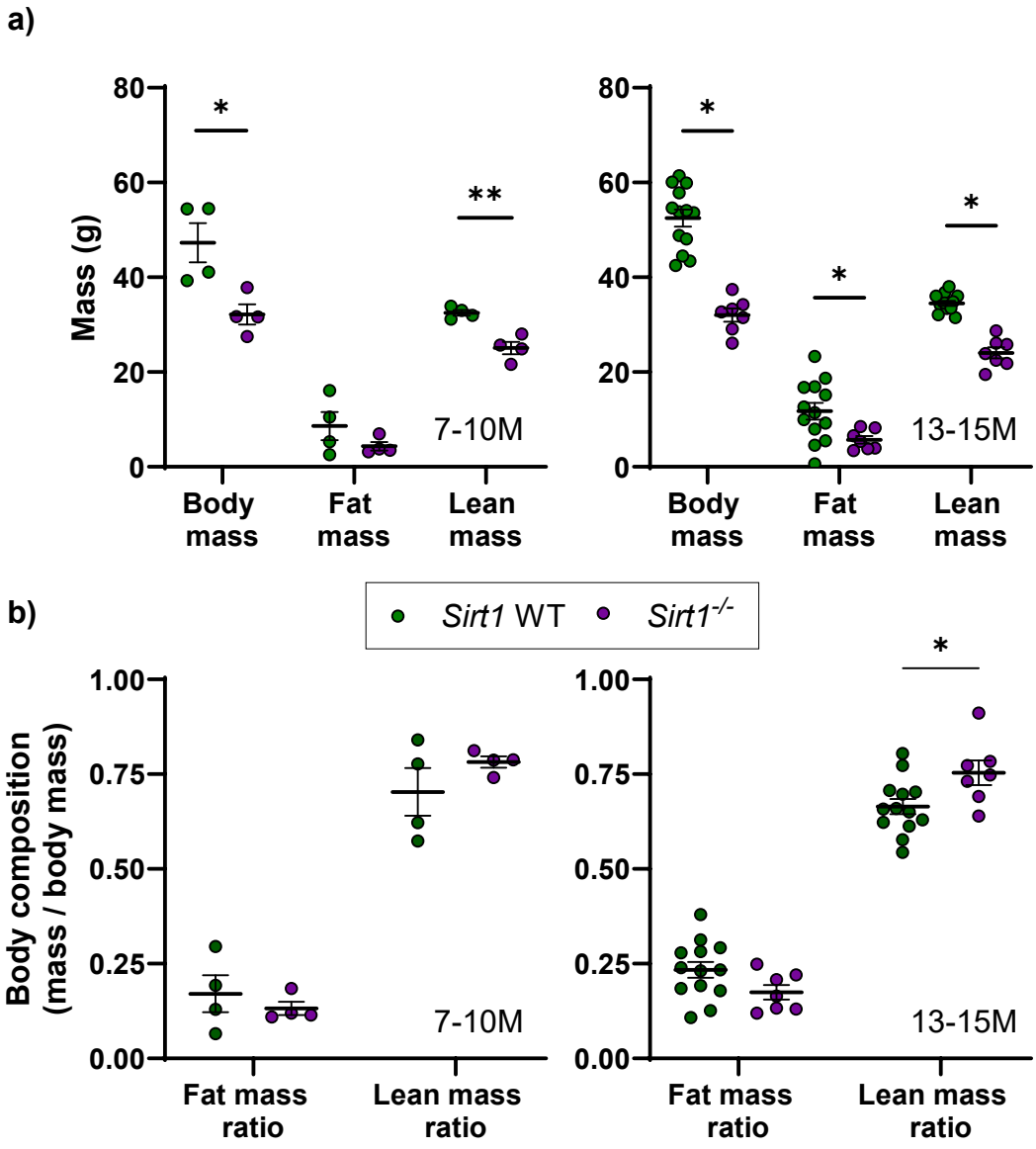

Figure 17.2.1 Body composition of *Sirt1* WT vs. *Sirt1*$^{-/-}$ mice.

WT vs. *Sirt1*$^{-/-}$ mice at ages 7-10 months (7-10M; WT n=4; *Sirt1*$^{-/-}$ n=4) and 13-15 months (13-15M; WT n=13; *Sirt1*$^{-/-}$ n=7).

a) *Sirt1*$^{-/-}$ are significantly smaller than WT, although

b) the relative fat and lean mass compositions are no different between *Sirt1*$^{-/-}$ and WT. Values are means ± SE; * $p<0.05$; ** $p<0.01$.

7-10M – 7-10 months; 13-15M – 13-15 months; SE – standard error; WT – wildtype

.

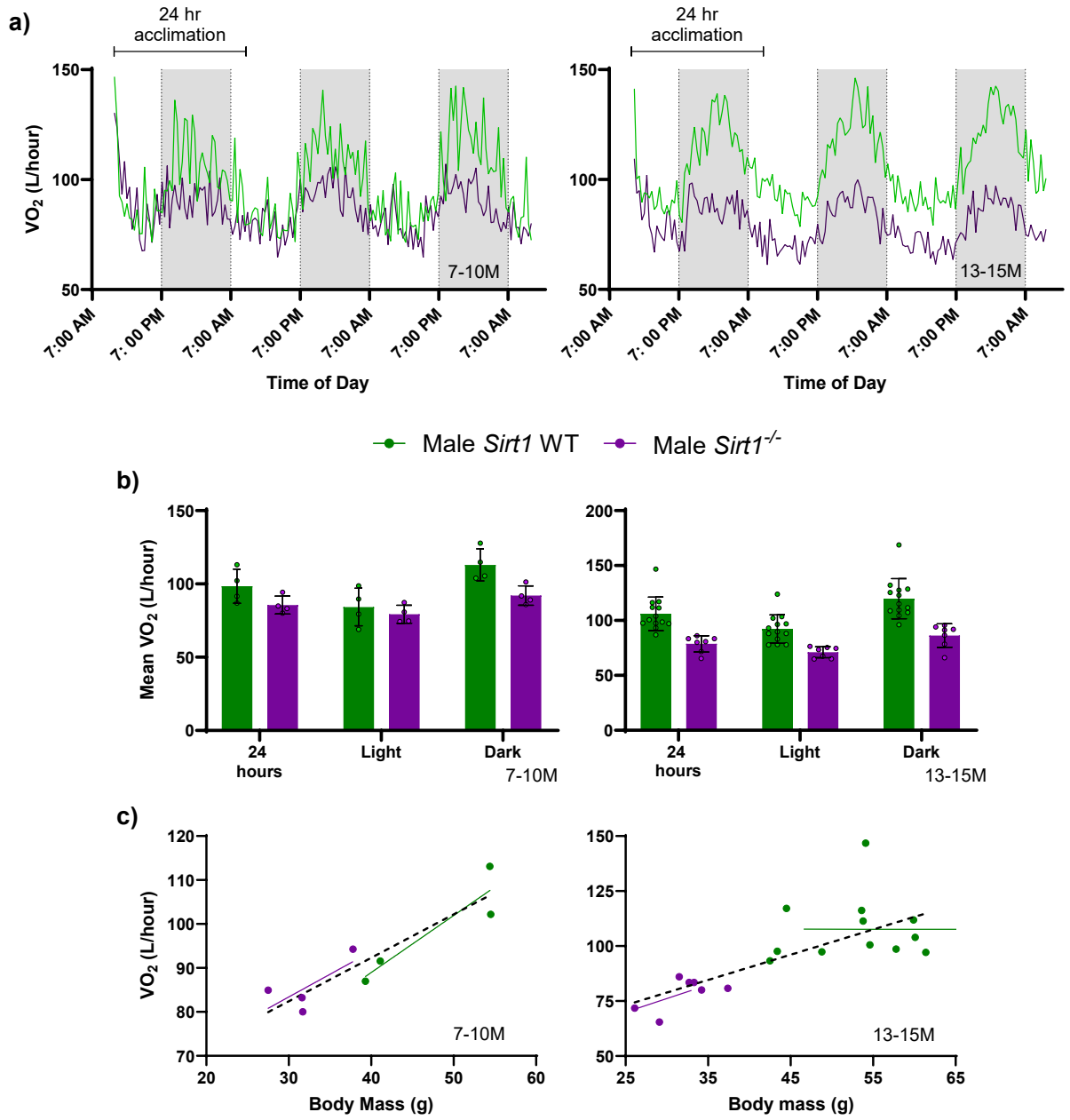

Figure 17.2.2 Mean volume of O_2 inhalation (VO_2 in L/hour) in *Sirt1*$^{-/-}$ and WT mice.

Using indirect calorimetry,
a-b) *Sirt1*$^{-/-}$ mice display lower O_2 consumption during the active phase at 7-10M (WT n=4; *Sirt1*$^{-/-}$ n=4) and at both light dark phases at 13-15M (WT n=13; *Sirt1*$^{-/-}$ n=7).

c) However, the differences in 24-hour VO_2 can be explained by a lower body mass in *Sirt1*$^{-/-}$ mice. Values are means ± SE; * $p<0.05$; *** $p<0.001$.

7-10M – 7-10 months; 13-15M – 13-15 months; SE – standard error; WT – wildtype

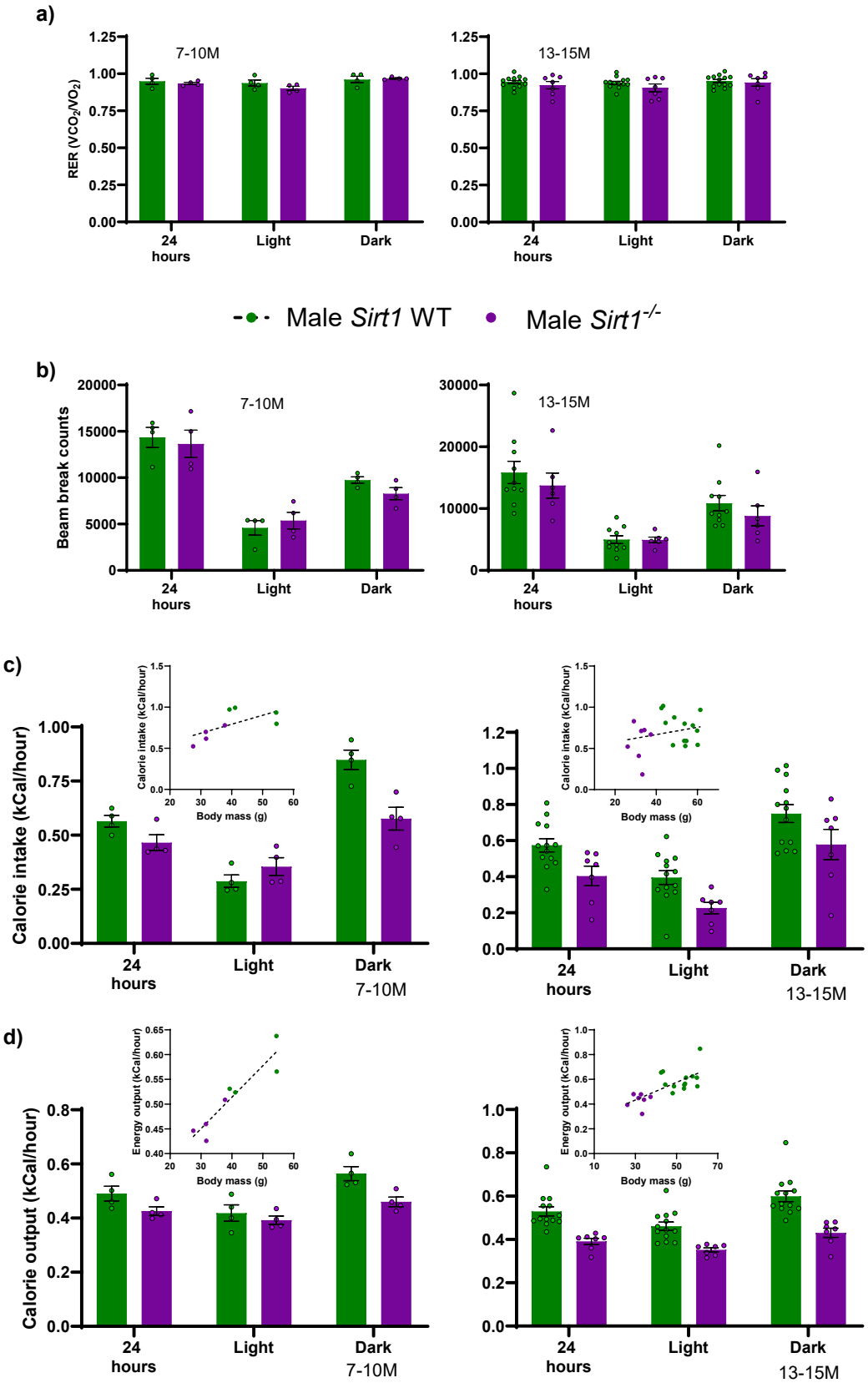
a)
7-10M
13-15M
RER (VCO_2/VO_2)
24 hours
Light
Dark
Male Sirt1 WT
Male Sirt1-/-
b)
Beam break counts
c)
Calorie intake (kCal/hour)
Body mass (g)
7-10M
13-15M
d)
Calorie output (kCal/hour)
Energy output (kCal/hour)

Figure 17.2.3 Indirect calorimetry parameters comparing *Sirt1*$^{-/-}$ and WT mice.

Sirt1$^{-/-}$ and WT mice at 7-10M (WT n=4; *Sirt1*$^{-/-}$ n=4) and 13-15M (WT n=13; *Sirt1*$^{-/-}$ n=7).

a) No difference in RER between WT and *Sirt1*$^{-/-}$ mice.

b) No difference in ambulatory motion between WT and *Sirt1*$^{-/-}$ mice.

c-d) Calorie intake and output were lower in *Sirt1*$^{-/-}$ mice; however, these results were explained by the lower body mass of *Sirt1*$^{-/-}$ mice (c-d insets showing dark period calorie intake and energy output regressed against body mass).

Values are means ± SE.

7-10M – 7-10 months; 13-15M – 13-15 months; RER – respiratory exchange ratio; WT – wildtype

17.3 Work in-progress – high-throughput testing of anti-aging compounds

Houtkooper *et al*. (2013) demonstrated that invoking the UPR^{mt} by targeting mitochondrial translation and generating a mitonuclear protein imbalance will improve lifespan and health span in *C. elegans.* Alzheimer's Disease (AD) is an age-related disorder characterized by aggregation of amyloid protein peptides that invokes the UPR^{mt} (Sorrentino 2017). Intriguingly, Sorrentino *et al.* (2017) targeted mitochondrial translation to successfully invoke a mitonuclear protein imbalance, induce the UPR^{mt}, and delay aggregation of amyloid-β peptide (Aβ). Use of doxycycline to target mitochondrial translation in human SH-SY5Y neuroblastoma cells (with Swedish mutation K670N/M671L in the amyloid precursor protein [*APP*] gene) induces a mitonuclear protein imbalance and the UPR^{mt} and reduces intracellular Aβ deposits (Sorrentino et al., 2017). Likewise, inducing a mitonuclear protein imbalance and the UPR^{mt} using doxycycline or reducing *Mrps5* expression reduced Aβ aggregation in a *C. elegans* model (Sorrentino et al., 2017). These results indicate that targeting mitochondrial translation and invoking the UPR^{mt} can improve mitochondrial proteostasis and potentially delay amyloid-proteotoxic diseases like AD.

The Worm Tracker high-throughput system is designed to rapidly screen compounds that could potentially affect lifespan or health span through the induction of UPR^{mt} (Perni et al., 2018).

It is based on increased protein aggregation (i.e., disrupted proteostasis) – a known hall mark of aging (López-Otín et al., 2013, 2023). The GMC101 *C. elegans* model expresses full-length human Aβ peptide in its body muscle, driven by a temperature-dependent heavy chain muscle myosin promoter (Mccoll et al., 2012). Once the roundworms are moved from 20°C to 25°C, Aβ aggregation begins, and the worms become paralysed over the span of two days. The Worm Tracker system can quantify both thrashing and crawling worm behaviours, both of which decrease with age and, in the GMC101 roundworm, with the onset of Aβ-mediated paralysis. A compound that induces a mitonuclear protein imbalance and the UPR^{mt} and then decreases or delays age-related protein aggregation is thought to also be a good candidate to increase lifespan or health span through the delay in the onset of age-related diseases (e.g., AD and Inclusion Body Myositis, both of which have Aβ aggregation in neuronal and muscle tissue, respectively (Blagosklonny, 2017; Lilleker et al., 2019)).

As proof of concept, GMC101 roundworms were treated with doxycycline to target mitochondrial translation, induce a mitonuclear protein imbalance and the UPR^{mt}, and extend *C. elegans* lifespan in a dose-dependent manner (Houtkooper et al., 2013; Sorrentino et al., 2017). As measured by the Worm Tracker thrashing assay, 25°C GMC101 roundworms treated with doxycycline had similar levels of motion as 20°C worms treated with vehicle (H_2O) only, indicating that doxycycline rescued Aβ-mediated paralysis (Fig. 17.3).

Ideally, anti-aging compounds could be combined to provide an additive or synergistic anti-aging effect; however, to be additive, the mode of action of individual compounds need to follow different biochemical pathways. Two compounds that fulfill this criterion are rapamycin and low-dose lithium. Rapamycin is a recognized anti-aging compound that induces a mitonuclear imbalance and the UPR^{mt}, and extends *C. elegans* lifespan (Houtkooper et al., 2013). Low-dose

lithium likewise extends *C. elegans* lifespan through pleiotropic effects including increased mitochondrial biogenesis (Singulani et al., 2021). Rapamycin's anti-aging effects act primarily through the inhibition of the mTOR (mammalian target of rapamycin) nutrient sensing pathway, through a reduction in global mRNA translation (i.e., reducing energetic demands) or through activation of autophagy, which allows clearance of damaged cells (Robida-Stubbs et al., 2012). The anti-aging effects of low-dose lithium are thought to include mTOR-independent autophagy and telomere lengthening (Coutts et al., 2018; McColl et al., 2008; Sarkar et al., 2005). Low-dose lithium is also an inhibitor of HDAC 1 and so HDAC inhibition may also play a role in lithium's anti-aging effects (Wu et al., 2013). Rapamycin and low-dose lithium were shown to have an additive effect against neurodegeneration in a Huntington's Disease *Drosophila* model (Sarkar et al., 2008). They were also tested in combination in a mouse model of protein-aggregating Machado-Joseph disease (Duarte-Silva et al., 2016). Unfortunately, the lithium/rapamycin-treated mice experienced neurotoxicity and the authors concluded that the lithium dose was too high. Indeed, lithium at high doses will activate mTOR through the inhibition of glycogen synthase kinase-3β, effectively reducing autophagy (Sarkar et al., 2008).

Using the Worm Tracker system, the mobility of temperature-induced GMC101 worms were tested after separate rapamycin and low-dose lithium treatments, using doxycycline as a positive control. Compared to vehicle (H_2O), both LiCl (5 mM) and the positive control (15 μg/mL doxycycline) successfully rescued muscle paralysis in GMC101 worms with temperature induced Aβ expression (Fig. 17.3); however, rapamycin (100 μM) failed to dissolve in nematode media. The next steps are to optimize the dissolution of rapamycin in nematode media, then test separately and in combination with low dose lithium for additive/synergistic effects.

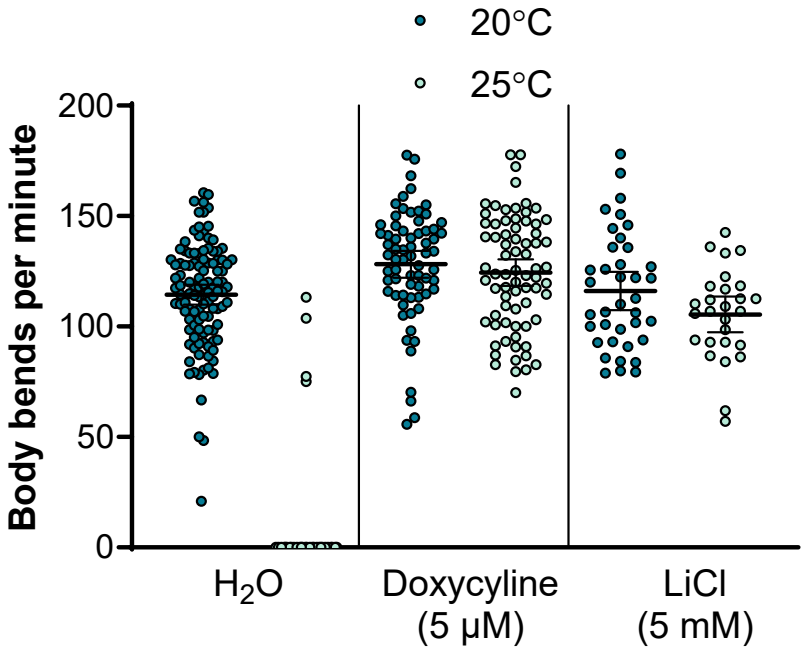

.

Figure 17.3 Worm Tracker thrasher test for compounds that can rescue temperature-induce Aβ aggregation and worm paralysis.

After induction at 25°C, GMC101 worms become paralyzed from the aggregation of Aβ in the body muscle. Both doxycycline (15 µg/mL) and LiCl (5 mM) rescues paralysis.

Values are means ± SE.

Aβ – amyloid-beta peptide; LiCl – lithium chloride

17.4 Work in-progress – *Polypterus senegalus* land-acclimation model

One of the central and least well-answered questions relating to the fish-tetrapod transition asks what are the factors that facilitate the transition from water to land locomotion (Long & Gordon, 2004)? It may be that phenotypic plasticity (where a new environment induces an organism to change morphology and physiology) plays an important role in facilitating the evolution of novel traits (West-Eberhard, 2003). Alternately, phenotypic plasticity may play a role in facilitating the evolutionary transition between pre-adaptations to adaptations (i.e., the re-emergence of a previous adaptation when encountering a similar environment) or co-opting an old trait for a new function (i.e., exaptation) (Rodgers & Gomez Isaza, 2023). In other words, phenotypic plasticity may allow an organism to survive and reproduce in a novel (often extreme) environment long enough for successful adaptions or acclimations to become fixed heritable adaptations. Rogers & Isaza (2023) place this hypothesis in the context of cross-protection (i.e., hormesis) where exposure to complex stressors (i.e., alterations to an organism's environment that challenge performance or fitness) increases resilience to future stressors. In this regard, cross-protection is seen as a pre-adaptation (Rodgers & Gomez Isaza, 2023). In the fish-tetrapod transition, exposure to an air environment and terrestrial locomotion may have provided a complex stressor with a hormetic (cross-protective) response that permitted survival as well as facilitated adaptation. In this regard, studying extant amphibious fish and how they acclimate to a terrestrial environment can give insight into the fish-tetrapod transition.

P. senegalus belongs to an ancient class of fish, the bichirs, which are a basal group of ray-finned fishes (i.e., a basal actinopterygian) and possibly the most primitive of living bony fish (Noack et al., 1996; Yang et al., 2015). Due to their ability to breathe air along with muscular pectoral fins, *P. senegalus* is capable of terrestrial locomotion (Du et al., 2016). These features

make *P. senegalus* an ideal model to study land-acclimation and the tetrapod water-to-land transition (Hale et al., 2022; Standen et al., 2014).

In their natural environment, *P. senegalus* can move on land using a contralateral gait and can successfully acclimate to an air environment – at least for short stints during seasonal drying of their habitat (Du et al., 2016). Standen *et al.* (2014) asked what happens to *P. senegalus* behaviour and developmental morphology after juveniles are exposed to an air-breathing terrestrial environment (water depth 3 mm) for 8-months. They found that fish raised on land developed a more predictable and efficient walking gait, raised their heads higher, and their pectoral anatomy displayed phenotypic plasticity in response to the change in forces experienced by the skeleton. Intriguingly, the skeletal changes observed in land-raised *P. senegalus* resemble what is observed in the fossil remains of stem tetrapods (Andrews & Westoll, 1970). Additional anatomical and physiological changes in land-raised *P. senegalus* include 28% more fast-twitch (i.e., glycolytic) muscle fibers in the pectoral fins used in the terrestrial contralateral gait (Du & Standen, 2017). The proportion of fast-twitch muscle fibers near the pectoral girdle increases in land-raised fish and there is a larger proportion of small diameter fibers (<5 μm), suggesting increased muscle fiber growth potential (i.e., hyperplasia) in land-raised *P. senegalus* (Du & Standen, 2017). These changes in muscle fiber type, location, and growth potential are evidence of adaptive plasticity that allow *P. senegalus* to harness greater bursts of power during locomotion on land. Whether the anatomical and physiological changes in land-raised *P. senegalus* constitute a hormetic response to a stressful environment and facilitate the evolution of traits conducive to terrestrial locomotion requires multigenerational experiments. However, breeding *P. senegalus* in a laboratory setting has proved challenging.

A major area of functional change during the transition from water to land is respiration, with a switch from sufficient to poor gas exchange across the gills. For *P. senegalus* raised in a terrestrial environment, poor gas exchange across the gills (diffusion of O_2) necessitates the switch to a reliance on air-sacs (convection of O_2) possibly via spiracle respiration (paired tubes that extend from the dorsal surface of the skull to the buccopharyngeal chamber) (Graham et al., 2014). In facultative air-breathing fish, the gills have a different respiratory potential than air-breathing organs, and so the switch to lungs will likely impact energetic costs (da Cruz & Fernandes, 2016; Fernandes & Moron, 2020; McMahon, 1970). To examine the effect on ATP production after 7.5-months in a terrestrial environment and the switch from gills to lungs, we isolated mitochondria from body muscle using differential centrifugation (Djafarzadeh & Jakob, 2017). We raised juvenile fish raised in terrestrial (gravel with ~3 mm water, n=13), aquatic plus exercise (aquatic conditions plus 30 cm daily walk down a 5° ramp, n=11), and aquatic (control, n=11) environments (Fig 17.4.1a) (Du & Standen, 2020), and then tested OXPHOS efficiency using respiration polarography (Clark-type electrode, Hansatech Instruments) (Banh et al., 2016).

Pre- versus post-study comparison of fish body mass and length indicated that juvenile *P. senegalus* raised in terrestrial conditions did not grow appreciably during the 7.5-month study (Fig. 17.4.1b), despite consuming the same amount of food as control fish (Du & Standen, 2020). In contrast, *P. senegalus* raised in aquatic conditions increased their body mass by 50-60% and their body length by ~25%. These results indicate that *P. senegalus* is expending energy at the expense of growth while in a terrestrial environment. The yield of isolated mitochondria per mg of *P. senegalus* body muscle tissue was high; however, OXPHOS activity was not consistently measurable using current methodology to isolate mitochondria via differential centrifugation. To preserve mitochondrial function, the time between muscle dissection and measurement of O_2

consumption was minimized by adding muscle homogenate directly to the Clarke-type electrode and bypassing differential centrifugation (Doerrier et al., 2018). The results indicated a strong response to mitochondrial substrates and inhibitors (Fig. 17.4.2a); however, the variation between individuals was too high to allow comparison between land-raised and control fish. Isolated intact body and fin muscle fibers from an aquatic control *P. senegalus* were then tested using real-time cell metabolic analysis (Seahorse XF Analyzer, Agilent) (Spangenburg & Ward, 2016). Preliminary results successfully generated an OXPHOS profile, except for the absence of oligomycin-mediated ATP synthase inhibition (an old aliquot of oligomycin is suspected) (Fig. 17.4.2b). The next steps will be to replicate the muscle fiber respiration results and optimize the method to produce consistent results between technical replicates. Once this is achieved, then the method can be applied to compare muscle fiber respiration between terrestrial and aquatic control fish.

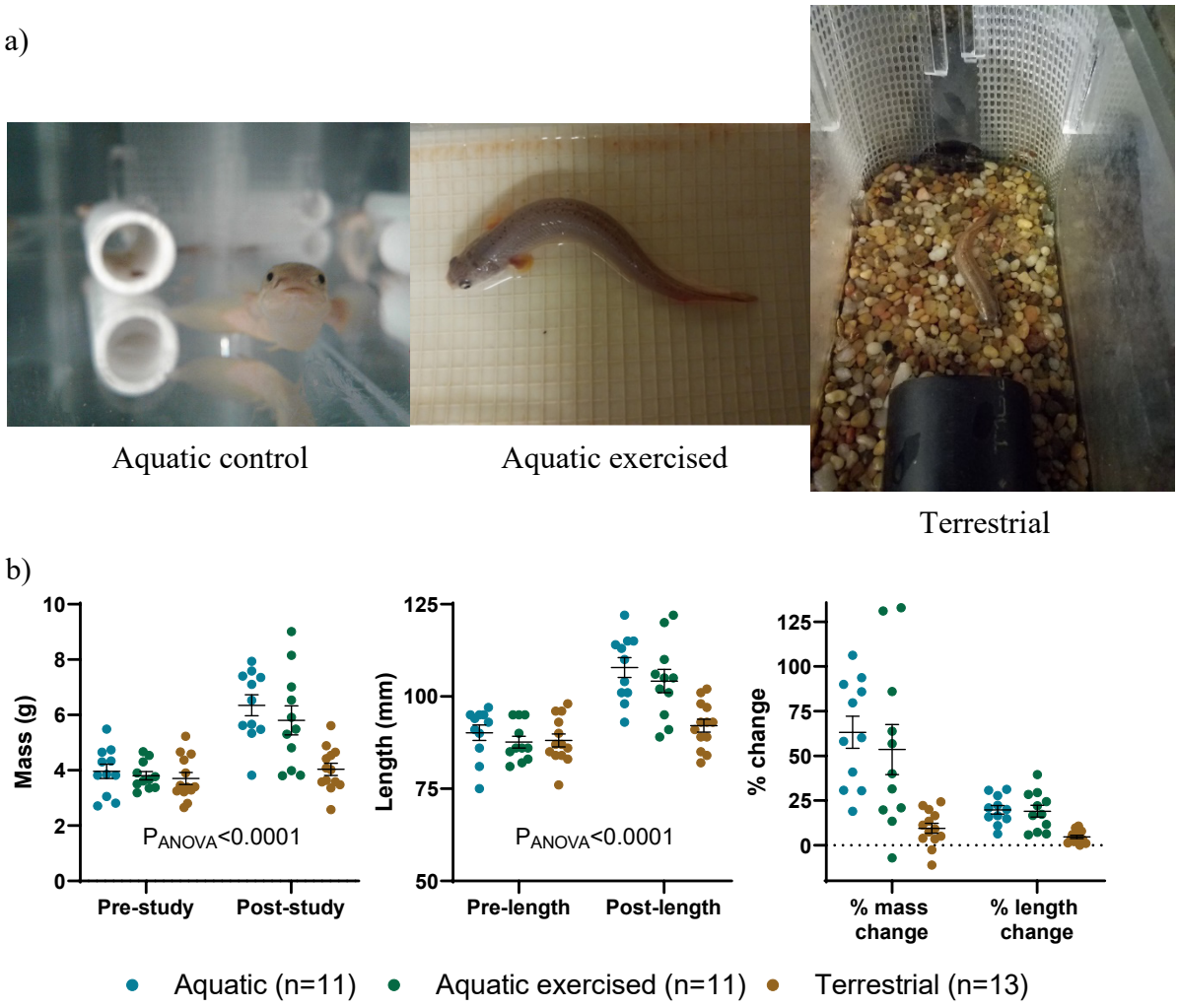

Figure 17.4.1 *P. senegalus* experimental conditions and change in body mass and length.

a) Juvenile *P. senegalus* raised in aquatic control, aquatic exercised (aquatic plus ~30 cm daily walk on 5° ramp), and terrestrial (gravel with 3 mm water) conditions.

b) After 7.5 months, juvenile *P. senegalus* raised in an aquatic environment increased both body mass and length whereas *P. senegalus* raised in a terrestrial environment maintained both body mass and length.

Values are means ± SE; 2-way ANOVA with Dunnett's multiple comparisons test (aquatic control vs. terrestrial) and Tukey's correction for multiple comparisons.

ANOVA – analysis of variance; SE – standard error

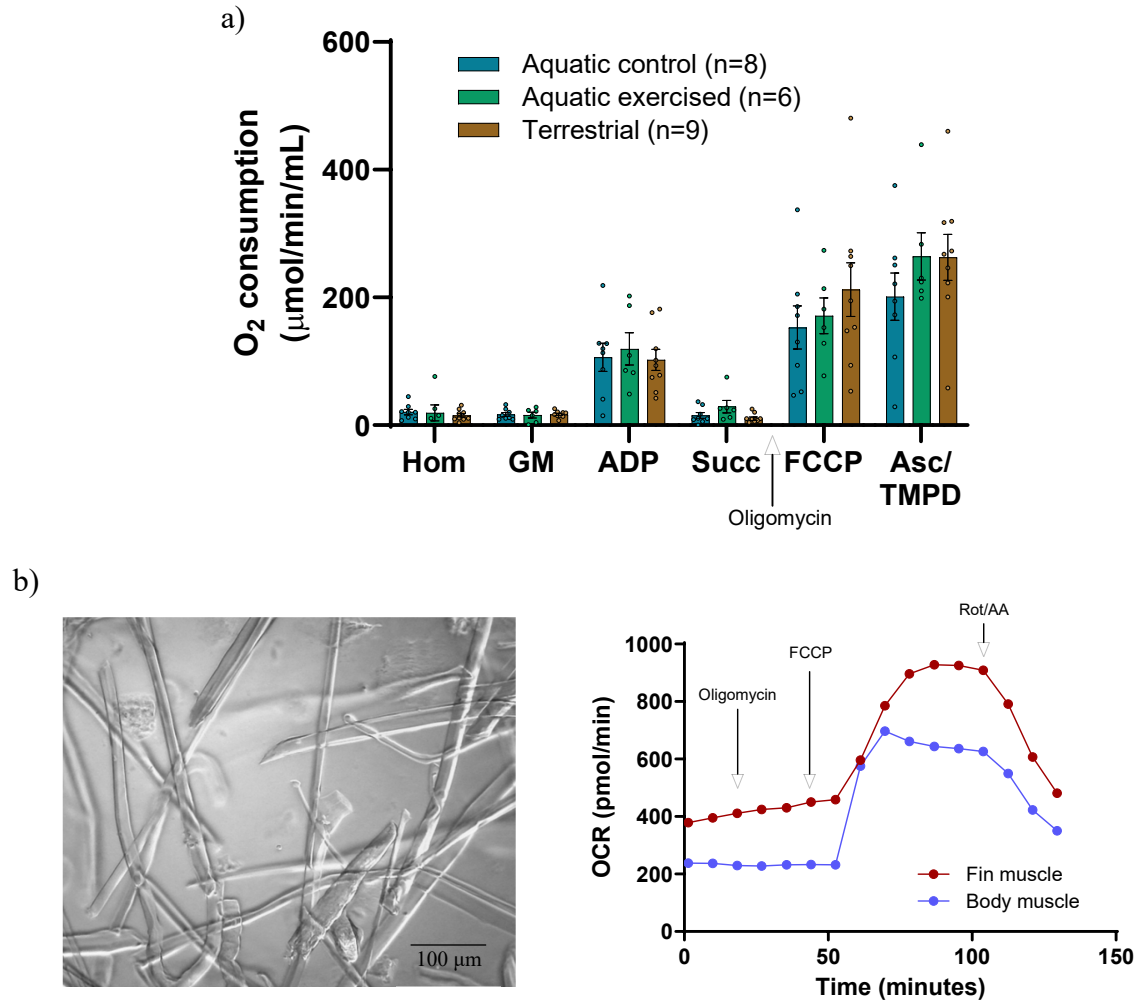

Figure 17.4.2 Assessment of OXPHOS efficiency in *P. senegalus* body muscle.

a) Polarography of homogenized body muscle (Hom) indicating O_2 consumption after the stepwise addition of Complex I substrate (GM), ATP-synthase substrate (ADP + Pi), Complex II substrate (Succ), ATP-synthase inhibitor (oligomycin), OXPHOS uncoupler (FCCP, depolarises mitochondrial inner membrane), and Complex IV substrate (Asc/TMPD).

b) Isolated intact body and fin muscle fibers from *P. senegalus* aquatic control under compound microscope (representative image at 100X; left) immediately followed by real-time cell metabolic analysis (Seahorse XF Analyzer, Agilent) (right) using a modified Seahorse XF Mito Stress Test (Spangenburg & Ward, 2016)

AA – antimycin A (Complex III inhibitor); ADP – adenosine diphosphate; Asc – ascorbate (maintains TMPD in a reduced state); ATP – adenosine triphosphate; FCCP – carbonyl cyanide-p-trifluoromethoxyphenylhydrazine (OXPHOS uncoupler); GM – glutamate plus malate (substrate for Complex I); Hom – body muscle tissue homogenate; OXPHOS – oxidative phosphorylation; Pi – inorganic phosphate; Rot – rotenone (Complex I inhibitor); Succ – succinate (substrate for Complex II); TMPD – tetramethyl-p-phenylenediamine dihydrochloride (substrate for Complex IV)

18. Discussion

Maintaining mitochondrial function with age is required to extend human health span and possibly lifespan (López-Otín et al., 2013, 2023). Likewise, survival in new challenging environments hinges on maintaining energy levels through mitochondrial adaption, which may facilitate evolutionary change (Sokolova, 2018). The mitochondrial unfolded protein response (UPR^{mt}) is a cross-species biochemical process that helps an organism respond to external and internal stressors and maintain mitochondrial proteostasis and function. The UPR^{mt} contributes to robustness where mitochondrial function is maintained in the face of perturbations (Plech et al., 2017). Invoking the UPR^{mt} before the onset of adulthood in the roundworm *C. elegans*, through the generation of a mitonuclear protein imbalance, acts as a hormetic and provides resilience (the ability to resist future stressors) and extends both health span and lifespan (Houtkooper et al., 2013). This thesis aims to investigate the potential hormetic role of the UPR^{mt} in a mammalian model; to determine whether a mild stressor that challenges mitochondrial translation would improve health span or lifespan. Additional investigations were conducted on the role of mitochondrial adaption in *P. senegalus*, which is a fish model for water to land transition and tetrapod evolution.

18.1 Mitochondrial adaption in *P. senegalus*, a fish model for water to land transition

Like aging, acclimation to a new environment involves responding to external stressors to maintain homeostasis or to achieve allostasis. Likewise, maintaining energy levels is necessary for both healthy aging and for thriving in a new environment, and so maintaining or enhancing mitochondrial health and efficiency is essential for both healthy aging and acclimation.

The roundworm *C. elegans* has harnessed the UPR^{mt} in a species-specific manner to enhance survival against xenobiotic stressors in its soil environment, which is an example of adaptation (Q.

Zhang et al., 2021). Other stress response pathways are implicated in adaptation – for example, the endoplasmic reticulum UPR is integral to acclimation of plants to low O_2 levels (Beaugelin et al., 2020). An intriguing proposition is that the UPR^{mt}, and/or other stress response pathways, in *P. senegalus* is involved in responding and adapting to external stressors as it transitions from water to land.

The first question to ask is how a stress response system gives a selective advantage (Ness, Bhatnagar, & Ellis, 2016). In the *P. senegalus* water to land transition model, two land interventions were compared to an aquatic control. The functionality of isolated body muscle mitochondria was compared to determine whether living or walking on land affects mitochondria efficiency. Variation between individuals was high, which is not unusual for laboratory animals that come from the pet trade. Real-time cell metabolic analysis was successfully employed on body muscle fibers from an aquatic *P. senegalus*. Future work will 1) optimize the muscle fiber assay to generate consistent and reproducible results, 2) compare muscle fiber respiration between land-raised and aquatic control *P. senegalus*, and then 3) examine the role of stress response pathways, such as the UPR^{mt}, in the *P. senegalus* land-acclimation response.

18.2 Reduced *Mrpl54* gene expression has no hormetic effect in C57BL/6N mice

The *Mrpl54*$^{+/-}$ mouse model was designed to test whether the hormetic response observed in the reduced *Mrp C. elegans* model (i.e., an increased health span and lifespan) (Houtkooper et al., 2013) could be duplicated in a mammalian model. The prediction was that a ~50% germ-line reduction in *Mrpl54*, encoding a critical mitochondrial ribosomal protein, would improve mouse metabolic health span and/or lifespan through a proteostatic stress-mediated upregulation of the UPR^{mt}. Following *Mrpl54*$^{+/-}$ and *Mrpl54* WT mice for the duration of their natural lifespan revealed no differences in growth, median lifespan, or maximum lifespan in either males or

females (Reid et al., 2023). Likewise, no differences were observed in metabolic health at 6-, 18- or 24-months.

Characterization of the *Mrpl54*$^{+/-}$ mouse model revealed that a ~50% reduction in *Mrpl54* gene expression had no effect on basal UPR^{mt} levels in the liver nor was there any evidence of a mitonuclear protein imbalance. Reduced levels of OXPHOS protein subunits were detected in primary myoblasts retrieved from hind limb skeletal muscle; although, the relative concentrations of nDNA- to mtDNA-encoded proteins were the same as WT (i.e., no mitonuclear protein imbalance nor UPR^{mt} signal was detected). Further examination of the model revealed that male *Mrpl54*$^{+/-}$ mice experienced reduced grip strength (also observed in other *Mrp* heterozygous mouse models (Groza et al., 2023)) from age 12-months onward, coupled with improved treadmill endurance, decreased *ex vivo* tetanic force, increased *ex vivo* fatigue recovery, and disrupted sarcomeres as evidenced through transmission electron micrographs. However, by age 18-months *Mrpl54*$^{+/-}$ male treadmill endurance was no different than WT. Rather than improving health span or lifespan, reduction in *Mrpl54* gene expression instead points to an aged skeletal muscle phenotype in males by age 12-months. Up to this age, there appears to be a compensatory mechanism to maintain overall muscle function, which may have manifested as improved *ex vivo* fatigue recovery and an improved treadmill endurance that was maintained between age 12- and 18-months (equivalent to age ~42-56 years in a human (Hagan, 2017)) but lost thereafter when compared to WT animals.

The conclusion is that a ~50% germline reduction of a critical *Mrp* gene has no discernible hormetic effect in the tested mammalian model. This result counters the observations in *C. elegans,* where RNAi-mediated ~50% *Mrp* reduction and germline heterozygous *tars-1* (mitochondrial threonyl-tRNA synthetase) reduction both result in health span and lifespan extensions through a

mitonuclear protein imbalance-mediated upregulation of the UPR^{mt} (M. Guo et al., 2023; Houtkooper et al., 2013).

18.3 Why does reducing *Mrpl54* result in hormesis in *C. elegans* but not in the mouse?

18.3.1 Strain-specific effect

In Houtkooper et al. (2013), quantitative trait locus (QTL) mapping of BXD mice revealed an association between *Mrp* levels and lifespan, where BXD strains with lower *Mrp* expression were longer lived (Houtkooper et al., 2013). BXD mice are multigenerational C57BL/6J intercrosses with DBA/2J mouse strains to mimic the genetic diversity of human cohorts (Martins et al., 2021).

The background mouse strain used in this study was C57BL/6N from Taconic Biosciences (Taconic Biosciences, 2024). C57BL/6 strains are relatively long lived (mean 2.5 years for males) when compared to short-lived strains like DBA/2J (mean 1.9 years for males) (Yuan et al., 2009). It may be that the reduced *Mrp* effects on lifespan from the BXD QTL mapping study were driven by the DBA/2J genetic background rather than the C57BL/6 background. Reducing the expression of a critical *Mrp* in a short-lived strain like DBA/2J may yet result in a mitohormetic effect on health span or lifespan.

18.3.2 Species-specific effect

Recall the *Surf1* knock out mouse model, where the ablation of SURF1 protein (which assists in the assembly of mtDNA-encoded subunits of respiratory complex CIV) yields a UPR^{mt}-mediated phenotype that is beneficial in the mouse (e.g., increased lifespan) but harmful to humans (e.g., Leigh Syndrome) (Dell'Agnello et al., 2007). It may be that reduction of *Mrp* expression in *C. elegans* has a beneficial effect (i.e., increased health span and lifespan) (Houtkooper et al., 2013) but the same heterozygous *Mrp* mutation in a mammalian model has no appreciable benefit (i.e.,

no difference in metabolic health with age or lifespan) (Reid et al., 2023) or possibly a deficit (i.e., *Mrpl54*$^{+/-}$ exhibit early age-related reduced grip strength and sarcomere disruption) (Reid et al., manuscript in progress).

18.3.3 Species-specific adaptation

Alternately, the answer as to why *C. elegans* exhibits lifespan extension in response to mitoproteostatic stress may lie in a *C. elegans*-specific adaptation. Specifically, the UPR^{mt} in the roundworm is adapted to respond to a soil-based environmental stressor that then primes the roundworm (and subsequent generations) to withstand future environmental stress. This is an example of hormesis or what Rogers & Isaza (2023) would call “cross-protection", where exposure to complex stressors (i.e., alterations to an organism’s environment that challenge performance or fitness) increases resilience to future stressors.

The evidence for a *C. elegans*-specific UPR^{mt} adaptation comes from a relatively recent publication (Q. Zhang et al., 2021) where the presence of a soil xenobiotic (e.g., *Pseudomonas aeruginosa*, an opportunistic *C. elegans* pathogen (Ambreetha & Balachandar, 2022)) is picked up by the roundworm's sensory neurons. The xenobiotic triggers both mitochondrial proteostatic stress (i.e.., mitonuclear protein imbalance) and a local UPR^{mt} signal in the neurons that are then propagated cell non-autonomously (via Wnt cytokine signaling (Q. Zhang et al., 2018)) to the gut as well as the maternal gonad. The neuron-mediated induction of proteostatic stress and the UPR^{mt} in the gut primes the roundworm for imminent ingestion of *P. aeruginosa*. The result is stress resistance to the soil xenobiotic (i.e., hormesis) coupled with a tradeoff in fitness (delayed development and reduced brood size). However, the proteostatic stress-mediated UPR^{mt} signal triggered by the soil xenobiotic also increases the roundworm’s health span and lifespan (Q. Zhang et al., 2021), which is also observed in Houtkooper *et al.* (2013). An increased life span could

potentially help offset the fitness cost – a xenobiotic-resistant roundworm may have a reduced brood size, but it also has a longer lifespan and so can have a greater number of broods than an unstressed roundworm.

Most intriguingly, a mitonuclear protein imbalance and the UPR^{mt} signal are both transmitted to the roundworm's gonad where they are maternally transmitted (through an increase in mtDNA levels) for up to 50 generations of roundworm descendants (even after the original neuronal stressor is removed), priming future progeny to survive a hostile environment of pathogenic xenobiotics (Q. Zhang et al., 2021). Each subsequent generation maternally inherits a mitonuclear protein imbalance and an upregulated UPR^{mt} signal. Descendants live longer than unstressed roundworms and are resistant to heat stress, paraquat treatment, as well as infection with *P. aeruginosa*, but again at the cost of slow development and reduced fecundity. This is an example of transgenerational epigenetic inheritance, where a stressor encountered by the parent is maternally transmitted to the offspring to improve the survival of future generations.

Comparing the nematode and mammalian UPR^{mt} signaling pathways also gives clues as to why sensing mitoproteostatic stress and invoking the UPR^{mt} affects lifespan in the roundworm but not in the mouse. In *C. elegans*, the UPR^{mt} appears to be a standalone pathway that operates independently of Atf-5 (the orthologue of mammalian ATF4, which is the master regulator of the mammalian integrated stress response [ISR]) (Molenaars et al., 2020). Independent activation of the *C. elegans* UPR^{mt} makes sense if the UPR^{mt} is adapted in a species-specific manner to respond to and propagate externally sensed environmental stressors (e.g., xenobiotics like *P. aeruginosa*) – the *C. elegans* UPR^{mt} stress response remains local and therefore controllable and focused (i.e., on priming the roundworm and its progeny to resist future environmental stressors). In contrast,

the mammalian UPR^{mt} is downstream and dependent on ATF4 signaling and the ISR with a focus on re-establishing proteostasis in response to perturbation.

18.4 Why do male *Mrpl54*$^{+/-}$ mice display an early skeletal muscle phenotype?

With age, Ca^{2+} leakage from the sarcoplasmic reticulum results in increased Ca^{2+} within the mitochondria (Endlicher et al., 2023). Calcium overload triggers the opening of the mitochondrial permeability transition pore (mPTP), which is exacerbated with age because the Ca^{2+} threshold that triggers the mPTP is lower in aged mammals (Gouspillou et al. 2014). The result is a reduced membrane potential, release of Ca^{2+} into the cytosol, and activation of caspase-3, which in skeletal muscle can lead to muscle fiber atrophy (Skinner et al., 2021) Prolonged opening of the mPTP can lead to enlarged swollen mitochondria through osmosis, which is a hallmark of aged skeletal muscle in mice (Pietrangelo et al., 2015).

By age 12-months the male *Mrpl54*$^{+/-}$ mouse had reduced grip strength, reduced *ex vivo* skeletal muscle tetanic force, disrupted sarcomeres, misaligned Ca^{2+} release units, and enlarged intermyofibrillar mitochondria. This aged phenotype is typically not observed in mice before the age of 24-months (Pietrangelo et al., 2015). It may be that by age 12 months, *Mrpl54*$^{+/-}$ male mice experience an early loss in Ca^{2+} homeostasis in skeletal muscle fibers along with prolonged opening of the mPTP, which may explain the reduced grip strength and enlarged mitochondria phenotype.

18.5 Sex-specific differences in the *Mrpl54*$^{+/-}$ mouse model

Differences between male and female *Mrpl54*$^{+/-}$ mice were observed at age 6-months during the metabolic health tests and again during the grip strength tests at age 8-weeks, 6-months, and 12-months. While no metabolic differences were observed between male *Mrpl54*$^{+/-}$ and WT mice at any time point, female *Mrpl54*$^{+/-}$ mice at age 6-months were smaller, had increased activity

during daytime, and had better treadmill endurance when compared to 6-month-old WT females, although these differences disappeared by age 18-months. And while male *Mrpl54*$^{+/-}$ mice had decreased grip strength by age 12-months compared to WT males, no differences in grip strength were observed between female *Mrpl54*$^{+/-}$ and WT mice at any time point measured (up to age 12-months).

Mammalian mitochondria are maternally inherited, and they are replete with estrogen receptor in both the inner and outer mitochondria membranes (Liao et al., 2015). Estrogen effects within mitochondria include improved Ca^{2+} retention capacity and increased resistance to Ca^{2+} overload, where estrogen provides a protective function especially within skeletal muscle (Ventura-Clapier et al., 2019). With age, Ca^{2+} leakage from the sarcoplasmic reticulum results in increased Ca^{2+} within the mitochondria (Endlicher et al., 2023). Ca^{2+} overload triggers the opening of the mPTP, which reduces membrane potential and results in enlarged hypertrophic mitochondria (Endlicher et al., 2023). Since females have higher estrogen levels than males, they may be better protected from the Ca^{2+} overload effects through a delayed opening of the mPTP. And so, if the aged *Mrpl54*$^{+/-}$ reduced grip strength phenotype in males is due to increased sensitivity to mitochondrial Ca^{2+} levels that lead to hypertrophic mitochondria, then it follows that the maintenance of grip strength with age in female *Mrpl54*$^{+/-}$ mice may be attributed to estrogen-mediated resistance to Ca^{2+} overload.

18.6 Conclusion

Mitochondria are at the centre of ATP production and cellular energy transduction and are therefore in a unique position to sense the metabolic health of the cell and communicate this status to the nucleus through retrograde communication. One communication pathway is the UPR^{mt}, where mitochondrial proteostatic stress (e.g., mitonuclear protein imbalance) generates a signal to

the mammalian nucleus via ATF5 (Atfs-1 in *C. elegans*). The nucleus responds by reducing global protein translation, and upregulating those functional proteins involved in the UPR^{mt} to resolve the proteostatic stress. In *C. elegans*, the UPR^{mt} is harnessed not only as a stress signal to resolve mitoproteostatic stress, but also as a hormetic to prime the organism and subsequent generations to withstand pathogenic xenobiotic stress in its natural soil environment. In mammals, the role of the UPR^{mt} as a mitohormetic that affects health span or lifespan is less clear. Unlike the nematode UPR^{mt}, the mammalian UPR^{mt} is tightly coupled to the ISR and plays a supporting role in resolving proteostatic stress and mitigating the effects of age-related diseases like Alzheimer's and Parkinson's. Future work can investigate whether a threshold level of UPR^{mt} induction will invoke a hormetic response; however, the results in this thesis does not support this hypothesis in mammals.

19. References for Sections 13, 17, and 18

Aibara, S., Singh, V., Modelska, A., & Amunts, A. (2020). Structural basis of mitochondrial translation. *ELife*, *9*, 1–17. https://doi.org/10.7554/ELIFE.58362

Al-Furoukh, N., Ianni, A., Nolte, H., Hölper, S., Krüger, M., Wanrooij, S., & Braun, T. (2015). ClpX stimulates the mitochondrial unfolded protein response (UPRmt) in mammalian cells. *Biochimica et Biophysica Acta*, *1853*(10 Pt A), 2580–2591. https://doi.org/10.1016/J.BBAMCR.2015.06.016

Ambreetha, S., & Balachandar, D. (2022). Pathogenesis of plant-associated Pseudomonas aeruginosa in Caenorhabditis elegans model. *BMC Microbiology*, *22*(1), 1–10. https://doi.org/10.1186/S12866-022-02682-Z/TABLES/2

Amunts, A., Brown, A., Toots, J., Scheres, S. H. W., & Ramakrishnan, V. (2015). The structure of the human mitochondrial ribosome. *Science*, *348*(6230), 95–98. https://doi.org/10.1126/SCIENCE.AAA1193/SUPPL_FILE/AMUNTS-SM.PDF

Anderson, N. S., & Haynes, C. M. (2020). Folding the Mitochondrial UPR into the Integrated Stress Response. *Trends in Cell Biology*, *30*(6), 428–439. https://doi.org/10.1016/J.TCB.2020.03.001

André, V., Gau, C., Scheideler, A., Aguilar-Pimentel, J. A., Amarie, O. V., Becker, L., Garrett, L., Hans, W., Hölter, S. M., Janik, D., Moreth, K., Neff, F., Östereicher, M., Racz, I., Rathkolb, B., Rozman, J., Bekeredjian, R., Graw, J., Klingenspor, M., … Hrabé de Angelis, M. (2018). Laboratory mouse housing conditions can be improved using common environmental enrichment without compromising data. *PLOS Biology*, *16*(4), e2005019. https://doi.org/10.1371/JOURNAL.PBIO.2005019

Andrews, S. M., & Westoll, T. S. (1970). IX.—The Postcranial Skeleton of Ensthenopteron foordi Whiteaves. *Transactions of the Royal Society of Edinburgh*, *68*(9), 207–329. https://doi.org/10.1017/S008045680001471X

Antonicka, H., & Shoubridge, E. A. (2015). Mitochondrial RNA Granules Are Centers for Posttranscriptional RNA Processing and Ribosome Biogenesis. *Cell Reports*, *10*(6), 920–932. https://doi.org/10.1016/J.CELREP.2015.01.030

Arem, H., Moore, S. C., Patel, A., Hartge, P., Berrington de Gonzalez, A., Visvanathan, K., Campbell, P. T., Freedman, M., Weiderpass, E., Adami, H. O., Linet, M. S., Lee, I.-M., & Matthews, C. E. (2015). Leisure Time Physical Activity and Mortality: A Detailed Pooled Analysis of the Dose-Response Relationship. *JAMA Internal Medicine*, *175*(6), 959–967. https://doi.org/10.1001/jamainternmed.2015.0533

Banh, S., Wiens, L., Sotiri, E., & Treberg, J. R. (2016). Mitochondrial reactive oxygen species production by fish muscle mitochondria: Potential role in acute heat-induced oxidative stress. *Comparative Biochemistry and Physiology Part B: Biochemistry and Molecular Biology*, *191*, 99–107. https://doi.org/10.1016/J.CBPB.2015.10.001

Beard, J. R., Jotheeswaran, A. T., Cesari, M., & Araujo De Carvalho, I. (2019). The structure and predictive value of intrinsic capacity in a longitudinal study of ageing. *BMJ Open*, *9*(11), e026119. https://doi.org/10.1136/BMJOPEN-2018-026119

Beard, J. R., Officer, A., De Carvalho, I. A., Sadana, R., Pot, A. M., Michel, J. P., Lloyd-Sherlock, P., Epping-Jordan, J. E., Peeters, G. M. E. E., Mahanani, W. R., Thiyagarajan, J. A., & Chatterji, S. (2016). The World report on ageing and health: a policy framework for

healthy ageing. *The Lancet*, *387*(10033), 2145–2154. https://doi.org/10.1016/S0140-6736(15)00516-4

Beck, J. S., Mufson, E. J., & Counts, S. E. (2016). Evidence for Mitochondrial UPR Gene Activation in Familial and Sporadic Alzheimer's Disease. *Current Alzheimer Research*, *13*(6), 610–614.

Betts, H. C., Puttick, M. N., Clark, J. W., Williams, T. A., Donoghue, P. C. J., & Pisani, D. (2018). Integrated genomic and fossil evidence illuminates life's early evolution and eukaryote origin. *Nature Ecology & Evolution*, *2*(10), 1556–1562. https://doi.org/10.1038/s41559-018-0644-x

Beaugelin, I., Chevalier, A., D'Alessandro, S., Ksas, B., & Havaux, M. (2020). Endoplasmic reticulum-mediated unfolded protein response is an integral part of singlet oxygen signalling in plants. *The Plant journal : for cell and molecular biology*, *102*(6), 1266–1280. https://doi.org/10.1111/tpj.14700

Blagosklonny, M. V. (2017). From rapalogs to anti-aging formula. *Oncotarget*, *8*(22), 35492. https://doi.org/10.18632/ONCOTARGET.18033

Bogenhagen, D. F., & Haley, J. D. (2020). Pulse-chase SILAC-based analyses reveal selective oversynthesis and rapid turnover of mitochondrial protein components of respiratory complexes. *The Journal of Biological Chemistry*, *295*(9), 2544–2554. https://doi.org/10.1074/JBC.RA119.011791

Bogenhagen, D. F., Martin, D. W., & Koller, A. (2014). Initial Steps in RNA Processing and Ribosome Assembly Occur at Mitochondrial DNA Nucleoids. *Cell Metabolism*, *19*(4), 618–629. https://doi.org/10.1016/J.CMET.2014.03.013

Bogenhagen, D. F., Ostermeyer-Fay, A. G., Haley, J. D., & Garcia-Diaz, M. (2018). Kinetics and Mechanism of Mammalian Mitochondrial Ribosome Assembly. *Cell Reports*, *22*(7), 1935–1944. https://doi.org/10.1016/J.CELREP.2018.01.066

Boily, G., Seifert, E. L., Bevilacqua, L., He, X. H., Sabourin, G., Estey, C., Moffat, C., Crawford, S., Saliba, S., Jardine, K., Xuan, J., Evans, M., Harper, M. E., & McBurney, M. W. (2008). SirT1 Regulates Energy Metabolism and Response to Caloric Restriction in Mice. *PLOS ONE*, *3*(3), e1759. https://doi.org/10.1371/JOURNAL.PONE.0001759

Brand, M. D. (2016). Mitochondrial generation of superoxide and hydrogen peroxide as the source of mitochondrial redox signaling. *Free Radical Biology & Medicine*, *100*, 14–31. https://doi.org/10.1016/J.FREERADBIOMED.2016.04.001

Bremer, N., Tria, F. D. K., Skejo, J., Garg, S. G., & Martin, W. F. (2022). Ancestral State Reconstructions Trace Mitochondria but Not Phagocytosis to the Last Eukaryotic Common Ancestor. *Genome Biology and Evolution*, *14*(6), evac079. https://doi.org/10.1093/gbe/evac079

Brown, A., Amunts, A., Bai, X. C., Sugimoto, Y., Edwards, P. C., Murshudov, G., Scheres, S. H. W., & Ramakrishnan, V. (2014). Structure of the large ribosomal subunit from human mitochondria. *Science*, *346*(6210), 718–722. https://doi.org/10.1126/SCIENCE.1258026/SUPPL_FILE/BROWN.SM.PDF

Calabrese, V., Cornelius, C., Dinkova-Kostova, A. T., Iavicoli, I., Di Paola, R., Koverech, A., Cuzzocrea, S., Rizzarelli, E., & Calabrese, E. J. (2012). Cellular stress responses, hormetic phytochemicals and vitagenes in aging and longevity. *Biochimica et Biophysica Acta*, *1822*(5), 753–783. https://doi.org/10.1016/J.BBADIS.2011.11.002

Campbell, J. E., & Drucker, D. J. (2015). Islet α cells and glucagon—critical regulators of energy homeostasis. *Nature Reviews Endocrinology 2015 11:6*, *11*(6), 329–338. https://doi.org/10.1038/NRENDO.2015.51

Chakravarty, E., Hubert, H., Lingala, V., & JF, F. (2008). Reduced disability and mortality among aging runners: A 21-year longitudinal study. *Archives of Internal Medicine*, *168*(15), 1638–1646. http://dx.doi.org/10.1001/archinte.168.15.1638

Chapman, J., Fielder, E., & Passos, J. F. (2019). Mitochondrial dysfunction and cell senescence: deciphering a complex relationship. *FEBS Letters*, *593*(13), 1566–1579. https://doi.org/10.1002/1873-3468.13498

Chaveroux, C., Lambert-Langlais, S., Parry, L., Carraro, V., Jousse, C., Maurin, A. C., Bruhat, A., Marceau, G., Sapin, V., Averous, J., & Fafournoux, P. (2011). Identification of GCN2 as new redox regulator for oxidative stress prevention in vivo. *Biochemical and Biophysical Research Communications*, *415*(1), 120–124. https://doi.org/10.1016/J.BBRC.2011.10.027

Chen, C., Zhou, M., Ge, Y., & Wang, X. (2020). SIRT1 and aging related signaling pathways. *Mechanisms of Ageing and Development*, *187*, 111215. https://doi.org/10.1016/J.MAD.2020.111215

Chen, Q., Young, L., & Barsotti, R. (2023). Mitochondria in cell senescence: A Friend or Foe? *Advances in Protein Chemistry and Structural Biology*. https://doi.org/10.1016/BS.APCSB.2023.02.019

Conte, D., MacNei, L. T., Walhout, A. J. M., & Mello, C. C. (2015). RNA Interference in Caenorhabditis Elegans. *Current Protocols in Molecular Biology*, *109*, 26.3.1. https://doi.org/10.1002/0471142727.MB2603S109

Cordeiro, A. V., Bricola, R. S., Braga, R. R., Lenhare, L., Silva, V. R. R., Anaruma, C. P., Katashima, C. K., Crisol, B. M., Simabuco, F. M., Silva, A. S. R., Cintra, D. E., Moura, L. P., Pauli, J. R., & Ropelle, E. R. (2020). Aerobic Exercise Training Induces the Mitonuclear Imbalance and UPRmt in the Skeletal Muscle of Aged Mice. *The Journals of Gerontology: Series A*, *75*(12), 2258–2261. https://doi.org/10.1093/GERONA/GLAA059

Coutts, F., Palmos, A. B., Duarte, R. R. R., de Jong, S., Lewis, C. M., Dima, D., & Powell, T. R. (2018). The polygenic nature of telomere length and the anti-ageing properties of lithium. *Neuropsychopharmacology 2018 44:4*, *44*(4), 757–765. https://doi.org/10.1038/S41386-018-0289-0

Couvillion, M. T., Soto, I. C., Shipkovenska, G., & Churchman, L. S. (2016). Synchronized mitochondrial and cytosolic translation programs. *Nature 2016 533:7604*, *533*(7604), 499–503. https://doi.org/10.1038/NATURE18015

Cox, C. S., McKay, S. E., Holmbeck, M. A., Christian, B. E., Scortea, A. C., Tsay, A. J., Newman, L. E., & Shadel, G. S. (2018). Mitohormesis in Mice via Sustained Basal Activation of Mitochondrial and Antioxidant Signaling. *Cell Metabolism*, *28*(5), 776-786.e5. https://doi.org/10.1016/J.CMET.2018.07.011

Cruz-Jentoft, A. J., Bahat, G., Bauer, J., Boirie, Y., Bruyère, O., Cederholm, T., Cooper, C., Landi, F., Rolland, Y., Sayer, A. A., Schneider, S. M., Sieber, C. C., Topinkova, E., Vandewoude, M., Visser, M., Zamboni, M., Bautmans, I., Baeyens, J. P., Cesari, M., … Schols, J. (2019). Sarcopenia: revised European consensus on definition and diagnosis. *Age and Ageing*, *48*(1), 16–31. https://doi.org/10.1093/AGEING/AFY169

da Cruz, A. L., & Fernandes, M. N. (2016). What is the most efficient respiratory organ for the loricariid air-breathing fish Pterygoplichthys anisitsi, gills or stomach? A quantitative morphological study. *Zoology*, *119*(6), 526–533. https://doi.org/10.1016/J.ZOOL.2016.08.003

Daley, D. O., & Whelan, J. (2005). Why genes persist in organelle genomes. *Genome Biology*, *6*(5), 110. https://doi.org/10.1186/gb-2005-6-5-110

Dasgupta, D., Delmotte, P., & Sieck, G. C. (2020). Inflammation-Induced Protein Unfolding in Airway Smooth Muscle Triggers a Homeostatic Response in Mitochondria. *International Journal of Molecular Sciences*, *22*(1), 1–13. https://doi.org/10.3390/IJMS22010363

De Silva, D., Tu, Y. T., Amunts, A., Fontanesi, F., & Barrientos, A. (2015). Mitochondrial ribosome assembly in health and disease. *Cell Cycle (Georgetown, Tex.)*, *14*(14), 2226–2250. https://doi.org/10.1080/15384101.2015.1053672

Dell'Agnello, C., Leo, S., Agostino, A., Szabadkai, G., Tiveron, C. C., Zulian, A. A., Prelle, A., Roubertoux, P., Rizzuto, R., & Zeviani, M. (2007). Increased longevity and refractoriness to Ca(2+)-dependent neurodegeneration in Surf1 knockout mice. *Human Molecular Genetics*, *16*(4), 431–444. https://doi.org/10.1093/HMG/DDL477

Diaconu, M., Kothe, U., Schlünzen, F., Fischer, N., Harms, J. M., Tonevitsky, A. G., Stark, H., Rodnina, M. V., & Wahl, M. C. (2005). Structural Basis for the Function of the Ribosomal L7/12 Stalk in Factor Binding and GTPase Activation. *Cell*, *121*(7), 991–1004. https://doi.org/10.1016/J.CELL.2005.04.015

Djafarzadeh, S., & Jakob, S. M. (2017). Isolation of Intact Mitochondria from Skeletal Muscle by Differential Centrifugation for High-resolution Respirometry Measurements. *Journal of Visualized Experiments : JoVE*, *2017*(121), 55251. https://doi.org/10.3791/55251

Doerrier, C., Garcia-Souza, L. F., Krumschnabel, G., Wohlfarter, Y., Mészáros, A. T., & Gnaiger, E. (2018). High-resolution fluorespirometry and oxphos protocols for human cells, permeabilized fibers from small biopsies of muscle, and isolated mitochondria. *Methods in Molecular Biology*, *1782*, 31–70. https://doi.org/10.1007/978-1-4939-7831-1_3/COVER

Du, T. Y., Larsson, H. C. E., & Standen, E. M. (2016). Observations of terrestrial locomotion in wild Polypterus senegalus from Lake Albert, Uganda. *African Journal of Aquatic Science*, *41*(1), 67–71. https://doi.org/10.2989/16085914.2015.1125337

Du, T. Y., & Standen, E. M. (2017). Phenotypic plasticity of muscle fiber type in the pectoral fins of Polypterus senegalus reared in a terrestrial environment. *Journal of Experimental Biology*, *220*(19), 3406–3410. https://doi.org/10.1242/JEB.162909/262810/AM/PHENOTYPIC-PLASTICITY-OF-MUSCLE-FIBER-TYPE-IN-THE

Du, T. Y., & Standen, E. M. (2020). Terrestrial acclimation and exercise lead to bone functional response in Polypterus senegalus pectoral fins. *Journal of Experimental Biology*, *223*(11). https://doi.org/10.1242/JEB.217554/267603/AM/TERRESTRIAL-ACCLIMATION-AND-EXERCISE-LEAD-TO-BONE

Duarte-Silva, S., Silva-Fernandes, A., Neves-Carvalho, A., Soares-Cunha, C., Teixeira-Castro, A., & Maciel, P. (2016). Combined therapy with m-TOR-dependent and -independent

autophagy inducers cause neurotoxicity in a mouse model of Machado–Joseph disease. *Neuroscience*, *313*, 162–173. https://doi.org/10.1016/J.NEUROSCIENCE.2015.11.030

Edwards, M. G., Anderson, R. M., Yuan, M., Kendziorski, C. M., Weindruch, R., & Prolla, T. A. (2007). Gene expression profiling of aging reveals activation of a p53-mediated transcriptional program. *BMC Genomics*, *8*(1), 1–13. https://doi.org/10.1186/1471-2164-8-80/TABLES/3

Endlicher, R., Drahota, Z., Štefková, K., Červinková, Z., & Kučera, O. (2023). The Mitochondrial Permeability Transition Pore-Current Knowledge of Its Structure, Function, and Regulation, and Optimized Methods for Evaluating Its Functional State. *Cells*, *12*(9), 1273. https://doi.org/10.3390/cells12091273

Falcón, P., Escandón, M., Brito, Á., & Matus, S. (2019). Nutrient sensing and redox balance: GCN2 as a new integrator in aging. *Oxidative Medicine and Cellular Longevity*, *2019*. https://doi.org/10.1155/2019/5730532

Fang, E. F., Scheibye-Knudsen, M., Chua, K. F., Mattson, M. P., Croteau, D. L., & Bohr, V. A. (2016). Nuclear DNA damage signalling to mitochondria in ageing. *Nature Reviews Molecular Cell Biology 2016 17:5*, *17*(5), 308–321. https://doi.org/10.1038/nrm.2016.14

Fernandes, M. N., & Moron, S. E. (2020). Breathing and respiratory adaptations. *Biology and Physiology of Freshwater Neotropical Fish*, 217–250. https://doi.org/10.1016/B978-0-12-815872-2.00010-5

Fiorese, C. J., Schulz, A. M., Lin, Y. F., Rosin, N., Pellegrino, M. W., & Haynes, C. M. (2016). The Transcription Factor ATF5 Mediates a Mammalian Mitochondrial UPR. *Current Biology : CB*, *26*(15), 2037–2043. https://doi.org/10.1016/J.CUB.2016.06.002

Flurkey, K., Papaconstantinou, J., & Harrison, D. E. (2002). The Snell dwarf mutation Pit1dw can increase life span in mice. *Mechanisms of Ageing and Development*, *123*(2–3), 121–130. https://doi.org/10.1016/S0047-6374(01)00339-6

Forsström, S., Jackson, C. B., Carroll, C. J., Kuronen, M., Pirinen, E., Pradhan, S., Marmyleva, A., Auranen, M., Kleine, I. M., Khan, N. A., Roivainen, A., Marjamäki, P., Liljenbäck, H., Wang, L., Battersby, B. J., Richter, U., Velagapudi, V., Nikkanen, J., Euro, L., & Suomalainen, A. (2019). Fibroblast Growth Factor 21 Drives Dynamics of Local and Systemic Stress Responses in Mitochondrial Myopathy with mtDNA Deletions. *Cell Metabolism*, *30*(6), 1040-1054.e7. https://doi.org/10.1016/J.CMET.2019.08.019

Ghosh, J. C., Seo, J. H., Agarwal, E., Wang, Y., Kossenkov, A. V., Tang, H. Y., Speicher, D. W., & Altieri, D. C. (2019). Akt phosphorylation of mitochondrial Lonp1 protease enables oxidative metabolism and advanced tumor traits. *Oncogene 2019 38:43*, *38*(43), 6926–6939. https://doi.org/10.1038/s41388-019-0939-7

Girardin, S. E., Cuziol, C., Philpott, D. J., & Arnoult, D. (2021). The eIF2α kinase HRI in innate immunity, proteostasis, and mitochondrial stress. *The FEBS Journal*, *288*(10), 3094–3107. https://doi.org/10.1111/FEBS.15553

Goh, J., Wong, E., Soh, J., Maier, A. B., & Kennedy, B. K. (2023). Targeting the molecular & cellular pillars of human aging with exercise. *The FEBS Journal*, *290*(3), 649–668. https://doi.org/10.1111/FEBS.16337

Gomez-Llorente, Y., Jebara, F., Patra, M., Malik, R., Nisemblat, S., Chomsky-Hecht, O., Parnas, A., Azem, A., Hirsch, J. A., & Ubarretxena-Belandia, I. (2020). Structural basis for active single and double ring complexes in human mitochondrial Hsp60-Hsp10 chaperonin.

Nature Communications 2020 11:1, *11*(1), 1–14. https://doi.org/10.1038/s41467-020-15698-8

Gouspillou, G., Sgarioto, N., Kapchinsky, S., Purves-Smith, F., Norris, B., Pion, C. H., Barbat-Artigas, S., Lemieux, F., Taivassalo, T., Morais, J. A., Aubertin-Leheudre, M., & Hepple, R. T. (2014). Increased sensitivity to mitochondrial permeability transition and myonuclear translocation of endonuclease G in atrophied muscle of physically active older humans. *FASEB journal : official publication of the Federation of American Societies for Experimental Biology*, *28*(4), 1621–1633. https://doi.org/10.1096/fj.13-242750

Graham, J. B., Wegner, N. C., Miller, L. A., Jew, C. J., Lai, N. C., Berquist, R. M., Frank, L. R., & Long, J. A. (2014). Spiracular air breathing in polypterid fishes and its implications for aerial respiration in stem tetrapods. *Nature Communications 2014 5:1*, *5*(1), 1–6. https://doi.org/10.1038/ncomms4022

Greber, B. J., Boehringer, D., Leibundgut, M., Bieri, P., Leitner, A., Schmitz, N., Aebersold, R., & Ban, N. (2014). The complete structure of the large subunit of the mammalian mitochondrial ribosome. *Nature 2014 515:7526*, *515*(7526), 283–286. https://doi.org/10.1038/nature13895

Groza, T., Gomez Lopez, F. L., Mashhadi, H. H., Muñoz-Fuentes, V., Gunes, O., Wilson, R., Cacheiro, P., Frost, A., Keskivali-Bond, P., Vardal, B., McCoy, A., Cheng, T. K., Santos, L., Wells, S., Smedley, D., Mallon, A. M., & Parkinson, H. (2023). The International Mouse Phenotyping Consortium: comprehensive knockout phenotyping underpinning the study of human disease. *Nucleic Acids Research*, *51*(D1), D1038–D1045. https://doi.org/10.1093/NAR/GKAC972

Guo, M., Qiao, X., Wang, Y., Li, Z. H., Shi, C., Chen, Y., Kang, L., Chen, C., & Zhou, X. L. (2023). Mitochondrial translational defect extends lifespan in C. elegans by activating UPRmt. *Redox Biology*, *63*, 102722. https://doi.org/10.1016/J.REDOX.2023.102722

Guo, X., Aviles, G., Liu, Y., Tian, R., Unger, B. A., Lin, Y. H. T., Wiita, A. P., Xu, K., Correia, M. A., & Kampmann, M. (2020). Mitochondrial stress is relayed to the cytosol by an OMA1-DELE1-HRI pathway. *Nature*, *579*(7799), 427. https://doi.org/10.1038/S41586-020-2078-2

Guo, Y., Guan, T., Shafiq, K., Yu, Q., Jiao, X., Na, D., Li, M., Zhang, G., & Kong, J. (2023). Mitochondrial dysfunction in aging. *Ageing Research Reviews*, *88*, 101955. https://doi.org/10.1016/J.ARR.2023.101955

Hagan, C. (2017, November 7). *When are mice considered old?* The Jackson Laboratory.

Hale, M. E., Galdston, S., Arnold, B. W., & Song, C. (2022). The Water to Land Transition Submerged: Multifunctional Design of Pectoral Fins for Use in Swimming and in Association with Underwater Substrate. *Integrative and Comparative Biology*, *62*(4), 908–921. https://doi.org/10.1093/ICB/ICAC061

Harris, M. P., Zeng, S., Zhu, Z., Lira, V. A., Yu, L., Hodgson-Zingman, D. M., & Zingman, L. V. (2023). Myokine Musclin Is Critical for Exercise-Induced Cardiac Conditioning. *International Journal of Molecular Sciences*, *24*(7), 6525. https://doi.org/10.3390/IJMS24076525/S1

Haynes, C. M., Petrova, K., Benedetti, C., Yang, Y., & Ron, D. (2007). ClpP mediates activation of a mitochondrial unfolded protein response in C. elegans. *Developmental Cell*, *13*(4), 467–480. https://doi.org/10.1016/J.DEVCEL.2007.07.016

Hector, K. L., Lagisz, M., & Nakagawa, S. (2012). The effect of resveratrol on longevity across species: a meta-analysis. *Biology Letters*, *8*(5), 790. https://doi.org/10.1098/RSBL.2012.0316

Herranz, D., Muñoz-Martin, M., Cañamero, M., Mulero, F., Martinez-Pastor, B., Fernandez-Capetillo, O., & Serrano, M. (2010). Sirt1 improves healthy ageing and protects from metabolic syndrome-associated cancer. *Nature Communications 2010 1:1*, *1*(1), 1–8. https://doi.org/10.1038/ncomms1001

Hirst, J., Carroll, J., Fearnley, I. M., Shannon, R. J., & Walker, J. E. (2003). The nuclear encoded subunits of complex I from bovine heart mitochondria. *Biochimica et Biophysica Acta (BBA) - Bioenergetics*, *1604*(3), 135–150. https://doi.org/10.1016/S0005-2728(03)00059-8

Holzenberger, M., Dupont, J., Ducos, B., Leneuve, P., Géloën, A., Even, P. C., Cervera, P., & Le Bouc, Y. (2002). IGF-1 receptor regulates lifespan and resistance to oxidative stress in mice. *Nature 2003 421:6919*, *421*(6919), 182–187. https://doi.org/10.1038/NATURE01298

Houtkooper, R. H., Mouchiroud, L., Ryu, D., Moullan, N., Katsyuba, E., Knott, G., Williams, R. W., & Auwerx, J. (2013). Mitonuclear protein imbalance as a conserved longevity mechanism. *Nature*, *497*(7450), 451–457. https://doi.org/10.1038/NATURE12188

Hu, D., Liu, Z., & Qi, X. (2021). UPRmt activation protects against MPP+-induced toxicity in a cell culture model of Parkinson's disease. *Biochemical and Biophysical Research Communications*, *569*, 17–22. https://doi.org/10.1016/J.BBRC.2021.06.079

Hu, D., Sun, X., Liao, X., Zhang, X., Zarabi, S., Schimmer, A., Hong, Y., Ford, C., Luo, Y., & Qi, X. (2019). Alpha-synuclein suppresses mitochondrial protease ClpP to trigger

mitochondrial oxidative damage and neurotoxicity. *Acta Neuropathologica*, *137*(6), 939–960. https://doi.org/10.1007/S00401-019-01993-2/FIGURES/7

Human Mortality Database. (2023). *Data by country and area*. https://www.mortality.org/Home/Index

Iborra, F. J., Kimura, H., & Cook, P. R. (2004). The functional organization of mitochondrial genomes in human cells. *BMC Biology*, *2*(1), 1–14. https://doi.org/10.1186/1741-7007-2-9/FIGURES/9

Inigo, J. R., & Chandra, D. (2022). The mitochondrial unfolded protein response (UPRmt): shielding against toxicity to mitochondria in cancer. *Journal of Hematology & Oncology 2022 15:1*, *15*(1), 1–18. https://doi.org/10.1186/S13045-022-01317-0

Itoh, Y., Andréll, J., Choi, A., Richter, U., Maiti, P., Best, R. B., Barrientos, A., Battersby, B. J., & Amunts, A. (2021). Mechanism of membrane-tethered mitochondrial protein synthesis. *Science*, *371*(6531), 846–849. https://doi.org/10.1126/SCIENCE.ABE0763/SUPPL_FILE/ABE0763S1.MOV

Janouškovec, J., Tikhonenkov, D. V, Burki, F., Howe, A. T., Rohwer, F. L., Mylnikov, A. P., & Keeling, P. J. (2017). A New Lineage of Eukaryotes Illuminates Early Mitochondrial Genome Reduction. *Current Biology*, *27*(23), 3717-3724.e5. https://doi.org/https://doi.org/10.1016/j.cub.2017.10.051

Jin, L., Geng, L., Ying, L., Shu, L., Ye, K., Yang, R., Liu, Y., Wang, Y., Cai, Y., Jiang, X., Wang, Q., Yan, X., Liao, B., Liu, J., Duan, F., Sweeney, G., Woo, C. W. H., Wang, Y., Xia, Z., … Xu, A. (2022). FGF21–Sirtuin 3 Axis Confers the Protective Effects of Exercise

Against Diabetic Cardiomyopathy by Governing Mitochondrial Integrity. *Circulation*, *146*(20), 1537–1557. https://doi.org/10.1161/CIRCULATIONAHA.122.059631

Kang, G. M., Min, S. H., Lee, C. H., Kim, J. Y., Lim, H. S., Choi, M. J., Jung, S. B., Park, J. W., Kim, S., Park, C. B., Dugu, H., Choi, J. H., Jang, W. H., Park, S. E., Cho, Y. M., Kim, J. G., Kim, K. G., Choi, C. S., Kim, Y. B., … Kim, M. S. (2021). Mitohormesis in Hypothalamic POMC Neurons Mediates Regular Exercise-Induced High-Turnover Metabolism. *Cell Metabolism*, *33*(2), 334-349.e6. https://doi.org/10.1016/J.CMET.2021.01.003

Kasai, S., Shimizu, S., Tatara, Y., Mimura, J., & Itoh, K. (2020). Regulation of Nrf2 by Mitochondrial Reactive Oxygen Species in Physiology and Pathology. *Biomolecules 2020, Vol. 10, Page 320*, *10*(2), 320. https://doi.org/10.3390/BIOM10020320

Kaspar, S., Oertlin, C., Szczepanowska, K., Kukat, A., Senft, K., Lucas, C., Brodesser, S., Hatzoglou, M., Larsson, O., Topisirovic, I., & Trifunovic, A. (2021). Adaptation to mitochondrial stress requires CHOP-directed tuning of ISR. *Science Advances*, *7*(22), 971–997. https://doi.org/10.1126/SCIADV.ABF0971/SUPPL_FILE/SCIADV.ABF0971_TABLES

Kayani, A. C., Close, G. L., Dillmann, W. H., Mestril, R., Jackson, M. J., & McArdle, A. (2010). Overexpression of HSP10 in skeletal muscle of transgenic mice prevents the age-related fall in maximum tetanic force generation and muscle cross-sectional area. *American Journal of Physiology - Regulatory Integrative and Comparative Physiology*, *299*(1), 268–276. https://doi.org/10.1152/AJPREGU.00334.2009/ASSET/IMAGES/LARGE/ZH600710724400006.JPEG

Kemoun, P., Ader, I., Planat-Benard, V., Dray, C., Fazilleau, N., Monsarrat, P., Cousin, B., Paupert, J., Ousset, M., Lorsignol, A., Raymond-Letron, I., Vellas, B., Valet, P., Kirkwood, T., Beard, J., Pénicaud, L., & Casteilla, L. (2022). A gerophysiology perspective on healthy ageing. *Ageing Research Reviews*, *73*. https://doi.org/10.1016/J.ARR.2021.101537

Kennedy, B. K., Berger, S. L., Brunet, A., Campisi, J., Cuervo, A. M., Epel, E. S., Franceschi, C., Lithgow, G. J., Morimoto, R. I., Pessin, J. E., Rando, T. A., Richardson, A., Schadt, E. E., Wyss-Coray, T., & Sierra, F. (2014). Geroscience: linking aging to chronic disease. *Cell*, *159*(4), 709–713. https://doi.org/10.1016/J.CELL.2014.10.039

Kerndt, P., Naughton, J., Driscoll, C., & Loxterkamp, D. (1982). Fasting: The History, Pathophysiology and Complications. *Western Journal of Medicine*, *137*(5), 379–399. https://www.ncbi.nlm.nih.gov/pmc/articles/PMC1274154/

Khawaja, A., Cipullo, M., Krüger, A., & Rorbach, J. (2023). Insights into mitoribosomal biogenesis from recent structural studies. *Trends in Biochemical Sciences*, *48*(7), 629–641. https://doi.org/10.1016/J.TIBS.2023.04.002

Kirkland, J. L., Stout, M. B., & Sierra, F. (2016). Resilience in Aging Mice. *The Journals of Gerontology. Series A, Biological Sciences and Medical Sciences*, *71*(11), 1407–1414. https://doi.org/10.1093/GERONA/GLW086

Kitano, H., Oda, K., Kimura, T., Matsuoka, Y., Csete, M., Doyle, J., & Muramatsu, M. (2004). Metabolic syndrome and robustness tradeoffs. *Diabetes*, *53*(SUPPL. 3). https://doi.org/10.2337/diabetes.53.suppl_3.S6

Kubota, H., Obata, T., Ota, K., Sasaki, T., & Ito, T. (2003). Rapamycin-induced Translational Derepression of GCN4 mRNA Involves a Novel Mechanism for Activation of the eIF2α

Kinase GCN2. *Journal of Biological Chemistry*, *278*(23), 20457–20460. https://doi.org/10.1074/JBC.C300133200

Kudin, A. P., Bimpong-Buta, N. Y. B., Vielhaber, S., Elger, C. E., & Kunz, W. S. (2004). Characterization of Superoxide-producing Sites in Isolated Brain Mitochondria. *Journal of Biological Chemistry*, *279*(6), 4127–4135. https://doi.org/10.1074/jbc.M310341200

Lane, N., & Martin, W. (2010). The energetics of genome complexity. *Nature*, *467*(7318), 929–934. https://doi.org/10.1038/nature09486

Lee, R. G., Gao, J., Siira, S. J., Shearwood, A. M., Ermer, J. A., Hofferek, V., Mathews, J. C., Zheng, M., Reid, G. E., Rackham, O., & Filipovska, A. (2020). Cardiolipin is required for membrane docking of mitochondrial ribosomes and protein synthesis. *Journal of Cell Science*, *133*(14). https://doi.org/10.1242/JCS.240374

Lee, T. Y., Huang, L. J., Dong, H. P., Tohru, Y., Liu, B. H., & Yang, R. C. (2020). Impairment of mitochondrial unfolded protein response contribute to resistance declination of H_2O_2-induced injury in senescent MRC-5 cell model. *The Kaohsiung Journal of Medical Sciences*, *36*(2), 89–97. https://doi.org/10.1002/KJM2.12146

Liao, T. L., Tzeng, C. R., Yu, C. L., Wang, Y. P., & Kao, S. H. (2015). Estrogen receptor-β in mitochondria: implications for mitochondrial bioenergetics and tumorigenesis. *Annals of the New York Academy of Sciences*, *1350*, 52–60. https://doi.org/10.1111/nyas.12872

Lilleker, J. B., Hodgson, R., Roberts, M., Herholz, K., Howard, J., Hinz, R., & Chinoy, H. (2019). [18F]Florbetapir positron emission tomography: identification of muscle amyloid in inclusion body myositis and differentiation from polymyositis. *Annals of the Rheumatic Diseases*, *78*(5), 657–662. https://doi.org/10.1136/ANNRHEUMDIS-2018-214644

Liu, M., & Spremulli, L. (2000). Interaction of mammalian mitochondrial ribosomes with the inner membrane. *Journal of Biological Chemistry*, *275*(38), 29400–29406. https://doi.org/10.1074/jbc.M002173200

Long, J. A., & Gordon, M. S. (2004). The greatest step in vertebrate history: A paleobiological review of the fish-tetrapod transition. *Physiological and Biochemical Zoology*, *77*(5), 700–719. https://doi.org/10.1086/425183

Lopez Sanchez, M. I. G., Krüger, A., Shiriaev, D. I., Liu, Y., & Rorbach, J. (2021). Human Mitoribosome Biogenesis and Its Emerging Links to Disease. *International Journal of Molecular Sciences*, *22*(8). https://doi.org/10.3390/IJMS22083827

López-Otín, C., Blasco, M. A., Partridge, L., Serrano, M., & Kroemer, G. (2013). The Hallmarks of Aging. *Cell*, *153*(6), 1194–1217. https://doi.org/10.1016/J.CELL.2013.05.039

López-Otín, C., Blasco, M. A., Partridge, L., Serrano, M., & Kroemer, G. (2023). Hallmarks of aging: An expanding universe. *Cell*, *186*(2), 243–278. https://doi.org/10.1016/J.CELL.2022.11.001

Macena, M. de L., & Bueno, N. B. (2023). Letter to the editor: The use of resting energy expenditure divided by body weight (kcal/kg) may yield inconsistencies and should be avoided. *Clinical Nutrition*, *42*(4), 609–610. https://doi.org/10.1016/J.CLNU.2023.02.017

Mair, W., Goymer, P., Pletcher, S. D., & Partridge, L. (2003). Demography of dietary restriction and death in Drosophila. *Science*, *301*(5640), 1731–1734. https://go-gale-com.proxy.bib.uottawa.ca/ps/i.do?p=AONE&sw=w&issn=00368075&v=2.1&it=r&id=GALE%7CA110152907&sid=googleScholar&linkaccess=fulltext

Martin, W. F., Tielens, A. G. M., & Mentel, M. (2020). 4 Energy metabolism and redox balance. *Mitochondria and Anaerobic Energy Metabolism in Eukaryotes*, 23–25. https://doi.org/10.1515/9783110612417-005/HTML

Martins, A. C., López-Granero, C., Ferrer, B., Tinkov, A. A., Skalny, A. V., Paoliello, M. M. B., & Aschner, M. (2021). BXD Recombinant Inbred Mice as a Model to Study Neurotoxicity. *Biomolecules*, *11*(12), 1762. https://doi.org/10.3390/biom11121762

Mathers, C. D., Stevens, G. A., Boerma, T., White, R. A., & Tobias, M. I. (2015). Causes of international increases in older age life expectancy. *The Lancet*, *385*(9967), 540–548. https://doi.org/10.1016/S0140-6736(14)60569-9

McBurney, M. W., Yang, X., Jardine, K., Hixon, M., Boekelheide, K., Webb, J. R., Lansdorp, P. M., & Lemieux, M. (2003). The Mammalian SIR2α Protein Has a Role in Embryogenesis and Gametogenesis. *Molecular and Cellular Biology*, *23*(1), 38–54. https://doi.org/10.1128/MCB.23.1.38-54.2003

McColl, G., Killilea, D. W., Hubbard, A. E., Vantipalli, M. C., Melov, S., & Lithgow, G. J. (2008). Pharmacogenetic Analysis of Lithium-induced Delayed Aging in Caenorhabditis elegans. *Journal of Biological Chemistry*, *283*(1), 350–357. https://doi.org/10.1074/JBC.M705028200

Mccoll, G., Roberts, B. R., Pukala, T. L., Kenche, V. B., Roberts, C. M., Link, C. D., Ryan, T. M., Masters, C. L., Barnham, K. J., Bush, A. I., & Cherny, R. A. (2012). Utility of an improved model of amyloid-beta (Aβ1-42) toxicity in Caenorhabditis elegans for drug screening for Alzheimer's disease. *Molecular Neurodegeneration*, *7*(1), 1–9. https://doi.org/10.1186/1750-1326-7-57/FIGURES/5

McMahon, B. R. (1970). The Relative Efficiency of Gaseous Exchange Across the Lungs and Gills of an African Lungfish Protopterus Aethiopicus. *Journal of Experimental Biology*, *52*(1), 1–15. https://doi.org/10.1242/JEB.52.1.1

Melber, A., & Haynes, C. M. (2018). UPR mt regulation and output: A stress response mediated by mitochondrial-nuclear communication. *Cell Research*, *28*(3), 281–295. https://doi.org/10.1038/CR.2018.16

Memme, J. M., Oliveira, A. N., & Hood, D. A. (2016). Chronology of UPR activation in skeletal muscle adaptations to chronic contractile activity. *American Journal of Physiology - Cell Physiology*, *310*(11), C1024–C1036. https://doi.org/10.1152/AJPCELL.00009.2016/ASSET/IMAGES/LARGE/ZH00111679510008.JPEG

Mercer, T. R., Neph, S., Dinger, M. E., Crawford, J., Smith, M. A., Shearwood, A. M. J., Haugen, E., Bracken, C. P., Rackham, O., Stamatoyannopoulos, J. A., Filipovska, A., & Mattick, J. S. (2011). The human mitochondrial transcriptome. *Cell*, *146*(4), 645–658. https://doi.org/10.1016/J.CELL.2011.06.051

Merkwirth, C., Jovaisaite, V., Durieux, J., Matilainen, O., Jordan, S. D., Quiros, P. M., Steffen, K. K., Williams, E. G., Mouchiroud, L., Tronnes, S. U., Murillo, V., Wolff, S. C., Shaw, R. J., Auwerx, J., & Dillin, A. (2016). Two Conserved Histone Demethylases Regulate Mitochondrial Stress-Induced Longevity. *Cell*, *165*(5), 1209–1223. https://doi.org/10.1016/J.CELL.2016.04.012

Mick, E., Titov, D. V., Skinner, O. S., Sharma, R., Jourdain, A. A., & Mootha, V. K. (2020). Distinct mitochondrial defects trigger the integrated stress response depending on the metabolic state of the cell. *ELife*, *9*. https://doi.org/10.7554/ELIFE.49178

Mitchell, P. (1961). Coupling of Phosphorylation to Electron and Hydrogen Transfer by a Chemi-Osmotic type of Mechanism. *Nature 1961 191:4784*, *191*(4784), 144–148. https://doi.org/10.1038/191144a0

Mitchell, P. (1970). Aspects of the chemiosmotic hypothesis. *Biochemical Journal*, *116*(4), 5P-6P. https://doi.org/10.1042/BJ1160005P

Moehle, E. A., Shen, K., & Dillin, A. (2019). Mitochondrial proteostasis in the context of cellular and organismal health and aging. *The Journal of Biological Chemistry*, *294*(14), 5396. https://doi.org/10.1074/JBC.TM117.000893

Molenaars, M., Daniels, E. G., Meurs, A., Janssens, G. E., & Houtkooper, R. H. (2020). Mitochondrial cross-compartmental signalling to maintain proteostasis and longevity. *Philosophical Transactions of the Royal Society of London. Series B, Biological Sciences*, *375*(1801). https://doi.org/10.1098/RSTB.2019.0414

Mouchiroud, L., Houtkooper, R. H., Moullan, N., Katsyuba, E., Ryu, D., Cantó, C., Mottis, A., Jo, Y. S., Viswanathan, M., Schoonjans, K., Guarente, L., & Auwerx, J. (2013). The NAD+/Sirtuin Pathway Modulates Longevity through Activation of Mitochondrial UPR and FOXO Signaling. *Cell*, *154*(2), 430–441. https://doi.org/10.1016/J.CELL.2013.06.016

Murphy, C. T., McCarroll, S. A., Bargmann, C. I., Fraser, A., Kamath, R. S., Ahringer, J., Li, H., & Kenyon, C. (2003). Genes that act downstream of DAF-16 to influence the lifespan of

Caenorhabditis elegans. *Nature*, *424*(6946), 277–284. https://doi.org/10.1038/NATURE01789

Musci, R. V., Hamilton, K. L., & Linden, M. A. (2019). Exercise-Induced Mitohormesis for the Maintenance of Skeletal Muscle and Healthspan Extension. *Sports 2019, Vol. 7, Page 170*, *7*(7), 170. https://doi.org/10.3390/SPORTS7070170

Musci, R. V, Hamilton, K. L., & Miller, B. F. (2018). Targeting mitochondrial function and proteostasis to mitigate dynapenia. *European Journal of Applied Physiology*, *118*(1), 1–9. https://doi.org/10.1007/s00421-017-3730-x

Nargund, A. M., Pellegrino, M. W., Fiorese, C. J., Baker, B. M., & Haynes, C. M. (2012). Mitochondrial import efficiency of ATFS-1 regulates mitochondrial UPR activation. *Science (New York, N.Y.)*, *337*(6094), 587–590. https://doi.org/10.1126/SCIENCE.1223560

Nesse, R., Bhatnager, S., & Ellis, B. (2016). Evolutionary Origins and Functions of the Stress Response System. In G. Fink (Ed.), *Stress: Concepts, Cognition, Emotion, and Behavior* (pp. 95-101). Academic Press. ISBN 9780128009512

Noack, K., Zardoya, R., & Meyer, A. (1996). *The Complete Mitochondrial DNA Sequence of the Bichir (Polypterus ornutipinnis), a Basal Ray-Finned Fish: Ancient Establishment of the Consensus Vertebrate Gene Order*.

Okado-Matsumoto, A., & Fridovich, I. (2001). Subcellular distribution of superoxide dismutases (SOD) in rat liver: Cu,Zn-SOD in mitochondria. *The Journal of Biological Chemistry*, *276*(42), 38388–38393. https://doi.org/10.1074/JBC.M105395200

Olagunju, A. S., Ahammad, F., Alagbe, A. A., Otenaike, T. A., Teibo, J. O., Mohammad, F., Alsaiari, A. A., Omotoso, O., & Talukder, M. E. K. (2023). Mitochondrial dysfunction: A notable contributor to the progression of Alzheimer's and Parkinson's disease. *Heliyon*, *9*(3), e14387. https://doi.org/10.1016/J.HELIYON.2023.E14387

Owusu-Ansah, E., Song, W., & Perrimon, N. (2013). Muscle mitohormesis promotes longevity via systemic repression of insulin signaling. *Cell*, *155*(3), 699. https://doi.org/10.1016/J.CELL.2013.09.021

Ozkurede, U., & Miller, R. A. (2019). Improved mitochondrial stress response in long-lived Snell dwarf mice. *Aging Cell*, *18*(6), e13030. https://doi.org/10.1111/ACEL.13030

Peirce, J. L., Lu, L., Gu, J., Silver, L. M., & Williams, R. W. (2004). A new set of BXD recombinant inbred lines from advanced intercross populations in mice. *BMC Genetics*, *5*(1), 1–17. https://doi.org/10.1186/1471-2156-5-7/FIGURES/4

Perni, M., Challa, P. K., Kirkegaard, J. B., Limbocker, R., Koopman, M., Hardenberg, M. C., Sormanni, P., Müller, T., Saar, K. L., Roode, L. W. Y., Habchi, J., Vecchi, G., Fernando, N., Casford, S., Nollen, E. A. A., Vendruscolo, M., Dobson, C. M., & Knowles, T. P. J. (2018). Massively parallel C. elegans tracking provides multi-dimensional fingerprints for phenotypic discovery. *Journal of Neuroscience Methods*, *306*, 57–67. https://doi.org/10.1016/J.JNEUMETH.2018.02.005

Perry, E. A., Bennett, C. F., Luo, C., Balsa, E., Jedrychowski, M., O'Malley, K. E., Latorre-Muro, P., Ladley, R. P., Reda, K., Wright, P. M., Gygi, S. P., Myers, A. G., & Puigserver, P. (2021). Tetracyclines promote survival and fitness in mitochondrial disease models. *Nature Metabolism*, *3*(1), 33–42. https://doi.org/10.1038/S42255-020-00334-Y

Pharaoh, G., Pulliam, D., Hill, S., Sataranatarajan, K., & Van Remmen, H. (2016). Ablation of the mitochondrial complex IV assembly protein Surf1 leads to increased expression of the UPRMT and increased resistance to oxidative stress in primary cultures of fibroblasts. *Redox Biology*, *8*, 430–438. https://doi.org/10.1016/J.REDOX.2016.05.001

Pietrangelo, L., D'Incecco, A., Ainbinder, A., Michelucci, A., Kern, H., Dirksen, R. T., Boncompagni, S., & Protasi, F. (2015). Age-dependent uncoupling of mitochondria from $Ca2^{+}$ release units in skeletal muscle. *Oncotarget*, *6*(34), 35358–35371. https://doi.org/10.18632/oncotarget.6139

Plech, M., Tomala, K., Tutaj, H., Piwcewicz, D. E., de Visser, J. A. G. M., & Korona, R. (2017). Power provides protection: Genetic robustness in yeast depends on the capacity to generate energy. *PLOS Genetics*, *13*(5), e1006768. https://doi.org/10.1371/JOURNAL.PGEN.1006768

Pulliam, D. A., Deepa, S. S., Liu, Y., Hill, S., Lin, A. L., Bhattacharya, A., Shi, Y., Sloane, L., Viscomi, C., Zeviani, M., & Van Remmen, H. (2014). Complex IV-deficient $Surf1^{-/-}$ mice initiate mitochondrial stress responses. *Biochemical Journal*, *462*(2), 359–371. https://doi.org/10.1042/BJ20140291

Qiu, Y., Fernández-García, B., Lehmann, H. I., Li, G., Kroemer, G., López-Otín, C., & Xiao, J. (2023). Exercise sustains the hallmarks of health. *Journal of Sport and Health Science*, *12*(1), 8–35. https://doi.org/https://doi.org/10.1016/j.jshs.2022.10.003

Quirós, P. M., Prado, M. A., Zamboni, N., D'Amico, D., Williams, R. W., Finley, D., Gygi, S. P., & Auwerx, J. (2017). Multi-omics analysis identifies ATF4 as a key regulator of the

mitochondrial stress response in mammals. *The Journal of Cell Biology*, *216*(7), 2027–2045. https://doi.org/10.1083/JCB.201702058

Ramsay, D. S., & Woods, S. C. (2014). Clarifying the roles of homeostasis and allostasis in physiological regulation. *Psychological Review*, *121*(2), 225–247. https://doi.org/10.1037/A0035942

Razzoli, M., Nyuyki-Dufe, K., Gurney, A., Erickson, C., McCallum, J., Spielman, N., Marzullo, M., Patricelli, J., Kurata, M., Pope, E. A., Touma, C., Palme, R., Largaespada, D. A., Allison, D. B., & Bartolomucci, A. (2018). Social stress shortens lifespan in mice. *Aging Cell*, *17*(4), e12778. https://doi.org/10.1111/ACEL.12778

Regulski, M. J. (2017). Cellular Senescence: What, Why, and How. *Wounds : A Compendium of Clinical Research and Practice*, *29*(6), 168–174.

Reid, K., Daniels, E. G., Vasam, G., Kamble, R., Janssens, G. E., Hu, I. M., Green, A. E., Houtkooper, R. H., & Menzies, K. J. (2023). Reducing mitochondrial ribosomal gene expression does not alter metabolic health or lifespan in mice. *Scientific Reports 2023 13:1*, *13*(1), 1–15. https://doi.org/10.1038/s41598-023-35196-3

Richter-Dennerlein, R., Oeljeklaus, S., Lorenzi, I., Ronsör, C., Bareth, B., Schendzielorz, A. B., Wang, C., Warscheid, B., Rehling, P., & Dennerlein, S. (2016). Mitochondrial Protein Synthesis Adapts to Influx of Nuclear-Encoded Protein. *Cell*, *167*(2), 471-483.e10. https://doi.org/10.1016/J.CELL.2016.09.003

Robida-Stubbs, S., Glover-Cutter, K., Lamming, D. W., Mizunuma, M., Narasimhan, S. D., Neumann-Haefelin, E., Sabatini, D. M., & Blackwell, T. K. (2012). TOR Signaling and

Rapamycin Influence Longevity by Regulating SKN-1/Nrf and DAF-16/FoxO. *Cell Metabolism*, *15*(5), 713–724. https://doi.org/10.1016/J.CMET.2012.04.007

Rodgers, E. M., & Gomez Isaza, D. F. (2023). The mechanistic basis and adaptive significance of cross-tolerance: a “pre-adaptation” to a changing world? *The Journal of Experimental Biology*, *226*(11). https://doi.org/10.1242/JEB.245644/316631

Roger, A. J., Muñoz-Gómez, S. A., & Kamikawa, R. (2017). The Origin and Diversification of Mitochondria. *Current Biology*, *27*(21), R1177–R1192. https://doi.org/https://doi.org/10.1016/j.cub.2017.09.015

Rolland, S. G., Schneid, S., Schwarz, M., Rackles, E., Fischer, C., Haeussler, S., Regmi, S. G., Yeroslaviz, A., Habermann, B., Mokranjac, D., Lambie, E., & Conradt, B. (2019). Compromised Mitochondrial Protein Import Acts as a Signal for UPRmt. *Cell Reports*, *28*(7), 1659-1669.e5. https://doi.org/10.1016/J.CELREP.2019.07.049

Sadat, A., Tiwari, S., Sunidhi, S., Chaphalkar, A., Kochar, M., Ali, M., Zaidi, Z., Sharma, A., Verma, K., Rao, K. B. N., Tripathi, M., Ghosh, A., Gautam, D., Atul, Ray, A., Mapa, K., & Chakraborty, K. (2022). Conserved and divergent chaperoning effects of Hsp60/10 chaperonins on protein folding landscapes. *Proceedings of the National Academy of Sciences of the United States of America*, *119*(18), e2118465119. https://doi.org/10.1073/PNAS.2118465119/SUPPL_FILE/PNAS.2118465119.SD02.XLSX

Sarkar, S., Floto, R. A., Berger, Z., Imarisio, S., Cordenier, A., Pasco, M., Cook, L. J., & Rubinsztein, D. C. (2005). Lithium induces autophagy by inhibiting inositol monophosphatase. *The Journal of Cell Biology*, *170*(7), 1101. https://doi.org/10.1083/JCB.200504035

Sarkar, S., Krishna, G., Imarisio, S., Saiki, S., O'Kane, C. J., & Rubinsztein, D. C. (2008). A rational mechanism for combination treatment of Huntington's disease using lithium and rapamycin. *Human Molecular Genetics*, *17*(2), 170–178. https://doi.org/10.1093/HMG/DDM294

Satoh, A., Brace, C. S., Rensing, N., Cliften, P., Wozniak, D. F., Herzog, E. D., Yamada, K. A., & Imai, S. I. (2013). Sirt1 extends life span and delays aging in mice through the regulation of Nk2 homeobox 1 in the DMH and LH. *Cell Metabolism*, *18*(3), 416. https://doi.org/10.1016/J.CMET.2013.07.013

Schmidt, R. H., Nickerson, J. M., & Boatright, J. H. (2016). Exercise as Gene Therapy: BDNF and DNA Damage Repair. *Asia-Pacific Journal of Ophthalmology (Philadelphia, Pa.)*, *5*(4), 309—311. https://doi.org/10.1097/apo.0000000000000226

Seely, S. M., & Gagnon, M. G. (2022). Mechanisms of ribosome recycling in bacteria and mitochondria: a structural perspective. *RNA Biology*, *19*(1), 662. https://doi.org/10.1080/15476286.2022.2067712

Shen, Y., Ding, M., Xie, Z., Liu, X., Yang, H., Jin, S., Xu, S., Zhu, Z., Wang, Y., Wang, D., Xu, L., Zhou, X., Wang, P., & Bi, J. (2020). Activation of Mitochondrial Unfolded Protein Response in SHSY5Y Expressing APP Cells and APP/PS1 Mice. *Frontiers in Cellular Neuroscience*, *13*, 495529. https://doi.org/10.3389/FNCEL.2019.00568/BIBTEX

Sherratt, H. S. (1991). Mitochondria: structure and function. *Revue Neurologique*, *147*(6–7), 417–430.

Shin, C. S., Meng, S., Garbis, S. D., Moradian, A., Taylor, R. W., Sweredoski, M. J., Lomenick, B., & Chan, D. C. (2021). LONP1 and mtHSP70 cooperate to promote mitochondrial

protein folding. *Nature Communications 2021 12:1*, *12*(1), 1–10. https://doi.org/10.1038/s41467-020-20597-z

Sies, H. (2017). Hydrogen peroxide as a central redox signaling molecule in physiological oxidative stress: Oxidative eustress. *Redox Biology*, *11*, 613. https://doi.org/10.1016/J.REDOX.2016.12.035

Singulani, M. P., De Paula, V. J. R., & Forlenza, O. V. (2021). Mini review: Mitochondrial dysfunction in Alzheimer's disease: Therapeutic implications of lithium. *Neuroscience Letters*, *760*, 136078. https://doi.org/10.1016/J.NEULET.2021.136078

Skinner, S. K., Solania, A., Wolan, D. W., Cohen, M. S., Ryan, T. E., & Hepple, R. T. (2021). Mitochondrial Permeability Transition Causes Mitochondrial Reactive Oxygen Species- and Caspase 3-Dependent Atrophy of Single Adult Mouse Skeletal Muscle Fibers. *Cells*, *10*(10), 2586. https://doi.org/10.3390/cells10102586

Slavin, M. B., Kumari, R., & Hood, D. A. (2022). ATF5 is a regulator of exercise-induced mitochondrial quality control in skeletal muscle. *Molecular Metabolism*, *66*, 101623. https://doi.org/10.1016/J.MOLMET.2022.101623

Sloan, D. B., Warren, J. M., Williams, A. M., Wu, Z., Abdel-Ghany, S. E., Chicco, A. J., & Havird, J. C. (2018). Cytonuclear integration and co-evolution. *Nature Reviews Genetics*, *19*(10), 635–648. https://doi.org/10.1038/s41576-018-0035-9

Snigdha, S., Aleph Prieto, G., Petrosyan, A., Loertscher, B. M., Dieskau, A. P., Overman, L. E., & Cotman, C. W. (2016). H3K9me3 Inhibition Improves Memory, Promotes Spine Formation, and Increases BDNF Levels in the Aged Hippocampus. *The Journal of*

Neuroscience : The Official Journal of the Society for Neuroscience, *36*(12), 3611–3622. https://doi.org/10.1523/JNEUROSCI.2693-15.2016

Sokolova, I. (2018). Mitochondrial Adaptations to Variable Environments and Their Role in Animals' Stress Tolerance. *Integrative and Comparative Biology*, *58*(3), 519–531. https://doi.org/10.1093/ICB/ICY017

Sorrentino, V., Romani, M., Mouchiroud, L., Beck, J. S., Zhang, H., D'Amico, D., Moullan, N., Potenza, F., Schmid, A. W., Rietsch, S., Counts, S. E., & Auwerx, J. (2017). Enhancing mitochondrial proteostasis reduces amyloid- proteotoxicity. *Nature*, *552*(7684), 187–187. https://doi.org/10.1038/NATURE25143

Soto, I., Couvillion, M., Hansen, K. G., McShane, E., Moran, J. C., Barrientos, A., & Churchman, L. S. (2022). Balanced mitochondrial and cytosolic translatomes underlie the biogenesis of human respiratory complexes. *Genome Biology*, *23*(1), 1–24. https://doi.org/10.1186/S13059-022-02732-9/FIGURES/4

Spangenburg, E. E., & Ward, C. W. (2016). Measuring mitochondrial respiration in intact skeletal muscle fibers Technical Brief. *Seahorse Bioscience Technical Brief*.

Standen, E. M., Du, T. Y., & Larsson, H. C. E. (2014). Developmental plasticity and the origin of tetrapods. *Nature 2014 513:7516*, *513*(7516), 54–58. https://doi.org/10.1038/NATURE13708

Statistics Canada. (2022, January 24). *Life expectancy and other elements of the complete life table, single-year estimates, Canada, all provinces except Prince Edward Island*. https://www150.statcan.gc.ca/t1/tbl1/en/tv.action?pid=1310083701

Taconic Biosciences. (2024). *Black 6 (B6NTac)*. Retrieved January 31, 2024, from Taconic Biosciences | Models for Life: https://www.taconic.com/products/mouse-rat/standard-strains-and-stocks/black-6-b6ntac

Tamura, Y., Matsunaga, Y., Kitaoka, Y., & Hatta, H. (2017). Effects of Heat Stress Treatment on Age-dependent Unfolded Protein Response in Different Types of Skeletal Muscle. *The Journals of Gerontology: Series A*, *72*(3), 299–308. https://doi.org/10.1093/GERONA/GLW063

Tan, K. T., Ang, S. T. J., & Tsai, S. Y. (2020). Sarcopenia: Tilting the Balance of Protein Homeostasis. *Proteomics*, *20*(5–6), 1800411. https://doi.org/10.1002/PMIC.201800411

Tapia, A., Palomino-Schätzlein, M., Roca, M., Lahoz, A., Pineda-Lucena, A., López Del Amo, V., & Galindo, M. I. (2021). Mild muscle mitochondrial fusion distress extends drosophila lifespan through an early and systemic metabolome reorganization. *International Journal of Molecular Sciences*, *22*(22), 12133. https://doi.org/10.3390/IJMS222212133/S1

Tapia, P. C. (2006). Sublethal mitochondrial stress with an attendant stoichiometric augmentation of reactive oxygen species may precipitate many of the beneficial alterations in cellular physiology produced by caloric restriction, intermittent fasting, exercise and dietary phytonutrients: “Mitohormesis” for health and vitality. *Medical Hypotheses*, *66*(4), 832–843. https://doi.org/10.1016/J.MEHY.2005.09.009

Teske, B. F., Fusakio, M. E., Zhou, D., Shan, J., McClintick, J. N., Kilberg, M. S., & Wek, R. C. (2013). CHOP induces activating transcription factor 5 (ATF5) to trigger apoptosis in response to perturbations in protein homeostasis. *Molecular Biology of the Cell*, *24*(15),

2477–2490. https://doi.org/10.1091/MBC.E13-01-0067/ASSET/IMAGES/LARGE/2477FIG8.JPEG

Tian, Y., Garcia, G., Bian, Q., Steffen, K. K., Joe, L., Wolff, S., Meyer, B. J., & Dillin, A. (2016). Mitochondrial Stress Induces Chromatin Reorganization to Promote Longevity and UPR(mt). *Cell*, *165*(5), 1197–1208. https://doi.org/10.1016/J.CELL.2016.04.011

Tiernan, C. T., Ginsberg, S. D., Guillozet-Bongaarts, A. L., Ward, S. M., He, B., Kanaan, N. M., Mufson, E. J., Binder, L. I., & Counts, S. E. (2016). Protein homeostasis gene dysregulation in pretangle-bearing nucleus basalis neurons during the progression of Alzheimer's disease. *Neurobiology of Aging*, *42*, 80–90. https://doi.org/10.1016/J.NEUROBIOLAGING.2016.02.031

Tobiasson, V., Gahura, O., Aibara, S., Baradaran, R., Zíková, A., & Amunts, A. (2021). Interconnected assembly factors regulate the biogenesis of mitoribosomal large subunit. *The EMBO Journal*, *40*(6). https://doi.org/10.15252/EMBJ.2020106292

Tomtheelnganbee, E., Sah, P., & Sharma, R. (2022). Mitochondrial function and nutrient sensing pathways in ageing: enhancing longevity through dietary interventions. *Biogerontology*, *23*(6), 657–680. https://doi.org/10.1007/S10522-022-09978-7

Tria, F. D. K., Brueckner, J., Skejo, J., Xavier, J. C., Kapust, N., Knopp, M., Wimmer, J. L. E., Nagies, F. S. P., Zimorski, V., Gould, S. B., Garg, S. G., & Martin, W. F. (2021). Gene Duplications Trace Mitochondria to the Onset of Eukaryote Complexity. *Genome Biology and Evolution*, *13*(5), evab055. https://doi.org/10.1093/gbe/evab055

Tsang, W. Y., Sayles, L. C., Grad, L. I., Pilgrim, D. B., & Lemire, B. D. (2001). Mitochondrial respiratory chain deficiency in Caenorhabditis elegans results in developmental arrest and

increased life span. *The Journal of Biological Chemistry*, *276*(34), 32240–32246. https://doi.org/10.1074/JBC.M103999200

Tschöp, M. H., Speakman, J. R., Arch, J. R. S., Auwerx, J., Brüning, J. C., Chan, L., Eckel, R. H., Farese, R. V., Galgani, J. E., Hambly, C., Herman, M. A., Horvath, T. L., Kahn, B. B., Kozma, S. C., Maratos-Flier, E., Müller, T. D., Münzberg, H., Pfluger, P. T., Plum, L., … Ravussin, E. (2012). A guide to analysis of mouse energy metabolism. *Nature Methods*, *9*(1), 57–63. https://doi.org/10.1038/NMETH.1806

Urbina-Varela, R., Castillo, N., Videla, L. A., & Del Campo, A. (2020). Impact of Mitophagy and Mitochondrial Unfolded Protein Response as New Adaptive Mechanisms Underlying Old Pathologies: Sarcopenia and Non-Alcoholic Fatty Liver Disease. *International Journal of Molecular Sciences 2020, Vol. 21, Page 7704*, *21*(20), 7704. https://doi.org/10.3390/IJMS21207704

Vachon, P. J., & Sestier, F. (2013). Life Expectancy Determination. *Physical Medicine and Rehabilitation Clinics of North America*, *24*(3), 539–551. https://doi.org/10.1016/J.PMR.2013.03.007

Vaupel, J. W., Villavicencio, F., & Bergeron-Boucher, M. P. (2021). Demographic perspectives on the rise of longevity. *Proceedings of the National Academy of Sciences*, *118*(9), e2019536118. https://doi.org/10.1073/PNAS.2019536118

Ventura-Clapier, R., Piquereau, J., Veksler, V., & Garnier, A. (2019). Estrogens, Estrogen Receptors Effects on Cardiac and Skeletal Muscle Mitochondria. *Frontiers in endocrinology*, *10*, 557. https://doi.org/10.3389/fendo.2019.00557

Viswanathan, M., & Guarente, L. (2011). Regulation of Caenorhabditis elegans lifespan by sir-2.1 transgenes. *Nature 2011 477:7365*, *477*(7365), E1–E2. https://doi.org/10.1038/nature10440

Võikar, V., Polus, A., Vasar, E., & Rauvala, H. (2005). Long-term individual housing in C57BL/6J and DBA/2 mice: assessment of behavioral consequences. *Genes, Brain, and Behavior*, *4*(4), 240–252. https://doi.org/10.1111/J.1601-183X.2004.00106.X

Wagner, K.-H., Reichhold, S., & Neubauer, O. (2011). Impact of endurance and ultraendurance exercise on DNA damage. *Annals of the New York Academy of Sciences*, *1229*(1), 115–123. https://doi.org/https://doi.org/10.1111/j.1749-6632.2011.06106.x

Wälti, M. A., Canagarajah, B., Schwieters, C. D., & Clore, G. M. (2021). Visualization of Sparsely-populated Lower-order Oligomeric States of Human Mitochondrial Hsp60 by Cryo-electron Microscopy. *Journal of Molecular Biology*, *433*(24). https://doi.org/10.1016/J.JMB.2021.167322

Wang, C. L., Ohkubo, R., Mu, W. C., Chen, W., Fan, J. L., Song, Z., Maruichi, A., Sudmant, P. H., Pisco, A. O., Dubal, D. B., Ji, N., & Chen, D. (2023). The mitochondrial unfolded protein response regulates hippocampal neural stem cell aging. *Cell Metabolism*, *35*(6), 996-1008.e7. https://doi.org/10.1016/J.CMET.2023.04.012

Wang, S. F., Chen, S., Tseng, L. M., & Lee, H. C. (2020). Role of the mitochondrial stress response in human cancer progression. *Experimental Biology and Medicine*, *245*(10), 861–878. https://doi.org/10.1177/1535370220920558/ASSET/IMAGES/LARGE/10.1177_1535370220920558-FIG3.JPEG

Wang, Z., Bo, H., Song, Y., Li, C., & Zhang, Y. (2022). Mitochondrial ROS Produced by Skeletal Muscle Mitochondria Promote the Decisive Signal for UPRmt Activation. *BioMed Research International*, *2022*. https://doi.org/10.1155/2022/7436577

Webb, R., Hughes, M. G., Thomas, A. W., & Morris, K. (2017). The Ability of Exercise-Associated Oxidative Stress to Trigger Redox-Sensitive Signalling Responses. *Antioxidants (Basel, Switzerland)*, *6*(3). https://doi.org/10.3390/ANTIOX6030063

Wedatilake, Y., Brown, R. M., McFarland, R., Yaplito-Lee, J., Morris, A. A. M., Champion, M., Jardine, P. E., Clarke, A., Thorburn, D. R., Taylor, R. W., Land, J. M., Forrest, K., Dobbie, A., Simmons, L., Aasheim, E. T., Ketteridge, D., Hanrahan, D., Chakrapani, A., Brown, G. K., & Rahman, S. (2013). SURF1 deficiency: A multi-centre natural history study. *Orphanet Journal of Rare Diseases*, *8*(1), 1–13. https://doi.org/10.1186/1750-1172-8-96/FIGURES/3

Weichhart, T. (2018). mTOR as regulator of lifespan, aging and cellular senescence. *Gerontology*, *64*(2), 127. https://doi.org/10.1159/000484629

West-Eberhard, M. J. (2003). Developmental Plasticity and Evolution. *Developmental Plasticity and Evolution*. https://doi.org/10.1093/OSO/9780195122343.001.0001

World Health Organization. (2022, May 19). *World Health Statistics 2022: Monitoring health for the SDGs, sustainable development goals*. https://www.who.int/publications/i/item/9789240051157

Wu, S., Zheng, S. Di, Huang, H. L., Yan, L. C., Yin, X. F., Xu, H. N., Zhang, K. J., Gui, J. H., Chu, L., & Liu, X. Y. (2013). Lithium Down-regulates Histone Deacetylase 1 (HDAC1)

and Induces Degradation of Mutant Huntingtin. *Journal of Biological Chemistry*, *288*(49), 35500–35510. https://doi.org/10.1074/JBC.M113.479865

Xu, H., Liu, Y.-Y., Li, L.-S., & Liu, Y.-S. (2023). Sirtuins at the Crossroads between Mitochondrial Quality Control and Neurodegenerative Diseases: Structure, Regulation, Modifications, and Modulators. *Aging and Disease*, *14*(3), 794–824. https://doi.org/10.14336/AD.2022.1123

Yang, L., Zhang, Z., & He, S. (2015). Bichir microRNA repertoire suggests a ray-finned fish affinity of Polypteriforme. *Gene*, *566*(2), 242–247. https://doi.org/10.1016/J.GENE.2015.04.058

Yuan, R., Tsaih, S. W., Petkova, S. B., Marin de Evsikova, C., Xing, S., Marion, M. A., Bogue, M. A., Mills, K. D., Peters, L. L., Bult, C. J., Rosen, C. J., Sundberg, J. P., Harrison, D. E., Churchill, G. A., & Paigen, B. (2009). Aging in inbred strains of mice: study design and interim report on median lifespans and circulating IGF1 levels. *Aging cell*, *8*(3), 277–287. https://doi.org/10.1111/j.1474-9726.2009.00478.x

Yun, J., & Finkel, T. (2014). Mitohormesis. *Cell Metabolism*, *19*(5), 757–766. https://doi.org/10.1016/j.cmet.2014.01.011

Zhang, L., Lv, J., Wang, C., Ren, Y., & Yong, M. (2022). Myokine, a key cytokine for physical exercise to alleviate sarcopenic obesity. *Molecular Biology Reports 2022 50:3*, *50*(3), 2723–2734. https://doi.org/10.1007/S11033-022-07821-3

Zhang, Q., Wang, Z., Zhang, W., Wen, Q., Li, X., Zhou, J., Wu, X., Guo, Y., Liu, Y., Wei, C., Qian, W., & Tian, Y. (2021). The memory of neuronal mitochondrial stress is inherited

transgenerationally via elevated mitochondrial DNA levels. *Nature Cell Biology 2021 23:8*, *23*(8), 870–880. https://doi.org/10.1038/s41556-021-00724-8

Zhang, Q., Wu, X., Chen, P., Liu, L., Xin, N., Tian, Y., & Dillin, A. (2018). The Mitochondrial Unfolded Protein Response Is Mediated Cell-Non-autonomously by Retromer-Dependent Wnt Signaling. *Cell*, *174*(4), 870-883.e17. https://doi.org/10.1016/J.CELL.2018.06.029

Zhao, Q., Wang, J., Levichkin, I. V., Stasinopoulos, S., Ryan, M. T., & Hoogenraad, N. J. (2002). A mitochondrial specific stress response in mammalian cells. *The EMBO Journal*, *21*(17), 4411–4419. https://doi.org/10.1093/EMBOJ/CDF445

Zimmermann, A., Madreiter-Sokolowski, C., Stryeck, S., & Abdellatif, M. (2021). Targeting the Mitochondria-Proteostasis Axis to Delay Aging. *Frontiers in Cell and Developmental Biology*, *9*, 656201. https://doi.org/10.3389/FCELL.2021.656201/BIBTEX